BEHAVIOUR OF UNSATURATED SOILS FOR ROAD PAVEMENT STRUCTURE UNDER CYCLIC LOADING

by

ANEKE FRANK IKECHUKWU

A dissertation submitted to the Faculty of Engineering and information Technology
Central University of Technology, Free State, South Africa
In fulfilment of the requirement for the degree of
Doctor of Engineering in Civil Engineering

SUPERVISOR: Prof. Mohamed M H Mostafa

CO- SUPERVISOR: Dr. Azza Moubarak

BLOEMFONTEIN
October 2018

DECLARATION

I, Aneke Frank Ikechukwu hereby declare that the work presented in this thesis titled **'BEHAVIOUR OF UNSATURATED SOILS FOR ROAD PAVEMENT STRUCTURE UNDER CYCLIC LOADING'** submitted to Central University of Technology for a Doctoral degree of Engineering (D. Eng.) in Civil Engineering, is my personal distinctive research work carried out by me under the supervision of Prof. Mostafa and Dr. Moubarak. I therefore confirm that no part of this thesis has been presented for any other degree or examined in any other University.

Signature…

Date: October 2018

Bloemfontein, South Africa

ABSTRACT

The geotechnical engineering practice has not been advanced in South Africa. As no significant integration of unsaturated soil mechanics (USM) is yet to be covered in pavement design. Stiffness of subgrade soils that is determined by resilient modulus (Mr), is an important component in the design of flexible pavement structures and railway embankments. Environmental effects, such as seasonal variations in moisture content considerably influence the subgrade properties that are failed to be considered in any realistic pavement and railway embankment design. The seasonal changes in moisture condition affects the stress state of subgrade due to changes in the matric suction and this is considered an important stress state variable in unsaturated soil mechanics. Therefore, particular attention was directed in this research towards evaluating the response of unsaturated pavement structure under cyclic loading.

Several factors are needed to be considered during pavement design, which are dependent on Mr in order to provide an accurate assessment of the support provide by the subgrade. Roadbed with high plasticity index (PI) and swelling potential, are prevalent across Free State and Northern Cape and this possess an uncommon challenges to design Engineers. This challenge is majorly as a result of Mr value of high plasticity index subgrades depends on the moisture content. Furthermore, the pavement structures are generally under unsaturated conditions, such that the Groundwater Table depth is below the depth of the subgrade in consideration for pavement design. The classic soil mechanics considers the pavement structures to be under saturated conditions. This means, that the soil mass under consideration consists of two phases, solids (soil particles) and water. This assumption is generally acceptable, as it makes it possible to develop simple analytical solutions that lay the foundation for geotechnical engineering. However, since subgrade soils for pavements exist largely in an unsaturated state. It is reasonably realistic to employ the fundamentals of unsaturated soil mechanics in order to explore the resilient performance and deformation characteristics of subgrades using Mr- suction correlation.

The evaluation of Mr properties of unsaturated subgrade soils and evaluation effects of suction and swelling stress on Mr of the studied subgrades were summerized in this research. Furthermore, this study developed mathematical predictive models. As well,

reviewed the design of flexible pavement, as per AASHTO 1993 flexible pavement design guide by comparing designs made with both unsaturated Mr design value and conventional laboratory Mr design value. Prior to the design of flexible pavement exercise carried out in this study, some geotechnical tests were laboratory conducted using both the unsaturated soil mechanics and classic soil mechanics approach i.e. unsaturated CBR, shear stress, resilient modulus tests and filter paper test to measure suction.

The laboratory result of the tested soils reveal that the unsaturated CBR and Mr values were 1.5 to 2.5 times higher than that of the conventional CBR and Mr values. Among other results, are shear strength result that followed similar trend, on the contrary, the shear stress parameter i.e. $\emptyset^b$ of the tested soils were 1 to 1.5% lower than that of the classical soil mechanics.

The SWRC curves were evaluated through the entire range of volumetric water content using filter paper techniques. It is evident that Mr depends on matric suction, which also varies with moisture content, thereby, a Mr -matric suction relationship provides sound theoretical framework to account for moisture variation in unsaturated subgrade soils. Three different SWRC models (Seki, Van Genuchten, and Fredlund and Xing) were used for curve fitting, the SWRC revealed that Seki's SWRC model best fitted the laboratory data with coefficient of determination, R^2 values ranging from 0.95458 - 0.99986. Whereas, Van Genuchten R^2 values were in the bracket of 0.85796 - 0.93317, and Fredlund and Xing R^2 values were within the range of 0.89959 – 0.96142.

The SWRC curves evidenced that the subgrade soils with fine content (50%>P_{200}) like FSS 1, 2 and NCS 2 and 3 recorded higher air entry values (AEV) within the range of 152 kPa – 250 kPa. Whereas, the subgrade soils with lower fine content yielded AEV between the range of 90kPa -120kPa. The means that soils with high fine content starts to desaturate at a very high AEV compared to soils with lower fine content, due to inability of the soils to maintain saturation.

The analysis of experimental data obtained from the prepared specimens at different moisture contents were used for multi-regression analysis using "NCSS11" software package. The predictive mathematical models were developed for unsaturated CBR. This model performed well against Ampadu's (2007) model for prediction of unsaturated CBR.

In addition, all the predictive models developed in this study i.e. Models 7, 8, and extended Yang et.al model yielded more satisfactorily results than, Yang et.al (2005) model, Liang et. al (2008) model and when compared with the laboratory measured Mr. Thus, the predicted Mr values using all these models were 1.2 to 1.5 times higher than laboratory measured Mr values with R^2 within the range of 0.91 – 0.96 on curve validation. The results showed that all the tested subgrade soils are highly depended on k_1 parameter. Whereas, the effects of k_2, and k_3 are proportional to deviatoric and confining stresses relatively to Mr values.

Lastly, AASHTO 1993 pavement design guide was used for the design exercise, on the samples prepared on the dry side of optimum. Subgrade Mr reflect the range of stress states, commonly developed beneath the pavements that are subjected to moving wheel loads. According to the design exercise in this study, the predicted Mr design value for the subgrade provided sufficient thickness that can support the entire pavement structure. Whereas, the measure resilient modulus design value, under-designed the pavement thus, required higher asphalt thickness layer.

Keywords: Subgrade soils, unsaturated CBR, CBR, swelling stress, soil suction, soil water retention curve (SWRC) properties, unsaturated shear strength, shear strength unsaturated resilient modulus, resilient modulus regression analysis, pavement design.

ACKNOWLEDGEMENTS

It has been my gratification to pursue a Doctoral degree program in Civil Engineering with a speciality in application of Geotechnical engineering in pavement. My Doctoral degree program offered me a true reflection of Geotechnical engineering, as a unique and versatile discipline with the challenges Geotechnical engineers solves. Pursuing a Doctoral degree to me, has been challenging, time consuming, somewhat requires sacrifices through the strength of my courage though it was truly an effectual experience.

My profound gratitude goes to my puissant main supervisor Prof. Mohamed Mostafa, for his expert guidance, valuable assistance, constructive suggestions and positive criticisms throughout the course of this study. I also want to say a very good thanks to Dr. Azza Moubarak of Civil Engineering Department Suez Canal University for accepting to serve as a co-supervisor and also for her valuable guidance and assistance towards this dissertation.

My sincere thanks go to Central University of Technology, for providing me scholarship and opportunity to be part of their special graduate program. Truthfully, I appreciate the provision of workspace, through which all my laboratory programs were conducted.

Similarly, my gratitude and appreciations are due to my mom Mrs Hanna Aneke who has been a great pillar of support ever since my father died. To my Father, late Mr Innocent Nzekwe Aneke, this is the part you have always wanted for me, to be an academic Doctor. Further greetings and thanks go to my brothers: Chinedu Aneke, Emeka Aneke and Onyebuchi Aneke for their unconditional love and words of admonition given to me throughout the period of my research study.

TABLE OF CONTENTS

LIST OF ABBREVIATIONS

AASHTO	American Association of State Highway and Transportation Officials
AIC	Akaike Information Criterion
AEV	Air Entry Value
ASTM	American Society for Testing and Material
AWI	Air-Water Interface
CBR	California Bearing Ratio
CBRu	Unsaturated California Bearing Ratio
CH	High Plastic Clay
CL	Medium Plastic Clay
CPC	Capillary Pressure Curve
CSIR	Council of scientific and Industrial Research
CU	Consolidated Undrained
CUT	Consolidated Undrain Test
DOP	Dry Side of the Optimum
DCP	Dynamic Cone Penetration (DCP)
EICM	Enhanced Integrated Climatic Model (EICM)
FSI	Free Swell Index
FSS	Free State Soil
FPM	Filter Paper Method
GPS	Gauteng Province Soil
GWT	Ground-Water Table
IS	Indian Standards
LFWD	Light Falling Weight Deflectometer
LVDT	Linear Variable Differential Transducer
Mc	Moisture Content
MDD	Maximum Dry Density
M-E	Mechanistic-Empirical
MEPDG	Mechanistic-Empirical Pavement Design Guide
M_{ER}	Effective Resilient Modulus Adjusted for Seasonal Variation
ML	Low Plastic Silt
-PWP	Negative Pore-Water Pressure
NCS	Northern Cape Soil
NCHRP	National Cooperative Highway Research Program

OMC	Optimum Moisture Content
OC	Percentage Organic Content
Ps	Swelling Stress
PSD	Particles Size Distribution
PVC	Poly-Vinyl Chloride
RAM	Recycled Asphalt Material
RAP	Recycled asphalt pavement
RLTT	Repeated Load Triaxial Test
S_0	Combined Standard Error of the Traffic and Performance Predictions
SAPDA	South Africa Pavement Design Methods
SSR	Sum of Squared Residuals
SSCC	Suction Stress Characteristic Curve
SN	Structural Number of the Total Pavement Thickness
SWCC	Soil Water Characteristic Curve
SWRC	Soil Water Retention Curve
TMH	Technical Method for Highways
UCS	Unconfined Compressive Strength
USCS	Unified Soil Classification System
USM	Unsaturated soil mechanics
XRF	X-ray fluorescence
XRD	X - Ray Diffraction
WOP	Wet Side of the Optimum
Z_R	Standard normal Deviate
ZST	Zero Swelling Test
ΔPSI	Difference Between the $PSIo$ and Terminal $PSIt$ Serviceability Indices

NOTATIONS AND SYMBOLS

Roman letters

A	The corresponding cross−sectional area
A_0	The initial cross−sectional area of the specimen
a_f	Soil parameter related to the air entry of the soil
ai	Layer coefficient
A_c	Activity of clay
a,n and m	Fitting Parameters for SWRC
br	Beam ratio
C	Correction factor
C'	Intercept of the Mohr-Coulomb failure envelope at specific suction
C_c	Coefficient of curvature
C_u	Coefficient of uniformity
Di	Layer thickness
e	Void ratio
e_c	Unit electron charge
e	Natural constant 2.718
*f**	Interaction function between the equilibrium of the soil structure and the equilibrium of the contractile skin.
g	Gravitational acceleration
G_s	Specific gravity
H	Relative humidity of the pore air above the meniscus
h_c	Capillary height
$k1$, $k2$, $k3$	Regression constant
K	Boltzmann's constant
K_o	Number of estimated parameter
L_o	The initial length of the specimen
LL	Liquid limit
m	Number of relevant soil parameter
m_1	Mass of wet filter paper + cold tare
m_2	Mass of wet filter paper + hot tare mass
m_f	Soil parameter related to the residual water content condition
mi	Layer Drainage Coefficient

M	Total mass
M_1	Empty mass of volumetric flask
M_2	Mass of pycnometer+ oven dry soil
M_3	Mass of pycnometer+ oven dry soil+ filled water
M_4	Mass of pycnometer+ filled with water only
M_a	Mass of air
M_w	Mass of water
M_s	Mass of solids
M_c	Mass of the contractile skin
M_c	Mass of container
M_f	Mass of the dry filter paper
M_i	Unit mass of surcharge
M_m	Mass of the mould and base plate
Mr	Resilient modulus
M_{soil}	Mass of the dry soil
M_t	Mass of the mould, base plate, and wet soil
M_w	Mass of water to be added
M_v	Mass of water in the filter paper
n	Number of surcharge
n_f	Soil parameter related to the rate of desaturation
n_w	Porosity relative to the water phase
n_c	Porosity relative to the contractile skin
n_s	Porosity relative to the soil particles
P	Plunger−load KN/m2 for the tested soil
p′	Pressure Deficiency
P_a	Atmospheric pressure
PI	Plasticity index
P_s	Plunger−load in KN/m2 for the standard soil
P_s	Swelling stress
PL	Plastic limit
P200	Percentage of passing #200 sieve (75μm)
q	Unconfined compressive strength
R	Radius of the capillary tube
R^2	Correlation coefficient

R	Universal gas constant
Rd	Relative density of water according to temperature
R_s	Sheath radius of curvature/ Radius of curvature of the meniscus
R_1, R_2	Radius of curvature of warped membrane
S	Degree of Saturation
S_r	Residual of saturation
S_e	Effective saturation
T	Absolute Temperature
T	Temperature
T_c	Cold tare mass
T_h	Hot tare mass
T_s	Surface Tension
T_k	Absolute temperature
T_{zy}	Shear stress on the z-plan in y direction
U_a	Pore air pressure
U_w	Pore water pressure
U_v	Partial pressure of pore
U_{v0}	Saturation pressure of water
V	Total volume
V_{w0}	Specific Volume of Water
V_a	Volume of air
V_c	Volume of contractile skin
V_f	Final volume of the specimen
V_i	Initial volume of the specimen
V_k	Volume of the soil containing Kerosene.
V_r	Residual Water Volume
V_s	Volume of solids in water
V_m	Volume of the mould
V_w	Volume of water
W_v	Molecular mass of water vapour
W	Moisture content
W_1	Mass of container + wet soil
W_2	Mass of container + wet soil
W_c	Moisture content

W_f	Water content of the filter paper
W_i	Initial water content
W_{opt}	Optimum moisture content
W_t	Targeted moisture content
W_{18}	Predicted Number of 18−kip (80kN) Single Axle Load
X_{ij}	Independent variables
Y	Dependent variables

Greek letters

α_1	Angle of contact
β	Angle between the tension surface and horizontal.
ε_c	Dielectric constant medium
$\varepsilon_r = \varepsilon_2 - \varepsilon_1$	Recoverable strain
ε	Random error representing the discrepancies in the approximation
ε_r	Resilient strain
u_e	Air entry value
η	Electrolyte concentration
q_u	Unconfined compressive strength
$\theta = \sigma_1 + \sigma_2 + \sigma_3$	Bulk stress
θg	Gravimetric water content
θv	Volumetric water content
τ_{oct}	Octahedral shear stress
ρ_w	Density of water
ρ_s	Soil particle density
ψ_t	Total soil suction
ψ_m	Matric suction
$u_a - u_w$	Matric suction
ψ_o	Osmotic suction
τ_{xy}	Shear stress on the x-plan in y-direction
τ_{zy}	Shear stress on the z-plan in y-direction
σ_y	Total normal stress in y-direction
θ_s	Volumetric water at saturation
θ_r	Residual volumetric water content
θ_ω	Volumetric water content
γ_d	Dry density
τ	Shear strength of unsaturated soil
γ_{dmax}	Maximum dry density
$\sigma - u_a$	Net normal stress

σ_3	Minor principal stress or confining stress in the triaxial
θ	Bulk stress
$\sigma_d = \sigma_1$-σ_3	Deviator stress
σ_{cyc}	Applied cyclical stress
σ'	Effective stress
ϕ′	Effective angle of friction
ϕ^b	Angle of friction due to suction
$\lambda_o, \eta_o, \xi_o, \zeta_o, \beta_o, \mu_o$	Intercepts
$\lambda_i, \eta_i, \xi_i, \zeta_i, \beta_i, \mu_i$	Multi-regression analysis coefficient
$\phi(x)$	Normalized form of the cumulative normal distribution function
ϕ	Internal diameter of the consolidation ring
Θ	Normalised water content between saturation and residual water content
α,k,β	Fitting constants
α	Intercept of Mr at given $\theta\tau oct$ against suction relationship
β	Slope of Mr at given $\theta\tau oct$ against suction relations
τ_{sr}	Shear strength at residual suction
P_a	Atmospheric pressure
Δ_C	Chemical concentration difference across a semipermeable membrane
$\Delta\mu c$	Change due to curvature of the air−water interface (capillarity)
$\Delta\mu_0$	Change due to osmotic effects (dissolved solutes)
$\Delta\mu e$	Change due to electric field $\Delta\mu f$=change due to Van der Waals forces
ΔU	Difference in stress on a two dimension curved arc
ΔV	Initial change in volume of a specimen
ΔP	Pressure Difference
σ^s	Air entry pressure of water saturated soil

LIST OF TABLES

Page

LIST OF FIGURES

Page

LIST OF APPENDICES

APPENDIX A: Pages

APPENDIX B:

APPENDIX C:

APPENDIX D:

CHAPER 1: INTRODUCTION

1.1 Overview

The unsaturated subgrade layer plays major role in the overall performance of flexible pavement structure. The cyclic response of subgrade layer depends greatly upon moisture content and matric suction, but these effects have been conventionally difficult to quantify. Following the development of Mechanistic-Empirical (M-E) design technique. Resilient modulus (M_r) is considered an essential input design parameter in characterising cyclic behaviour of pavement structure under cyclic loading. The M_r values are determined in laboratory through repeated load triaxial test (RLTT). Basically, M-E design analysis is currently been used by American Association of State Highway and Transportation Officials (AASHTO) and other transportation agencies around the globe. Perhaps, pavement structures are typically constructed under unsaturated condition within the degrees of saturation that ranges from 75 to 90%. In spite of this fact, design engineers still uses the conventional pavement design approach that are based on saturated soil mechanics, rather than unsaturated soil mechanics (USM) principles. Scholars like: Fredlund and Morgenstern, (1977), Fredlund et al., (1978), Fredlund and Rahardjo, (1993), Fredlund, (1996), and Vanapalli et al., (1996) introduced a theoretical network, for expressing moisture response of unsaturated soils as regards pavement design.

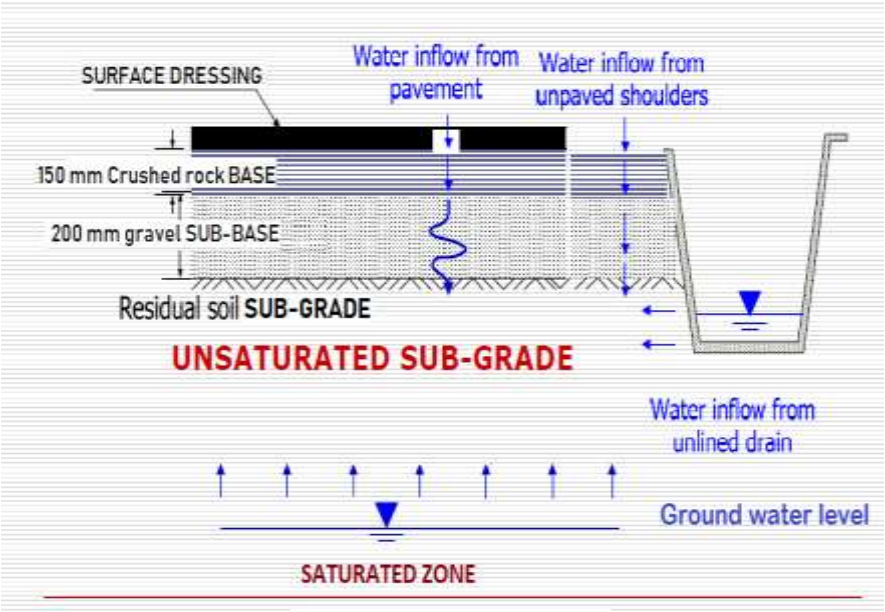

Figure1. 1: Typical unsaturated pavement structure Ampadu, (2007)

According to Figure 1.1, it becomes imperative to analyse pavement response under unsaturated condition, by considering resilient modulus with respect to matric suction.

1.2 Problem Statement

The climatic state around the earth, ranges from very humid to dry and the climatic stratification depend on the standard annual net moisture influx at the surface level.

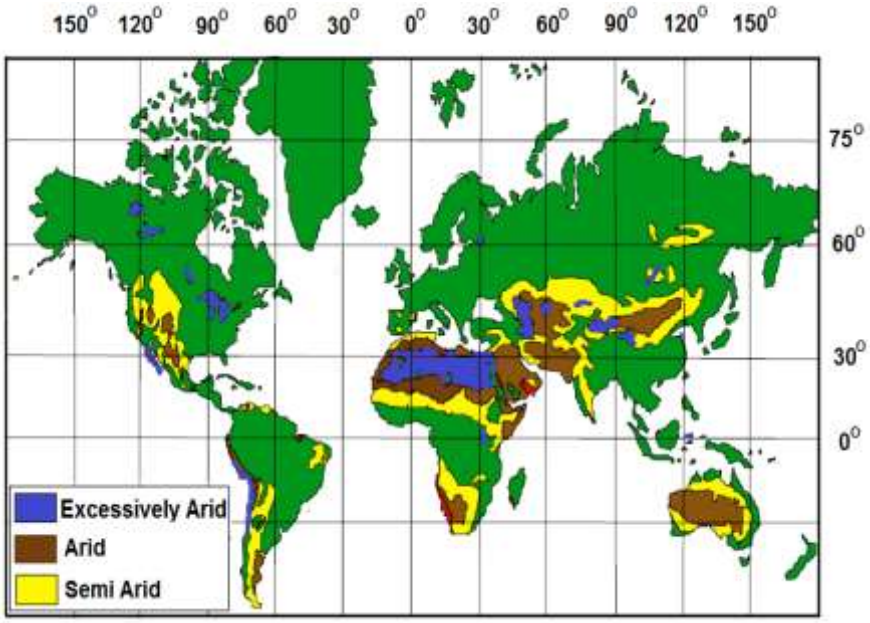

Figure1.2: Extremely arid, and semiarid regions (Fredlund &Rahardjo, 1993)

Figure 1.2 shows that South Africa is cut-across within arid and semi-arid zone, and this implies that 95% of roadbed in South African are under unsaturated condition. Despite this factors, design engineers failed to account for negative pore-water pressure (-PWP) or matric suction, as this might lead to an inappropriate design of pavement structure. Resilient response of subgrade is measured using expensive laboratory tests, that is somewhat time-consuming. Design engineers sometimes, uses overestimated backcalculated values, that in turn lead to over-design of pavement. These challenges encourage the need for a valuable and inexpensive geotechnical testing procedures, that can easily and directly determine unsaturated M_r of subgrades. As most of this testing equipment are not readily available in the university laboratories and highway engineering research centres in south Africa. Therefore, it becomes very difficult to perform obtain unsaturated M_r value.

1.3 Hypothesis

Matric suction, swelling pressure and soil type influences the shear strength, resilient modulus of unsaturated soils.

1.4 Justification for USM

Approximately, South Africa is constituted of arid and semi-arid regions. This means that groundwater table (GWT) is deep and soils are identified under unsaturated state. Hence, stresses associated with pavement structure are active above GWT. These stresses are negative with respect to the atmospheric pressure (i.e. matric suction). This implies that rational design of pavement in arid and semi-arid regions should be carried out based on the principles of USM.

1.5 Research Objectives

With the view to realise the objectives of this dissertation, the following masterplan were directly pursued to investigate the geotechnical behaviour of unsaturated soils for road pavement structure under cyclic loading:

- Firstly, the objective is to characterise the studied subgrade soils, identified across South Africa, using particles size distribution (PSD) analyses, consistency limit, among others are X-Ray Diffraction (XRD) and X-ray fluorescence (XRF) as to quantify the mineralogical constituents and elemental compounds of the this identified soils.

- To evaluate the geotechnical properties of the identified subgrades, through laboratory testing, by conducting standard civil engineering tests in both saturated and unsaturated conditions, ranging from compaction test, California bearing ratio (CBR) test, free swell index (FSI) test, zero swelling stress, suction test, consolidated undrain test (CUT), unconfined compressive strength (UCS) test, and repeated load triaxial (RLT) test.

- To develop linear mathematical predictive model for unsaturated CBR and M_r using other soil mechanical properties. As well, compare the predicted CBR and M_r values with laboratory measured values.

- To review AASHTO pavement design method using saturated and unsaturated design parameters, in order to identify the most reliable, sustainable and conservative pavement design value.

1.6 Research Scope

The jurisdiction of this research is primarily experimental, with the objectives outlined above, the scopes are within the confinements of the following:

- Develop linear mathematical predictive model, that can predict CBR and resilient modulus, using other geotechnical properties.

- Analyse the experimental data for both saturated and unsaturated soil mechanics, and further use this data to empirically design a pavement.

- The design exercise did not consider Mechanistic-Empirical (M-E) design technique, rather AASHTO 1993 pavement design guide, that is purely empirical method is considered.

1.7 Research Organization

This dissertation is presented in seven-chapter format, listed as follows:

Chapter 1 is the introductory chapter and it covers background to the research, problem statement, justification of study, objectives, scopes and lastly, the organisation of the research.

Chapter 2: presents the characteristics of unsaturated soils and provides technical background on the basic knowledge needed for good understanding of USM. These principles knowledge include: the three zones of unsaturated soil, stress state variables, suction matric and the soil-water retention curve. Furthermore, this Chapters presents previous studies on M_r, factors affecting M_r, M_r model, M_r generated from other geotechnical properties and some correlation between M_r and other geotechnical soil properties.

Chapter 3: gives a description of identified soils and methodology adopted to achieve the objectives of this research and this followed by standard civil engineering laboratory

testing methods, leading to the classification of this soils with their mineralogical contents. This chapter also provided illustrations of civil engineering testing procedure and equipment used to conduct these tests. i.e. consolidated undrained test (CUT), RLT test and filter paper test.

Chapter 4: Following the laboratory investigations, this chapter, covers basic test results, analyses and scientific report of all the laboratory tests conducted in this study.

Chapter 5: Provides the shear strength results of the studied soils, the effects of moulding water content, suction matric and swelling stress on shear strength of the roadbeds. This chapter further described the failure envelops and shear stress parameters of the subgrades under unsaturated soil mechanics.

Chapter 6: this chapter presents M_r results of the tested soils and further evaluates the influenced of confining pressure, swelling pressure moisture content and suction on M_r. subsequently, validation of existing and developed M_r predictive models were carried out ,through comparing the models with laboratory measured M_r. This chapter further demonstrates a superlative comparison between unsaturated soil mechanics concept of pavement design method and conventional pavement method, using unsaturated M_r values and laboratory M_r values.

Chapter 7: serves as the summary, conclusions and recommendations.

CHAPTER 2: UNSATURATED SUBGRADES

2.1 Overview

Pavement structure is comprised of different layers, which collectively act to provide support for applied vehicular loads while serviceability measure is maintained. Pavement is usually situated in an unsaturated state, i.e. located above groundwater table (GWT) where it is considered an Active Zone. Fredlund's effective stress theory, basically explained shear strength of unsaturated soil, as partially saturated. Since, most natural subgrades are located above GWT. Whereas, in state the saturated subgrade is considered to be totally saturated. These conventional idealizations assume that the pore water pressures (PWP) for soils beneath the water table is positive (+PWP). On the other hand, the PWP above the GWT is certified to be negative (-PWP). Terzaghi's effective stress theory is widely accepted to evaluate the shear strength of saturated soils. Realistically, soil moisture is expected to vary seasonally, because moisture variation is known as negative pore-water pressure (-PWP). Thus, is prevalent in pavement hence its above GWT and is referred to as soil suction.

2.2 Fundamentals Of Unsaturated Geotechnics

Classical soil mechanics advanced from empirical to a science basis, after Karl Terzaghi, in 1936 developed the concept of effective stress. Conventionally, the differences between saturated and unsaturated states of soil are well explained using the phenomena of vadose zone region and water retention around soil porous system i.e. adhesive, cohesive and capillary pressures (Figure 2.1). Currently, applied soil mechanics is categorized within a horizontal line representing the GWT. Below GWT (+PWP) is considered positive, hence the soil is located on generally saturated zone. Aloft the GWT, the PWP is negative in reference to atmospheric pressure. The entire soil region above GWT is called vadose zone, above the GWT this zone is designated as capillary fringe, where degree of saturation (S_r), approaches 100%. This zone ranges from > 1m to approximately 10m in thickness, depending on soil type (Fredlund,1996). Water phase is deduced to be continuous within the capillary region, while air phase is regarded unsteady. Above this capillary region, two-distinct region is identified in which air and water phases are conceptualised as continuous.

Within this region, degree of saturation fluctuates ranging from 20% to 90%, depending on soil type. Above this two-distinct region, drier soil emerged and the water phase is

considered discontinuous. Whereas, the air phase remains continuous, as both the saturated and unsaturated zones are influenced by climatic feature i.e. evaporation, evapotranspiration and precipitation.

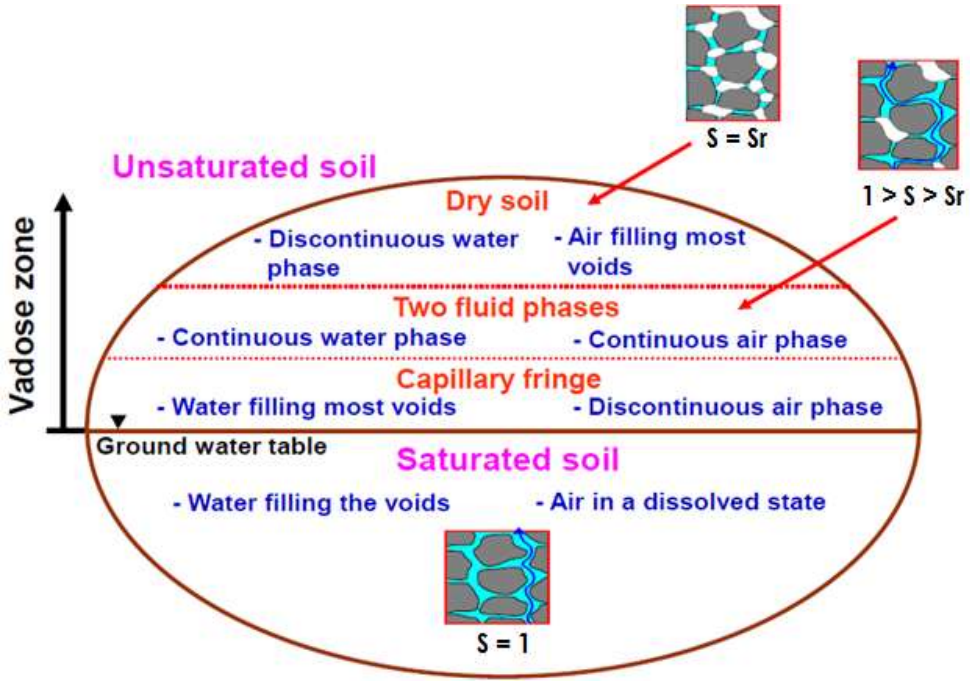

Figure 2. 1: Hydrologic system of unsaturated geotechnics (Fredlund, 1996)

The unsaturated zone is characterised by -PWP that is called suction and there are other terms synonymous to suction such as capillary suction, matric suction, capillary water stress, pore water tension, soil moisture deficiency, capillary potential, soil water pressure deficiency, soil water free energy and soil moisture tension. Moving towards zero atmospheric pressure near soil surface, PWP and increasing desiccation becomes highly negative. Curve liquid bridges can be clearly observed linking soil particles and this curvature at resultantly difference pressure, between air and water phase. The characteristics of the air-water interface (AWI) possess an important bearing on the hydro-mechanical characteristic of unsaturated soils. The saturated and the air-dried soil is made up of two phases, i.e., fluid in the voids (e.g., water or air). While, the soil structure includes other pursuant principles of unsaturated soil mechanics. Unsaturated soils have more than two phases, i.e., soil structure, water, and air according to Fredlund et al. (2012). Though, contract skin is another component phase of unsaturated soil as the air phase is continuous, AWI interacts with soil particles and provides an influence on the soils geotechnical behavior.

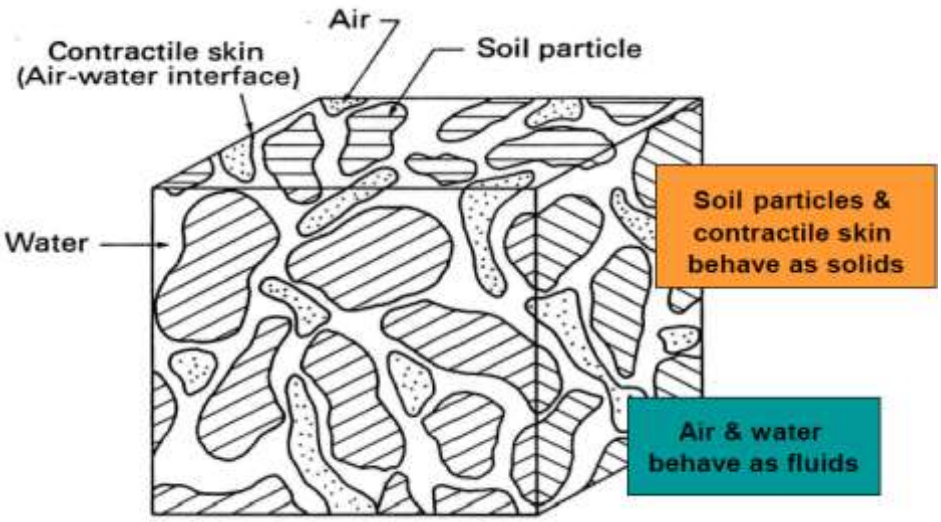

Figure 2. 2: Air water soil interphase (Fredlund et. al 2012)

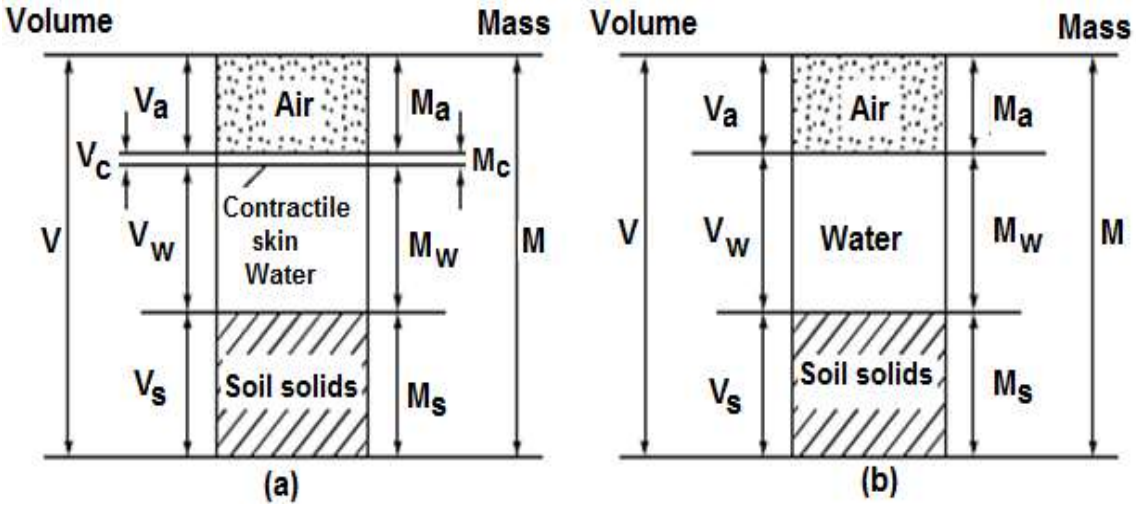

Figure 2. 3: Phase diagrams (a)Fourphase unsaturated soil system (b)Simplified three phase diagrams (Fredlund and Rahardjo, 1993)

Additionally, unsaturated soil is perceived as a four-phase system due to unique role of AWI on soil behaviour. The AWI portrayed a thin membrane interlinked through soil voids, forming a fixed layer within the air-water phases. Stress state varies around AWI causing changes in moisture content, volume and shear strength of unsaturated soils. Contractile skin forms barrier around air-water interphase and determines the air to the volume ratio in soil voids.

2.2.1 Capillarity

Basically, to understand the physical phenomenon of how negative pore-water pressure (-PWP) influences the effective stress (σ') in unsaturated soil. The principle of capillary forces, is necessary as capillarity is consistence with matric suction. When water level increases in the capillary tube, radius of curvature of AWI directly affects soil moisture content and matric suction, (ψ_m). Though rise in capillary differs from soil wetting-drying processes due to soil void discrepancy. More commonly, water increases in the capillary tube due to surface tension (T_s) and water tendency, to wet the surface of capillary tube. Furthermore, capillary activities could be analysed by considering T_s revolving within meniscus circumference. The T_s acts at an angle α_1 vertically to the capillary tube and this angle is called contact angle. The magnitude of capillary tube is controlled by adhesion between the molecules in the AWI. The perpendicular component of T_s, governs holding of water column weight, which has a height, h_c as expressed mathematically :

$$2\pi r T_s Cos\alpha_1 = \pi r^2 h_c \rho_w g \tag{2.1}$$

Where:

$\mathrm{r} = \text{radius of the capillary tube}$

$\mathrm{T_s} = \text{surface tension of water}$

$\alpha_1 = \text{contact angle}$

$h_c = \text{capillary heightcontact angle}$

$\mathrm{g} = \text{gravitional acceleration}$

When rearranged, Equation 2.2 could give the maximum water elevation in the capillary tube, h_c:

$$h_c = \frac{2T_s}{\rho_w g R_s} \tag{2.2}$$

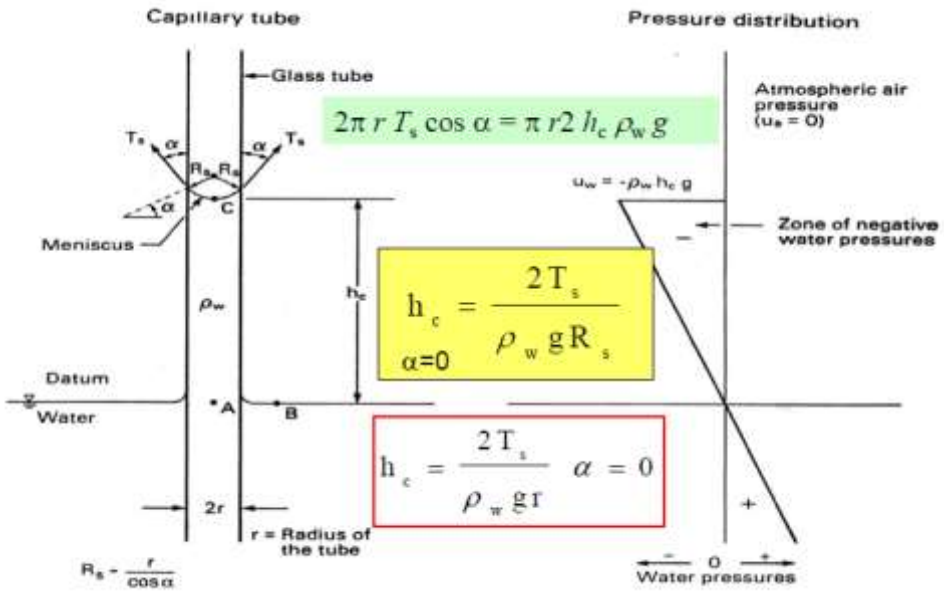

Figure 2.4: Capillarity model, (Fredlund and Rahardjo, 1993)

This factor contributes to soil water rise beyond water table and the pores in the soil, portrays tortuous capillary tubes with varying tube diameters. This is termed capillarity model. At the top of capillary bore, where the elastic film exists (contractile skin), the pressure difference (ΔP) over the film is demonstrated by the Young – Laplace equation:

$$\Delta P = (u_a - u_w) = 2T_s(1/r) \tag{2.3}$$

Where:

T_s = surface tension of water

r = radius of the capillary meniscus

Lu and Likos, (2004) presented mechanical equilibrium diagram for capillary rise in a small diameter tube $u_a - u_w$ acting within meniscus region, and the vertical projection of T_s acting over meniscus circumference lead to correlation in Equation 2.4:

$$(u_a - u_w)\frac{\pi}{4}d^2 = T_s \pi d Cos\alpha \tag{2.4}$$

It is evidenced that the term $u_a - u_w$, is equivalent to matric suction in Equation 2.4. Lu and Likos suggested that matric suction, depends on the tube diameter, relative to soil pore sizes.

This means that smaller the soil pores diameter, the larger the matric suction (ψ_m) values. Thus, this concept is important when in geotechnical engineering as matric suction is a state stress variables achieved by difference soils. The effect of -PWP and T_s gives rise to suction stress in soils under unsaturated condition. Suction stress denotes as free interparticle force gained around a matric of unsaturated soil particles due to combined effects of -PWP and T_s, which occurs at the pore water-air-soil grain interface. As suction pressure tends to pull soil particles towards each other and this gave rise to Kelvin equation:

$$\Delta P = -311 log_{10} H \tag{2.5}$$

Where:

$\mathrm{T_s} = \text{surface tension of water}$

$\mathrm{r} = \text{radius of the capillary meniscus}$

$\mathrm{H} = \text{relative humidiy of the pore air above the meniscus}$

Substituting the suction matric $(u_a - u_w)$ for ΔP in Equation 2.4 enables it to be demonstrated as a function of the relative humidity:

$$(u_a - u_w) = -311 log_{10} H \tag{2.5}$$

2.2.2 Soil potential energy

Soil suction is described as soil potential for water attraction. This is the key variable that regulates hydromechanical principles of unsaturated soils. Primarily, soil suction is the fundamental factors of unsaturated soils that is categorized into two parts i.e. osmotic suction (ψ_o) and matric suction (ψ_m). The summation of these two suction components is known as total suction, mathematically it is expressed as:

$$\psi_t = \psi_m + \psi_o \tag{2.6}$$

However, 'Total Suction', is considered as the potential energy of water in the soil and it describes potential thermodynamic difference (u_w) between the soil compared to free water. The thermodynamic potential of the soil u_w is decreased by capillarity effects, short-range adsorption, and effect of dissolved salts.

Thus, matric suction is triggered by short-range adsorption effects and capillarity; while osmotic suction is caused by dissolved salts effect. Osmotic suction is only present in marine and leached soils, because of short-range adsorption effects are only prominent at low water contents when the adsorbed water is mainly in the form of thin films around the soil particles. Basically, the soil potential energy, u_w is the mathematical expression of the potentials different:

$$\Delta\mu_t = \Delta\mu_c + \Delta\mu_0 + \Delta\mu_e + \Delta\mu_f \quad (2.7)$$

Where:

$\Delta\mu_c = \text{change due to curvature of the air} - \text{water interface (capillarity)}$

$\Delta\mu_0 = \text{change due to osmotic effects (dissolved solutes)}$

$\Delta\mu_e = \text{change due to electric field}$

$\Delta\mu_f = \text{change due to Van der Waals forces}$

Excluding dissolved solutes effects, all the other terms added up represent matric suction. While, all the terms represent a negative value, matric suction value is positive because it constitutes free water state potential change. Nam et. al, (2009) reported that matric potential contributes the highest potential of pore water during suction measurement. Matric suction is generally defined as $(u_a - u_w)$, and this stands for the amount of -PWP in unsaturated soils.

Fredlund and Rahardjo, (1993) developed a relationship that represented total suction as a function of partial vapour pressure (PVP) of the pore water, using the fundamentals of total suction and thermodynamic of the soil pore water:

$$\psi_T = \frac{-RT}{v_{w0}\, w_v} ln\left(\frac{u_v}{u_{v0}}\right) \quad (2.8)$$

Where:

$\mathrm{R} = \text{universal gas constant (J/mol K)}$

$\mathrm{T} = \text{absolute temperature (K)}$

$\mathrm{v_{w0}} = \text{specific volume of water } (\mathrm{m^3/k})$

$\mathrm{w_v} = \text{molecular mass of water vapour (g/mol)}$

$\mathrm{u_v} = \text{partial pressure of pore} - \text{water (kPa)}$

$\mathrm{u_{v0}} = \text{saturation pressure of water (kPa)}$

Note, the term $(^{u_v}/_{u_{v0}})$ stands for measured relative humidity (RH). Therefore, relative humidity of pore water vapor, can be employed to measure suction.

2.2.3 Matric suction

Matric suction $(u_a - u_w)$, is relatively determined as the different between partial pressure of water vapour in equilibrium with the soil water. Matric suction results through capillarity and surface absorptive forces of the soil.

$$\psi_m = (u_a - u_w) \tag{2.9}$$

2.2.4 Osmotic suction

Osmotic suction (ψ_o) is the expression of amount of dissolved salts in the pore fluid. Therefore, matric suction is caused by capillary pressure in soil structure, thus its relates to mechano-chemical interactions between soil minerals and u_w (Wan et. al, 1995). However, matric suction is of high interest, as many pavement problems related to unsaturated soil due to variation in moisture content, which principally influence soil matric suction (Nishimura et. al 2007). Osmotic changes are less significant in geotechnical engineering, because change in total suction, (ψ_T) is equivalent to different in matric suction i.e.

$$\Delta\psi = \Delta(u_a - u_w) \tag{2.10}$$

Furthermore, mechanics of unsaturated soil is considered as a three-phase system that is made up of pore-air, pore-water and granular solid particles. Matric suction in such system made-up off two parts: the hydration forces and capillary forces that arises from capillary activities attributed to interactions within air-water menisci that are originated from soil particles and T_s. The two forces are available in high clays content soil, such as bentonite (Pusch and Yong, 2003; Arifin and Schanz, 2009). In case of sands and low plastic clays, suction matric is associated to capillary pressure (Fredlund and Rahardjo,1993).

2.3 Soil-Water Retention Curve (SWRC)

Thermodynamic potential decrease of pore water is associated with degree of pore water present in the soil and a correlation exists within soil suction and moisture content of the soil. This link is described by the Soil Water Retention Curve (SWRC). The SWRC consists of different suction ranges, where the main moisture holding mechanism is different and differs by soil type. Various researchers have successfully applied axis-translation technique, to study SWRC of unsaturated soils (Ng and Pang, 2000a, b), by considering volume change and shear strength characteristic of unsaturated soils (Ng and Chiu, 2001; Ng and Chiu, 2003a, b; Zhan, 2003; Ng and Zhou, 2005). Therefore, SWRC is relationship between suction and the corresponding soil wetness. Moisture quantity, could be gravimetric water content, w, volumetric water content, θ, or degree of saturation (Sr). SWRC could also be called capillary pressure curve (CPC). The SWRC categorises soil behaviour into three distinct classes of desaturation (Figure 2.5). The classes of desaturation are designated as the "boundary effect class" at a very low suction of soil, the "transition class" at intermediate soil suction, and the "residual class" at a great soil suction that extend to 1,000,000 kPa (Fredlund, 2006).

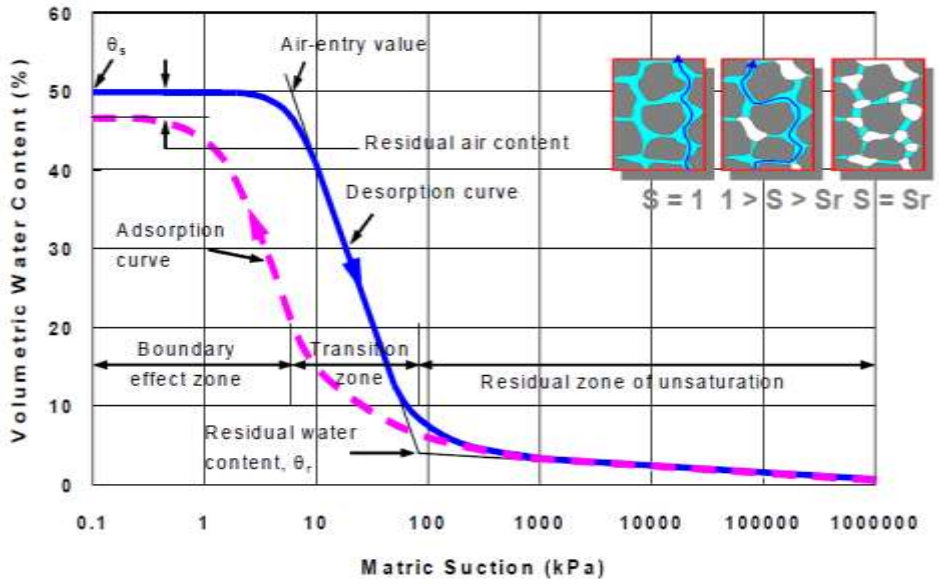

Figure: 2. 5: Soil – water retention curve (Fredlund and Xing, 1994)

The hysteresis in the SWRC is triggered by non-uniformity of pore-size distribution in the soil. During the wetting and drying process, the soil water-content varies at any particular matric suction (Fredlund and Rahardjo, 1993). Figure 2.5 above, illustrated that the end-point of adsorption curve differs from the start-point of the curve; due to

hedged air in the soil (Fredlund and Xing, 1994). The slope steepness over a range of soil suctions is representative of the soil storage potential (Leong and Rahardjo, 1997). Whereas, the difference between soil matric suction and moisture content is presences soil's adsorption potential. In addition, soil subjected to wetting may never reach full saturation due to the entrapped air bubbles (Pham, 2005). Therefore, hysteresis effect exists for SWRCs for two major reasons and this include:

I. Hysteresis is mainly present in the capillary regime, which explains the importance of the pore-size distribution effect.

II. Changes in geometry of the pore-size distribution (Lu and Likos, 2004).

2.3.1 SWRC models

The most widely utilised models were formulated by (Fredlund and Xing, 1994), as presented in Equations 2.11 and 2.12. Van Genuchten, (1980), proposed Equation 2.13, though the models was used to describe a SWRC exist in 3 or 4 parameter forms. These models allow analytical correlation with soil suction and volumetric water content. Moreover, the sigmoidal shape of this model, replicates that of particle size distribution (PSD) curve, as it was originally derived based on relationships from the pore-size distribution of soils.

$$\theta_w = \frac{\theta_s}{(\ln(e+\psi/a)^n))^m} \tag{2.11}$$

$$\theta_w = \left[1 - \frac{\ln\left(1+\frac{\psi}{\psi_r}\right)}{ln\left(1+\frac{1{,}000{,}000}{\psi_r}\right)}\right] \frac{\theta_s}{(\ln(e+\psi/a)^n))^m} \tag{2.12}$$

$$\theta_w = \theta_r + \frac{\theta_s - \theta_r}{[1+(\psi/a)^n]^m} \tag{2.13}$$

Where:

θ_w = volumetric water content

θ_s = saturated water content

θ_r = residual water content

ψ = suction matric/ soil moisture deficiency

ψ_r = residual suction

a, n and m = fitting parameters

Leong and Rahardjo, (1997) suggested that 'a' in the three models presented above, is related to suction at inflection point of the curve (i.e., air-entry value), parameter 'n' affects the gradient of the curve in the desaturation zone, and the parameter 'm' affects the symmetry of the slope of the curve about the inflection point. The degree of saturation (S_r) or gravimetric water content (w) or volumetric water content (θ_w) are used to illustrates the SWRC. Mathematically, the relations between volumetric water content θ_w, gravimetric water content, w, and degree of saturation, S_r are given by the relation below:

For saturated soil condition:

$$\theta_w = \frac{V_w}{V_w + V_s}$$

$$W = \frac{M_w}{M_s} = \frac{V_v \rho_w}{G_s \rho_w V_s} = \frac{V_w}{G_s V_s} = \frac{e}{G_s}, e = wG_s$$

$$\theta_w = \frac{S_r e}{1+e} = \frac{W G_s}{1+wG_s} \quad (2.15)$$

For not saturated soil condition:

$$e = \frac{wG_s}{S_r}$$

$$\theta_w = \frac{wG_S}{1+{}^{wG_s}/_{S_r}} = \frac{S_r wG_s}{S_r+wG_S} \quad (2.16)$$

Where:

$e =$ void ratio

$G_s =$ specific gravity

$\rho_w =$ density of water

$M_s =$ mass of soil solids

$M_w =$ mass of water

Equations 2.15 and 2.16 are useful theoretical relationships. For practical purposes, SWRCs is always measured in line with gravimetric water content, w non-recoverable energy consumed by compressed soil due to hysteresis (Blight, 2013).

Conclusively, SWRC can vary according to a number of factors and these includes hydraulic hysteresis, transient nature of the pore size distribution of a deformable soil. The account of these factors should be considered, during modelling of SWRC.

2.4 Unsaturated Soil Shear Strength

Bishop, (1959) propounded an equation to evaluate shear strength of unsaturated soil, while exploring effective stress concept, as stated in Equation 2.17 below:

$$\tau = c' + (\sigma - u_a)tan\phi' + (u_a - u_w)\chi tan\phi' \quad (2.17)$$

Where:

$\tau =$ shear strength of unsaturated soil,

$c' =$ effective cohesion,

$\phi' =$ effective angle of friction

$(\sigma - u_a) =$ net normal stress,

$(u_a - u_a) =$ is matric suction; and χ is parameter dependent on the degree of saturation (between 0 and 1).

Fredlund et al. (1978) extended the shear strength equation of saturated soil, by suggesting an equation that demonstrates the shear strength of unsaturated soils.

$$\tau = c' + (\sigma_n - u_a)tan\phi' + (u_a - u_w)tan\phi^b \quad (2.18)$$

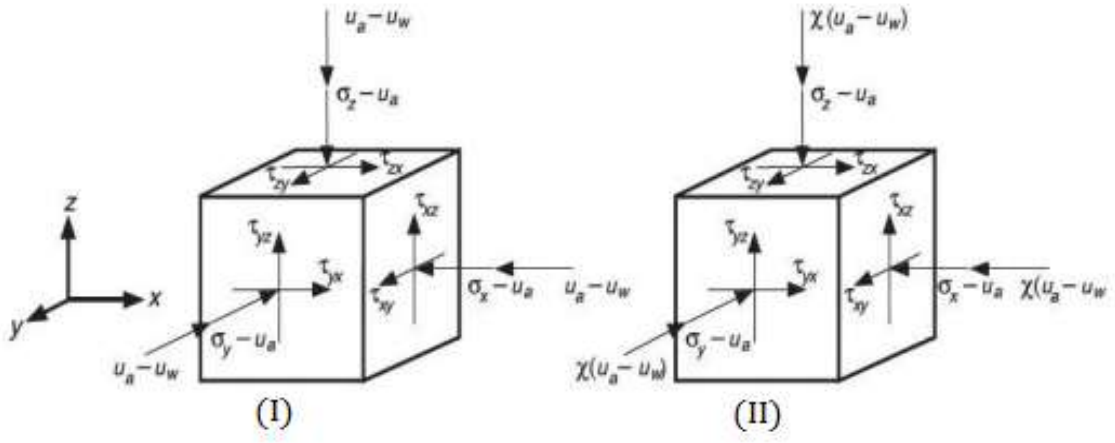

Figure 2.6: Normal and shear stresses in unsaturated geotechnics:

(I) independent stress state variable, (Fredlund 1993)

(II) effective stress approach (Lu and Likos, 2004)

Furthermore, the principal concept of unsaturated soil mechanics can be grouped into three categories: (i) effective stress approach by (Bishop,1960), (Bishop and Blight,1967), (ii) independent stress variable approach of (Fredlund and Morgenstern, 1977) and (Fredlund et. al, 1978) and (iii) suction stress characteristic curve (Lu and Likos, 2006) and (Lu et. al, 2010).

2.4.1 Effective stress approach:

Shear strength of soil is the resistance a soil needed to sustain, before slide on a failure plane (Das, 2006). Shear strength measurements are based on Mohr's theory of material rupture. The theory states that material failure occurs at a critical combination of shear (τ) and normal (σ_n) stresses. Thus, shear strength at failure (τ_f) could be demonstrated with Mohr-Coulomb law as:

$$\tau_f = c' + \sigma_n tan\phi' \tag{2.19}$$

Where:

$c' =$ cohesion of the soil

$\phi' =$ angle of internal friction

Equation 2.19 was later modified by (Terzaghi, 1936), through the incorporation of PWP in saturated soils. It was argued that total normal stress, σ' is summation of stress supported by soil, and the stress due to PWP (u_w). Thus, shear stress is defined as the stress carried by soils, as effective stress($\sigma' = \sigma_n - u_w$) and Mohr-Coulomb formulation for saturated soils is stated as:

$$\tau_f = c' + (\sigma_n - u_w)tan\phi' \tag{2.20}$$

This equation was further revised by (Bishop et. al, 1960) for unsaturated soil, as to account for suction effects, $(u_a - u_w)$ in the soil. They suggested that, since unsaturated soil is a three-phase system (solid, pore water, and pore air) and water in voids is not continuous.

The total stress will be the sum of intergranular stress, the pore air pressure, u_a and pore water pressure, u_w and they further stated that effective stress(σ') in unsaturated soils could be demonstrated as:

$$\sigma' = (\sigma_n - u_a) + \chi\,(u_a - u_w) \tag{2.21}$$

Where:

χ = fractional cross − sectional area of the water in voids, For dry soil, χ = 0 and for saturated soil $\chi = 1$.

Thus, Equation 2.22 is for Mohr-Coulomb relationship shear strength for unsaturated soils:

$$\tau_f = c' + [(\sigma_n - u_a) + \chi(u_a - u_w)] + tan\emptyset' \tag{2.22}$$

Jennings and Burland, (1962) explored the limitations in the use of effective stress principles and discovered that it may not be adequate for description of collapse behaviour of soils. Also, the material parameter χ includes single valued effective stress equation, which leads to difficulties both in theory and its measurement. The material parameter χ depends on the soil mineralogy and stress path (Khalili, N. et al, 2004; Alsherif, N.A et. al, 2014; Baille, W. et.al 2014). Similarly, other researchers presented the relationships in Equation 2.20 and all pointed out to the challenges of using effective stress concept due to the error in prediction of χ value.

Bishop's approach received wide criticism concerning the use of χ which some researchers call an elusive parameter. Coleman, (1962) argued that χ is associated with soil structure and no correlation can be found between χ and volumetric parameter such as the saturation degree. Fredlund, et al. (1978) presented suction as an independent state variable, but prediction of shear strength from the concept of effective stress is rarely utilised. Basically, efforts were made by (Khalili and Khabbaz,1998) and (Khalili et .al, 2004), when shear strength data from 17 studies were used (including that of Fredlund and his associates) for the evaluation of χ value and this showed that χ value was uniquely correlated with suction ratio and air-entry value.

$$\chi = \left[\frac{(u_a - u_w)}{(u_a - u_w)_b}\right]^{\eta} \quad (2.23)$$

Where:

χ = effective stress coefficient

$(u_a - u_w)$ = matrix suction in the soil samples at failure conditions

$(u_a - u_w)_b$ = soil air − entry value

η = -0.55. which is the correlation coefficient.

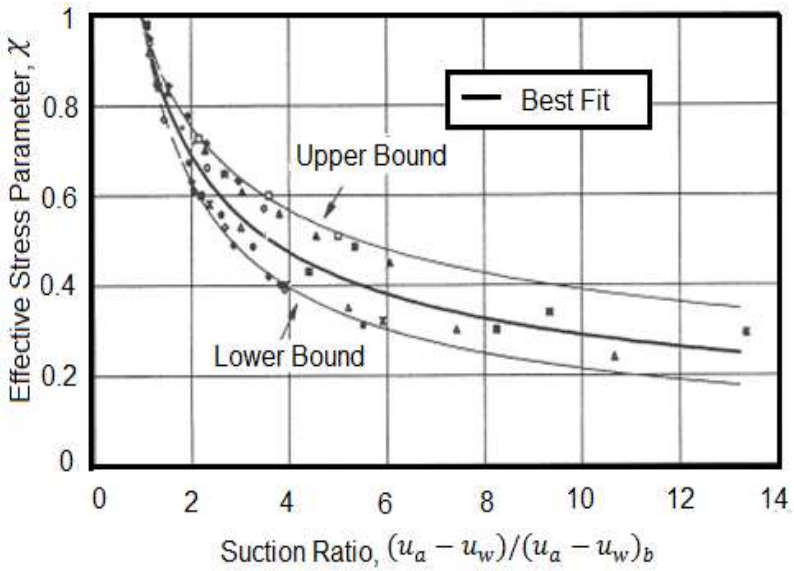

Figure 2.7: Effective stress parameter versus suction ration (from Khalili and Khabbaz, 1998)

Khalili et al. (2004) additionally reviewed previous studies from other researchers and concluded that shear strength can be predicted using effective stress concept. These scholars further proposed a sequential progression form of effective stress parameter to account for suction effects. They further suggested that for suctions > air entry values, χ values should vary as demonstrated in Equation 2.23. whereas, for suction < air entry, χ value was equal to 1.0. These scholars tested their concept of sequential progression for effective stress on shear strength data from (Cui and Delage,1996, Maatouk et. al, 1995, and Geiser, et. al 2000), and volume change data from (Fleureau et. al, 1993) observed a good curve of fit between the measured and predicted values in all cases.

The effective stress σ' controls stiffness and strength of soil and its application is important in design of pavement and other geotechnical structure.

Basically, three phases presences changes in equilibrium equation, as relative air and water pressure also contribute to the behaviour. Therefore, evaluation of strength parameter in soils, modified effective stresses equation for unsaturated soil. These equivalent effective stresses equation for unsaturated soils requires independent stress variables, which might be computed combining total stress, PWP, and pore air pressure, (PAP). The commonly used stress variables are formed by the net normal stress $(\sigma - u_a)$ and matric suction $(u_a - u_w)$ (Fredlund and Rahardjo, 1993). Clearly, matric suction is one of the variables, because it increases the existing forces at interparticle points contact due to capillary pressure presence. Variable, like net normal stress, uses the air pressure as a reference which is almost constant if taken as the atmospheric pressure.

$$\sigma' = \underbrace{(\sigma - u_a)} + \chi(u_a - u_w) \quad \text{Unsaturated soils} \tag{2.24}$$

where χ = zero for dry condition and one for full saturation. It is necessary to state that the impact of suction matric and net stresses induced by external loads at particle contact points are uncoupled. Thus, the stress variables must be independent (Vinale et.al, 2001; Cho and Santamarina, 2001). Although the Bishop's single tensor equation is often used and it summed menisci water pressure and total stress effects, but it has several limitations because it mixes local and global conditions within the medium. it is better to present stress-strain results in terms of the two state variables, to avoid challenges: net pressure$(\sigma - u_a)$ and suction $(u_a - u_w)$. Equation 2.25 is applicable to pure water only as the presence of soluble will add another term to suction. Osmotic suction π is also important in soil systems (Tindall and Kunkel, 1999):

$$\pi = KT\Delta_c \tag{2.25}$$

Where:

$\mathrm{K} =$ Boltzmann's constant

$\mathrm{T} =$ absolute temperature

$\Delta\_\mathrm{c} =$ chemical concentration difference across a semipermeable membrane

Aitchison, (1961) proposed the equation:

$$\sigma' = \sigma + \psi p' \tag{2.26}$$

Where:

$p' = \text{pressure deficiency} = (u_a - u_w)$

The Aitchison equation is a special case of Bishop equation, when the air pressure is zero (atmospheric). Whereas, (Jennings, 1961) proposed an equation similar to that of Aitchison using a different symbol, β, in place of either χ or ψ. This equation was formulated in 1958, though it was made public in 1960s:

2.4.2 Independent state stress variable approach

This approach was recommended by Fredlund and associates in a series of publications (Fredlund and Morgenstern, 1977; and Fredlund et al., 1978; Fredlund and Rahardjo, 1993; Fredlund, 1996). These researchers demonstrated that stress state of unsaturated soil can be stated using any two of the three-possible stress variables correlation namely: total normal stress(σ), pore air pressure (u_a), and pore water pressure (u_w). Possible combinations are: $(\sigma - u_a)$ and $(u_a - u_w)$, $(\sigma - u_w)$ and $(u_a - u_w)$ and $(\sigma - u_a)$ and $(\sigma - u_w)$. These researchers argued that $(\sigma - u_a)$ and $(u_a - u_w)$, were the most benefited combination as only one stress state variable was affected when pore water pressure changes. Using these combinations, the following correlation was demonstrated for describing shear strength of unsaturated soils.

$$\tau_{ff} = C' + (\sigma_f - u_a)_f \, tan\emptyset' + (u_a - u_w)_f tan\emptyset^b \quad (2.27)$$

Where:

tan $\emptyset^b$ = angle indicating the rate of increase in shear strength with respect to a change suction matric, $(u_a - u_w)_f$.

These researchers further observed that Mohr-Coulomb failure plot for saturated soil is plotted in two dimensions, while the corresponding plot for unsaturated soil must be a 3-dimensional diagram. Equation 2.28 additionally expressed that since the intercept of the failure envelop intersects the shear stress versus suction matric plane the correlation between the shear stress versus matric suction, see Figure. 2.9.

$$c = c' + (u_a - u_w)tan\emptyset^b \quad (2.28)$$

Where:

c = intercept of the Mohr-Coulomb failure envelope at specific suction and zero net normal stress.

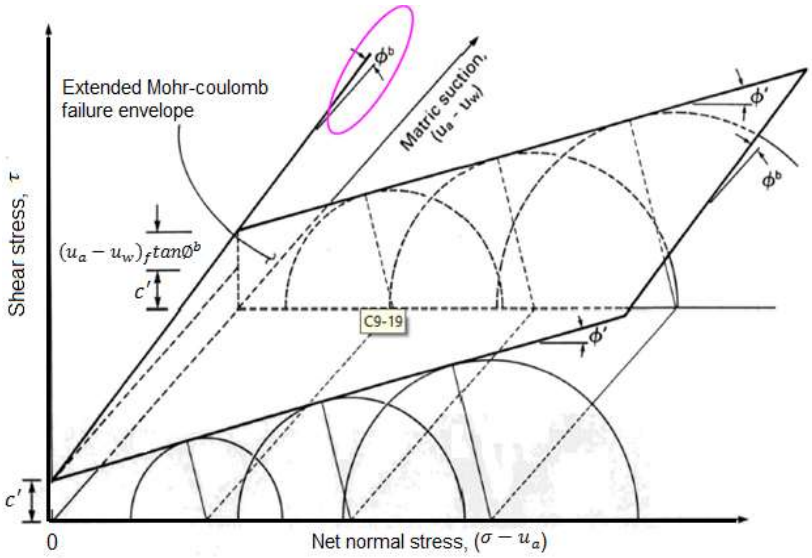

Figure2.8: Unsaturated soil Mohr – Coulomb failure envelope (Fredlund 1993)

The pair of two profitable stress state variables formed was $(\sigma - u_a)$ and $(u_a - u_w)$ and it was applied in formulation of constitutive models describing strength and deformation of unsaturated soils. Muraleetharan and Wei, (2000) develop sets of governing equations for unsaturated porous media. These equations stand on the theory of Interfaces that explicitly considers the interfacial effects and provides a theoretical basis for the use of two independent stress variables. Generally, stress tensors are required to illustrate three-dimensional state of stress in soils:

$$\sigma - u_a = \begin{bmatrix} \sigma_x - u_a & \tau_{yx} & \tau_{zx} \\ \tau_{xy} & \sigma_y - u_a & \tau_{zy} \\ \tau_{xz} & \tau_{yz} & \sigma_z - u_a \end{bmatrix} \quad (2.29)$$

$$u_a - u_w = \begin{bmatrix} u_a - u_w & 0 & 0 \\ 0 & u_a - u_w & 0 \\ 0 & 0 & u_a - u_w \end{bmatrix} \quad (2.30)$$

Some boundary conditions exist, accurate components value for state stress is limited as demonstrated by the inequality: $\sigma \geq u_a \geq u_w$.

In the condition that, air pressure must exceed total pressure, the solid particles would not intercept the soil at the extreme, but rather deform or shear. In fact, this restriction

is often applicable in pressure plate apparatus and specimen surrounded by a flexible membrane, could be considered and this makes air pressure to acts as the total pressure. The water pressure can rise until it equates the air pressure. In this case, the suction matric will be zero and the soil condition is fully saturated. Additionally, the water pressure cannot exceed the external pressure. This case is studied in classical soil mechanics.

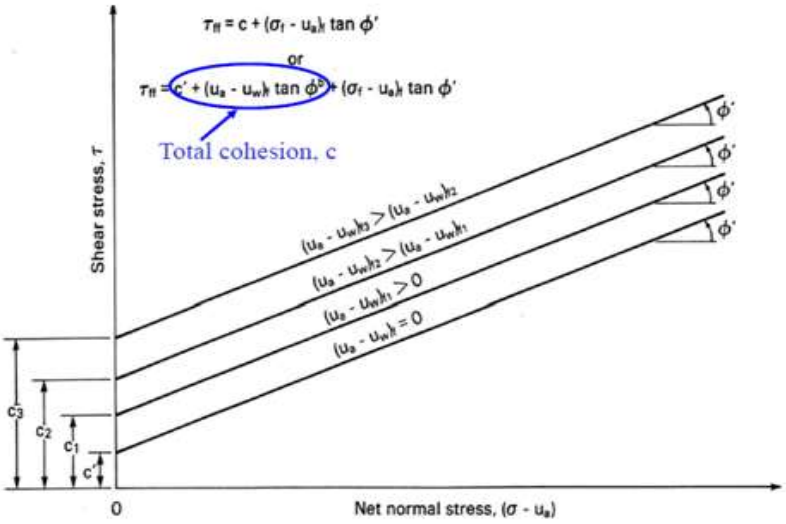

Figure 2.9: Two dimensional projections of failure envelopes at various suctions (Fredlund 1993)

Equation 2.28 implies that shear strength is linearly a function of suction. However, several equations demonstrated this correlation a non-liner parameter. Furthermore, this non-linearity is somewhat similar to the variation in χ as a function of saturation degree in effective stress concept. Different types of revised equations have been submitted and some of these revised equations included the same parameters to that of degree of saturation (Vanapalli et al., 1996; Oberg and Sallfours, 1997). Whereas other revised equation deal with inclusion of parameters related to suction (Abramento and Carvalho, 1989; Rassamand and Cook, 2002).

Oberg and Sallfours (1997):

$$\tau_f = c' + (\sigma_n - \mu_a)tan\emptyset' + (S)(\mu_a - \mu_w)tan\emptyset^b \quad (2.31)$$

Fredlund et al (1996) and Vanapalli et al (1996):

$$\tau_f = c'(\sigma_n - \mu_a)tan\emptyset' + (\theta^k)(\mu_a - \mu_w)tan\emptyset^b \quad (2.32)$$

(Abramento and Carvalho,1989)

$$\tau_f = c' + (\sigma_n - \mu_a)tan\emptyset' + \alpha(\mu_a - \mu_w)^{\beta} \quad (2.33)$$

(Rassam and Cook, 2002)

$$\tau_f = c' + (\sigma_n - \mu_a)tan\emptyset' + (\mu_a - \mu_w)tan\emptyset - \varphi((\mu_a - \mu_w) - (\mu_a - \mu_w)^{\beta} \quad (2.34)$$

$$\varphi = \frac{(\mu_a - \mu_w)\tan\emptyset - \tau_{sr}}{((\mu_a - \mu_w) - (\mu_a - \mu_w)^{\beta}} \quad (2.35)$$

$$\beta = \frac{\tan\emptyset((\mu_a - \mu_w)_r - (\mu_a - \mu_w)_b)}{(\mu_a - \mu_w)_r \tan\emptyset - \tau_{sr}} \quad (2.36)$$

Where:

$S_r =$ degree of saturation

$\Theta =$ normalised water content between saturation and residual water content;

α, k, β are fitting constants.

$\tau_{sr} =$ shear strength at residual suction.

Oberg and Sallfours,(1997) included saturation degree in Equations 2.31 and 2.32 while Fredlund et. al, (1996) and Vanapalli et. al (1996) equation was on a conceptual basis like Bishop's formulation. These authors also argued that since water is present only in a fraction of cross-sectional area in unsaturated soils, the effect of soil suction needs to be reduced by saturation degree. This provides a mechanism to account for the variation in SWRC between soil types. The fitting factor "k" in Equation 2.32 was based on the best fit of experimental data.

Nonetheless, this approach was supported by null-type triaxial tests, which showed unsaturated soil volume specimen remains constant while decreasing and increasing the stress state variables by an equal amount. Very small discrepancies in the specimen volume under null-type test condition prove the applicability of stress state variables in unsaturated soils.

Through the concept, for solving unsaturated soils mechanics problems using a realistic approach was established. Although, effective stress principles have proved workable in explaining stress and volume changes that occur in saturated soils due to differences in the applied external load. Thus, extending these principles to unsaturated soils has

been problematic because of the presence of pore fluid consisting of two phases; air and water.

Sridharan and Venkatappa Rao, (1973) asserted that osmotic suction plays part in illustration of soil behaviour. This implies that current formulations of the effective stress equation do not account for osmotic suction.

Allam and Sridharan, (1987) brought modifications to the effective stress and stress state variables approach to include osmotic suction and the effect of air-water interface. The modification, showed that high salt content contributes to a high suction which in turn greatly influences the physical and volumetric changes of soil according to the studies conducted by (Noorany, 1984, Feng et al., 2003).

$$\sigma' = (\sigma - u_a) + \chi_w(u_a - u_w) \tag{2.37}$$

Equation 2.37 was used by (Khalili and Khabbaz, 1998; Zienkiewicz et .al, 1999 and Gallipoli et. al, 2003), but other researchers like (Muraleetharan and Wei, 2000) indicated that Equation 2.38 is valid under certain conditions. This is because χ_w primarily depends on degree of saturation S_τ, soil type, compaction procedures and stress path. This parameter is equal to the saturation for the completely dry and saturated cases, which are governed by the same limits as saturation ($0 \leq \chi_w \leq 1$). The relationship between S_τ and χ_ω of various soils was illustrated by (Blight, 1967). The relation in this range, is not quite explanatory, due to lack of data at very low saturation. Thus, the consequence is very insignificant to unsaturated granular subgrade. However, modelling at low saturation levels are improbable to pose error under field conditions.

2.4.3 Suction stress characteristic curve (SSCC) approach

The third concept explains stress state of unsaturated soil is called the suction stress characteristic curve approach. Lu & Likos, (2006) proposed a form of suction stress that is similar to Terzaghi's effective stress for saturated soils (Terzaghi, 1943) and Bishop's effective stress for unsaturated soil (Bishop, 1954).

This concept aimed at proposing a single stress variable that can model hydro-mechanical response of soil. Forces such as the van der Waals, double layer forces, surface tension and adhesive forces are interactive within soil solid surface. These

forces generate energy that triggers suction stress variables. Consequently, suction stress characteristic curve approach involves thermodynamic method and this approach is better than the both effect stress and independent state variable approach, due to these reasons:

(i) Suction stress is solely a function of soil suction and therefore does not require that the effective stress coefficient χ be used to define effective stress.

(ii) The SSCC is similar to the soil water characteristic curve, so a single valued function is not required.

(iii) Hysteresis could also be conveniently handled in the SSCC

The effective stress equation by the SSCC is expressed as:

$$\sigma' = (\sigma - u_a) - \sigma^s \tag{2.38}$$

Where:

u_a = pore air pressure

σ = total stress,

σ' = effective stress

σ^s = the SSCC of soil

Where:

$\sigma^s = -(\sigma - u_a)S$ and S = saturation proportion

$(\sigma - u_a)$ = is the matric suction

Using functions of thermodynamic justifications (Lu et. al, 2010) also evaluated tensile stress using virtual work by increasing the volume of the soil system with bound residual water. They arrived at an expression for the SSCC as:

$$\sigma^s = -(u_a - u_w)S_e \text{ for } V_w > V_r \tag{2.39}$$

Where:

S_e = effective saturation

$(u_a - u_w)$ = suction matric

V_w = total water volume

V_r = residual water volume

From equation 2.38, (Lu et. al, 2010) suggested an effective stress equation as an extension of Bishop's equation and an expansion of Terzaghi's equation for all saturations by modifying the contribution to effective stress as:

$$\sigma' = -(\sigma - u_w) - [-S_e(u_a - u_w)] \tag{2.40}$$

$$= (\sigma - u_a) - \frac{S - S_r}{1 - S_r}(u_a - u_w) = (\sigma - u_a) - \sigma^s \tag{2.41}$$

Where:

S_r = residual saturation

The above equation is different from Bishop's equation with respect to the degree of saturation, but can become Terzaghi's effective stress equation, $\sigma' = u_a - u_w$, when it is saturated. An additional extension could be carried out by applying the correlation, linking degree of saturation and suction matric. Using (Van Genuchten, 1980) soil water content curve model, the normalised saturation degree is expressed as:

$$S_e = \left\{\frac{1}{1+[\alpha(u_a - u_w)]^n}\right\}^{1-1/n} \tag{2.42}$$

where n and α are empirical fitting parameters of unsaturated soil properties, n being the pore size distribution parameter and α the inverse of the air entry pressure of water saturated soil.

$$\sigma^s = \frac{s_e}{\alpha}\left(s_e^{\frac{1}{1-n}} - 1\right)^{\frac{1}{n}} \qquad 0 \le S_e \le 1 \tag{2.43}$$

Similar suction stress closed-form equation for full range of matric suction is obtained when equation (2.43) is substituted into equation (2.44) and eliminating the degree of saturation giving equation 2.45 un saturated soils:

$$\sigma^s = -(u_a - u_w) \qquad u_a - u_w \le 0 \tag{2.44}$$

$$\sigma^s = \left\{\frac{1}{1+[\alpha(u_a - u_w)]^n}\right\}^{1-1/n} \qquad u_a - u_w \ge 0 \tag{2.45}$$

Substituting equations (2.44) and (2.46) into (2.45) yields equation 2.47, for unsaturated soils:

$$\sigma' = \sigma - u_a + (u_a - u_w) \qquad u_a - u_w \leq 0 \tag{2.46}$$

$$\sigma' = \sigma - u_a + \left\{\frac{(u_a - u_w)}{1+[\alpha(u_a - u_w)]^n}\right\}^{1-1/n} \qquad u_a - u_w \geq 0 \tag{2.47}$$

Because of scarcity of data for SWCC and SSCC for same soils Lu et al, 2010 used existing data to validate this model. Soils, which have both the SWCC and SSCC their data was validated by comparing them with equations 2.42 for SWCC and equations 2.45 for SSCC. Table 2.1 gives some characteristics of the used soils.

Table 2.1: Soil properties used to validate the closed equation (Lu et. al. 2010)

Name	Soil properties	ub = 1/α	n	Ø′	c
Kaolin	LL = 63%, PI = 33% Percent finer than 3µmm = 70, γ_{dmax} = 1.4g /cm3	395	1.20	22	24
Jossigny Silt		182	1.54	22	25
Madrid clay	LL = 37%, PI = 18% Clay fraction = 34, γ_{dmax} = 1.7g/cm3	127	1.63	38	0
Sandy clay	LL = 32%, PI = 15% Clay fraction = 17, γ_{dmax} = 1.91g/cm3 No Data	35	1.59	37	0

In conclusion, it is evidenced that three schools of thought have been established with regard to unsaturated soil behaviour. The revised effective stress approach was attributed to Bishop, the two-independent stress approach was propounded by (Fredlund and Morgenstern, 1977) and the SSCC, was suggested by (Lu and Likos, 2006) and (Lu et. al, 2010).

2.5 Previous Studies on Resilient Modulus

2.5.1 Overview

One of the functions of pavement structure, is to provide support at different layers. The key factor in determining the thicknesses of other layers is the support specified through the subgrade resilient modulus (M_r). Generally, subgrade is elucidate as having an infinite thickness and the support given by subgrade is commonly compute from modulus of subgrade reaction (k). This reaction is `expressed as the sustained pressure of the soil under a rigid plate at a specified settlement. However, pavement design has

evolved over time, with regards to quantifying brace provided by pavement layers, under repeated loading rather than static loading condition. Formerly, plate load tests under static loading is use to evaluate modulus of subgrade reaction and as well use to quantify subgrade provided support. Although, pavements experience series of loading as a result of vehicular traffic load, perhaps loading due to vehicular traffic can be fittingly evaluated in the laboratory using repeated load triaxial test (RLTT) through mathematical use of cyclic stress equations.

2.6 Resilient Modulus (M_r) Concept

The key pavement design parameter, is M_r and it is considered an important input design property particularly during application of mechanistic-empirical pavement design guide (MEPDG). Recently, National Cooperative Highway Research Program (NCHRP) for flexible pavement design guide was developed in the united states and the current South Africa pavement design methods (SAPDM) requires repeated load triaxial testing to determine the M_r for characterising subgrade soil (NCHRP, 2004, SANRAL, 2008). M_r is illustrated as the ratio of maximum cyclical stress to elastic strain under repeated loading.

$$M_r = \frac{\sigma_d}{\varepsilon_r} \tag{2.48}$$

Where:

$\mathrm{M_r} = \text{ resilient modulus (Mpa)}$

$\sigma_\mathrm{d} = \sigma_1 - \sigma_3 = \text{ deviator stress (kPa)}$

$\varepsilon_\mathrm{r} = \varepsilon_2 - \varepsilon_1 = \text{ recoverable strain } (\mu\mathrm{m})$

Since pavement materials are repeatedly loaded and unloaded when subjected to cyclic loading. Most pavements materials, like soil, exhibits both elastic and plastic behaviour when subjected to loading and unloading. Plastic strain is permanent while elastic strain is recoverable. This means that M_r is analogous to the stiffness of subgrade under repeated loading thus M_r is determined with regards to recoverable strain (i.e., elastic strain). Figure 2.11 shows the strain behaviour of a specimen subjected to repeated axial loading. Initially, there is considerable plastic strain. However, the plastic strain caused by each load cycle decreases as the number of cycles increases.

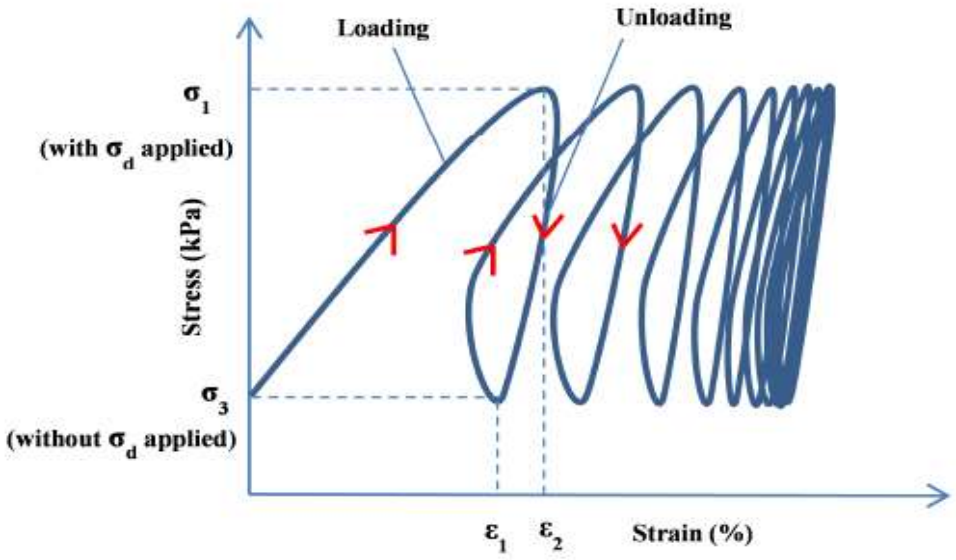

Figure 2.10: Subgrade resilient modulus behaviour (Hopkins et al., 2004)

Notably, as the number of loading cycles increases, an accumulation of plastic strain occurs (i.e., non-recoverable deformation). While M_r is based just on the elastic strain, pavements experiences both plastic and elastic strain under repeated loading. Plastic deformation manifests itself in a pavement as rutting (permanent deformation) and is an undesirable property that could trigger failure in pavement.

Generally, the larger the M_r value the better the subgrade soil would be considered. A large M_r value could indicate that the subgrade can handle certain repeated loading with little deformation (i.e. subgrade is stiff). In reality M_r continually changes due to the effects of moisture flux, therefore it becomes imperative to appropriately evaluate M_r pavement with respect to matric suction. Darter et al., (1991) proved that a decrease in M_r of pavement during its service life, results in increased deflection of the pavement structure, which in turn causes fatigue and cracks.

2.6.1 Resilient Modulus Correlation With Soil Geotechnical Properties

Although, M_r laboratory testing procedures is overly tricky, time-dependent and somewhat costly. On that regard, attempts have been made to correlate M_r with other geotechnical properties, such as CBR and unconfined compressive strength (UCS) etc. However, it is acknowledged that these reported correlations are empirical, whereas M_r values are mechanistic parameter and it depends on soil stress despite the correlated values been reasonably close to the measured values in most cases.

Thus, this gave reasons for many correlations been proposed to evaluate M_r based on in-situ and laboratory testing results such as: Geogauge, and Light Falling Weight Deflectometer (LFWD), Dynamic Cone Penetration (DCP) test. Among other, is the laboratory civil engineering test method i.e. unconfined compressive strength (UCS) and California Bearing Ratio (CBR), this method is widely utilized in correlating M_r to obtain a rational design values. These methods are acceptable and useful in obtaining M_r values for subgrades in design practice. Whereas in research, direct laboratory testing method is widely-accepted for measuring M_r because of its accuracy and ability to control multiple factors that directly affect M_r. Laboratory evaluation of M_r involves conducting RLTT and this test is generally conducted in a triaxial cell environment on a cylindrical either disturbed or undisturbed soil specimens. The main advantages of laboratory RLTT is the capability to apply multiple stress states to soil specimen by utilizing a combination of confining, deviatoric stresses among and recording the number of cyclic sequences required for a soil to fail.

Ng et al. (2013) performed RLLT, to investigate M_r of subgrade soil under various stress and matric suction conditions. The results revealed that matric suction influenced M_r of subgrade soil, as M_r depend mainly on the soil's stress states.

Ekblad and Isacsson (2008) presented experimental results from cyclic triaxial testing at various moisture content, by keeping confining pressure constant on two different graded granular materials. The result revealed increased moisture content caused a reduction in M_r and an increased in strain ratio. Therefore, it is important to evaluate effects of gravimetric moisture content on M_r.

2.6.2 Correlation between M_r and unconfined compressive strength

The estimation of M_r reported by Mallela et al. (2004) on lime-stabilized subgrade using unconfined compressive strength (q_u) tests and this is recommendation for M_r highway design. Mechanistic-Empirical Pavement Design Guide, Interim Edition: A Manual of Practice (MEPDG) (AASHTO 2008) is in conformity with this Mallela et al. (2004) approximation.

$$M_r(MPa) = 0.124q_u(kPa) + 68.8, \quad (R^2 = 0.46) \tag{2.49}$$

Where:

$\mathrm{q_u} = \text{unconfined compressive strength (MPa)}$

This equation was developed through comparing shear strength (kPa) and a secant modulus of elasticity E (MPa) obtained from static unconsolidated-undrained (UU) triaxial compression tests (Thompson 1966). Specifically, Equation 2.49 is based on q_u values from specimens tested at zero confining stress and E values from soil tested at 100 kPa confining stress. Thompson (1998) further performed three M_r and q_u tests (per AASHTO 1994) on one A-7-6 soil mixed with 6% quicklime. The results were identified as "duplicate" sets of three specimens in their referenced report. This test results generally agreed with Thompson's correlation for q_u values obtained between 1,000 and 1,400 kPa. In order to employ the above equation for M_r prediction, unconfined compressive test should be conducted in an in-situ conditions. Furthermore, the low value for coefficient of determination (COD), R^2 was as result of wide gap between strength (kPa) and secant modulus of elasticity E (MPa).

Lee et al (1997) suggested an alternative relationship to estimate M_r with small strain level and they proposed Equation 2.50 which has a strong COD and can be used for laboratory compacted samples.

$$M_r \text{ (MPa)} = 4.795\ (S_{u1.0\%}) - 0.041(S_{u1.0\%})^2\ (R^2 = 0.97) \quad (2.50)$$

Where:

$S_{(u1.0\%)} =$ stress at 1.0% strain in the unconfined compression test (strain rate is 1%/minute).

This concept of unconfined compression test was suggested as an option testing method to the laboratory RLTT for M_r values at the small strain levels Drumm et al. 1990 and Lee et al. 1997.

2.6.3 Correlation between M_r and CBR empirical

The correlation of CBR to estimate in-situ M_r of subgrade and granular materials, is extensively used empirical equation by pavement engineers. Moreover, National Cooperative Highway Program (NCHRP), AASHTO Guide (2008) and Austroads pavement design guide (2012) equally recommended this correlation. Some of the summarised correlations between M_r and CBR are shown below.

Table 2.2: M_r -CBR empirical correlations

References	Equation	Comments
Power et .al (1984)	$M_r(psi)=2555(CBR)^{0.64}$	None
Hopkins (1994a)	M_r (MPa)$=17.914(CBR)^{0.874}$	None
Webb and Campbell (1986)	$Mr(psi)= 3116\ (CBR)^{0.478}$	M_r showed no significant change within ± 1.5% of optimum moisture content. pavement sections (Lister and Powell 1987).
AASHTO Pavement Design Guide (2002)	$Mr\ (MPa)= 17.6\ (CBR)^{0.64}$	Valid from 5 x CBR to 20 x CBR (Sparks and Potter 1982).
Austroads Pavement Design Guide (2012)	Mr (MPa) = 10 (CBR)	(For Austroads 2012)

Though, CBR is technically a strength index parameter and could not necessarily be correlated with the modulus of reaction, k or stiffness, but correlation of CBR with M_r has comprehensively been applied by some pavement engineer and highway agencies to evaluate M_r with outstanding results. Furthermore, CBR is stress independent while M_r is basically a mechanistic parameter and it is represented as a repeated stress. Notably, the correlation between M_r and CBR is sensitive to soil mechanical properties, i.e. percentage of fines contents; environmental factors, and stress level. Logically, there should not good correlations between M_r and CBR, despite the wide use of this correlation among highway engineers.

Thompson and Robnett (1976) stated that developing a suitable correlation that can exactly predict M_r from CBR testing under certain experimental setup, could be challenging. Thus, some experimental data has shown that M_r values may differ over a wide range of CBR value, which can lead to a rough calculation of M_r value when it is empirically correlated for design purpose.

2.6.4 Correlation of M_r With Soil Physical Properties

Researchers like Thompson and Robnett (1979) proved that soil geotechnical properties affect M_r. Thus, the correlation of low plasticity index, liquid limit and specific gravity resulted in lower M_r value. In addition, Lekarp *et al.* (2000) recorded that M_r decreases with an increase in fines quantity. Janoo and Bayer II (2001) observed that an increased particle size lead to an increase in M_r value. Another observation by (Pezo and Hudson 1994), stated that the older the specimen, the lesser the resilient strain becomes. This implies that M_r of subgrade pavement will decrease with time. Majority of M_r values used for pavement design are not measured directly from laboratory test, but estimated either from experience based on previous projects or from physical properties George (2004). Nevertheless, AASHTO (2008) recommended estimation of M_r values from soil mechanical properties where direct measurement is not available. The good benefit of this method is that, it provides a means of taking seasonal variations into account for M_r calculation and these are reflected in the physical properties.

Jones and Witczak (1977) proposed two correlation equations for subgrade soils that combines moisture content and degree of saturation. RLTT were performed at deviator stresses of 6, 12, and 18 psi and confining stresses of 2, 4, 6, 8, and 12 psi for disturbed and undisturbed samples. The correlation portrayed some shocking results; thus, it was revealed that disturbed sample yielded reasonable M_r value compared to undisturbed sample.

For disturbed sample $(R^2 = 0.94)$

$$\mathrm{Log(M_r)} = -0.1328(\mathrm{Mc}) + 0.0134(\mathrm{S}) + 2.319 \quad (2.51)$$

For undisturbed sample $(R^2 = 0.45)$

$$Log(M_r) = -0.1111(Mc) + 0.0217(S) + 1.179 \quad (2.52)$$

Where:

$\mathrm{M_r} =$ resilient modulus (ksi)

$\mathrm{Mc} =$ moisture (%)

$\mathrm{S} =$ degree of saturation (%)

Carmichael and Stuart (1986) explored highway research information service database and proposed a correlation that compute M_r from mechanical properties, stress level and soil classification according to the Unified Soil Classification system (USCS) as follows. The correlated M_r outputted fair values as compared to directly measured value.

$$\mathrm{M_r} = 37.431 - 0.457(\mathrm{PI}) - 0.618(\mathrm{Mc}) - 0.1424(\mathrm{P_{200}}) + 0.179(\sigma_\mathrm{d}) + 36.722(\mathrm{CH}) + 17.097(\mathrm{MH}) \quad (2.53)$$

Where:

$\mathrm{M_r} =$ resilient modulus (psi)

$\mathrm{PI} =$ plasticity index (%)

$\mathrm{P_{200}} =$ percentage of passing #200 sieve (75μm)

$\sigma_\mathrm{d} =$ deviator stress (psi)

$\mathrm{CH} = 1$ for $(\mathrm{CH})_{\mathrm{soil}}$

$= 0$ for MH, ML and $(\mathrm{CL})_{\mathrm{soil}}$

$\mathrm{MH} = 1$ for $(\mathrm{MH})_{\mathrm{soil}}$

$= 0$ for CH, ML and $(\mathrm{CL})_{\mathrm{soil}}$

An investigation was conducted on thirteen Wyoming fine-grain soils and correlation was proposed to estimate M_r from index properties and stress level Farrar and Turner (1991). It was observed that M_r was negatively correlated to degree of saturation, (S) and positively correlated with PI and P_{200} as stated in Equation 2.54. This correlation was vigorously interrogated, but they were able to justify the equation, by stating that higher S will reduce the value of M_r, thereby argued that degree of saturation should be negatively correlated.

$$\mathrm{M_r} = 34280 - 359(\mathrm{S}) - 325(\sigma_\mathrm{d}) + 236(\sigma_3) + 86(\mathrm{PI}) + 107(\mathrm{P_{200}}) \quad (2.54)$$

Where:

$\mathrm{M_r} =$ resilient modulus (psi)

$\mathrm{S} =$ degree of saturation (%)

$\sigma_\mathrm{d} =$ deviator stress (psi)

$\sigma_3 =$ confining stress (psi)

$\mathrm{PI} =$ plasticity index (%)

$P_{200} =$ percentage of passing #200 sieve (75 micron) (%)

Hall and Thompson (1994) suggested an equation that corelated M_r with clay percentage, PI and organic percentage content. The value of M_r predicted from this correlation outputted significant value closely compared to M_r value measured directly. Even though percentage of organic content was negatively correlated, but the limitation of this equation is that it cannot be reasonably apply to inorganic soils.

$$\mathrm{M_r} = 6.90 + 0.0064(\mathrm{C}) + 0.216(\mathrm{PI}) - 1.970(\mathrm{OC})(\mathrm{R}^2 = 0.76) \quad (2.55)$$

Where:

$M_r =$ resilient modulus at the AASHTO T $-$ 99 optimum

Moisture content and 95% compaction (ksi)

$\mathrm{C} =$ percentage of clay ($< 2\mu\mathrm{m}$)

$\mathrm{OC} =$ percentage organic content (%)

An equation was presented by (Rahim and George, 2004), on an investigation carried out on soil properties index for predicting M_r of 12 fine-grained soils in Mississippi. The values of predicted M_r values from Equation 2.56, showed some impressive correlated values when compared with experimentally measured M_r.

$$M_r = 16.75\left\{1\left(\frac{LL}{M_c \times \gamma_{dr}}\right)^{2.06} + \left(\frac{P_{200}}{100}\right)^{-0.59}\right\} \quad (2.56)$$

Where:

$M_r =$ resilient modulus (psi)

$\mathrm{LL} =$ liquid limit (%)

$M_c =$ moisture content (%)

$\gamma_{dr} =$ confining stress (psi)

$P_{200} =$ percentage of passing #200 sieve (75 micron) (%)

However, several made attempts were recorded by (Lee at al. 1997; Burczyk et al. 1994; Santha 1994; Lee at al. 1995; Drumm et al. 1997; Von Quintus and Killingsworth 1998; Mohammad et al. 1999; Dai and Zollars 2002) to develop predictive equations for M_r using soil physical properties. The equations by these listed scholars, closely predicted

M_r of subgrade with an error of 0.05%. Furthermore, from equations 2.56 it is observed that moisture content, degree of saturation, material passing #200 sieve (75 micron), PI and dry density are the parameters used to predict M_r. Contrary to other equations, it is only Equation 2.54 that considered applied stresses such as σ_d and σ_3. Notably, the equations are dependent of experimental results from soils used in each corresponding study and can be used strictly for basic prediction of M_r values for pavement design.

2.7 Factors Affecting M_r

Illustration of non-linear behaviour of pavement materials under dynamic traffic loading is challenging, as M_r is a complicated parameter, due rigorous procedures involved. Although, many studies have been conducted in order to critically evaluate the factors that can possibly affect M_r of subgrade. Basically, it was discovered that applied stresses, moisture content, swelling pressure and density are the three factors that influences M_r.

2.7.1 Stress state effect

Stress state experienced by highway pavement layers, is affected by subgrade M_r. The stress state of a subgrade is considered by the deviatoric stress and confining pressure experienced on the subgrade during cyclic loading. Most importantly, pavement structures are under unsaturated conditions, therefore matric suction is an important factor that defines stress state of subgrade (Yang, 2008). Increase in deviatoric stress, causes decrease in M_r as the shear stresses experienced by the soil specimen increases. Whereas, increase in confining pressure serves to increase the M_r value of subgrade soil, as it increases the bulk stress resistance of the soil, therefore providing a stiffening effect on the specimen. Furthermore, effects of confining pressure are evidenced on granular soils, while the effect of deviatoric stress is observed on cohesive soils.

2.7.2 Moisture condition effects

Subgrades are compacted at a point close to optimum moisture content (OMC) with corresponding maximum dry density (MDD). Most times, it becomes difficult to achieve desired compaction moisture. Thus, leading to pavements been constructed on under in-situ moisture conditions.

However, during pavement service, subgrade moisture content comes to equilibrium with its surrounding moisture conditions and vary thereafter as a result of seasonal variation (Yang, 2005; Uzan, 1998). Although, subgrade is prepared at a particular moisture content and density, the moisture content of a subgrade will never be constant. Therefore, it is necessary to evaluate the impact of moisture content on the M_r value. Though, the post-construction moisture content (Mc) varies significantly and as such affects subgrade M_r. Researchers like: (Pezo et al. 1992, Fredlund et al. 1977; Mohammad et al. 1999; Huang 2001; Butalia et al. 2003; Heydinger 2003; Ooi et al. 2004; Wolfe and Butalia 2004; Hopkin et al. 2004; Richter 2006; Zaman and Khoury 2007; Cary and Zapata 2010) proved in their respective studies that M_r decreases drastically on the average between 42% and 60% with an increase in moisture content. Their studies further revealed that Mc of subgrade soils increases, while the stiffness tends to decrease, therefore contributed to reduced M_r values. Figure 2.12 demonstrates behaviour of subgrade M_r with four different Mc levels, including the (OMC), dry of OMC (OMC - 2.5%), wet of OMC (OMC + 2.5%) and soaked condition.

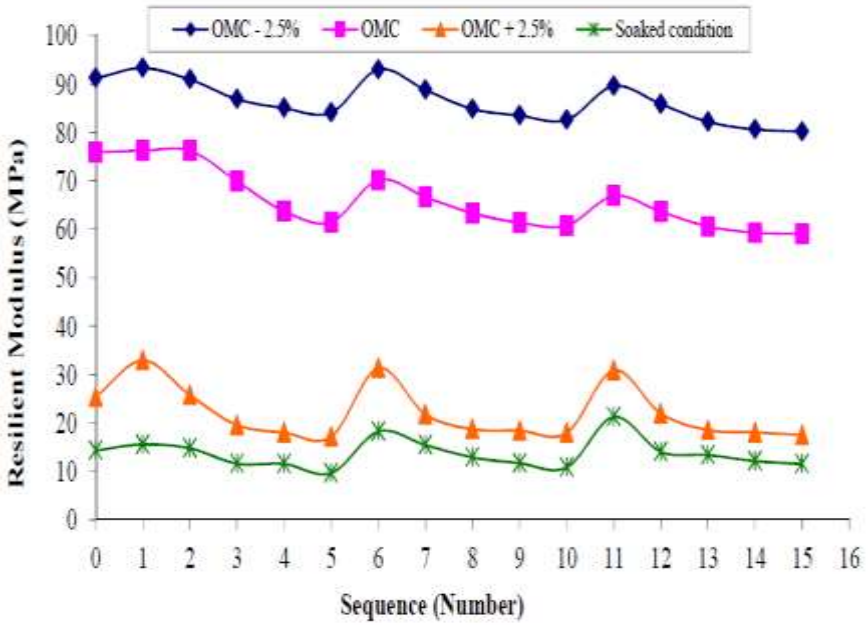

Figure 2.11: Variation of Mc on M_r (Nguyen and Mohajerani 2015)

Pavement under seasonal moisture variation, eventually absorbs moisture and increase the moisture content to the wet side. During the first five years of pavement service life, Uzan (1998) observed that the subgrades recorded an increase in Mc of about 30% higher than soil's initial plastic limit. Apparently, Von Quintus and Killingsworth (1998) argued that Mc of a pavement subgrade will continuously be on the wet-side of

Optimum, this result was published as 59 subgrade soils were tested for Mc after five years of construction. This report was an evidence, that subgrade's Mc increases subsequently after construction.

2.7.3 Effects of soil type

In the last section, it is well understood that increase in Mc results to a decrease in M_r. Reasonably, the influence of Mc on M_r differs with soil types. Drumm (1997) observed that A-7 soils tended to have higher M_r values at optimum conditions, compared to A-4 and A-6 soils, they also exhibited a larger decrease in M_r once the Mc increased to values greater than that of the optimum.

Furthermore, scholars like: Hicks and Monismith (1971), Thom and Brown (1987), Barksdale and Itani (1989) and Kamal et al. (1993) claimed that fine content has great influence on M_r. Hicks and Monismith (1971) reported on a M_r of partially crushed aggregates. The study showed that decrease in M_r, was triggered with an increase in fines content. Among other studies on fine content, was recorded by (Barksdale and Itani, 1989) and the study proved that M_r decreases with 60% fines content increased from 0% to 10% when fine content was reduced. Generally, it was observed that M_r value decreases as the fine contents increases Kancherla (2004).

2.7.4 Matric suction effect

Matric suction effects on M_r is necessary, because suction is fundamental to unsaturated soils that impart on stress state variables. Sauer and Monosmith (1968), conducted an in-situ study. The result showed that suction and pavement deflection are interrelated, such that suction values increases with decrease in deflection. Furthermore, suction increase will cause subgrade stiffness increase and thus increase M_r of not saturated subgrade soils. Because subgrade suction is composed of two components, matric suction and osmotic suction.

However, Khoury et al. (2004) demonstrated that changes in M_r for unsaturated soils are triggered by changings in matric suction. Thus, justifying matric suction definition as different between pore-air pressure and pore-water pressure $(u_a - u_w)$. The intensity of suction present in subgrade is related to Mc, which changes in subgrade over time.

Therefore, evaluation of suction influence, that will account for seasonal variation on M_r for unsaturated subgrades, become valuable. Yang et al. (2005) replicated field conditions, with laboratory compacted A-7 specimens at OMC and were then subjected to wetting. This was justified because subgrades are basically compacted at OMC and allowed to come to equilibrium with the surrounding soils. According to their study, suction was measured using the Filter Paper Method, followed by M_r testing. The soil samples were wetted at two different stages, equilibrium moisture content (EMC) and Mc between OMC and EMC. There result revealed a drastic decrease in M_r when moisture content increased from moisture content between OMC and EMC, therefor resulting in a low matric suction.

2.8 Resilient Modulus Models

2.8.1 Universal model

Various stress-dependent models are available to establish stress sensitive relationship between M_r and various stress state, for material parameter input in AASHTO 2002 design guide. This relationship, describes stress dependency of both fine-grained soils and unbound materials for mechanistic analysis (NCHRP 1-37A, 2004). In the same line, Witczak and Uzan (1998) proposed a model that is widely known as universal model. This model is adopted to evaluate M_r behaviour with respect to stress state. The generalized model adopted by MEPDG is presented in Equation 2.57

$$M_r = k_1 P_a \left(\frac{\theta}{P_a}\right)^{k_2} \left(\frac{\tau_{oct}}{P_a} + 1\right)^{k_3} \quad (2.57)$$

Where:

$\theta = \text{bulk stress} = \sigma_1 + \sigma_2 + \sigma_3$

$\sigma_1 = \text{major principal stress}$

$\sigma_2 = \sigma_3 = \text{for triaxial test on cylindrical specimen}$

$\sigma_3 = \text{minor principal stress or confining stress in the triaxial}$

$\tau_{oct} = \text{octahedra: shear stress} = \sqrt[\frac{1}{3}]{(\sigma_1 - \sigma_2)^2 + (\sigma_1 - \sigma_3)^2 + (\sigma_2 - \sigma_3)^2}$

$= \frac{\sqrt{2}}{3}(\sigma_1 - \sigma_3)$ for cylindrical specimen in triaxial test

$P_a = \text{normalising stress atmospheric pressure}$

$k_1, k_2, k_3 = \text{model parameter obtained from regression analysis}$

Equation 2.57 is useful and widely accepted, it only accounts for stress state effect on M_r but does not consider the effect of moisture disparity on M_r due to seasonal variation. Research have geared up towards solving this challenge by relating the regression constants to soil physical properties. Thus, incorporating seasonal variation effects on M_r predictions (Nazzal and Mohammad, 2010; Yau and Von Quintus 2002). Nazzal and Mohammad (2010) introduced physical meanings for the regression constants by evaluating them across different moisture conditions as to determine moisture change, can affect regression constants.

It was discovered that k_1 is related to the stiffness of the material, which increases with increasing effective stress. k_2 describes the stiffening increase effect of bulk stress on soil. Whereas, k_2 decreases with increase Mc; k_3 describes the softening of the material with increasing shear stress, such that k_3 decreases and becomes more negative as Moisture content increases and this implies that model parameters for regression constant greatly influenced by Moisture content.

2.8.2 Model incorporating moisture variation

Due to variation in Moisture content, several models were developed to accomplish the task of predicting the ability of changes in M_r values. However, the environmental effects particularly the seasonal variation MEPDG introduced Enhanced Integrated Climatic Model (EICM) to predict changes in properties of pavement structures. EICM evaluates changes in Mc for flexible asphalt pavements and it requires the user to input M_r at a specified moisture condition for subsequent evaluation of the effect of the seasonal changes in pavement structure. Most commonly, EICM is considered a powerful tool, due to its capability to creates a set of adjustment factors that account for moisture changes, freezing, thawing, and post thawing effects. MEPDG then combines the adjustment factors obtained from EICM with the effects of cyclical loading from the traffic and applies the total effect to the material properties. Once this is accomplished, MEPDG makes use of transfer functions to predict pavement performance considering the effect of EICM adjustment factor and the external loading on material properties. The link EICM adjustment factor is presented in Equation 2.58.

$$log\frac{\mathrm{M_r}}{\mathrm{M_{ropt}}} = \mathrm{a} + \frac{\mathrm{b-a}}{1\times\mathrm{Exp}(\ln\frac{-\mathrm{b}}{\mathrm{a}}+\mathrm{k_m}*(\mathrm{S-S_{opt}}))} \quad (2.58)$$

Where:

$\frac{M_r}{M_{ropt}} = \text{resilient modulus ratio}$

$a = \text{minimum of} \log \frac{M_r}{M_{ropt}}$

$b = \text{maxmum of} \log \frac{M_r}{M_{ropt}}$

$k_m = \text{regression parameter}$

$(S - S_{opt}) = \text{changes in degree of saturation}$

The right part of Equation 2.58 represents adjustment factor, this can be solved by applying the anti-logarithm to obtain the adjusted M_r by multiplying the adjustment factor with the M_r value at optimum moisture condition. The MEPDG recommends value of -0.5934 for a, 0.4 for b, and 6.1324 for k_m, for fine-grained soils. A graphical presentation of Equation 2.58 is given in Figure 2.13 for fine-grained soils. However, MEPDG provides a different set of values for a, b, and k_m for coarse-grained soils.

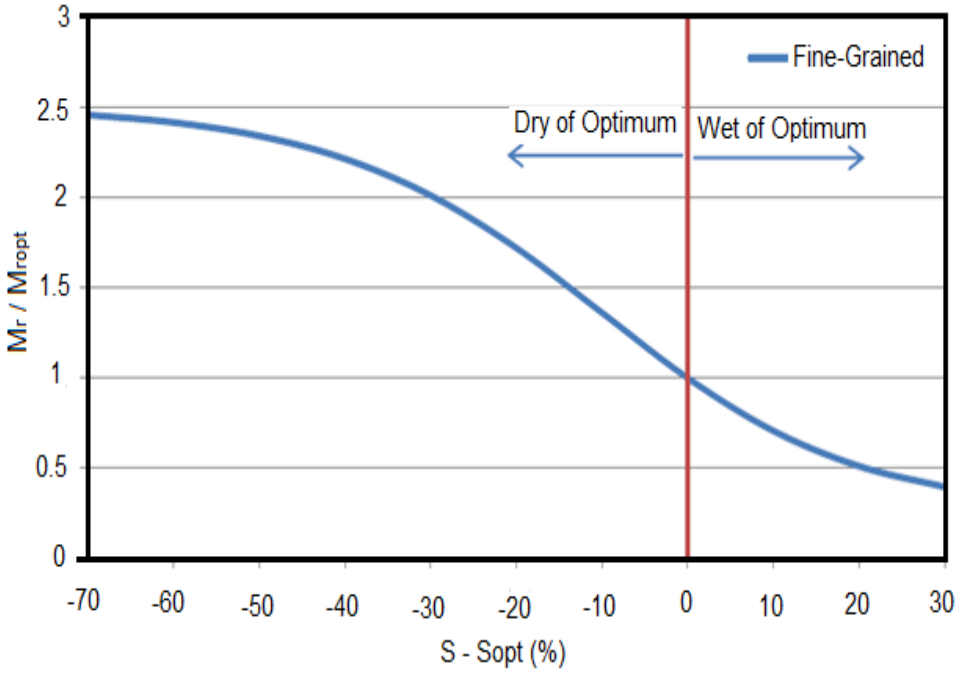

Figure 2.12: Typical moisture changes on M_r using EICM (NCHRP, 2004)

Cary and Zapata (2010), evaluated the rationality of Equation 2.58 for a broader range of moisture conditions and it was discovered that the EICM models tends to wrongly predict M_r in dry conditions, particularly for high PI soils. However, inadequate data was available to investigate the validity of the model for more wet conditions. Figure 2.14

illustrates how EICM model fits the data collected by Cary and Zapata (2010). There is remarkable data scatter when the S is below the optimum condition.

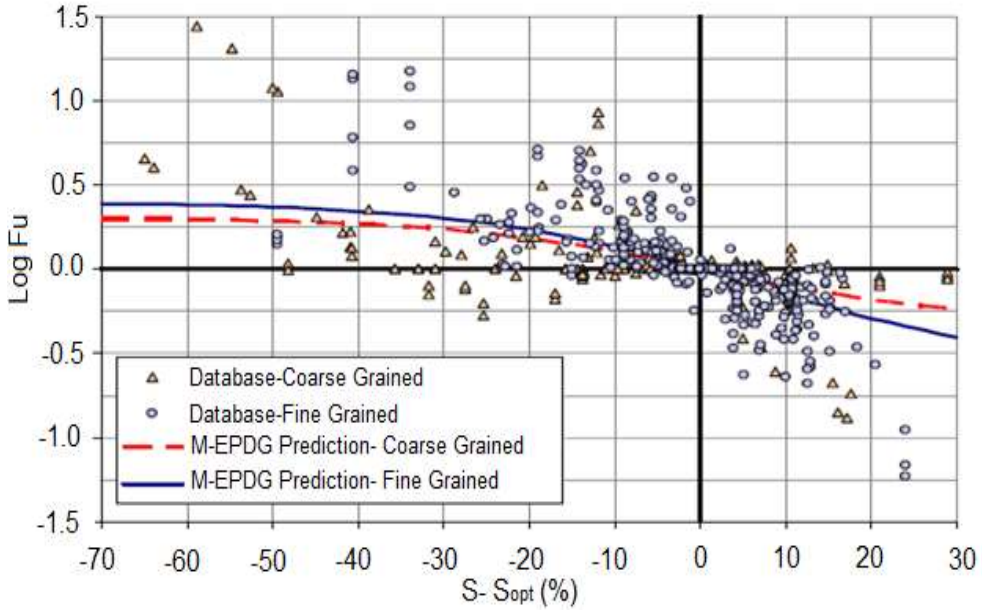

Figure 2.13: Collected database against EICM model (Cary and Zapata, 2010)

Cary and Zapata (2010) specified that the soil type effect is analytical, considering the rise in M_r value due to decrease in Mc, particularly for soils compacted on the dry side of optimum. Hence, soils with high plasticity index (PI) values tend to attain much higher suction values at lower degree of saturation, compared to soils with lower PI values, this postulation is considered based on Figure 2.15. Furthermore, they proposed a model to accommodate the effect of soil type on M_r, by including the term wPI, which is the product of PI and soil fine (No.200 sieve size). The model is presented in Equation 2.59

$$\mathrm{LogF_u} = \mathrm{mx}\left[(\alpha + \beta * \mathrm{e}^{-\mathrm{wPI}})^{-1} + \frac{(\delta+\gamma*\mathrm{wPI}^{.5})-(\alpha+\beta*\mathrm{e}^{-\mathrm{wPI}})^{-1}}{1+\mathrm{e}^{\left(\ln\left(\frac{-(\delta+\gamma*\mathrm{wPI}^{.5}}{\alpha+\beta*\mathrm{e}^{-\mathrm{wPI}})-1}\right)+(\rho+\mathrm{w}*\mathrm{e}^{-\mathrm{wPI}})^{.5}\left(\frac{\mathrm{S}-\mathrm{S_{opt}}}{100}\right)\right.}}\right] \quad (2.59)$$

Where:

$a = \alpha + \beta * \mathrm{e}^{-\mathrm{wPI}}$

$b = \delta + \gamma * \mathrm{wPI}^{.5}$

$k_m = (\rho + \mathrm{w} * \mathrm{e}^{-\mathrm{wPI}})^{.5}$

m = correction factor = 1.002

$\alpha = -0.600, \beta = -1.87194, \delta = 0.800, \gamma = 0.080, \rho = 11.96518, and\ \omega = -10.19111$

Similar to the EICM model presented in Figure 2.12, Equation 2.59 was used to create the model in Figure 2.14. As this model allows for more appropriate predictions in the dry range by considering additional stiffness gain by higher PI soils in the lower saturation range.

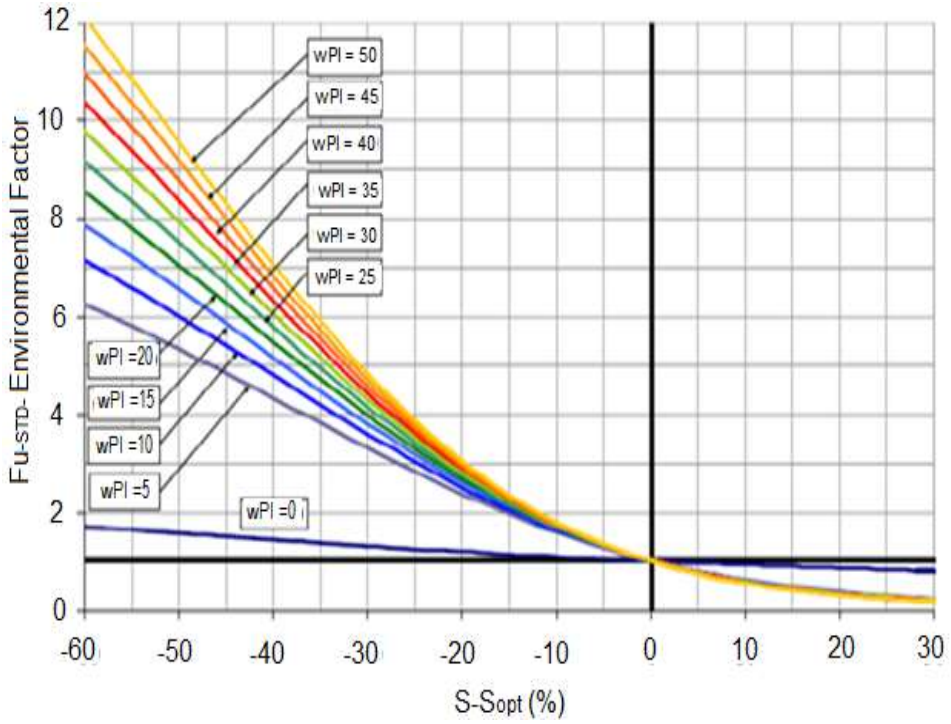

Figure 2. 14: Adjustment factor, Fu, for $(S - Sopt)$ and wPl (Cary and Zapata, 2010)

2.8.3 Models incorporating matric suction

The need to develop a model that incorporates soil suction in predicting M_r was also recognised by Yang et al. (2005), since suction has a direct effect on the stiffness of unsaturated soils. This model is a variation of the deviator stress model initially introduced by AASHTO T 292-91 and the original deviator stress model for M_r is presented in Equation 2.60.

$$M_r = k_1(\sigma_d)^{k_2} \tag{2.60}$$

Where:

$\sigma_d =$ deviatoric stress

$k_1, k_2 =$ regression constants

Yang et al. (2005) proposed a new correlation based on Equation 2.60 that considered soil suction as stated in Equation 2.61 by utilizing unsaturated soils effective stress concept in Equation 2.32 in chapter 2, this gives Equation 2.61.

$$M_r = k_1(\sigma_d + x\psi_m)^{k_2} \quad (2.61)$$

Where:

$x =$ parameter representing contribution of suction to effective stress

(Note: 0 for completely dry soil and 1 for saturated soils)

$\psi_m =$ suction matric

$k_1, k_2 =$ regression constants

Conclusively, Equation 2.61 accurately adopted the effect of suction, especially at decreased moisture contents because its effect is very remarkable and the effect of deviator stress which is significant at higher moisture content. Thus, changes in Mc affect suction, the effect of seasonal variation on M_r, is absolutely included in Equation 2.61. This equation provides a good fit between the measured and predicted M_r data.

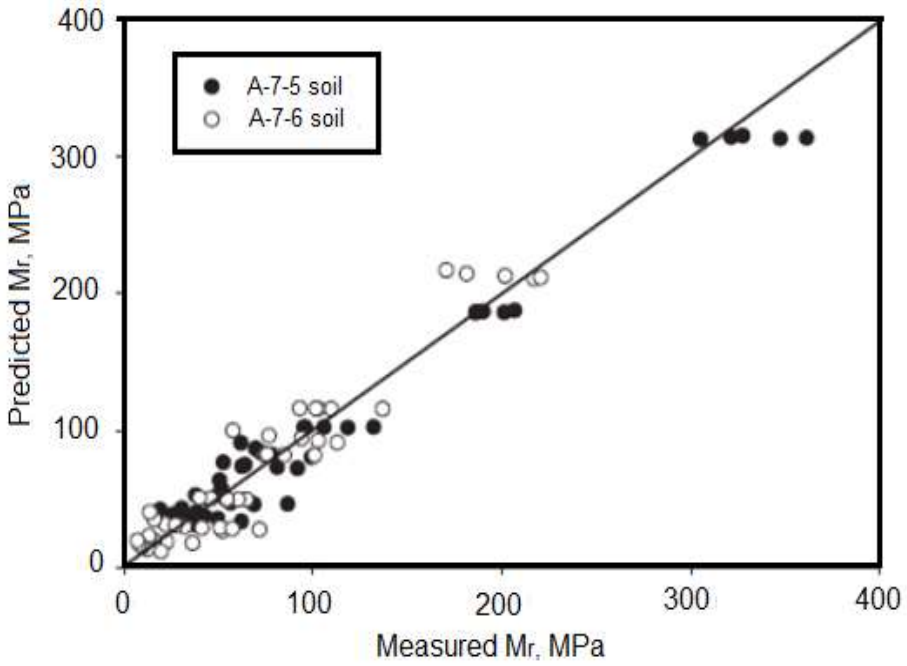

Figure 2.15: Predicted against measured M_r values using equation 2.75 (Yang et. al., 2005)

Based on three stress variables the bulk stress, matric suction $(u_a - u_w)$ and deviator stress, Gupta et al. (2007) developed a model to predict M_r for unsaturated soils. This model was based on the model proposed by Vanapalli et al. (1996), this describes the shear strength of unsaturated soils across the entire SWCC range.

$$\tau_{us} = C' + (\sigma_n - u_a)tan\emptyset' + (u_a - u_w)(\Theta^k tan\emptyset') \quad (2.62)$$

Where:

$C' = effective\ cohesion\ of\ a\ saturated\ soil$

$\emptyset' = effective\ friction\ angle\ of\ saturated\ soil$

$(\sigma_n - u_a) = net\ normal\ stress$

$\Theta = normalized\ volumetric\ water = \frac{\Theta}{\theta_s}$

$k = fitting\ parameters$

The first part of Equation 2.62 represents shear strength of soil under saturated condition. Whereas, the second part represents the contribution to shear strength due to matric suction. The volumetric water content, Θ was introduced into the model to reflect the quantities of water in the soil and it varies from large to a very small value at residual conditions when the soil is saturated. This model comprised normalizing Mc to actually evaluate the contribution of suction, since the area of contact between the soil particles, which is wetted, reduces with an increase in suction and when suction is decreased. The link between the increase and decrease of contact wetted area between soil particles is connected with the rate at which changes occurs in shear strength under unsaturated conditions. Therefore, there is a significant connection between the strength of unsaturated soil and the SWCC that explains the relationship between water content and suction (Vanapalli et al, 1996).

Gupta et al. (2007) explicitly expressed that the inclusion of one of the parameters that describes SWCC into Equation 2.62, generated a power correlation between soil suction and shear strength similar to the model presented in Equation 2.63.

$$\tau_{us} = (\sigma_n - u_a)tan\emptyset' + C'^{(\Theta^k tan\emptyset')\beta} \quad (2.63)$$

The advantage of Equation 2.56 over Equation 2.64 is that there is no need to evaluate normalized Mc and suction. Using the relationship presented in Equation 2.62 with the Universal M_r model presented by NCHRP 2003, Equation 2.63 can be formatted by considering suction in M_r equation.

$$M_r = (k_1 P_a \left(\frac{\theta}{P_a}\right)^{k_2} \left(\frac{\tau_{oct}}{P_a} + 1\right)^{k_3} + \alpha(u_a - u_w)^{\beta} \quad (2.64)$$

Where:

$\alpha =$ intercept of M_r at given $\theta_{\tau oct}$ against suction relationship

$\beta =$ slope of M_r at given $\theta_{\tau oct}$ against suction relationship

Liang et al. (2008) aimed at improving the model presented by Yang et al. (2005). As the model is devoid of regression constants calibration at each moisture content, for the same soil type, to be effective. Furthermore, Liang et al. (2008) also intended to propose a model which can accommodate seasonal variation effects in predicting M_r. This model is based upon the Universal Model utilized by MEPDG (NCHRP 2004).

$$M_r = (k_1 P_a \left(\frac{\theta}{P_a}\right)^{k_2} \left(\frac{\tau_{oct}}{P_a} + 1\right)^{k_3} \quad (2.65)$$

By incorporating the effective stress equation for unsaturated soils, Liang et al. (2008) w able to propose a new model to include suction for evaluating M_r as follows:

$$M_r = (k_1 P_a \left(\frac{\theta + x\psi_m}{P_a}\right)^{k_2} \left(\frac{\tau_{oct}}{P_a} + 1\right)^{k_3} \quad (2.66)$$

Where:

$P_a =$ atmospheric pressure (100kPa)

$x =$ Bishop's effective stress parameter

$\psi_m =$ matric suction

$\tau_{oct} =$ octahedral shear stress

$\theta =$ bulk stress

$k_1, k_2, k_3 =$ regression constants

Liang et al. (2008) suggested a model introduced by Khalili and Khabbaz (1998) for evaluation of χ parameters, which is presented in Equation 2.68. While, in Liang et al. (2008), χ was only computed at suction values greater than the air-entry value (AEV) since soil would be saturated before AEV and χ = will be equal to 1.

$$x_w = \left(\frac{(u_a - u_w)_b}{u_a - u_w}\right)^{0.55} \quad (2.68)$$

Where:

$(u_a - u_w)_b =$ air − entry pressure

$u_a - u_w =$ suction matric

Liang et al. (2008) further carried out repeated load triaxial test to validate the model for M_r values and filter paper method to obtain suction values. They conducted regression analysis at OMC during M_r test, as to obtain regression constants. Thus, regression constants along with the model in Equation 2.68, were introduced to specimens at different Mc to predict M_r values. Liang et al. (2008) also differentiated the total stress approach, by neglecting suction against the effective stress approach, but included suction, to predict M_r values. The M_r values predicted were significantly better compared to when suction was incorporated. A comparison between the total stress approach and effective stress approach for A-6 soil is displayed in Figure 2.17. It was observed that including matric suction helps in improved version of the predictive model for M_r values.

Cary and Zapata (2011) also expressed a model that included the effect of suction in evaluating M_r of unsaturated soils. Contrary to other models, this model included the effects of pore-water pressure (PWP) build up during cyclic loading. Dissipation happens in the delay time between applied loads, whereas excessive PWP in soil is usually generated under moving vehicle loads. When the delay in time is long, then the possibility of PWP accumulation between load cycles and PWP will not occur.

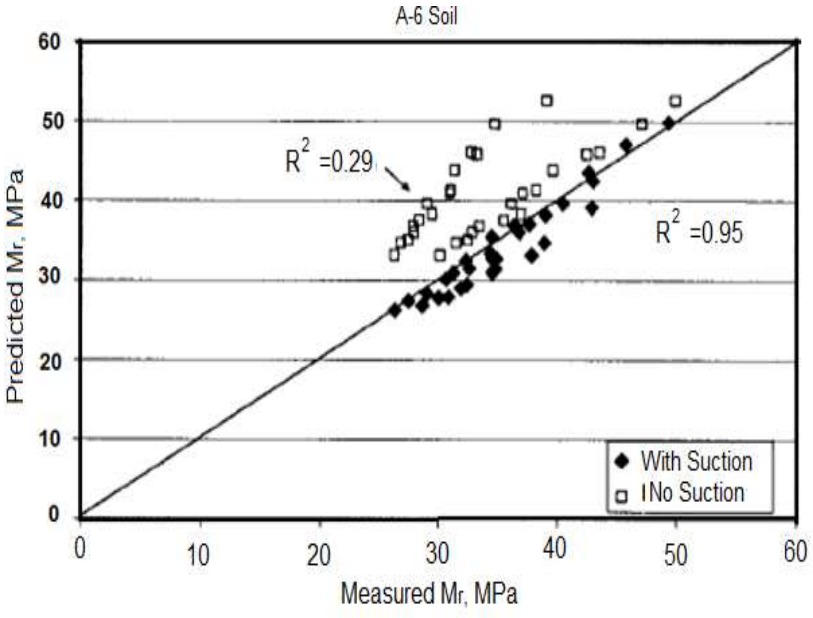

Figure 2.16: A − 6 soil predicted against measured M_r values (Liang et al., 2008)

Cary and Zapata, 2011 further stated that, if the delay time is short (i.e., fast moving traffic) there will be remarkable accumulation of excess PWP as the number of applied loads increases. The dissipation of PWP is a function of the coefficient of permeability, k and time delay between load repetitions. At high coefficient of permeability k or if there is large time delay between load repetitions, this condition can be simulated in the laboratory through performing a drained M_r test. Most commonly, at a low coefficient of permeability k, an undrained M_r test is recommended, as to accurately simulate field conditions.

$$M_r = k_1 P_a \left(\frac{\theta_{net} - 3*\Delta u_{w-sat}}{P_a}\right)^{k_2} \left(\frac{\tau_{oct}}{P_a} + 1\right)^{k_3} \left(\frac{(\psi_m - \Delta\psi_m)}{P_a} + 1\right)^{k_4} \quad (2.69)$$

Where:

P_a = atmospheric pressure

$\theta_{net} = \theta - 3u_a$= the net bulk stress ($\theta$=bulk stress $=\sigma_1+\sigma_2+\sigma_3$ and σ_a= Pore − air pressure)

Δu_{w-sat}=pore − water pressure build − up under saturated condition (ψ_m=0)

τ_{oct}= Octahedral shear stress= $\sqrt[1/3]{(\sigma_1-\sigma_2)^2+(\sigma_1-\sigma_3)^2+(\sigma_2-\sigma_3)^2}$

ψ_{m_o}=initial matric soil suction and

$\Delta\psi_m$ = relative change in soil matric suction with respect to ψ_{m_o} due to pore − water pressure build − up under unsaturated condition (Δu_{w-sat}=0)

$k_1 \geq 0, k_2 =\geq 0, k_3 \leq 0$ and $k_4 \geq 0$ are regression constants

The model presented in Equation 2.69 was formulated using M_r testing conducted with the concept of an unsaturated soil triaxial cell. That allows the use for axis-translation technique as to obtain suction and PWP during M_r testing. Thus, using θ_{net} instead of θ to represent the bulk stress ($\theta_{net} = \theta - u_a$) as the soil tends to reach saturation, u_a approaches towards 0 and θ_{net} becomes θ. Cary and Zapata (2011) validated Equation 2.69, by performing several different comparisons and there was no much divergence with these results.

Witicizak et al. (2000) suggested a model that incorporates environmental adjustment factor along with M_r at an applied effective stress to predict changes in M_r as a function of changes in degree of saturation.

$$M_r = 10^{\left(a+\frac{b-a}{1+EXP\left(\ln\frac{-b}{a}k_m*(S-S_{opt})\right)}\right)}*k_1 P_a\left(\frac{\theta}{P_a}\right)^{k_2}\left(\frac{\tau_{oct}}{P_a}+1\right)^{k_3} \quad (2.70)$$

Cara and Zapata (2011) used M_r test data to obtain regression constants, k_1 to k_4, in Equation 2.69. The predicted M_r results from Equation 2.69 were compared to those obtained using Equation 2.70. The comparison, is presented in Figure 2.18, shows that Equation 2.69 tends to give a better prediction of measured M_r values.

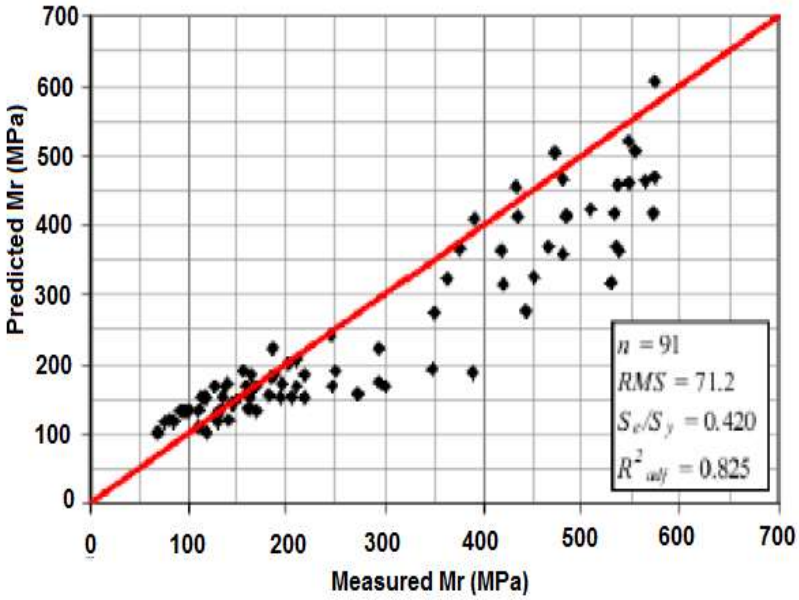

a.) Using Equation 2.70

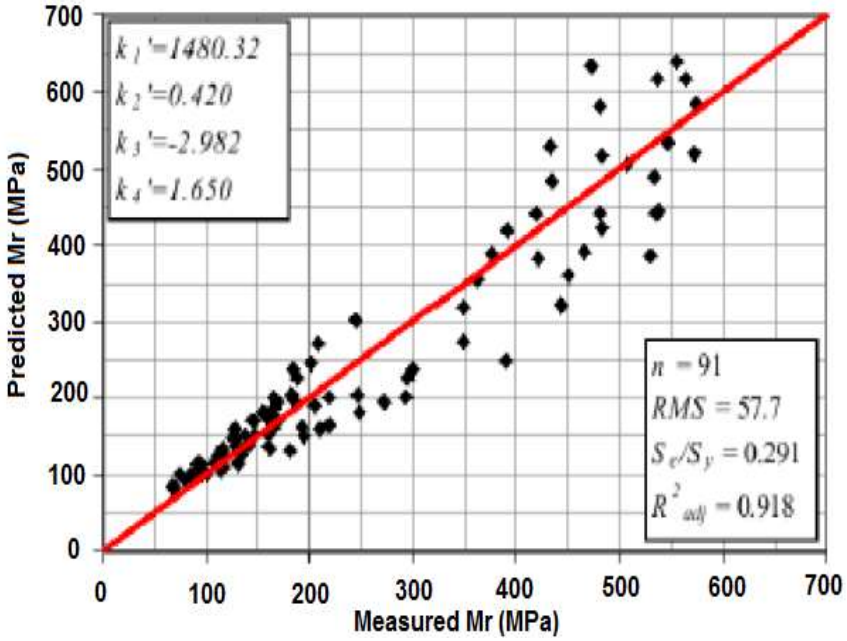

b.) Using Equation 2.69

Figure 2.17: good line fit measured against predicted M_r values for soil PI = 5 (Cary and Zapata, 2011).

Cary and Zapata (2011) did a comparison of the model presented in Equation 2.58 with that of Liang et al. (2008) suction dependent of M_r model. When compared with Figure 2.18 (part b), Cary and Zapata (2011) model provides a better prediction of M_r for this soil type.

Nokkaew et al. (2014) carried out a study, to investigate effects of matric suction on M_r of Recycled asphalt pavement (RAP) and Recycled Asphalt Material (RAM) in a post compaction state. These authors investigated the relationship further for RAP and RAM since this materials are repelling materials. In order, to determine the correlation between specimens prepared at OMC and 95% of Maximum Dry Density (MMD). Materials were subsequently saturated, and then dried to a target suction value before M_r testing commenced. In an attempt to dissect the data obtained from M_r testing, Nokkaew et al. (2014) employed the model proposed by Liang et al. (2008) to predict M_r values, however slight alteration was made, using the definition of χ presented in Equation 2.71.

$$x = \Theta^k = \left(\frac{\theta-\theta_r}{\theta_s-\theta_r}\right)^k \quad (2.71)$$

Where:

$\Theta =$ volumetric water content

$\theta_r =$ residual water content

$\theta_s =$ saturated water content

$k =$ fitting parameter to fit measured values to predicted values of x

This resulted in Equation 2.72 being utilized for the prediction of M_r.

$$M_r = k_1 P_a \left(\frac{\theta+\Theta^{k_\psi}}{P_a}\right)^{k_2} \left(\frac{\tau_{oct}}{P_a}+1\right)^{k_3} \quad (2.72)$$

Clearly, it was observed by Nokkaew et al (2014) that similar curve fitting of the measured data was observed when compared with Liang et .al (2008) equation. Nonetheless, Nokkaew et al. (2014) argued that Liang et al. (2008) model cannot fittingly predict M_r near saturation and at residual condition. As a result of the definition of χ used by Liang et al. (2008), that linearly assumes a relationship between χ and soil suction in a logarithmic scale when the suction value is greater than the air-entry pressure.

CHAPTER 3 : SOIL PROPERTIES AND TESTING PROGRAMS

3.1 Overview

This chapter illustrates the selection of natural subgrades for the experimental programme, together with the basic geotechnical properties of the soils. Standardised civil engineering tests procedures were followed, for all the experiments conducted in this study. This chapter further presents series of laboratory tests carried out on the nine selected subgrade soils as to accomplish the aim of this study:

- Modified compaction test
- Free swell index test (FSI)
- Zero swelling test (ZST)
- Filter paper test.
- California Bearing Ratio (CBR) test and unsaturated CBR test
- Triaxial tests (consolidated undrained test, CUT),
- Repeated load triaxial test (RLTT),

3.2 Materials

3.2.1 Soil geological location

The natural subgrade soils for this investigation were selected across three provinces in South Africa i.e. Free state, Northern cape and Gauteng province. These soils are metamorphosed by weathering of basic crystalline rock, to an expansive black clays known as cotton soils or turf. Lager area of South Africa is susceptible to subgrade problems triggered due to expansive activities. In addition, collapsible soil is among the problematic soil considered for this study. This soil is found largely in Gauteng province between Johannesburg and Pretoria area of South Africa. This soil stands higher risk of collapse and subsidence, as it is formed by weathering of dolomitic and limestone rocks. This type of soil undergoes precipitous decrease in volume due to wetting load and easily erodible by acidic water. As this causes sudden collapse or sinkholes on pavement structure. The studied soils, were sampled from three different locations at each province and labelled according to the province from which they were collected such as: Gauteng province soil (GPS 1 GPS 2 and GPS 3), Free State soil (FSS1, FSS 2 and FSS 3) and Northern Cape soil (NCS 1, NCS 2 and NCS 3), making it a total of nine different soil samples.

The precise locations from where the soils were collected are shown in Figure 4.1 with Global Positioning System (GPS) precision of 0.8m away from the borrowed pit. These soils represent a wide range of problematic soils ranging from expansive, collapsible and erodible soils throughout South Africa.

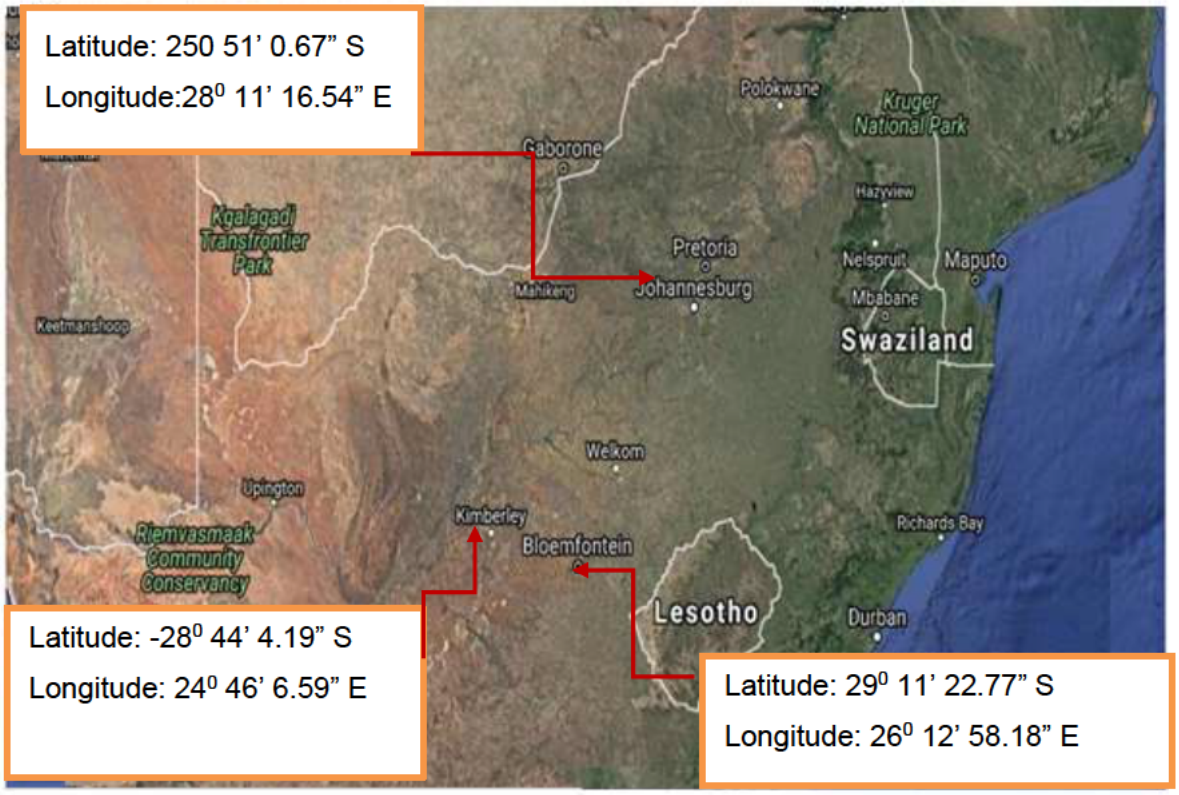

Figure 3.1: GPS Precision indicating visited site

Soils from each site were systematically collected at depth of 1.1m below the ground surface (Figure 3.2). Plastic bags were used to seal the collected samples as to minimise moisture lost. The soils were transported to both Central University of Technology Geotechnical and Pavement materials laboratory and Council of scientific and Industrial Research (CSIR) laboratory. Thirty-five grams of each soil were sent to the oven, at a temperature of 80^{0}C to determine the natural moisture content of each representative soils. Another 30kg of each soil samples, were oven-dried at a temperature of 80^{0}C for preliminary Geotechnical testing such as: particles size distribution (PSD) test, Atterberg limit test, X-Ray Diffraction (XRD) test and modified compaction test for basic soil classifications.

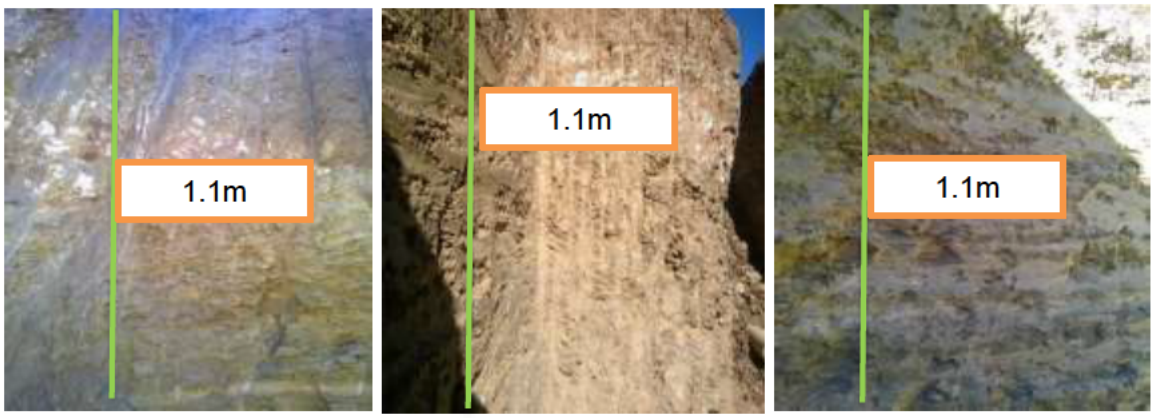

Figure 3. 2: Sample borrowed pits at different sites

3.3 Soil Chemical And Mineralogical Analysis

Prior knowledge of chemical and mineralogical composition of subgrade soil are required, before any pavement design could commence to avoid misleading of the subgrade response. Chemical analysis, using X-Ray Diffraction (XRD) and X-ray fluorescence (XRF) were carried out on the studied soils for evaluation of the chemical and mineralogical compositions. Thus, mineralogical composition of any soil depends largely on the weathering interaction of the host rocks. The mineralogical and chemical composition of the nine-studied soils are detailed in Appendix A.

3.3.1 soils XRD Test

X-ray powder diffraction technique with Cu Kα radiation (Rigaku, Ultimate IV) was used to determine the mineralogical composition of the soils. The soils mineralogy provides basic understanding of the hydro-mechanical response in pavement structure and it aid in the identification of clay minerals present in subgrade. The XRD result revealed that the dominant minerals in FSS sample are Quartz, Bentonite, Kaolinite, Muscovite and Illite-montmorillonite, this is an indication that the FSS sample is expansive. Whereas, GPS samples are dominated with minerals such as: Quartz, Anorthite, Rutile, Muscovite and Illite-montmorillonite. This implies that the GPS sample is slightly expansive with compressible and collapsible potentials. NCS sample results, revealed that the dominant minerals are: Quartz, Muscovite, Bentonite, Kaolinite and Goethite. This result depicts that NCS samples are of expansive and as such possesses slight potential of heave and erodibility. However, detailed XRD results of the studied soils are presented in Appendix A.

3.3.2 Soils XRF test

Chemical composition of the nine subgrade soils was determined using thermo scientific RIGAKU 3000 energy-dispersive x-ray fluorescence spectrometry analyser. Having an excitation source as miniaturised 30 kV X-ray tube. Dried pulverised soil passing through sieve size of 250 µm aperture were used. RIGAKU 300 XRF analyser was automatically adjusting for matrix effects, as to determine the various chemicals contented in the soils for an hour, without requiring any empirical input from the instrument operator. The XRF results of the subgrade soils, determined the existence of the following major and minor oxide: Al_2O_3, SiO_2, k_2O, CaO, MnO, Fe_2O_3 (major) and Na_2O, MgO, TiO_2 BaO (minor). The average concentrations of heavy metals CuO, Rb_2O, SrO, ZrO_2, Cr_2O_3, NiO, Rb_2O and Nb_2O_5 were detected to the lowest minimum, for the oxides such as AgO_2, CdO, HgO, Sb_2O_3, Se_2O_3 and SnO_2 were observed to have low concentrations and were below trace level. The chemical compositions of the nine studied soils are summarised in Tables 4.1 while the detailed results are presented in Appendix A.

Table 3.1: Soils Chemical Composition

Chemical oxides	FSS 1 Mass (%)	FSS 2 Mass (%)	FSS 3 Mass (%)	NCS 1 Mass (%)	NCS 2 Mass (%)	NCS 3 Mass (%)	GPS 1 Mass (%)	GPS 2 Mass (%)	GPS 3 Mass (%)
SiO_2	58.39	55.34	49.15	55.14	53.43	56.17	66.59	61.12	64.34
Al_2O_3	21.41	25.16	27.31	19.80	22.71	20.13	17.50	19.65	16.83
Fe_2O_3	12.09	12.09	13.93	18.99	11.56	12.56	8.29	11.34	10.29
TiO_2	1.13	0.25	2.12	0.76	0.88	1.57	0.78	0.92	0.72
MgO	1.96	4.37	1.81	0.64	3.23	2.35	0.72	0.56	0.63
CaO	1.75	2.25	0.23	0.22	0.56	0.54	1.27	1.74	1.46
Na_2O	0.53	2.13	0.89	0.052	0.11	0.13	0.37	0.52	0.61
K_2O	1.89	6.38	2.25	3.77	4.13	2.98	2.98	2.56	3.11
Others	0.85	3.12	2.31	0.628	4.87	3.57	1.50	1.68	2.01
LOI (%)	0.23	0.84	0.67	0.27	0.45	0.17	0.32	0.27	0.13

3.4 Soil Classification

The particle size distribution (PSD) analysis and Atterberg limits test were carried out for the classification of the soils. However, under unsaturated soils mechanics, soil classification takes an additional significance meaning. Though the PSD curve provides information on the percentage distribution of the soil particle sizes.

The distribution of the soil particles bears a correlation with pore sizes distribution. Information from pore-size distribution can be used to estimate water content–soil suction relationship for the soil (i.e., SWCC). Consequently, the PSD becomes of increased value for understanding the mechanics of unsaturated soil.

Furthermore, various standards are used for soil classification, though it depends on the geotechnical engineer's choice of standard. As long as the engineer provide justification that is in line with the local standard, besides most of these standards are written under the same principle. In this research, American Society for Testing and Materials (ASTM) and American Association of State Highway and Transportation Officials (AASHTO) which are in conformity with the local South Africa standard i.e. Technical Methods for Highways (TMH) were used.

3.4.1 Soils particles size distribution (PSD)

The objective of this research was to investigate the geotechnical response of natural subgrades that are prone to swelling, fatigue and cracks for pavement, when subjugated to cyclic moisture stresses and repeated loading. These problematic soils were carefully identified and collected from three provinces across South Africa. Figures 3.3 through 3.5 shows the PSD analysis of the respective studied soils. Whereas, summary of the average particle size (D_{60}), effective size (D_{10}), uniformity coefficient (C_u), coefficient of curvature (C_c) and the GPS coordinate location across nine sites from where the soils were sampled are summarized in Table 3.2. The result of PSD in Figures 3.3 through 3.5 reveal that fine content of the soils varies. Apparently, the curves show that FSS contained the highest number of fines among other studied soils, followed by NCS and GPS when traced from the curve. The soils particle content, ranges from well graded soils to poorly soils with no possibility of gap as the samples had very high percentages of fines with over 50% passed through No. 200 sieves.

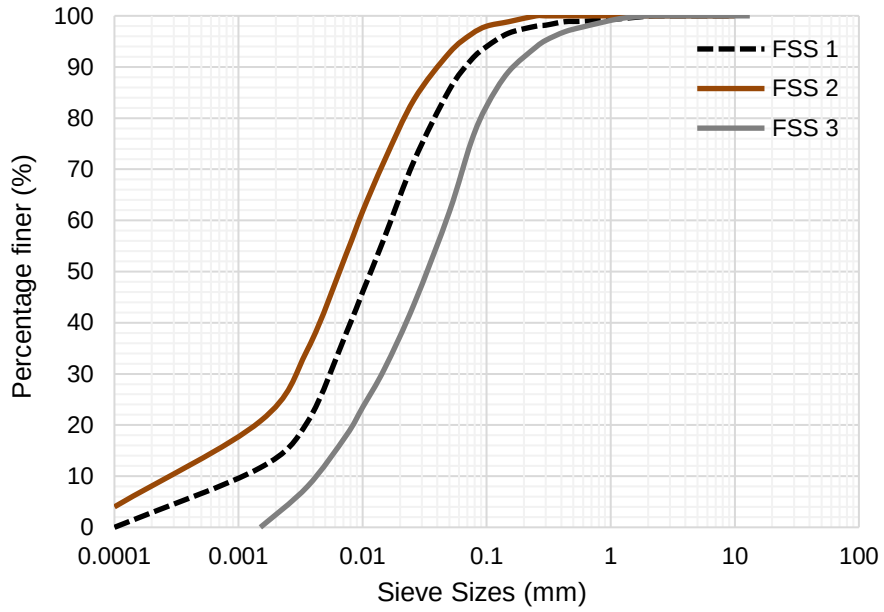

Figure 3.3: FSS grain size distribution curve

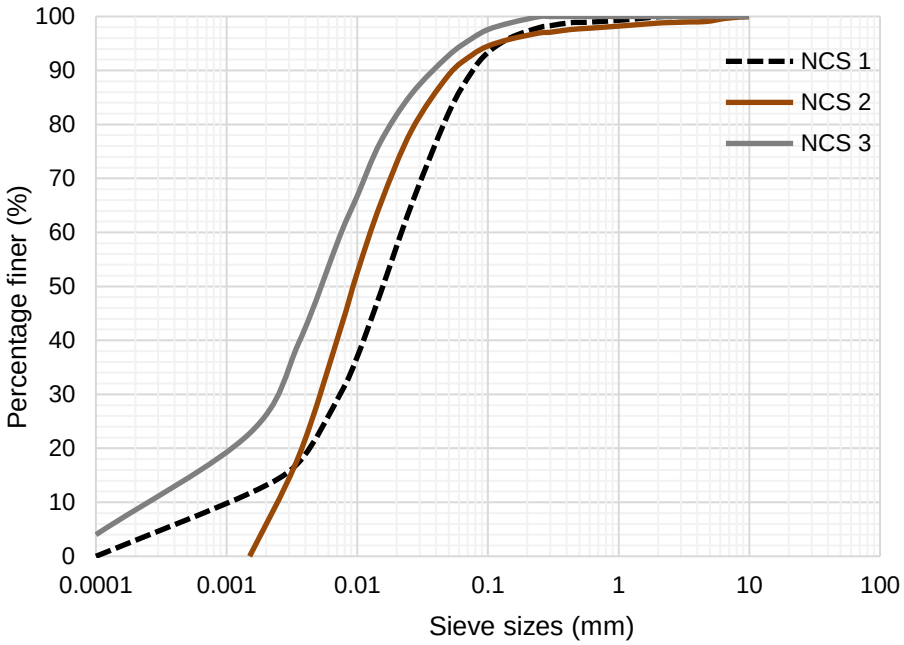

Figure 3.4: NCS grain size distribution curve

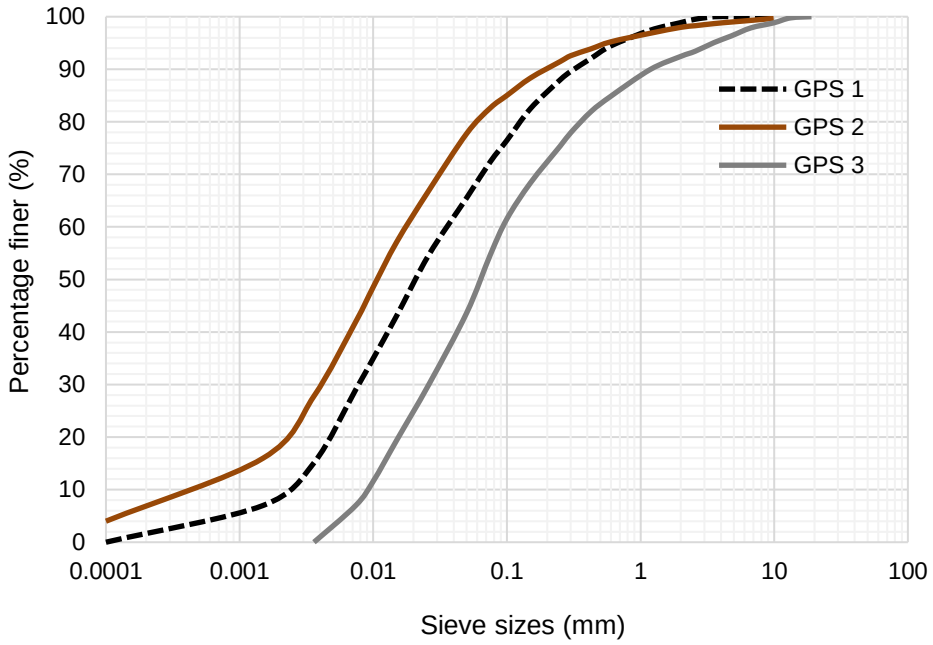

Figure 3.5: GPS grain size distribution curve

The coefficient of uniformity, (C_u) values for FSS 1, 2 and 3 are; C_u=19, 33 and 11, this depicted well-graded soils. While NCS 1, 2 and 3 have C_u values of 11, 5.2 and 52.3.7 which qualifies the soils as poorly-graded. Furthermore, C_u for GPS 1 and 3 are 15.3, 45 and 9, this show that GPS 1 and 3 are uniformly-graded, whereas GPS 2 is well-graded.

The Coefficient of curvature, (C_c) determines the shape of particle sizes. The values obtained for the studied soils are summerized in Table 3.2. The values of C_c for FSS 1, 2 and 3 are 1.89, 0.08 and 1. FSS 2 portrayed an irregular shape, because its value for C_c is not stipulated within the standard range i.e. 1 – 3 The NCS 1, 2 and 3 portrayed irregular shapes because they have C_c values to be15.8, 0.77 and 5.63 which are not within the range, due to high percentage of fines content. In addition, GPS 2 is within the stipulated range because it has C_c value 2.2 and GPS 1 and 3 is found to be outside the range. Therefore, GPS 2 is well-graded whereas GPS 1 and 3 are poorly graded. This result is in consistency with C_u results.

$$C_u = \text{Coefficient of uniformity } \left({}^{D_{60}}/_{D_{10}}\right) \quad (3.1)$$

$$C_c = \text{Coefficient of curvature } \left({}^{(D_{30})^2}/_{(D_{10}) \times (D_{60})}\right) \quad (3.2)$$

Table 3.2: Grain size analysis of the studied subgrades

Soils	Gradation (%)			Modulus of gradations					Coordinates
	Sand	Fines		D_{10}	D_{30}	D_{60}	C_u	C_c	Latitude
		Silt	Clay						longitude
FSS 1	8.62	34.44	56.94	0.001	0.006	0.019	19	1.89	29^0 11’ 22.77” S; 26^0 12’ 58.18” E
FSS 2	3.61	37.19	59.20	0.0003	0.003	0.01	33	0.08	-28^0 06’ 6.0” S; 26^0 53’ 59.99” E
FSS 3	24.62	31.21	44.17	0.0045	0.015	0.05	11	1.00	-27^0 58’ 6.0” S; 26^0 44’ 6.22” E
NCS 1	11.82	29.44	57.24	0.001	0.008	0.011	11	15.8	-28^0 44’ 4.19” S, 24^0 46’ 6.59” E
NCS 2	7.16	30.02	59.80	0.0025	0.005	0.013	5.2	0.77	-28^0 33’ 60” S, 24^0 17’ 60” E
NCS 3	4.11	39.14	55.75	0.00012	0.0025	0.008	53.3	5.63	29^0 2’ 19.2” S, 24^0 36’ 39.6” E
GPS 1	27.62	28.40	43.98	0.0022	0.008	0.035	15.9	0.83	25^0 51’ 0.67” S, 28^0 11’ 16.54” E
GPS 2	17.38	45.08	37.54	0.0004	0.004	0.018	45	2.2	-25°59'53.99" S 28°06'25.99" E
GPS3	45.34	28.57	26.09	0.01	0.028	0.09	9	0.87	25^0 51’ 6.84” S, 28^0 11’ 22.56” E

3.4.2 Atterberg limit test

Atterberg limit results are presented in Table 3.3. The soils were classified as fine-grained soils, because they have over 50% fine by dry weight of the soils that passes through sieves #200 (75-μm). The analysed test data and corresponding plasticity chart for the nine soil samples are illustrated in Figures 3.6 through 3.8. The plasticity curves demonstrate plasticity characteristics of the soils. Each symbol is explained using Universal Soil Classification System (USCS) from which the characteristic description of each soil is obtained. FSS and NCS, are of high Plasticity with Liquid limit greater than 35%, and GPS has a low plasticity. The data were recorded from three sets of performed tests, in order to obtain a reliable and most consistent results.

Table 3.3: Consistency limits values

Soil Samples	Liquid Limit (%)	Plastic Limit (%)	Plasticity Index (%)	Degree of expansion	Specific Gravity G_s	Natural Moisture Content, w_n (%)	AASHTO
FSS 1	62.10	21.32	40.78	High	2.71	26.00	A-7-6
FSS 2	68.03	23.82	44.21	High	2.73	24.23	A-7-6
FSS 3	60.28	23.56	36.72	High	2.69	25.64	A-7-6
NCS 1	54.91	20.93	33.98	Marginal	2.69	22.14	A-7-5
NCS 2	61.32	21.13	40.19	Marginal	2.70	23.11	A-7-5
NCS 3	66.88	21.21	45.67	Marginal	2.72	22.58	A-7-5
GPS 1	45.33	22.13	23.20	Low	2.68	17.58	A-6
GPS 2	52.28	24.34	27.94	Low	2.72	17.78	A-6
GPS 3	40.12	22.81	17.31	Low	2.65	16.90	A-6

Furthermore, FSS plotted data are positioned above A-line and their plasticity index is greater than 4% (PI>4%), NCS is classified as high plastic soils because the plotted data is traced above A-line. However, FSS 1, 2 and 3 has a liquid limit of 60.10%, 68.03 and 60.28% with plasticity index of 40.78%; 44.21% and 36.72% respectively. This area is identified as CH (high plastic clay). NCS 1, 2 and 3 are classified as CH as well, because the liquid limits obtained for these soils are: 54.91%, 66.88% and 66.88%. Whereas, the plasticity indexes of soils recorded are 33.98%, 40.91%, and 45.67% respectively. This area is identified as CH (high plastic clay), because it is positioned above A-line. The GPS 1 and 2 are classified as CL because they recorded liquid limits of 45.33% and 52.28% with corresponding plasticity indexes of 23.20% and 27.94% this area is identified as CL (low plastic clay) and it plotted above A-line but on the left side of the curve (Figure 3.8). GPS 3 is classified as low plastic silt (ML), because its plotted data is located below A-line on the left side of the chat with a liquid limit and a corresponding plasticity index of 40.12% and 17.31% respectively.

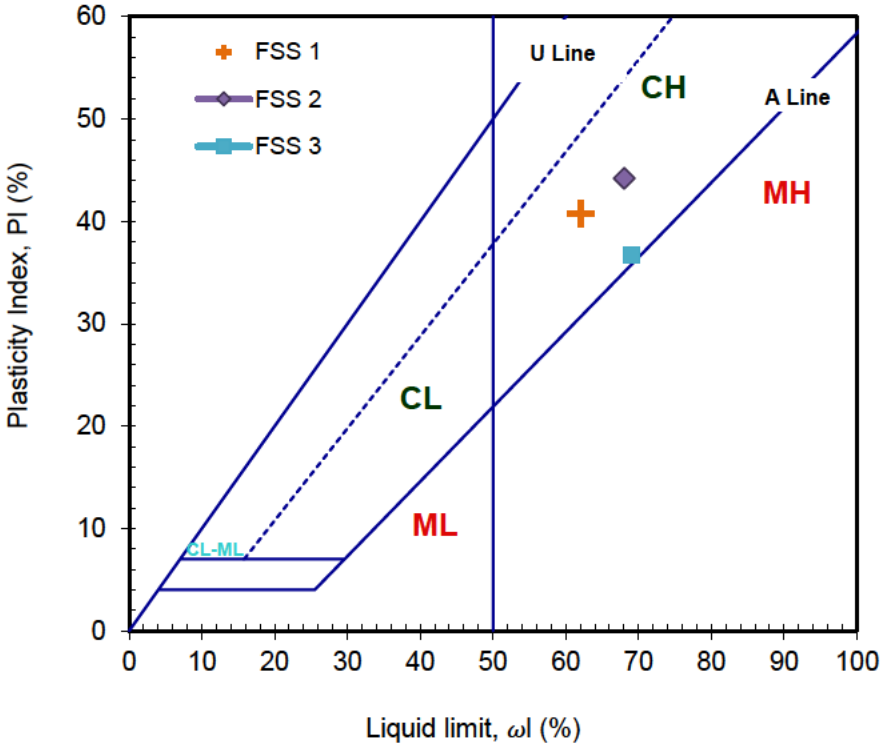

Figure 3.6: Casagrande plasticity chart for FSS

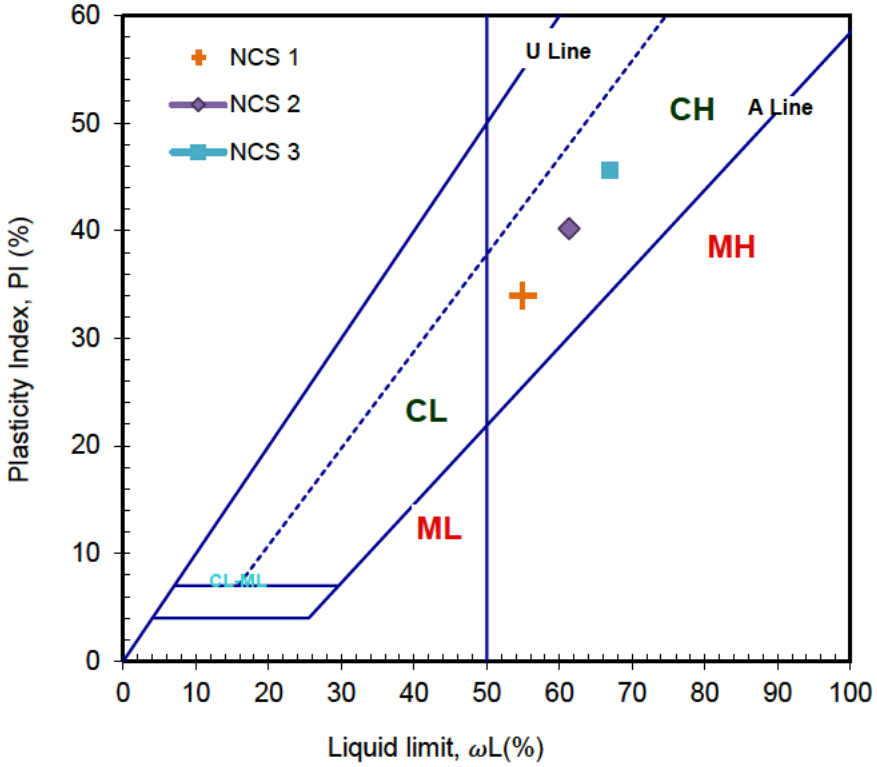

Figure 3.7: Casagrande plasticity chart for NCS

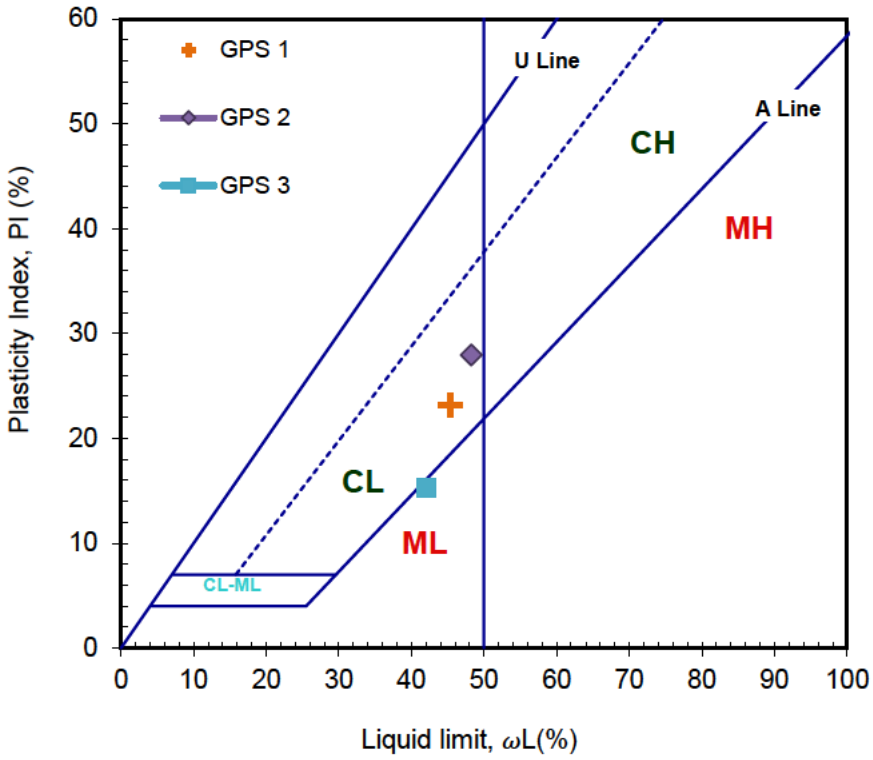

Figure 3.8: Casagrande plasticity chart for GPS

In addition, group classification of the studied soils, in accordance with AASHTO soil classification, group index equation was applied Equation 3.3:

$$\text{Group index} = (F - 35)[0.2 + 0.005(Wl - 40)] + 0.01(F - 15)(I_P - 10) \quad (3.3)$$

Where:

F = fines content (percent passing #200 sieve),

Wl = liquid limit

I_P = plasticity index

This group classification index revealed that the subgrade soils will make a very poor pavement foundation. Table 3.4 below shows the classification of the studied soil in terms of USCS, AASHTO and TRH.

Table 3.4: USCS, AASHTO and TRH Soil Classification

Soil Sample	Group Index	USCS	AASHTO	TRH
FSS 1	38.92	CH	A-7-6	G10
FSS 2	48.72	CH	A-7-6	G10
FSS 3	30.12	CH	A-7-6	G10
NCS 1	39.31	CH	A-7-6	G10
NCS 2	34.53	CH	A-7-6	G10
NCS 3	49.11	CH	A-7-6	G10
GPS 1	12.84	CL	A-7-5	G10
GPS 2	23.39	CL	A-7-5	G10
GPS 3	8.006	ML	A-7-5	G10

3.5 Geotechnical Testing Programs

With the view of realizing the objective of this study, some laboratory testing methods were adopted. However, both local and international testing specification were carefully crafted before laboratory testing commenced. These testing standards are: TMH, ASTM and AASHTO.

3.5.1 Free swell index (FSI) test

Free swell index test was conducted on the studied soils according to Indian standard (Is: 2720 (1977, Part 40) test method as to evaluate the swelling potential of the soils. These soils were passed through 425 μm sieve size (#40) and the soils were oven-dried at a temperature of 115°C. Ten grams of each soil samples were poured into two separate graduated cylindrical glass jars of 100 ml capacity, with one containing distilled water plus the 10g of the soil and the other 10g in a jar contained kerosene. The jars were allowed to stand for 48 hours and the final volumes of the soil were recorded and FSI of the soils were determined and recorded. Figure 3.5 shows the test setup.

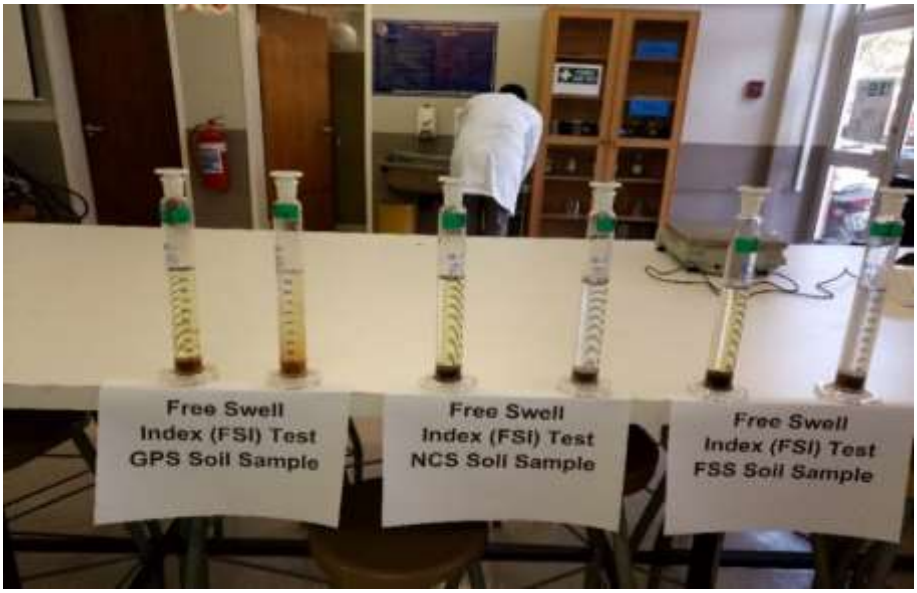

Figure 3.9: Free Swell Index setup of the subgrade soils

$$FSI = [(V_S - V_K)/V_K] \times 100\% \quad (3.4)$$

Where:

FSI= free Swell Index

V_k = volume of soil in kerosene,

V_s = volume of soil in water

3.5.2 Zero swelling test (ZST)

The method adapted for this research is zero swell test (ZST). The pressure which must be applied to the soil as to overcome the soil's swelling pressure from any further swelling through wetting process is called swelling stress. This procedure is also designated as Zero Swell Test (ZST) (Basma et al, 1995; Fattom and Barakat, 2000).

The ZST was conducted in line with ASTM D4546 (2013). The soil samples passing through ASTM sieve size of 4.75mm (#4) were used. The specimens were prepared at varying moisture content equivalent to the one gotten from compaction test. Hence, total of 5kg by weight of the soils were Oven-dried at a constant temperature of 105^0C for 48 hours. Followed by compaction in a modified mould at different dry unit weight, γ_d. The specimens were demoulded and cut into slices of 25mm height and 75 mm in diameter bearing the shape of the consolidation ring and oedometer ring was fitted into the sliced specimens.

Figure 3.10: Fitted Specimens in oedometer ring

The inner part of the ring, was greased to reduce resistance friction between the inner surface of the ring and the soil sample during testing. The specimen was held inside the metal ring and placed between two porous stones. The upper porous stone, which can easily move inside the ring with a small spacing, is positioned below a metal loading cap through which pressure can be applied to the specimen and a collar was attached. The sample was levelled and covered with filter in order to preserve the two exposed sides.

Figure 3.11: Zore swell test setup

The soils were then loaded under sustained stress condition equal to the overburden on the consolidation set-up. The representative soils were loaded and set at surcharge force. Upon wetting, the height of the specimen begins to increase and additional loads were applied each time change in height was recorded by the dial gauge, as to overcome swelling at that particular height. The same procedure continued, until no

additional swelling was recorded on the dial gauge. The applied loads that was on the prepared soils to counter the active swelling stress were recorded and the swelling stress of the soils were calculated using Equation 3.5.

$$P_s(kPa) = \left(\frac{(\sum_i^n = 1M_i) \times g \times b_r}{\frac{\pi(\emptyset^2)}{4}} \right) \Big/ 1000 \quad (3.5)$$

Where:

$P_s =$ swelling pressure in kPa

$(\sum_i^n = 1M_i) =$ total number of surcharges

$g =$ acceleration due to gravity $9.81\text{m}/s^2$

$b_r =$ beam ratio of the oedometer arm

$\frac{\pi(\emptyset^2)}{4} =$ internal area of the ring

3.5.3 Modified proctor compaction

The Proctor compaction test is a geotechnical laboratory testing procedure used to evaluate moisture-density relationship of soils. Specifically designed to determine the optimum moisture content of soils with their corresponding maximum dry density. The test procedure was carried out by adding water to each soil sample to bring it to the desired moisture content. Five layers of the soil were then compacted by evenly distributing 55 blows in a mould, having 127 ± 1mm height and 152.4 ± 1mm diameter using a modified Proctor hammer of weight 4.536kg, striking at a distance of 457.2 ± 1mm in accordance with TMH1 Method 7 (1986). After which, some small quantities of the soils were taken from top, bottom and middle to determine the moisture content.

$$w_c = \frac{M_1 - M_2}{M_2 - M_c} \times 100\% \quad (3.8)$$

where

$\text{M}_1 =$ mass of compacted sample + Can

$\text{M}_2 =$ oven dry mass of compacted sample + Can

$\text{M}_\text{c} =$ mass of Can

$\text{w}_\text{c} =$ Moisture content

3.5.4 Filter paper test (Whatman No. 42)

During sample preparation for each test i.e. CBR, ZST, consolidated undrain test, and resilient modulus test. The identical sets of specimens were prepared at different moisture content. One set of the identical specimens were used to determine the soils suction, while remaining specimens were used to measure the above-mentioned tests. Average of two results for each tested specimen were taken as the most consistence results determined in the laboratory. Filter paper test is considered in this study, due the ability of this methods to covers full range of suction. Soil suction tests were performed using filter paper technique according to ASTM D 5298-10 test method. The filter paper moisture contents were converted to matric suction using the calibration curves in ASTM 5298-10 and the soil water retention curve was established.

Though, several methods for measuring suction and the range of suction values vary from one standard to another. Measuring the negative pore water pressure directly can be limiting, because devices typically used for this measurement only measures very low suctions. Table 3.5 (Ridley 1993) summarized different devices used to measure suction and range of suction that can be measured.

Table 3.5: Time duration and various methods of measuring suction (Ridley 1993).

Device type	Suction value	Principal usage	Direct/indirect	Range: kPa	Equilibrium time
Vacuum desiccator	Total	Lab	Indirect	103-106	Months
psychrometer	Total	Field	Indirect	300-700	Months
Filter paper	Total Matrix	Field Lab	Indirect Indirect	1000-30000	Weeks 1 Week
Porous block	Matrix	Field	Indirect	30-3000	Weeks
Thermal block	Matrix	Field	Indirect	0-175	Days
Suction plate	Matrix	Lab	Direct	0-90	Hours
tensiometer	Matrix	Field	Direct	0-90	Hours
Pressure plate Osmotic	Matrix	Lab	Direct	0-5000	Hours
Tensiometer	Matrix	Field	Direct	0-1500	Days

The filter paper method for both the contact and non-contact filter papers to measure the matric and total suctions was selected for this research, because it can cover a wide range of suction measurement. The working principle behind the filter paper technique, is that the filter paper moisture content will come to equilibrium with the soil's moisture

content either through vapour flow or liquid flow. As the filter paper absorbs water through vapour flow (no contact between the filter paper and soil), then only total suction is measured. Whereas, absorption of moisture through fluid flow (contact between the filter paper and soil), allows for matric suction is measurement.

Following the ASTM D 5298 – 10 Standard Test Method for measurement of Soil Potential (Suction) Using Filter Paper. Dry filter papers were used, as obtained directly from their boxes. Throughout testing, the filter papers with a pair of clean tweezers with gloved hands were used to handle the filter papers, as to avoid contamination. A number of soil specimens were compacted and were carefully cut into sizes. Approximately, these cut specimens occupied 75% volume of the air-tight containers having 85 mm and 70 mm of diameter and height respectively. After which, the cylindrical specimens were equally sliced at the middle and three contact filter paper was sandwiched between the two sliced soils. Thus, the joint was sealed off using electrical tape to ensure no loss of moisture from the filter paper.

Figure 3.12: Sliced soil and sandwiched filter paper

The wrapped specimen is then placed into the air-tight container and A poly-vinyl chloride (PVC) ring (diameter 40mm and thickness 5mm) was placed on top of each soil specimens onto which the non-contact filter paper was placed.

The test specimens were then sealed in the air-tight container and transferred to an ice-chest box, for 14 days as to allow for moisture equilibrium between the filter papers and soil, under controlled temperature of 25^0C.

Figure 3.13: Sandwiched in temperature – controlled ice chest

After 14 days, the contact and no-contact filter papers were retrieved, weighed and their water contents were determined following the procedures suggested by Bulut et al. (2001).

Figure 3.14: Weighing the filter paper inside moisture can

Then, the filter paper calibration curve for water content versus suction, with the corresponding suction values were calculated from the curve. Therefore, a calibration curve was adopted (i.e., the one curve presented for two different filter papers in ASTM D 5298 – 10 Standard Test Method for Measurement of Soil Suction, Using Filter Paper).

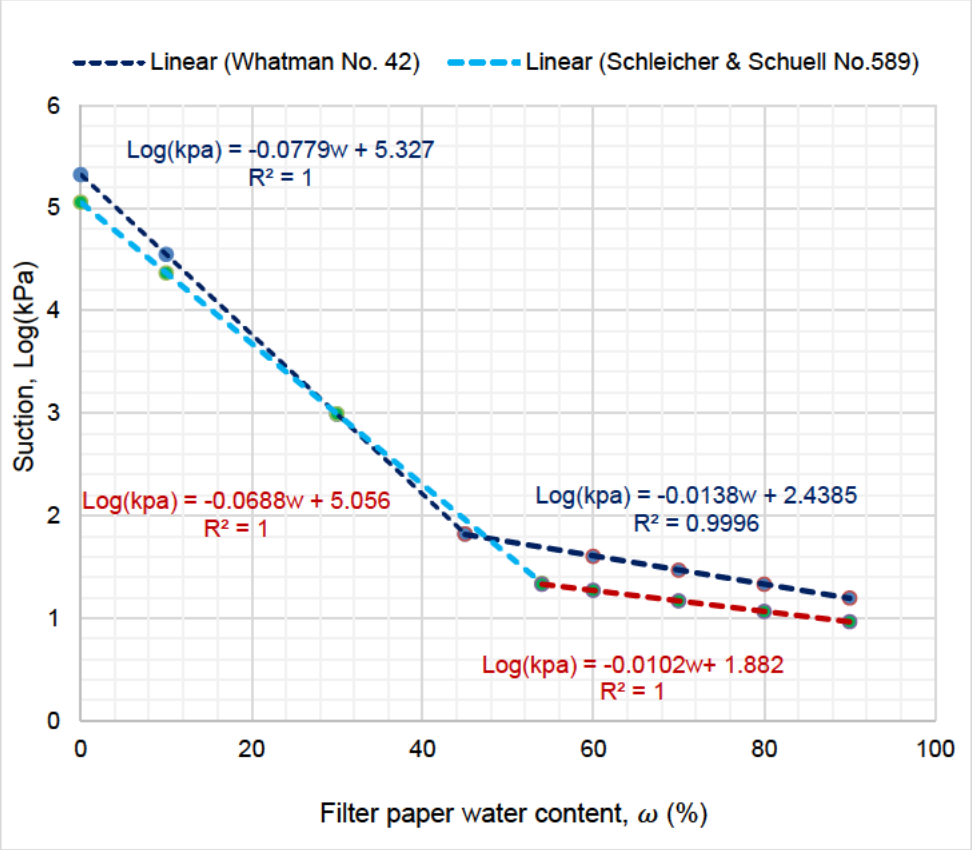

Figure 3. 15: Filter papers calibration curve

3.5.5 Filter paper calibration exercise

Calibration of the filter papers i.e. Whatman No. 42 and Schleicher and Schuell No.589, was reasonably performed, as two laboratory technician carefully took care of the moisture content estimation of the filter papers, as to confine the exposure time of the filter paper to the open air. This was to avoid minimum moisture, gain and lost during the exercise. All the utilized items were painstakingly cleaned. Tweezers and latex gloves were used to handle with the materials all through the duration of the calibration exercise. To evade moisture contamination, filter papers and moisture tins were never contacted with bare hands. The filter paper calibration curve was produced using salt solution as an osmotic potential source for suctions above 2.5 pF. NaCl solution set up ranges from 0 to 2.7 molality. The molality is the number of moles of NaCl in 1000ml of distilled water. For example, one mole of NaCl is 58.4428g. Hence, 2 molality NaCl means 2 times 58.4428g or 116.8856g NaCl in 1000ml distilled water. Figure3.16 illustrate the NaCl solution at various suction values. The filter paper calibration tests were carried out following the procedures listed below:

a) NaCl solutions were prepared from 0 to 2.7 molality. The molality is the number of moles of NaCl in 1000ml of distilled water. For example, one mole of NaCl is 58.4428g. Whereas, 2 molality of NaCl means 2 times 58.4428g which is equivalent to 116.8856g NaCl in 1000ml distilled water. Figure 3.16 gave the NaCl weight at various suction values.

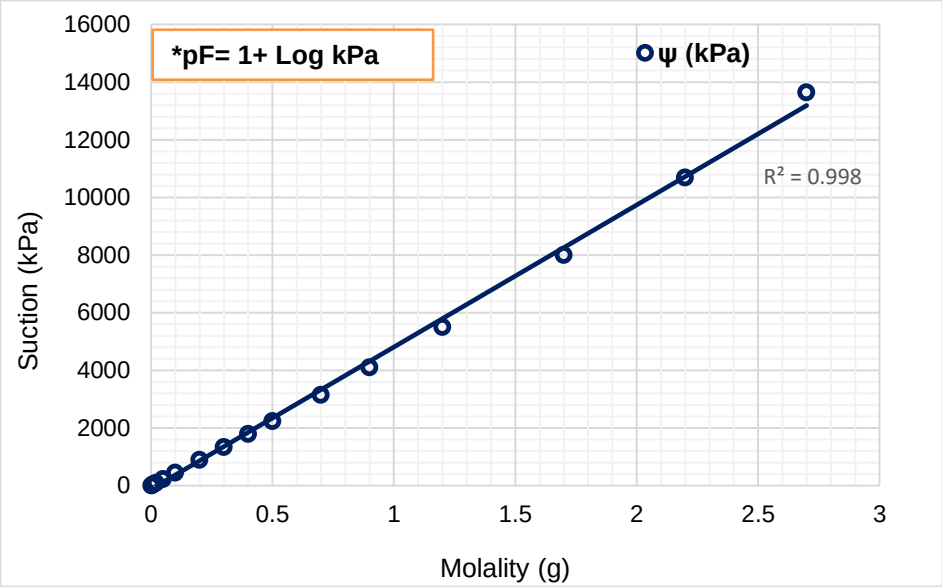

Figure. 3. 16: Total suction of NaCl at 20°C (adopted from Lang, 1967)

b) A 300 ml glass jar was filled with 200 ml of a known NaCl molality and the glass jar was labelled according to the solution molality the jar contained.

c) Then, a plastic support is put into the glass jar, Figure: 3.17 shows the setup of the glass jar, the plastic support and filter papers placed a few millimetres above the solution level.

d) Two filter papers were placed on top of the plastic support in order to minimise error scale readings and in case if one filter paper is mistakenly dropped during the exercise, the other filter will be used. The lid of the glass jar was air-tightened, and a plastic tape was used to seal off the glass jar, as shown in Figure 4b.

Figure: **3**. **17**: Plastic support hold filter papers; (b) glass jar tightly closed

a) Step b and d were repeatedly performed for each different NaCl concentrations. Then, glass jars were kept in a controlled temperature chamber, 2 weeks equilibrium period was adopted for the calibration exercise.

After equilibrium was attained, the filter paper moisture content was determined following the below listed procedures

a) Prior to filter papers moisture content determination, all the related items for calibration procedure were kept cleaned and the gloves were used throughout the entire exercise. Furthermore, each glass jars containing the filter paper, the NaCl solution and plastic support were retrieved from the controlled temperature chamber one at a time. The moisture tins were weighed to the nearest 0.0001g accuracy, and the filter paper moisture content of each NaCl concentration were recorded on the laboratory data sheet.
b) Throughout the entire exercise, all the measurements were performed buy two persons. i.e. one person was opening the sealed glass jar, while the other person was inserting the filter paper into the moisture tin swiftly in less than 5 seconds using the tweezers.
c) Following procedure “b” the mass of each moisture tin with the wet filter papers were recorded with the moisture tin labels for the bottom and the top filter paper.
d) Afterwards, all the moisture tins were placed in the oven at a temperature of 105 ± 5 °C for 24 hours with the lids half-closed as to allow for moisture evaporation.
e) The moisture tins were then fully closed with theirs lids, prior to retrieving from the oven and were allowed to equilibrate for 5 minutes in the oven, as the mass

of the dried filter papers and moisture tins were being taken. Immediately, each moisture tins were removed from the oven, they were placed on a metal block for 20 seconds, in order to step down the tins hotness. Then, each moisture tin containing the filter paper were weighed again. Subsequently, each dry filter paper was retrieved from the moisture tin and the weight of each cold tin were taken in few seconds. Thus, recording each value of the dry filter paper from each concentration on the laboratory data sheet.

f) Lastly, the values of each filter paper moisture content were used to calculate the suction values of each Nacl concentration. The curve of suction and each corresponding moisture content was plotted. Thus, the curve was designated as Authors calibration curve (Figure: 4.10).

The calibration curve of moisture content against the corresponding suction values of the filter paper was obtained from calibration process. The calibration curve of the filter paper is obtained when the suction value in pF or Log (kPa) units are represented with the corresponding moisture content. The curves were plotted using Whatman No. 42 type filter papers and Schleicher & Schuell No589 White Ribbon filter paper as previously given by ASTM D 5298 (1994) in Figure: 3.15. Therefore, the Author's calibration curve for Whatman No. 42 type filter papers was used for this study, for the calculation of suction.

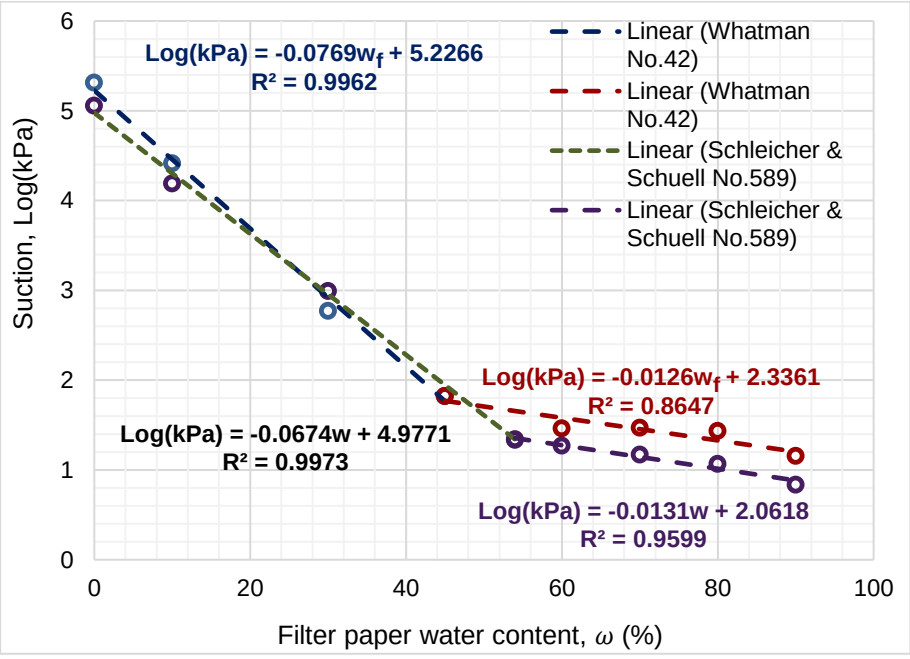

Figure 3.18: Authors filter papers calibration curve

3.5.6 California bearing ratio (CBR) test

CBR test is experimental approach for evaluating the bearing capacity of pavement subgrade. This test was performed by applying load on the penetration piston over compacted cylindrical specimens with the size of 152mm and height of 127mm inside a rigid mould at the rate of penetration which is approximately 1.27 mm/min. The load readings at penetrations was recorded as follows: 0.64mm, 1.27 mm, 1.91 mm, 2.54 mm, 3.18 mm, 3.81 mm, 4.45 mm, 5.08 mm, 5.72 mm, 6.35 mm, 7.62 mm, 8.26 mm, 8.90 mm and 9.53 mm as described in TMH1 Method 8. Essentially two types of CBR test associated with the testing of the soils was conducted i.e. soaked and unsoaked. The unsoaked CBR test was performed to simulate natural conditions. Whereas, the soaked test was performed to replicate severe and extreme conditions in the field, such as a high-water table rise in the pavement due to moisture variation.

Furthermore, specimens at different moisture content were prepared equivalent to the moisture content obtained from moisture-density test, as to determine moisture influence on the studied soils. Uniform compactive efforts were maintained to produce specimens with uniformed unit weight. The specimens were subjected to soaked and unsoaked curing conditions for four days. Subsequently, after four days soaking each specimen were weighed again and subjected to penetration by a cylindrical rod using automated CBR machine as shown below.

Figure 3.19: Automated CBR testing machine

The CBR values of the tested soils were determined by plotting CBR curve with the load on the vertical axis and penetration depth on the vertical axis. In addition, equation 3.9

was employed to calculate CBR values at three different strain loading level i.e. 2.54mm, 5.08mm and 7.62mm. The California standard values for these depths are 13,344, 20,016 and 25,354 kN respectively.

$$\mathrm{CBR} = \frac{\mathrm{P}}{\mathrm{P_s}} \times 100\% \tag{3.9}$$

Where:

$CBR = California\ bearings\ ratio$

$\mathrm{P} =$ is the plunger $-$ load KN/m2 for the tested soil.

$P_s =$ is the plunger $-$ load in KN/m2 for the standard soil.

Moisture content was determined using Equation 4.8 above

3.5.7 Unconfined compressive strength (UCS) Test

Unconfined compressive strength is the load per unit area at which an unconfined cylindrical specimen of soil will fail under axial compression. However, UCS of a soil is determined by measuring the load required to allow a standard compressive machine to crush a compacted soil according to (TMH1 METHOD 14). The UCS specimens were prepared at different moisture content, equivalent to the moisture content gotten from compaction test. Cylindrical specimens with diameter of 152mm and height of 127mm were stored in the curing chamber at a temperature of 23^0 and 98% relative humidity.

Figure 3.20: Cured soil specimens

Afterward, the compacted specimens were tested for 7 days curing period at the rate of 1.2 mm/min and UCS the compacted soils were determined using Equation 3.10.

$$q_u = \frac{\mathrm{P}}{\mathrm{A}} = \frac{\mathrm{kN}}{\pi \mathrm{r}^2} \tag{3.10}$$

Where:

$q =$ Unconfined compressive strength (kPa),

$kN =$ Load required to crush specimen (kN)

$r =$ radius of specimen face (0.025m),

Stress − strain values were calculated using Equation 3.11

$$\text{The axial strain, } \varepsilon = \frac{\Delta \mathrm{L}}{\mathrm{L_o}} \tag{3.11}$$

Where $\Delta \mathrm{L} =$ the change in the specimen length

$\mathrm{L_o} =$ the initial length of the specimen

$$\mathrm{A} = \frac{\mathrm{A_0}}{(1-\varepsilon)} \tag{3.12}$$

$A_0 =$ the initial cross − sectional area of the specimen (mm^2)

$A =$ the corresponding cross − sectional area (mm^2)

3.5.8 Consolidated undrain triaxial (CUT) test

Shear strength test such as CUT test procedures are described in this section. Samples, obtained from soil passing through No. 4 sieve, were used to prepare the specimens at different moisture content targeting the moisture content obtained from compaction test. The method used in this research to measure shear strength of the prepared specimens is consolidated undrained (CU) triaxial and the total stress was measured through consolidation phase. The shear strength test was conducted on the selected soil samples in accordance with ASTM D 4767 – 99. The shear strength parameters (C', $\emptyset^0$) of the soils were determined. The prepared specimens were cylindrical, having 150mm diameter and 300mm height corresponding with height-to-average diameter ratio of 2:1 with largest particle size smaller than 0.167mm of the specimen diameter. Specimens were allowed to drainage under initially applied normal stress only and full consolidation was allowed to take place. The curves of shear stress at failure against normal stress with the shear strength parameters at each moisture content were automatically plotted

by the Instron software. Thus, the shear strength of the studied soil was calculated at each moisture content using Equation 2.19.This is usually isotropic in most standard testing and it is denoted as consolidated isotropic undrained triaxial test (CIU) with or without pore pressure measurement. Different combinations of axial stress and cell pressure are possible only on the triaxial test. The triaxial equipment was preferable for this because both the saturated and unsaturated soil tests could be performed on them with very minimal adaptations.

Figure 3.21: Complete triaxial testing arrangement

Extension of the Mohr-Coulomb shear strength criterion to unsaturated soils requires determination of the shear strength parameters c' and ϕ'. conventional triaxial and direct shear apparatus are used to determine these parameters for saturated soils. However, for unsaturated soils this apparatuses needed some modification to make room for pore air and pore water pressure measurements simultaneously. Blight (2013) discovered several challenges for the experimentation of shear strength for unsaturated soils as:

- The need to make a large number of tests to establish the variation of shear strength with matric suction.
- The long time required to achieve equilibrium in soil samples before testing.
- Specialised equipment for unsaturated soil testing is complicated and costly.

As a result of these, filter paper method was adopted in this study to measure pore air and pore water pressure which equivalent to suction for the subgrade soils.

3.5.9 Repeated load triaxial test (RLTT)

This test was conducted as to evaluate the resilient modulus (M_r) of the studied soils. The soils were compacted at a different moisture content as obtained from the moisture-density relationship. To explore subsequent impact of seasonal moisture variation in pavement. Matric suction and M_r relationship of each soil was developed.

Samples, obtained from material passing through No. 4 sieve were oven-dried, as to eliminate possible hygroscopic moisture content. Once the samples had achieved constant weight in the oven, they were removed and allowed to cool. The M_r specimens were compacted and tested at different moisture contents equivalent to the moisture content gotten from compaction test. Standard RLTT was carried out to evaluate M_r of the investigated soils, following CSIR Protocols which is in line with AASHTO T 307, but differs only on specimen size: Standard method of test resilient modulus of soils and aggregate materials. The prepared specimens are 300 mm in height and 150 mm in diameter (Figure 3.22). The machine includes loading frame and software that controls the materials dynamic stress level.

Figure 3.22: Laboratory specimen for M_r testing

Prior to specimen preparation, good quantity of the soil samples were oven-dried at a temperature of 80° C. After which, the soil samples were passed through Sieve 4.75mm size. The maximum particles size material passing sieve 4.75mm was utilized for preparation of the M_r specimens. Once the samples had been processed through the sieve 4.75mm, and appropriate amount of demineralised water was added to achieve

the target moisture content. Following the addition of water, the samples were thoroughly mixed, covered with plastic bags and left overnight to attain mellowing and moisture equilibrium.

The specimens were compacted in the laboratory mould using a vibro-compaction machine, in five layers of equal weight, with the quantities of moisture content obtained from moisture-density relationship.

Figure 3.23: Vibro – compactor setup

The weight of each specimens was recorded after compaction using scale balance, thus height and diameter were of each specimen were measured using Vernier caliper to ensure that the specimens maintained 2:1 ratio of height to diameter. The specimens were wrap with plastic bags, labeled and kept in the chamber for three days to avoid moisture lost (Figure 3.24).

Figure 3.24: Wrapped specimens awaiting resilient modulus testing

Then the prepared specimens were tested one at a time by removing the plastic bag and placing latex membrane around the specimen to protect the inside part of the triaxial cell. A porous stone and filter paper were placed on the bottom base plate. The specimen is then placed on top of the filter paper and porous stone, and another filter paper and porous stone are placed on top of the specimen as well. Immediately, the specimen, porous stones, and filter papers are in place on the base plate, the prepared specimen was loaded to the triaxial frame.

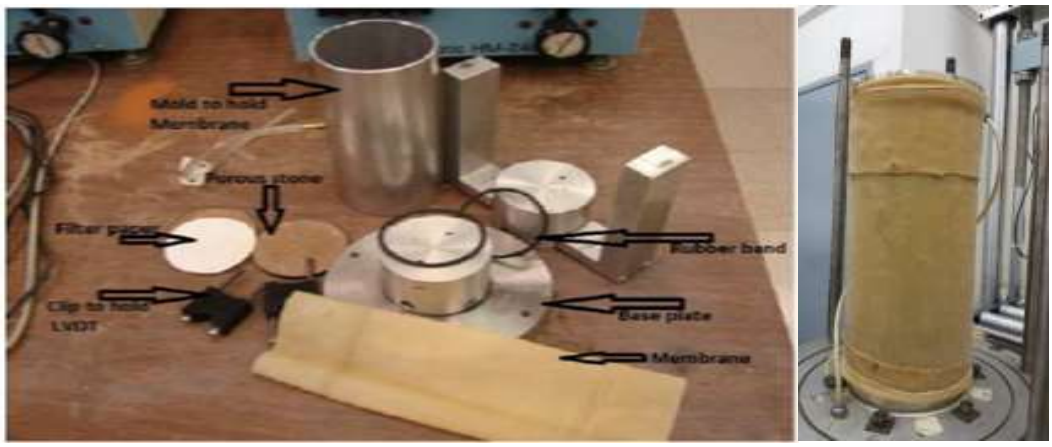

Figure 3.25: Setting – up of resilient modulus equipment

The applied load is measured by RLT device through a load cell, which is positioned around the specimen. This system helps minimise errors associated with the measured loads. Three linear variable differential transducers (LVDTs) were placed between the top plate, base plate and one on the load frame to record the axial displacements. The LVDTs on the body of specimen is installed to decrease the amount of error in the measured axial deformation. The filter paper and porous stone were allowed for free drainage of water from the specimen and the drainage valves were kept close during M_r testing.

Figure 3.26: Complete Repeated load triaxial device

Prior, to M_r testing, shear strength (Mohr circles) of the subgrade soils using static tests at a range of confining pressures was done. This is use as a basis of defining the stress regimes to be used for repeated load testing. Harmonized test methods for laboratory determination of resilient modulus for flexible pavement design," specifies 0.2 -second haversine load pulse and 0.8-second rest period. The total resilient axial deformation response and applied deviator stress were measured. The loading system are function of three different confining pressures, with five different cyclic deviatoric stresses applied at each confining pressure, however, seven different cyclic deviatoric stresses were used in this research. Moreover, each specimen was subjected to 15 different stress states during the course of the testing. A total of 1000 cycles were applied during the conditioning stage to remove imperfections on the top and bottom surface that might occur during compaction. The cyclical load was applied in the form of a sine-wave movement shaped load pulse and this loading sequence best represent the loading conditions experienced by a pavement structure under vehicular or rail track loading. During vehicular loading, some zone in the pavement experiences minimal deviatoric stresses when the wheel load is at considerable distance away from that point. The zone experiences the maximum deviatoric stress when the wheel load is directly on top.

The acquisition system records the data from the last seven load cycles at every stress state, the data obtained from the last five cycles, at each stress, is averaged to provide M_r value. The M_r values were automatically obtained from the software using Equation

3.13, with each test providing 21 M_r values, at different deviatoric stress each specimen.

$$M_r = \frac{\sigma_{cyc}}{\varepsilon_r} \tag{3.13}$$

Where:

σ_{cyc} = Applied cyclical stress

ε_r = Resilient strain

Following the completion of RLT testing, the specimens were carefully removed from the triaxial cell and as well from the latex membrane, and moisture content of the specimens were measured after M_r testing was completed. The test was considered acceptable as the moisture content of each tested specimens was within 0.5% of the target moisture content and the dry density was within 1.3% of the target dry density.

CHAPTER 4: GEOTCHNICAL TEST RESULTS OF THE SOILS

4.1 Overview

The following results and analysis are based on the data gathered from experimental tests conducted on the tested soils. The presented laboratory test results covered the following geotechnical tests: free swell index, swelling stress, modified compaction, suction, CBR, unsaturated CBR and UCS test. The laboratory testings analysis illustrated the geotechnical properties of these subgrades and the results were scientifically interpreted using an average of two specimens of each tested soils.

4.2 Density–Moisture Relationship

Soil compaction is one of the most critical components in the pavement construction, airfields, rail tracks, embankments, earth dam and foundations. Stability of structure depends mostly on the achievement of proper soil compaction. Failure to achieve proper ground compaction, is somewhat causes failure of pavement, rail track and airfield. However, higher compaction degree aggrandizes the geotechnical specifications of the subgrade. This aids to achieve the desired degree of relative compaction, required to ascertain specified properties, fittingly for shear strength resistance (Jaquin et al., 2009). Compaction process has proven the link between the density-moisture relationships with shear strength and helped in clarifying the aspects of cementation. Tarantino and De Cole, (2008) reported on the response of clay materials under compaction as the most important factor influencing compaction process (i.e. moisture status of soil).

4.2.1 Effect of moisture content on compacted FSS

Moisture-density relationships for FSS was established according to TMH1 method A7, using modified proctor compaction technique. Basically, it was observed that the density of the FSS decreases with increase in moisture content (Mc) and this lead to the soil displaying flocculated structure at moisture content less than the OPT. Whereas, at optimum moisture content (OPT) the soil portrayed a more aggrandize structure. Though, moisture content on the dry side is low due to more predominant attractive force compared to repulsive forces. This resulted into a flocculated structure as the Mc increased beyond the optimum, as a result of increased repulsive forces that caused the soil particles to orient into a more dispersed structure Figure 4.1.

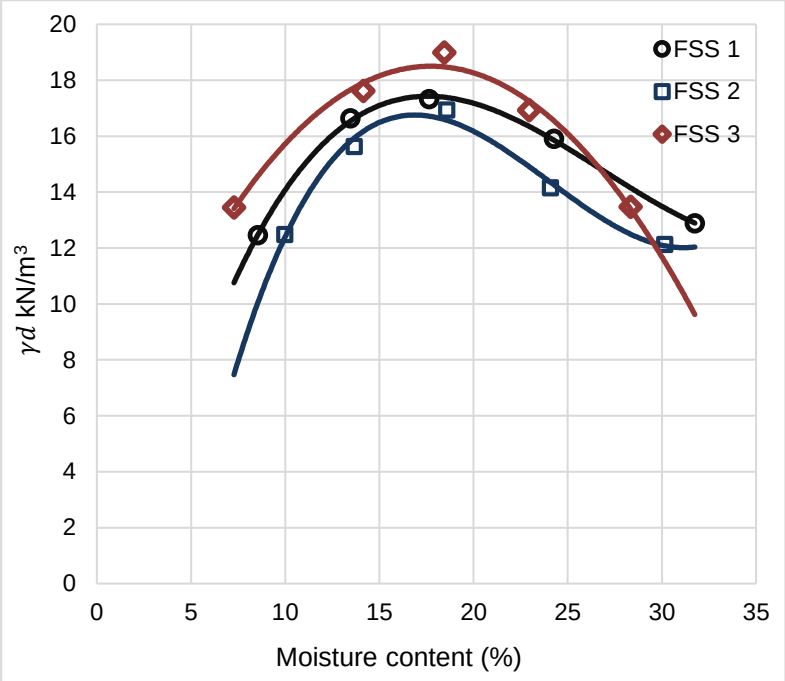

Figure 4.1: Moisture – Density Relationship of FSS

4.2.2 Effect of moisture content on compacted NCS

Moisture content strongly influenced NCS (Figure 4.2), due to high percentage of fine content in the soils > 50% with specific gravity of 2.69, 2.72 and 2.70 for NCS 1, 2 and 3 respectively. The curve showed that NCS portrayed bell-shaped compaction curves which confirmed the soils, typical clayey soil. Furthermore, the dry unity weight of the soil starts to drop as the moisture content begins to increase. This is caused by the capillary force effects, as the pore space of the soils begins to inhibits moisture. The soil particles tends to move around and portrayed less densely compacted soil matrix, due to more absorbed moisture on the wet side of the curves. However, the soil possesses a flocculent structure on the dry side of the optimum, as a result of the low moisture content. While on the wet-side, a diffused behaviour of the soil was observed causing the layers of ions surrounding the clay particles to be scattered. Hence, the interparticle repulsion was reduced resulting in a more random particle orientation thereby caused the soils to record higher MDD compared to FSS.

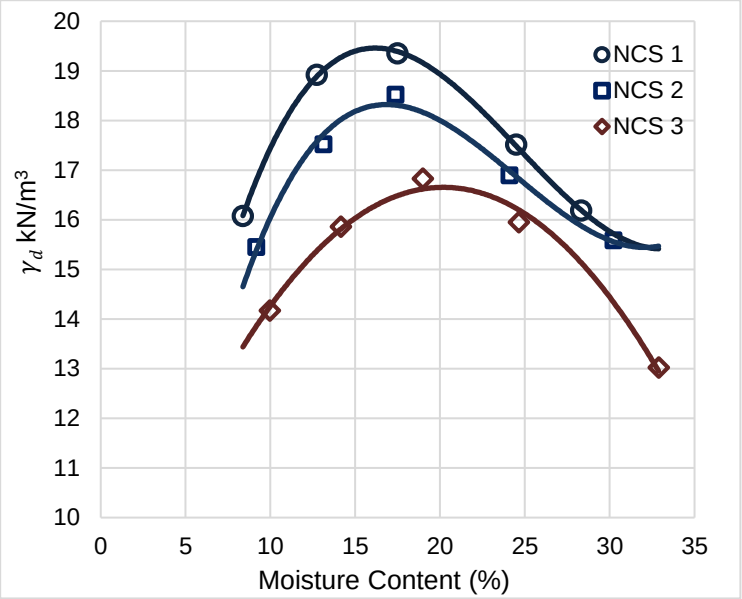

Figure 4. 2: Moisture – Density Relationship of NCS

4.2.3 Effect of moisture content on compacted GPS

Generally, the comprehensive results of compaction experiment displayed in the form of moisture content-unit weight showed in Figures 4. Considerably varied, but showed reasonable well-defined maximum dry unit weight at given moisture content. As the Mc of the compacted soil increases, the diffuse moisture around the soil particles expanded. This increased the repulsion forces within the clay particles of the soils and resulted in higher degree of flocculation that caused higher dry unit weight on the dry side.

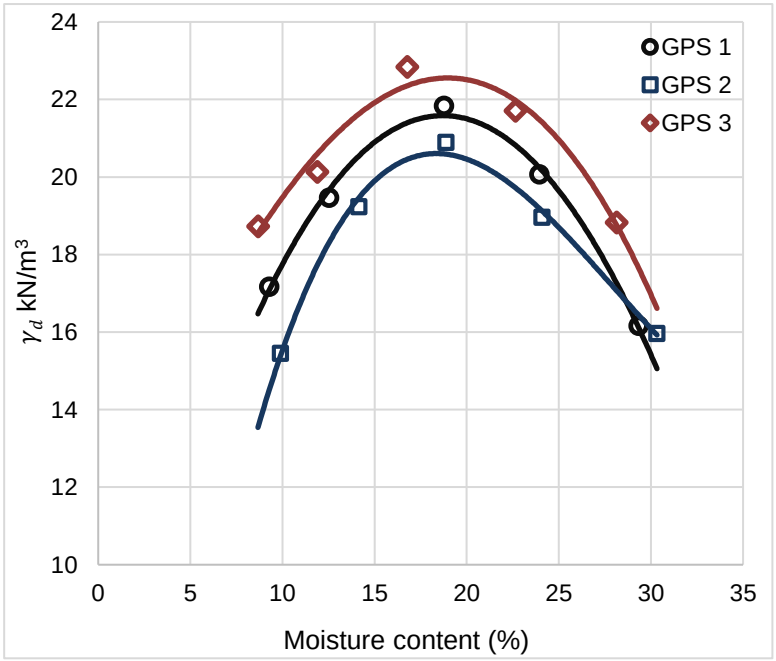

Figure 4. 3: Moisture – Density Relationship of GPS

The continued addition of moisture expanded the layers and resulted in a continued increase of repulsion within soil particles. Thus, causing greater degree of particle orientation and more dispersed structure on the wet-side. At given moisture content, compaction effort yielded more parallel orientation of the clay particles. This caused the soil particles to fuse more closely and trigged higher unit weight. Basically, similar trends were observed in Figures 4.1 through 4.3 which depicts that moisture contents increases with increase in dry unit weight and begins to drop rapidly at the point beyond the optimum moisture content.

4.2.4 Post-compaction soil behaviour

Compaction of soils is common in earthwork construction like: embankments/dams, fills for low-lying areas, pavement foundation, rail tracks and airfield. The primary aim of compaction is to achieve higher strength, lower compressibility, and lower permeability. Laboratory compaction test was carried out by applying modified Proctor compaction, as recommended by TMH1 method 7. Post-compaction soil behaviour of the tested subgrade soils was evaluated in laboratory, after MDD and OMC of the soil were determined, the soil specimens were kept under observation for various days i.e. 7, 14, 28, 56, 90 and 120 days, see Figure 4.2.

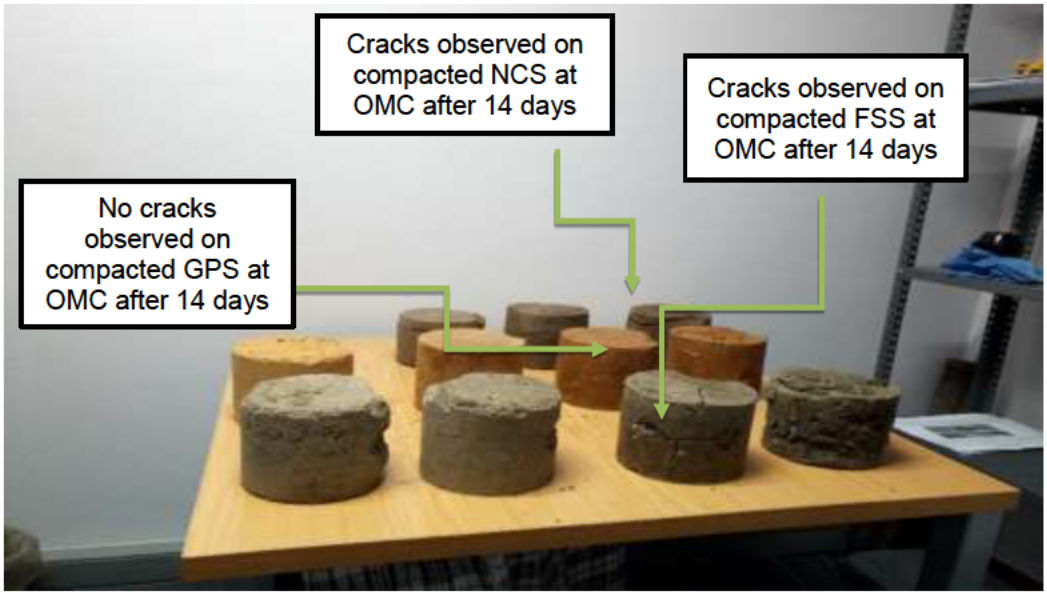

Figure 4.4: Post compacted soils Behaviour

The compacted subgrade soils especially FSS and NCS exhibited high swelling potential at the optimum and at a point beyond the optimum. Whereas, GPS does not

show any form of cracking. Nonetheless, at a point before the optimum, no cracks were observed. The post compaction behaviour of the soils is in line with the XDR result in Appendix A. The result classified FSS as highly expansive and NCS as moderate expansive. This is considered as one of the most serious challenges geotechnical engineer faces, due to potential danger of unpredictable upward movements of the subgrade. This swelling stress causes fatigue and cracks to the pavement structures identified across Free state and Northern cape. Hence, swelling behaviour of the compacted soils is importance, for pavements within this province. The high swelling potential of this studied soils could be attributed to the soil capillarity, as the voids within the soil structure are filled with moisture. Basically, during capillary process, moisture is absorbed by the interlayer particles of the clay minerals causing an increase in volume. After the moisture capillarity, voids are filled by the swollen expansive clay minerals like montmorillonite, kaolinite, bentonite etc. As such, the montmorillonite within the soil swells and the swelling increases as the amount of clay minerals increases until the swelling pressure equilibrates with the amount of moulding moisture content. However, after 3 days of compaction the total volume of the soil is restricted due to the compaction efforts. Furthermore, at a period beyond 7 days the soils swell and occupied all the volume available, thereby initiating cracking on the compacted soils.

The pressure caused by this process is known as the swelling pressure. Rationally, it will be ideal to compact expansive subgrade at a point below the optimum moisture content and provide high thickness of pavement wearing surface, in order to overcome swelling pressure during pavement design.

4.3 Analysis of Swell Potentials

Determination of swelling stress in expansive subgrade soil is important for numerous engineering applications. Damages caused per year by expansive soils has been reported to be more than all other natural hazards combined, including earthquakes, floods, and tornadoes (Chen, 1988). Expansion susceptible stress occurs as the Mc of the subgrade soils increases. Upon expansion, the soil exerts an upward stress on pavement and when this stress exceeds the limit state of stress in pavement, fatigue and cracks manifest. Then uplift or differential uplift occurs causing pavement to cracks. Therefore, assessing swelling pressure becomes important step in designing of pavement on expansive soil. Two swelling tests were used in this study to measure the swelling potential and swelling stress i.e. Free swell index test (FSI) and Zero swell test

(ZST) of the studied soils confirmed the tested soils to possess some expansive characteristic.

4.3.1 Free swell index (FSI) results

FSI results of the studied soils is consistent with Atterberg limit results, which identified FSS as high expansive soil, while NCS and GPS were quantified to be moderate with low degree of expansiveness.

Table 4.1: Free Swell Index Results

Soil Samples	V_k (ML)	V_s (ML)	FSI (%)	Degree of expansiveness
FSS 1	10	15	70	35-50 very high
FSS 2	10	15	80	Very high
FSS 3	10	15	65	Very high
NCS 1	10	15	70	35-50 high
NCS 2	10	15	80	Very high
NCS 3	10	15	80	Very high
GPS 1	10	15	30	20-35 moderate
GPS 2	10	15	50	50 high
GPS 3	10	15	20	<35 low

4.3.2 Zero swell stress result (P_s)

Figure 4.5 through 4.7 illustrates pressure stress against five sets of dry densities at varying Mc for the studied soils. This result shows that variables such as dry density, moisture content and percentage of clay fractions greatly affected swelling pressure of the subgrade soils. Furthermore, FSS 1, 2 and 3 in Figure 4.5 showed that higher P_s is obtained at lower moisture content and lower P_s is recorded at higher Mc. The soils behaviour is in consistence with the report published by (Rasheed, 1985). Values of P_s for different Mc are summarised in Table 4.2 Appendix B.

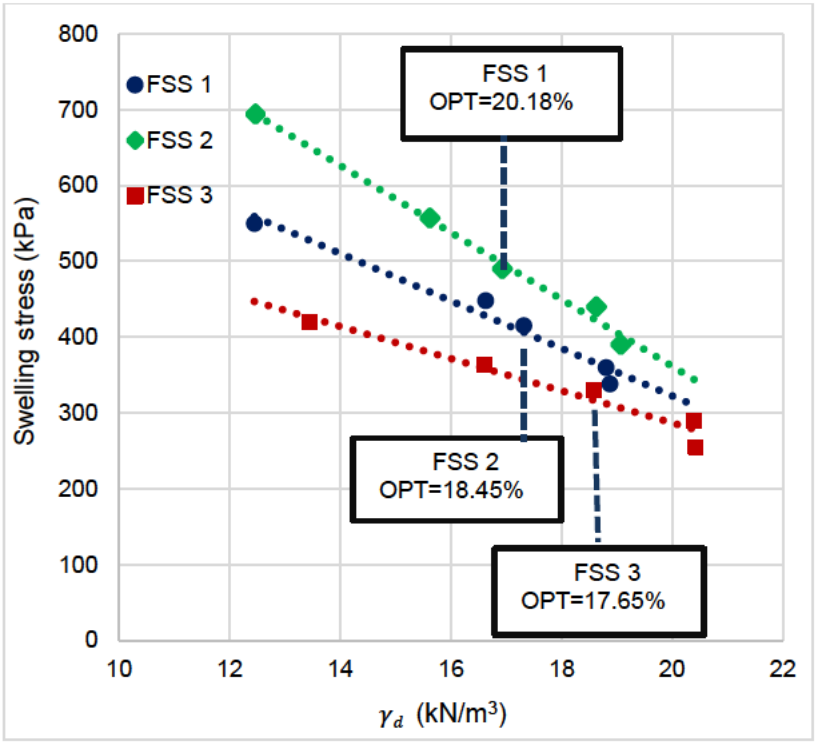

Figure 4. 5: Swelling pressure with varying dry density for FSS

Figure 4.6 illustrated the relationship between the measured P_s and initial dry density. The P_s increases with initial dry density of the soils. As the dry densities continues to increase the P_s begins to drop. The soil with higher percentage of clay minerals (i.e. bentonite and illite) according XRD result, recorded the highest value of P_s. This implies that higher P_s was recorded at lower Mc and swell stress varies with soil type, as a result of different clay minerals that are presence in the tested soils. Though, similar trend was observed in all the tested soils as NCS 1, 2 and 3 recorded P_s of 499 kPa, 553 kPa and 759 kPa respectively.

This shows that NCS 3 has 206 kPa and 260 kPa more P_s compared to NCS 2 and 1. As shown in Figure 4.6, NCS 3 will require more pressure either from compaction exercise or from the pavement surface course as to overcome the effect of P_s on the entire pavement structure. Therefore, designing the structure to counter the swelling stresses from the subgrade is important.

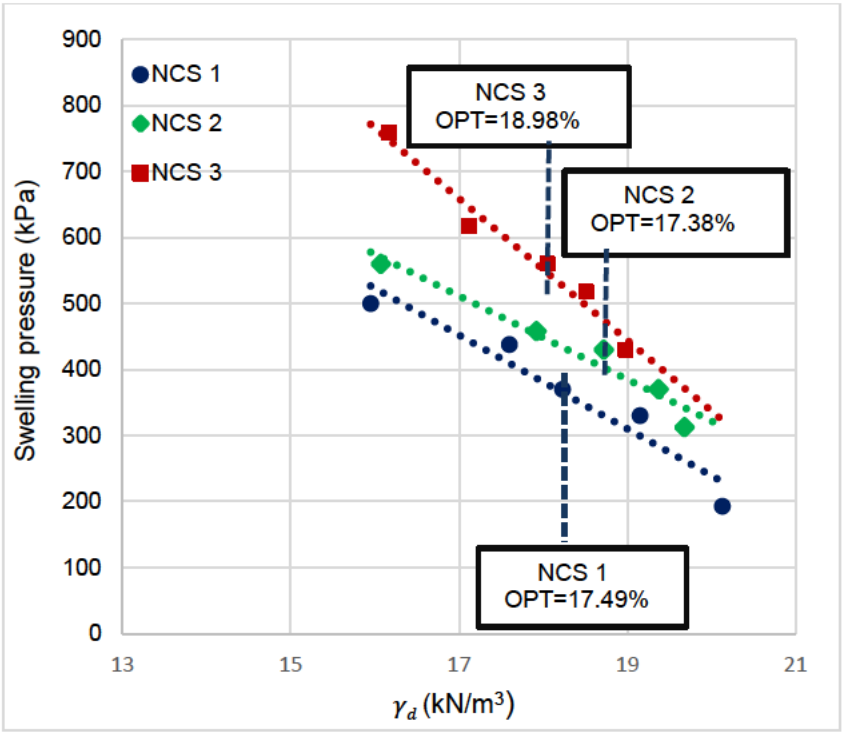

Figure 4.6: Swelling pressure with varying dry density for NCS

Figure 4.7 depicts the swelling stress results for GPS at various dry unit weights. The results indicated that P_s increases with dry unit weight for all the tested soils. Furthermore, the soil with higher fine content recorded the highest P_s. This result is in consistence with the study by Erzin and Erol, (2004) that states that the higher the value of initial dry density of a given soil, then lower the swelling potential. Therefore, the magnitude of P_s increases significantly with initial density of a particular soil. Based on the laboratory results, it was observed that the soil parameters that influenced P_s are: clay mineralogy, clay content, soil water chemistry, soil moisture deficiency, soil structure and fabric and dry density.

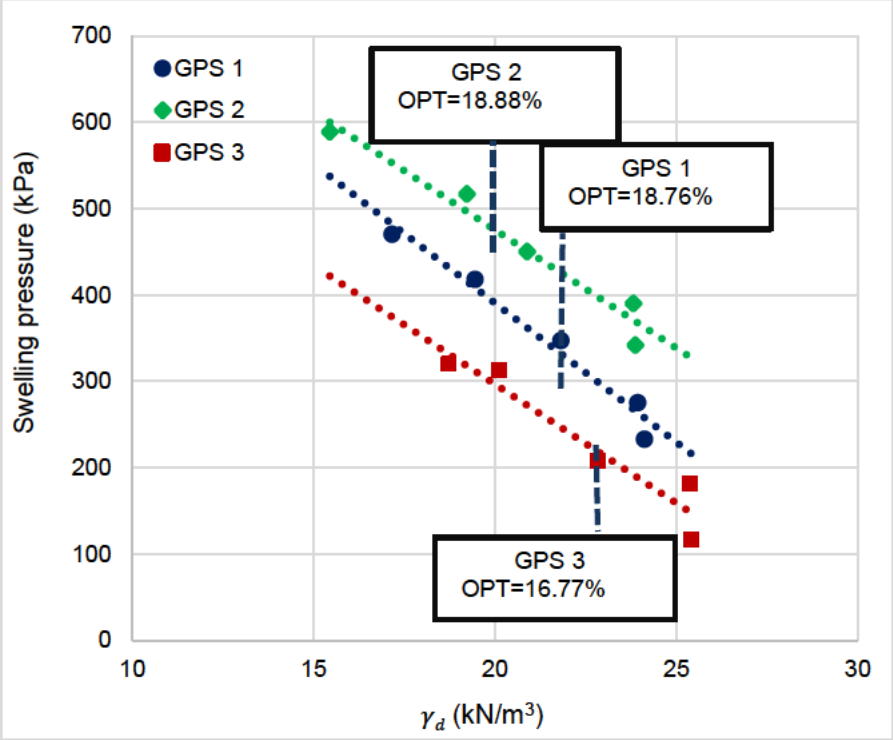

Figure 4. 7: Swelling pressure with varying dry density for GPS

The result from swelling pressure test, could be applied in pavement design, due to surcharge loading effects in subgrade swelling activity. In order, to apply surcharge load on pavement design procedure, it is required to determine the depth of the active unsaturated zone and the maximum swell pressures by employing ZST technique. The swelling stress values of the tested soils are summarised in Table 4.2 Appendix B.

4.4 Analysis of Filter Paper Results

Total, matric and osmotic suction values of the nine subgrade soils were obtained at different Mc. The shrinking and swelling of soil are caused by the movement of water within the soil voids. Thus, water is removed from the pores as the soil dries and suction sets in, causing the particles to settle and compact. This movement usually causes erratic damage to rail tracks and pavement structures This moisture movement causes structural load redistribution, that triggers failure due to large changes in shear forces on subgrade. The effects of P_s is usually neglected by design engineer during pavement design on expansive subgrade. Therefore, suction is considered important in the design of pavement structure.

4.4.1 Total, matric and osmotic suction results

Filter paper method was adopted to measure suction of the studied soils. This technique is on the basis that water potential of the soil reaches equilibrium with the filter paper water potential. Whatman No.42 filter paper calibration curve developed for this study was used to estimate the soil suction at equilibrium moisture content. Total and matric suctions were determined on the samples compacted at varying different moisture conditions. Whereas, osmotic suction was calculated from the difference between total and matric suction.

Various properties of unsaturated soil, such as the swelling stress, the volume variation, and hydraulic conductivity, is relative to moisture quantity within the soil's voids for a given soil potential. Thus, the relation between the water content (gravimetric water content, volumetric water content) and the soil potential is an essential feature under unsaturated soil mechanics. Suction curves against gravimetric moisture content for the soil sampled FSS 1, 2 and 3 are presented in (Figures 4.8 through 4.10). Generally, it was observed that total and matric suction recorded high suction values, due to low Mc. Whereas, FSS 2 yielded the highest matric suction values among FSS 2 and 3. This implied that high capillary stresses in the soils causes movement of water in an unsaturated state. This replicates real filed condition for typical unsaturated pavement structure. Thus, this result is consistence with the reported by Yang et al. (2005). Furthermore, on the dry side of the optimum FSS 2 recorded the highest matric suction value of 6517 kPa, while FSS 1 and 3 yielded 5941 kPa and 5598 kPa respectively. The curves demonstrated that matric suction dominates 82% component of the soils total suction (Leong et. al, 2003). This was as a result of soils capillarity, pore size distribution and the physiochemical interactions, which are highly dependent on the soil mineralogy that governs suction. The data for the curves is presented in Table 4.3, Appendix B.

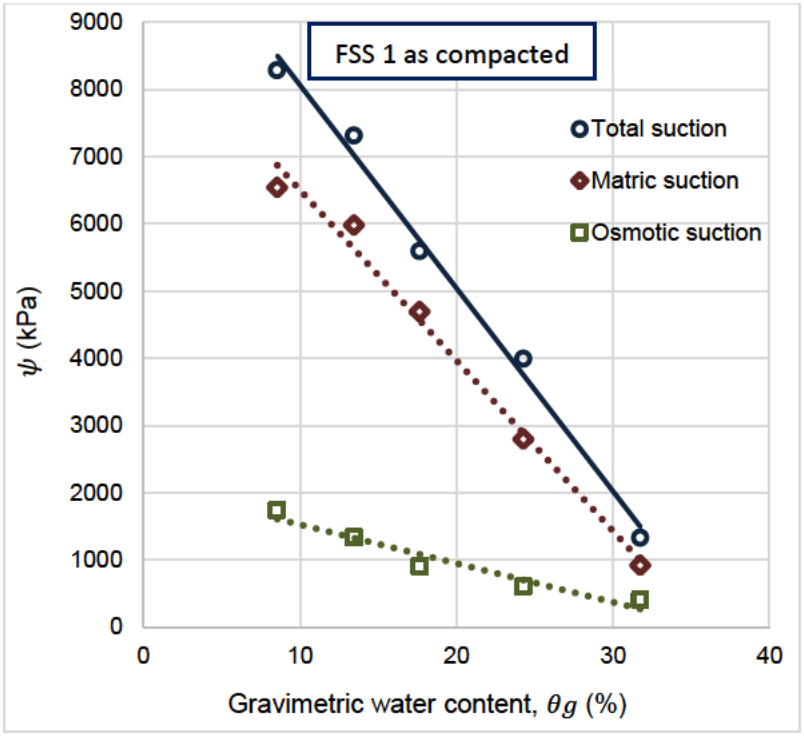

Figure 4.8: Suction, ψ versus gravimetric water content curve

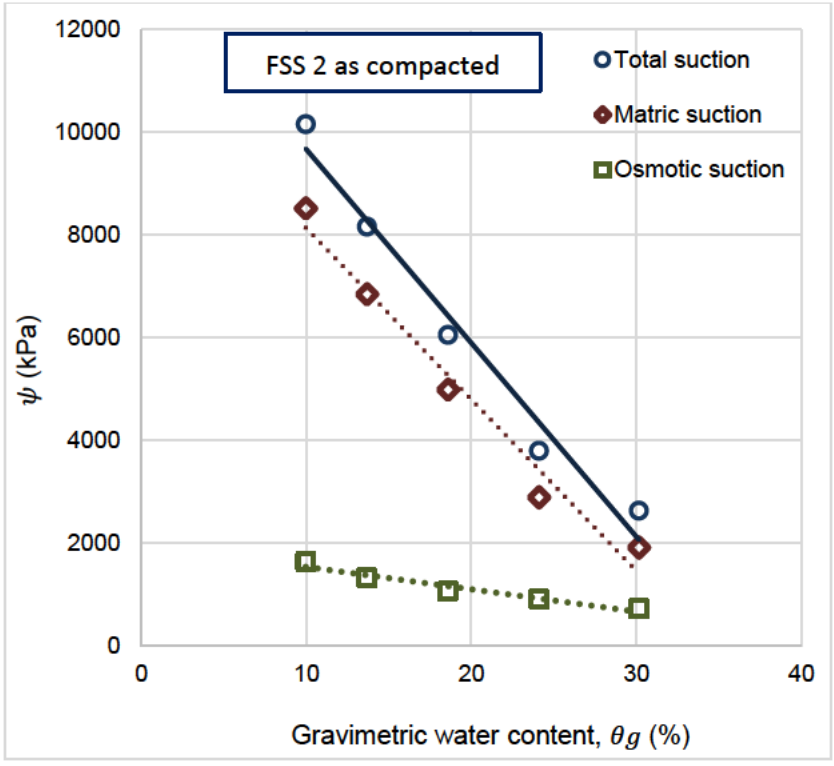

Figure 4.9: Suction, ψ versus gravimetric water content curve

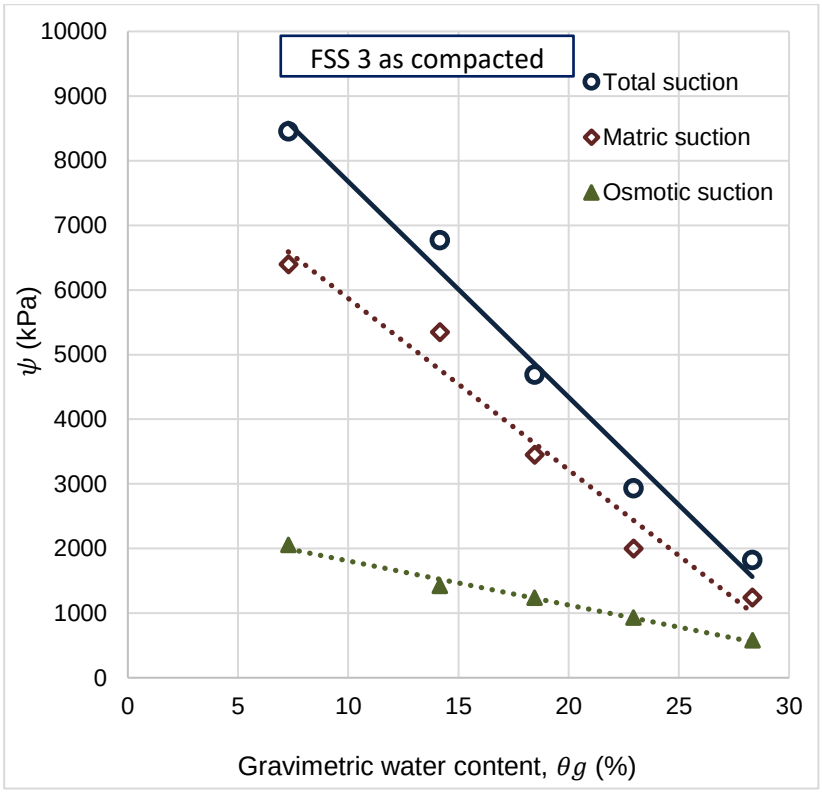

Figure 4.10: Suction, ψ versus gravimetric water content curve

Figure 4.11 through 4.14 depicts the suction matric behaviour of NCS. These curves demonstrated that the suction response of the soils is associated with capillary action. The interface tension between water and air within soils voids created a curve interface boundary in a narrow opening, leading to a high suction pressure. The capillary rise that occur within these soils was affected by its particle size and grading. It was observed that NCS, sustained large pressure difference between pore water and air, allowing large capillary rises, because of the qualities of soils fine-grained. The soils would have behaved differently, if it contained coarse grained with larger voids.

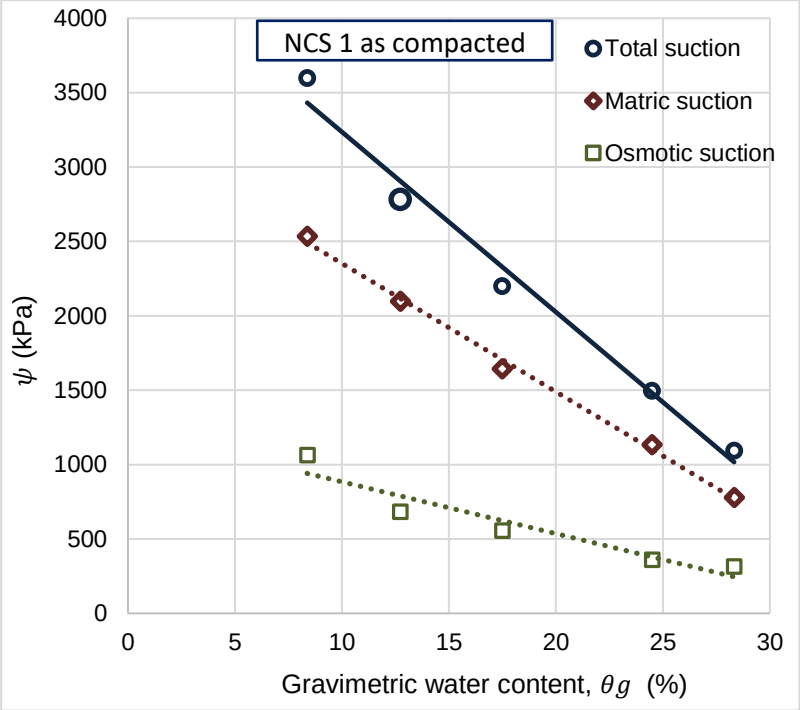

Figure 4. 11: Suction, ψ versus gravimetric water content curve

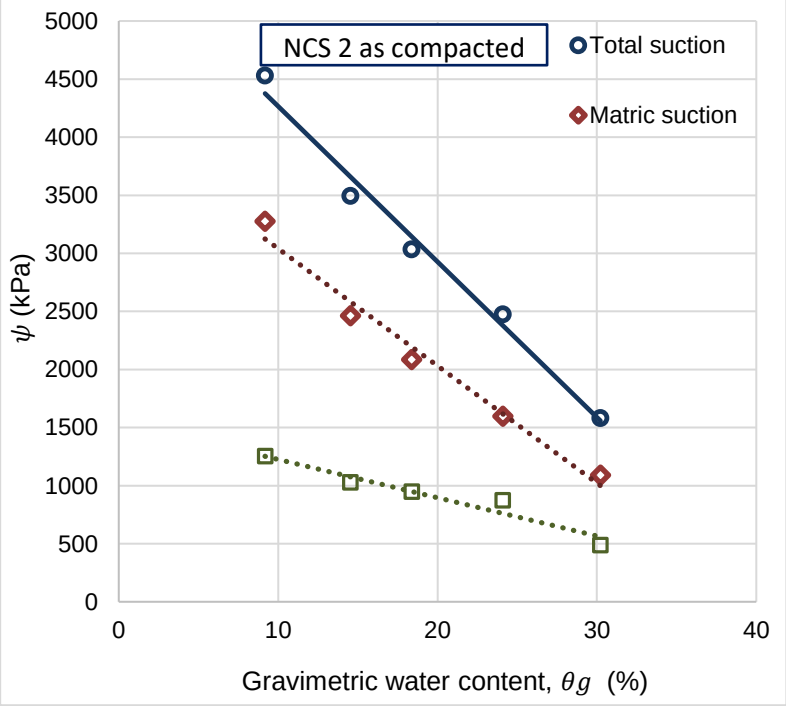

Figure 4. 12: Suction, ψ versus gravimetric water content curve

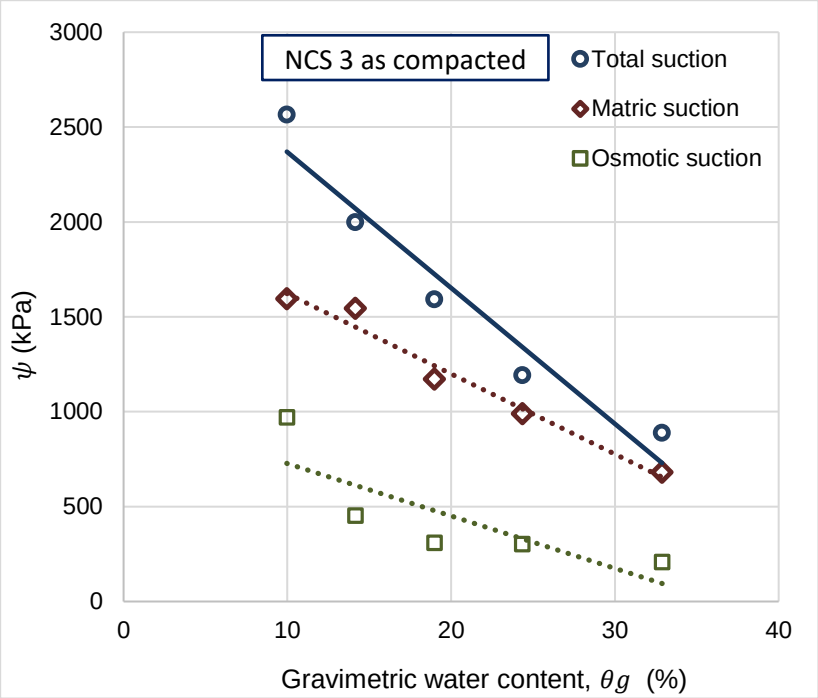

Figure 4. 13: Suction, ψ versus gravimetric water content curve

The relation between the soil suctions total, matric, and osmotic suction with the corresponding gravimetric water content was investigated for each tested soil and are depicted graphically. The compacted soils suction i.e. GPS 1, 2 and 3 obtained by filter paper method are presented in Figures 4.14 through 4.16. The curves of the tested soils showed that total and matric suctions insidiously decreased with an increase in the initial water content. The measured total and suction matric response of the tested GPS were found to be similar to FSS and NCS. The difference between total and matric suctions at low water content was as a result of proper contact between the filter paper and the soil specimens. The measured total suctions were greater than the measured matric suctions as was anticipated.

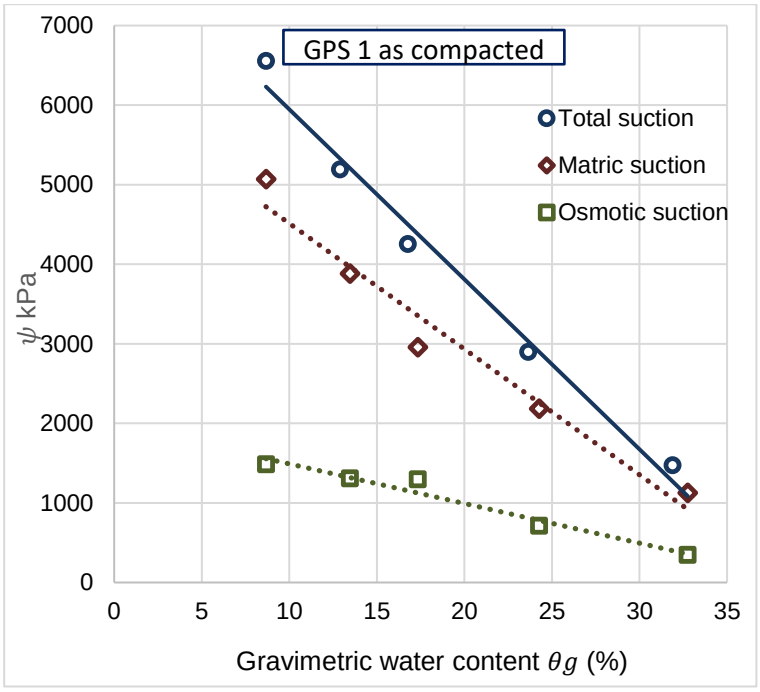

Figure 4. 14: Suction, ψ versus gravimetric water content curve

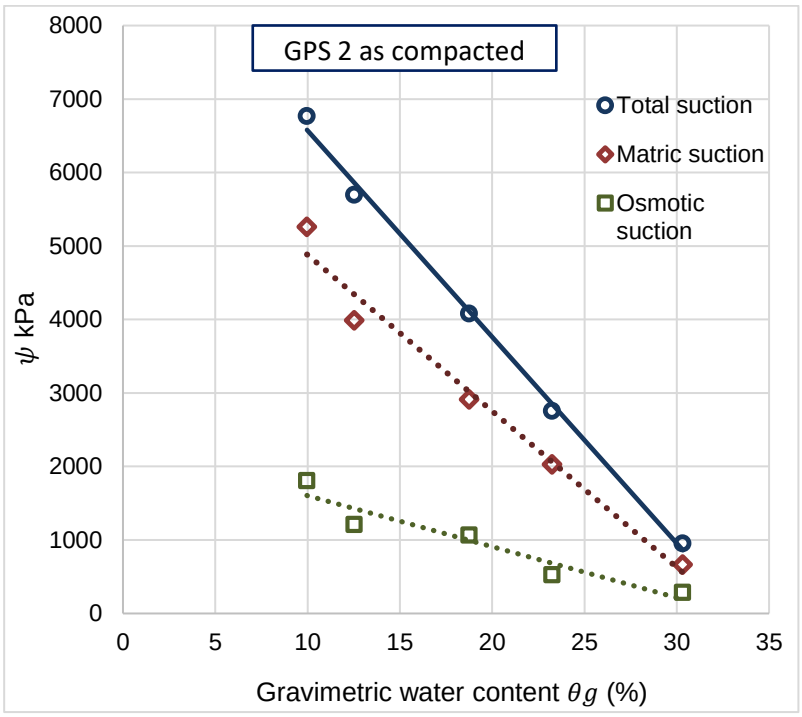

Figure 4. 15: Suction (ψ) versus gravimetric water content curve

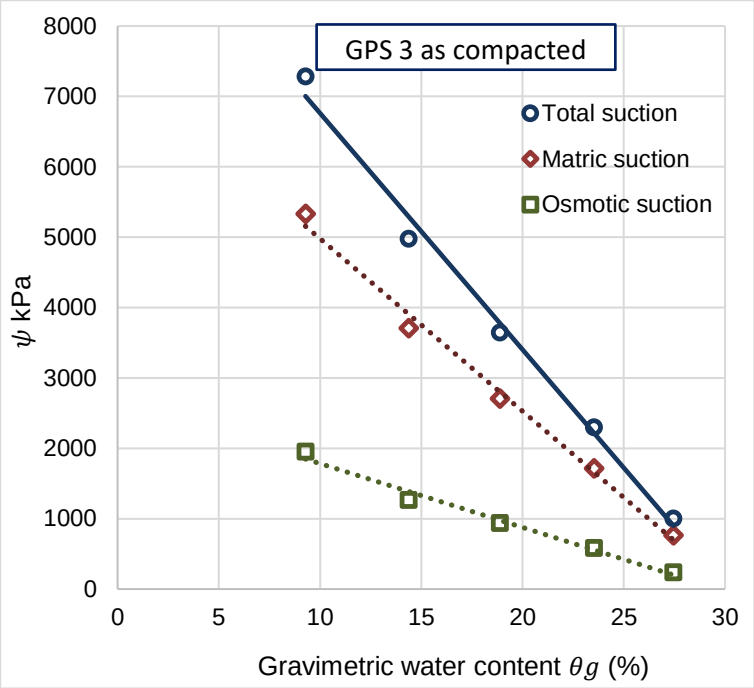

Figure 4.16: Suction (ψ) versus gravimetric water content curve

Conclusively, the difference between total and matric suction values for FSS 1, 2 and 3 varied from 1742 kPa to 404 kPa, 1641 kPa to 721 kPa and 2056 kPa to 578 kPa respectively from the dry side of the optimum (DOP) to the wet side of the optimum (WOP). While, the differences between total and matric suctions for NCS 1, 2 and 3 on the varies between 1064 kPa to 208 kPa, 1254 kPa to 490 kPa and 971 kPa to 208 kPa respectively. The differences between the total and matric suction values for GPS 1, 2 and 3 changes between 1483 kPa to 344 kPa, 1808 kPa to 289 kPa and 1949 kPa to 235 kPa. This result show that fine content and moulding water content of the soils have measurable effect on suction values of all the tested soils. In addition, the relationship between the total, matric suction and the filter paper water content. are approximately linear. This indicated decrease of suction with increase of the filter paper water content.

4.4.2 Soil-water retention curve (SWRC) of the tested soils

SWRC is the principle property of unsaturated soils (Fredlund et al., 2012). The SWRC for the studied soils are plotted using suction matric and volumetric water content ((θ_v) as recommended by Fredlund et al. (2001) for geotechnical engineering Figures 4.17 through 4.25.

Based on the filter paper for soil-water retentivity, FSS, NCS and GPS displayed adsorptive unimodal shapes. As such, the experimental test data were best fitted with three different SWRC models developed by Van Genuchten 1980; Fredlund and Xing 1994; and Seki 2007 with a correction factor using a least squares regression. An Optimizer was used to optimize the parametric models to the measured data, followed by an iterative exercise for the best sum of squared residuals (SSR) differences between the predicted and measured SWRC values. The sum of the SSR and Akaike information criterion (AIC) is an indication of how well the models fitted the measured data. Generally, it was observed that Seki's model best fitted the experimental data of the studied soils with R^2 ranging from 0.92 to 0.99, compared to the other models. The SWRC parameters are summarized in a Table 4.4 through 4.6 Appendix B after the each SWRC for the studied soils.

The SWRC for FSS 1, 2 and 3 demonstrated increased suction as the θ_v values decrease. This trend is consistent with other research studies reported by Sivakumar and Wheeler, (2000), and Agus and Schanz, (2006) that shows strong dependency of suction matric on the compaction Mc of the soil. The full saturation Mc remained constant up to the air entry value (AEV) of 132 kPa, 158 kPa and 113 kPa for FSS 1, 2 and 3 respectively. The soils with more fine content recorded the highest AEV, according to the particle size distribution of the investigated soils, FSS 2 contained 96.39% fine compared to FSS 1 and 3 that contained 91.38% and 75.38% respectively.

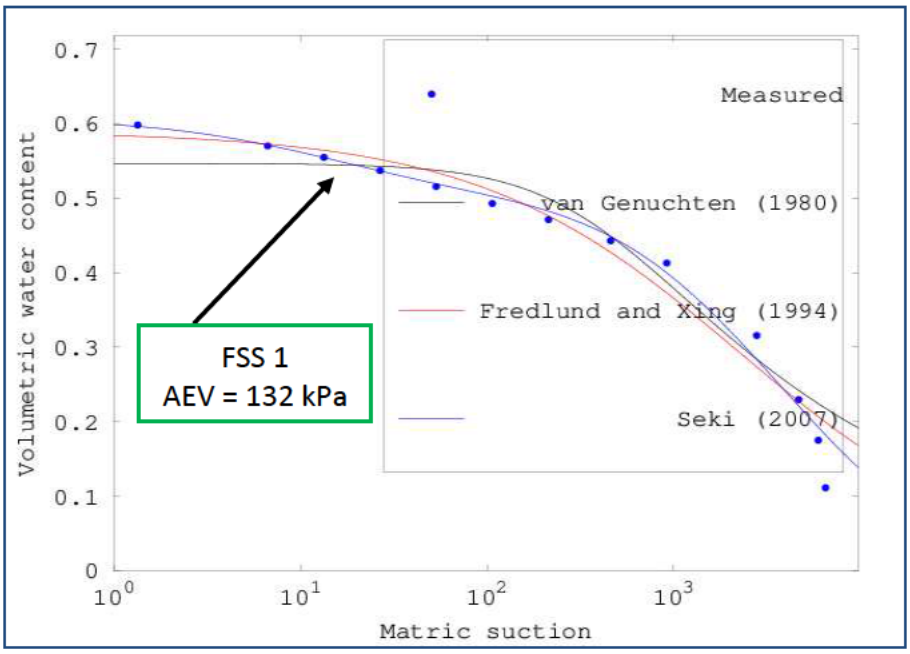

Figure 4. 17: FSS 1 soil water retention curve

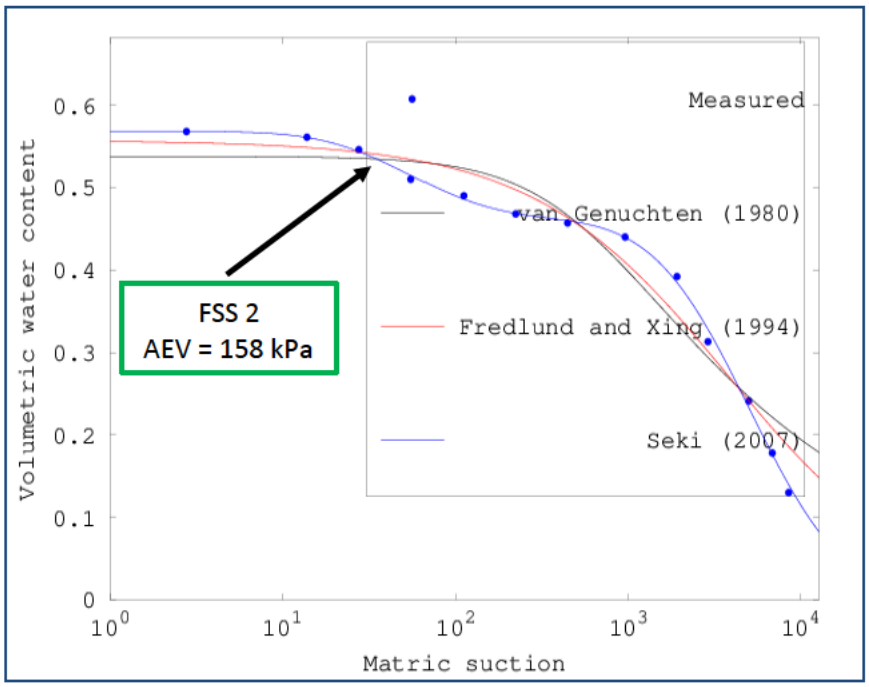

Figure 4. 18: FSS 2 soil water retention curve

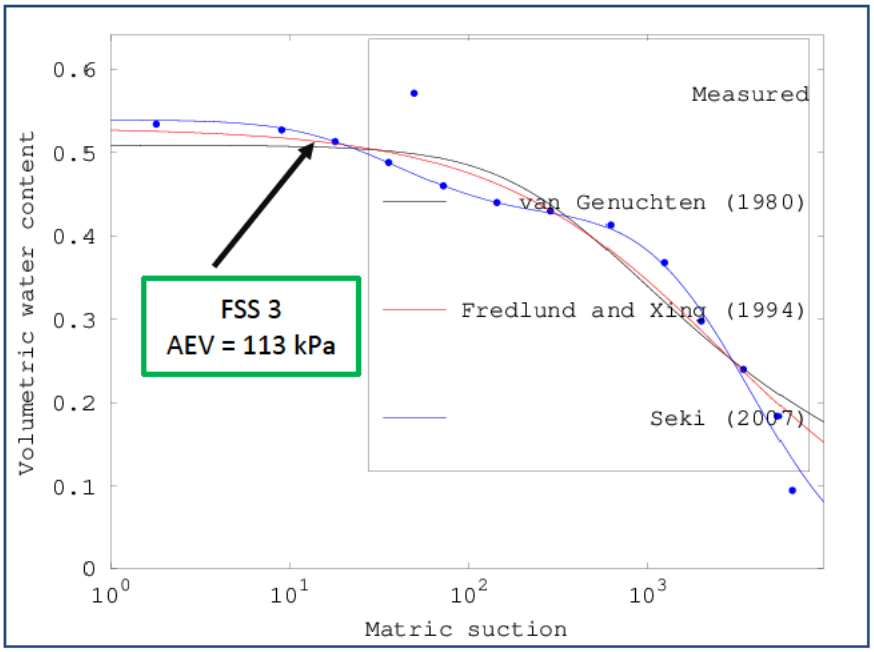

Figure 4. 19: FSS 3 soil water retention curve

The correlation between variation in θ_v and suction for the NCS 1, 2 and 3 are illustrated in Figure 4.20 through 4.22. NCS 1 revealed that Mc, begins to desaturation at AEV of 101 kPa. While, NCS 2 and 3 recorded AEV of 128 kPa and 135 kPa respectively.

This behaviour is best described by the different pore spares distribution possessed within the soils. Thus, this implied that matric suction at which NCS 1 starts to become desaturated is lower compared to NCS 2 and 3. Though, AEV of this subgrade soils varies because of their particle size distribution and intra-particle voids, therefore this contributed to increase in capacity of the soils to maintain saturation.

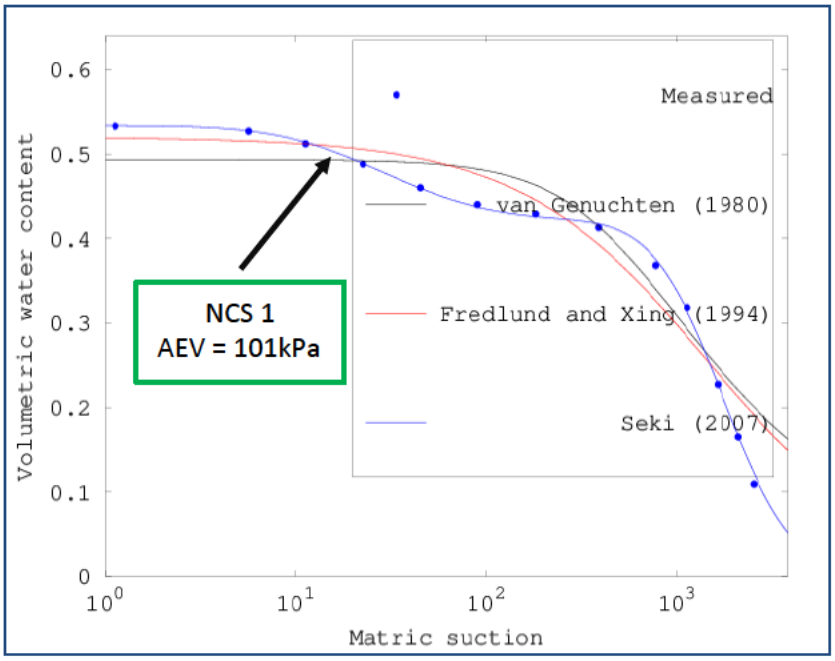

Figure 4.20: NCS 1 soil water retention curve

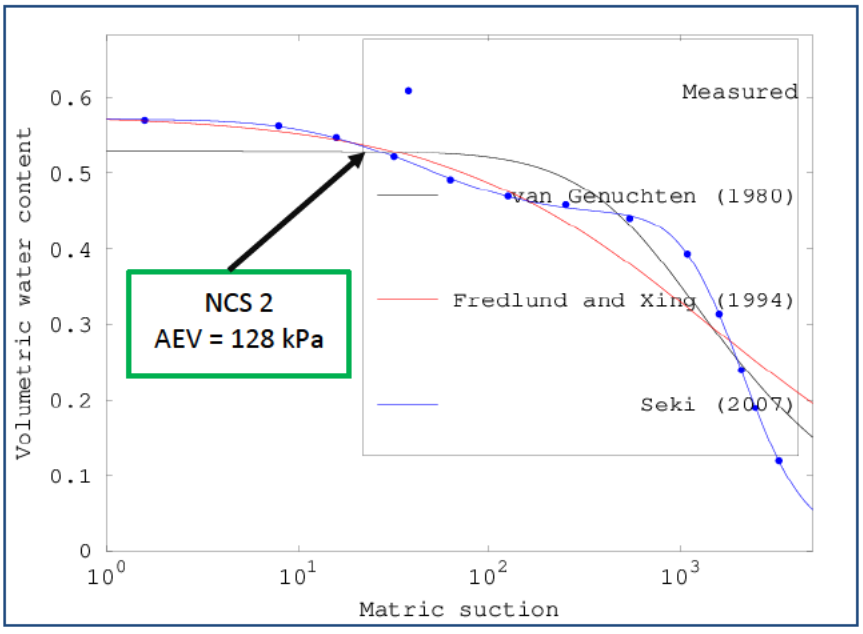

Figure 4.21: NCS 2 soil water retention curve

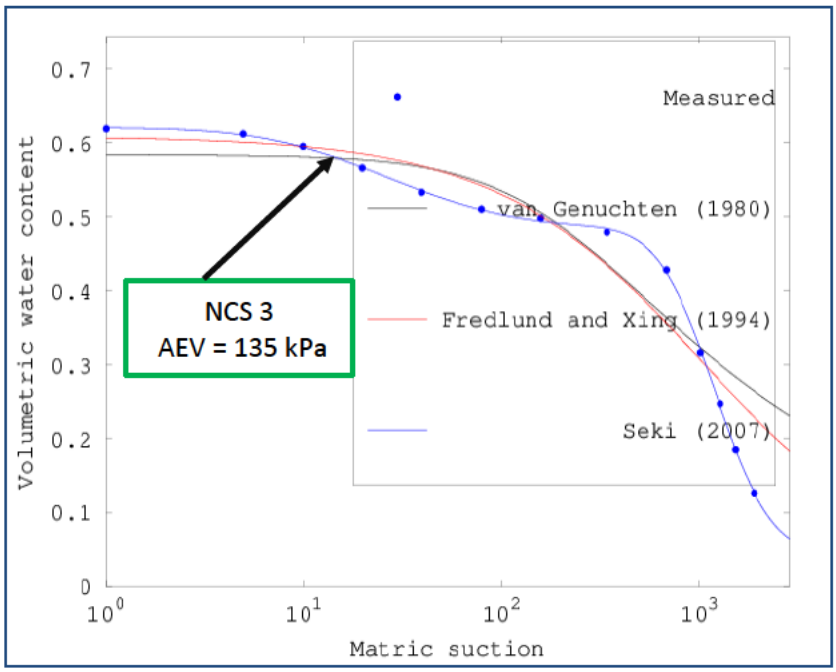

Figure 4.22: NCS 3 soil water retention curve

Figures 4.23 through 4.25 demonstrated SWRC of GPS and similar trend of hysteresis response were observed as the soils suction increase with θ_v decrease at suction range of 124 kPa to 105 kPa for all the soils. The AEV of the soils are 201 kPa, 215 kPa and 153 kPa for GPS 1, 2 and 3 respectively. In addition, the final Mc at the end of the adsorption curve is high than the start points of desorption curve. This finding is consistent with the results obtained by Wang (2000) for a similar expansive soil.

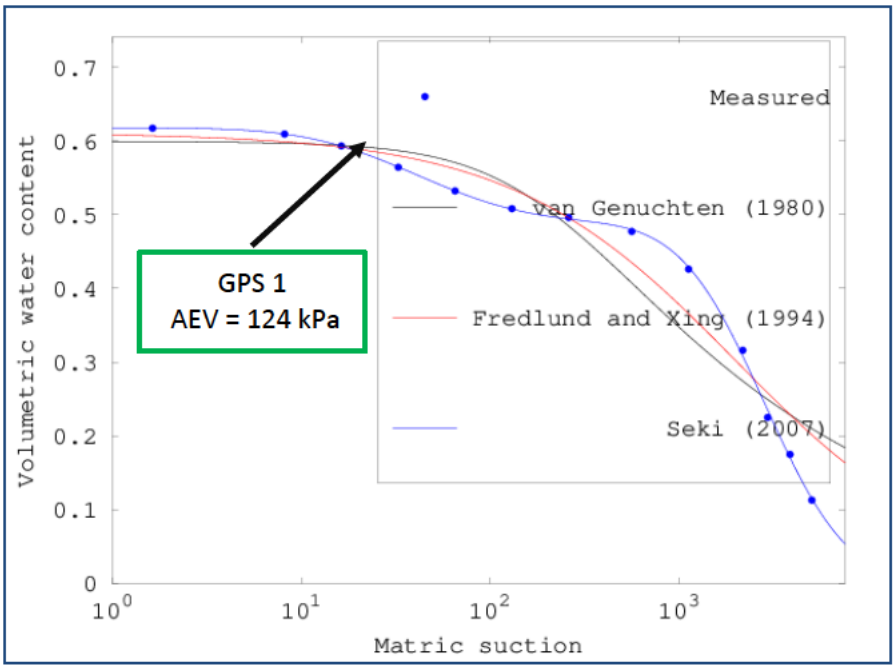

Figure 4.23: GPS 1 soil water retention curve

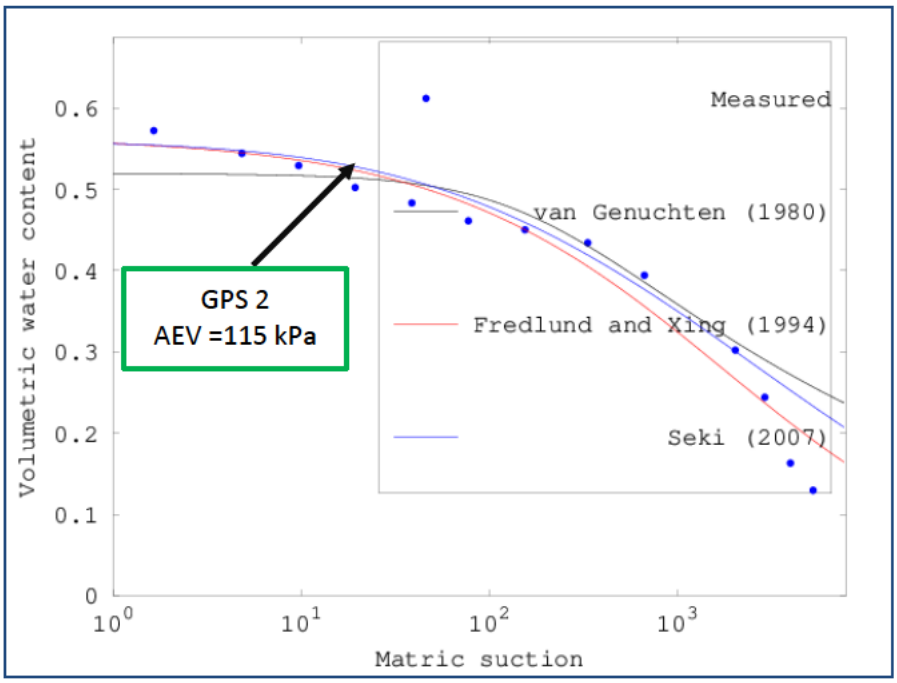

Figure 4.24: GPS 2 soil water retention curve

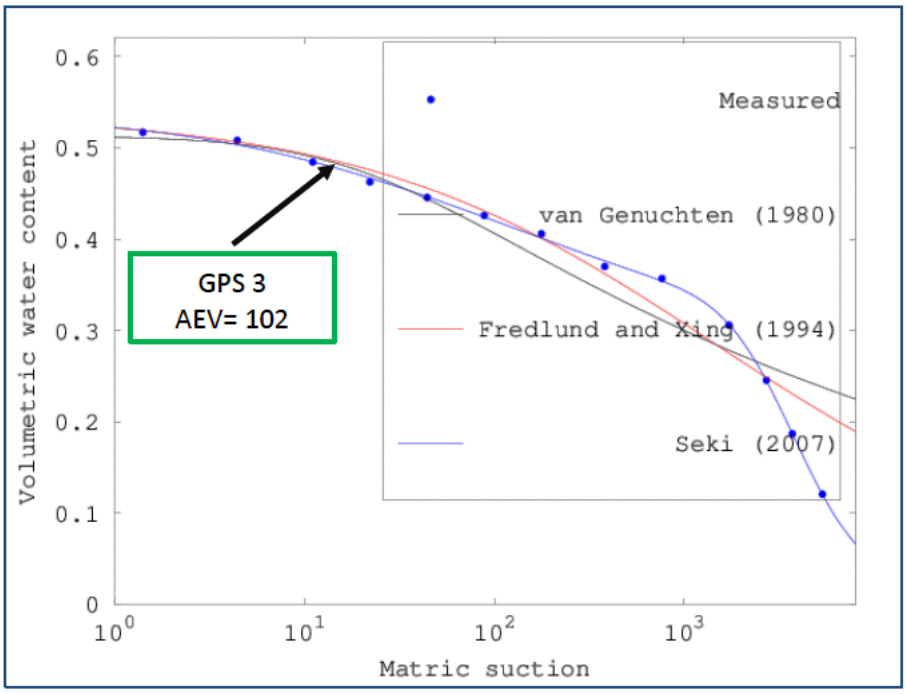

Figure 4.25: GPS 3 soil water retention curve

In conclusion, regardless of the θ_v presence, the shape of the SWRCs are inherently similar. However, FSS which has the largest clay fraction and smallest pores, amongst the tested soils recorded higher AEV values.

Based on the SWRC in Figures 4.17 through 4.25 it is clear that the matric suction-θ_v relationship is unique for each soil type due to the dependence of the soils pore size distribution and the physiochemical interactions, which are highly dependent on the clay minerals. Quick comparison of suction results with the soil plasticity test, revealed that high PI soils recorded higher range of suction during desaturation as compared to the soils with lower PI values that undergo desaturation over a small range of suction values. This was due to capillary forces, which is the main water holding mechanism in low PI soil and this dominates lower suction range of the soil. Whereas, surface adsorptive forces play a large role in holding water in high PI soils. As such, the AEV of the tested soils depends on the pore size distribution, such that soils with smaller pores have higher AEV than soils with larger pores. This is evidenced in particles sizes distribution analysis. Figures 3.3 through 3.5 show GPS with a significant silt content, yielded the lowest AEV value amongst soils evaluated.

4.5 Analysis of CBR Results

CBR values are used as an indication of index bearing capacity of soil strength. These values are predominantly used to execute the pavement design. Though CBR does not represent fundamental soil property. Thus, CBR is relevant on the basis of point load bearing capacity design method, rather than repetitive traffic load of pavement design. Nicholson et al. (1994) reported that CBR test is a common index test used for evaluation of strength of sub-base layers. In the same accord, CBR-test was conducted to characterise strength and bearing capacity of the studied subgrades. The CBR is influenced by different factors such as: moisture content, dry density, texture among other factors is clay minerals and soil's pore size distributions. The CBR test is conducted in the laboratory, under soaked and unsoaked conditions on soil samples prepared at the dry density and Mc likely to simulate field condition. The CBR test was carried out in this research, in order to use it as one of the independent variables for the prediction of resilient modulus.

Figure 4.26: Soaked and unsoaked compacted specimens

Table 4.7 below showed, the description of CBR values with respect to subgrades qualities, this table serves as a measure to determine the quality of subgrades as regards to the type of pavement required.

Table 4.7: Description of CBR-value subgrade quality

CBR-values	Subgrade quality	Subgrade status
0-3	very poor	subgrade
3-7	poor to fair	subgrade
7-20	fair	subgrade
20-50	good	subgrade
>50	excellent	subgrade

4.5.1 Behaviour of unsoaked compacted soils

The unsoaked CBR test was performed as stipulated in South African standard (Technical Methods for Highway (TMH) method 8, 1986). The load (kN) and penetration (mm) reading from a circular piston of 1935mm^2 were observed at a rate of 1,27 mm per minute. The loads at 2.54 mm, 5.08 mm and 7.62 mm were expressed as a percentage of standard load value for respective deformation level. CBR test were conducted at different dry densities and moisture content, as to evaluate the response of the subgrades over range of moisture content. The test results of unsoaked and soaked CBR are summarised in Tables in 4.8 and 4.9.

The calculation depicted the soils as fair subgrades from the dry side of the optimum. Whereas on the wet side, the subgrades are designated as poor to fair. The soils with clay fraction greater than 70%, recorded relatively smaller swelling values. Therefore, potential swelling for soil containing fine grain smaller than 70% is relatively small. At optimum moisture content (OPT), the CBR values of FSS 1, 2 and 3 are 12.59%,11.79% and 13.52% respectively. Whilst on the dry side of the optimum (DOP) the soils recorded the highest CBR values of 15.65%, 13.71% and 17.46%. Furthermore, wet side of the optimum (WOP) FSS 1, 2 and 3 obtained CBR values of 8.43%, 6.52% and 10.83% respectively. However, similar trend was observed in all the studied subgrades. In addition, significant decrease was observed in CBR values of the subgrades as the Mc increases. This could be ascribed to the arrangements of the soil particles, mineralogy and desperation of the soil particles because on increased moisture content. However, tabulated results of both the soaked and unsoaked subgrade soils are presented in Tables 4.8 and 4.9.

Table 4.8: Four days Unsoaked Soils for California Bearing Ration (CBR)

Soil moisture conditions:	**BEARING RATIO AT=** $\frac{Test\ Load}{Standard\ load} \times 100$			**SWELL (%)**	**MOD. AASHTO DATA**		**COMPACTION DATA**		
	CBR (%) at 2.54mm	CBR (%) at 5.08mm	CBR (%) at 7.62mm		MDD (Kg/m^3)	OPTIMUM MOISTURE (%)	DRY DENSITY (Kg/m^3)	COMPACTIONS (%)	MOISTURE QUANTITY (g)
FSS 1									
8.55	14.65	13.23	11.75	0.58	1766	17.65	1269	95	767
13.46	13.11	12.52	12.21	0.52	1766	17.65	1695	95	798
17.65	12.59	11.73	10.47	0.41	1766	17.65	1766	95	815
24.27	10.23	10.16	9.35	0.37	1766	17.65	1621	95	833
31.75	8.43	6.45	4.11	0.33	1766	17.65	1323	95	859
FSS 2									
9.97	12.11	11.22	10.09	0.65	1726	18.78	1271	95	799
13.67	11.11	11.54	10.42	0.58	1726	18.78	1592	95	812
18.78	10.19	9.76	8.96	0.52	1726	18.78	1726	95	832
24.09	8.14	6.83	4.28	0.46	1726	18.78	1443	95	856
30.16	6.52	4.56	3.49	0.44	1726	18.78	1236	95	894
FSS 3									
7.28	17.46	15.33	13.79	0.43	1895	18.45	1371	95	729
14.15	15.39	13.70	12.33	0.40	1895	18.45	1795	95	754
18.45	13.52	11.86	11.02	0.36	1895	18.45	1895	95	787
22.94	11.95	11.09	10.67	0.33	1895	18.45	1726	95	808
28.33	10.33	8.36	6.87	0.28	1895	18.45	1373	95	834

NCS 1									
8.38	17.52	13.56	11.34	0.78	1972	17.49	1638	95	727
12.73	15.49	15.76	14.19	0.67	1972	17.49	1929	95	815
17.49	13.66	11.87	10.67	0.52	1972	17.49	1972	95	833
24.49	12.83	10.99	8.73	0.48	1972	17.49	1785	95	856
28.33	10.75	7.78	5.88	0.40	1972	17.49	1588	95	892
NCS 2									
9.18	14.14	13.34	12.83	0.58	1888	17.38	1575	95	712
13.13	12.44	11.58	10.48	0.55	1888	17.38	1786	95	789
17.38	11.45	11.16	10.43	0.49	1888	17.38	1888	95	816
24.09	10.54	9.88	8.49	0.40	1888	17.38	1722	95	834
30.22	9.34	7.66	6.23	0.33	1888	17.38	1588	95	866
NCS 3									
9.97	12.34	11.59	10.88	0.53	1716	18.98	1445	95	718
14.15	10.89	11.45	10.32	0.47	1716	18.98	1617	95	756
18.98	9.74	8.73	7.89	0.43	1716	18.98	1716	95	788
24.64	8.83	6.45	5.56	0.40	1716	18.98	1626	95	809
32.88	7.67	6.84	4.56	0.36	1716	18.98	1327	95	818
GPS 1									
9.28	15.21	13.45	11.41	0.47	2225	18.76	1750	95	728
12.53	13.54	12.56	10.39	0.43	2225	18.76	1984	95	743
18.76	12.18	11.92	9.49	0.23	2225	18.76	2225	95	779
23.94	11.48	10.17	8.66	0.20	2225	18.76	2046	95	794
29.33	10.33	10.13	8.45	0.12	2225	18.76	1647	95	807
GPS 2									
9.89	12.16	11.56	8.76	0.52	2130	18.88	1575	95	743
14.15	11.88	9.62	6.34	0.48	2130	18.88	1960	95	756
18.88	10.84	8.88	6.63	0.43	2130	18.88	2130	95	776
24.09	10.31	8.48	6.31	0.40	2130	18.88	1933	95	818
30.33	9.21	6.76	4.33	0.38	2130	18.88	1627	95	883
GPS 3									
8.67	18.45	16.32	13.83	0.33	2328	16.77	1909	95	703
11.89	16.43	11.55	10.45	0.28	2328	16.77	2052	95	728
16.77	14.78	14.52	11.93	0.40	2328	16.77	2328	95	755
22.65	12.84	11.67	10.42	0.38	2328	16.77	2213	95	768
28.13	11.94	10.89	9.56	0.32	2328	16.77	1920	95	793

4.5.2 Behaviour of soaked compacted soils

The CBR values of soaked compacted soils are commonly used parameter for design of highway pavement, in the sense that it simulates worst field condition. The soaked CBR values of the subgrades dropped tremendously compared to unsoaked specimens. This was as result of absorbed water, that eventually led to higher voids ratio which caused the soils to yield lower CBR values.

Under soaked condition, the soils are considered as poor to fair subgrades from dry side to the optimum and very poor from optimum to wet side. Soaked CBR values of FSS 1, 2 and 3 decrease with respect to unsoaked CBR are 4.05%, 3.96% and 4.02% on the dry side of the optimum. This, indicated that on the dry side, the soil voids were less and the soil particles were more flocculated, thus causing the soils to be less affected by water during wetting period. In addition, the same trend of decrease in soaked CBR values with respect to unsoaked CBR was observed for the rest of the studied subgrades. The CBR value continues to decrease from dry side to the OMC up to the wet side, thus decrease in CBR values in soaked condition on dry side of the optimum for NCS 1, 2 and 3 were evaluated to be 4.95%, 4% and 1.04. These values showed that the difference in CBR values for soaked specimens continues to increase as the testing shifts from dry side to wet side.

This CBR-value of the soaked compacted soils was reported in the context of the general relationship between the CBR values and geotechnical quality of the soils used in pavement applications (Bowles, 1992). These values showed that unsoaked soils at wet side are classified as good subgrades, whilst under soaked condition, the soils are categorised as poor to fair. However, this CBR values cannot be recommended for the design pavement. Hence, it does not meet the minimum requirement for CBR design values. Thus, significant decrease in CBR value of the soaked subgrade soils were high compared to the unsoaked soils. This can be ascribed to the deformation of capillary forces under soaked conditions. Generally, the CBR values decreases significantly with number of soaking periods.

Table 4.9: Four days Soaked Soils for California Bearing Ration (CBR)

Soil moisture conditions:	**BEARING RATIO AT=** $\frac{Test\ Load}{Standard\ load} \times 100$			**SWELL (%)**	**MOD. AASHTO DATA**		**COMPACTION DATA**		
	CBR (%) at 2.54mm	CBR (%) at 5.08mm	CBR (%) at 7.62mm		MDD (Kg/m^3)	OPTIMUM MOISTURE (%)	DRY DENSITY (Kg/m^3)	COMPACTIONS (%)	MOISTURE QUANTITY (g)
FSS 1									
8.88	11.60	10.14	9.83	0.62	1772	17.93	1293	95	770
13.18	10.11	8.45	6.65	0.58	1772	17.93	1680	95	794
17.93	9.59	7.73	5.47	0.50	1772	17.93	1772	95	818
24.87	8.28	6.77	4.36	0.45	1772	17.93	1636	95	830
31.40	4.53	3.56	2.88	0.40	1772	17.93	1330	95	862
FSS 2									
9.28	9.73	7.28	5.15	0.68	1729	18.29	1274	95	801

13.82	7.80	5.58	3.42	0.60	1729	18.29	1589	95	809
18.29	5.79	4.76	3.96	0.55	1726	18.29	1729	95	835
24.33	5.14	4.54	3.23	0.50	1726	18.29	1440	95	859
29.71	4.52	3.28	2.60	0.48	1726	18.29	1233	95	891
FSS 3									
7.49	13.44	11.55	9.88	0.46	1891	18.63	1388	95	733
14.09	11.53	9.65	7.28	0.43	1891	18.63	1782	95	759
18.63	10.47	8.33	6.82	0.37	1891	18.63	1891	95	790
22.68	9.68	7.87	5.65	0.35	1891	18.63	1737	95	812
28.18	7.66	4.88	3.86	0.30	1891	18.63	1392	95	837
NCS 1									
8.47	13.31	11.59	10.44	0.75	1975	17.45	1641	95	731
12.69	12.94	10.66	9.45	0.70	1975	17.45	1926	95	812
17.45	10.66	9.89	8.75	0.55	1975	17.45	1975	95	836
24.71	8.45	6.99	4.16	0.51	1975	17.45	1788	95	853
28.25	7.47	5.78	3.88	0.45	1975	17.45	1585	95	895
NCS 2									
9.36	11.35	10.34	8.83	0.60	1885	17.55	1578	95	714
12.92	10.55	9.60	7.46	0.55	1885	17.55	1790	95	791
17.55	9.68	7.59	5.48	0.50	1885	17.55	1885	95	813
23.87	7.43	6.88	4.49	0.44	1885	17.55	1725	95	837
30.10	6.98	4.66	3.53	0.38	1885	17.55	1585	95	863
NCS 3									
9.89	9.84	8.29	6.45	0.56	1716	18.66	1445	95	718
14.38	9.17	8.33	7.22	0.50	1716	18.66	1617	95	756
18.66	7.48	5.66	3.45	0.47	1716	18.66	1716	95	788
24.48	5.87	4.32	3.76	0.45	1716	18.66	1626	95	809
32.67	4.94	2.84	1.59	0.40	1716	18.66	1327	95	818
GPS 1									
9.32	13.67	11.98	10.41	0.52	2225	18.56	1750	95	730
12.34	12.54	10.86	8.57	0.49	2225	18.56	1984	95	740
18.56	10.66	8.78	7.88	0.35	2225	18.56	2225	95	783
23.85	9.98	7.17	5.69	0.30	2225	18.56	2046	95	790
29.49	7.47	6.13	5.15	0.20	2225	18.56	1647	95	815
GPS 2									
9.84	11.23	10.76	9.89	0.55	2132	18.91	1571	95	746
14.18	10.13	8.86	5.89	0.50	2132	18.91	1963	95	73
18.91	9.45	7.75	5.68	0.48	2132	18.91	2132	95	779
24.03	7.31	5.41	4.54	0.44	2132	18.91	1928	95	813
30. 21	5.89	6.99	3.98	0.40	2132	18.91	1623	95	880
GPS 3									
8.46	15.55	13.44	11.86	0.36	2331	16.85	1912	95	708
11.65	13.96	10.63	8.45	0.30	2331	16.85	2049	95	725
16.85	12.73	10.52	7.93	0.45	2331	16.85	2331	95	758
22.63	11.84	9.67	7.49	0.38	2331	16.85	2209	95	763
28.28	10.94	8.89	6.56	0.32	2331	16.85	1923	95	795

4.5.3 Analysis of unsaturated CBR results

The CBR test is conducted to measure strength of subgrade for pavements design (Saklecha et al 2013). The wetting and drying moisture path is one of the factors that influences the performance of pavement. Therefore, to ascertain unsaturated CBR values, the wetting-drying cyclic is represented of suction stress. Thus, suction is a major geotechnical parameter to be considered in unsaturated CBR pavement design. However, variation occurred in CBR values due to varying Mc for all tested subgrades. The close values of CBR at higher Mc for both FSS and NCS could be relatively assigned to the soil's structural arrangement and dry density. Results showed that the CBR values of the soils continues to decrease as the soil Mc moves from dry side of the optimum to the wet side, irrespective the soil type. The percentage of reduction in CBR values for the soils during wetting cycle were relatively 5 to 8 times greater compared to drying path. Thus, the same trend was observed for all tested soils. The practical interpretation of the above soil's behaviour is that there is a benefit with respect to CBR increase on the drying path; as this will ensure well drained subgrade at lower Mc below the optimum value.

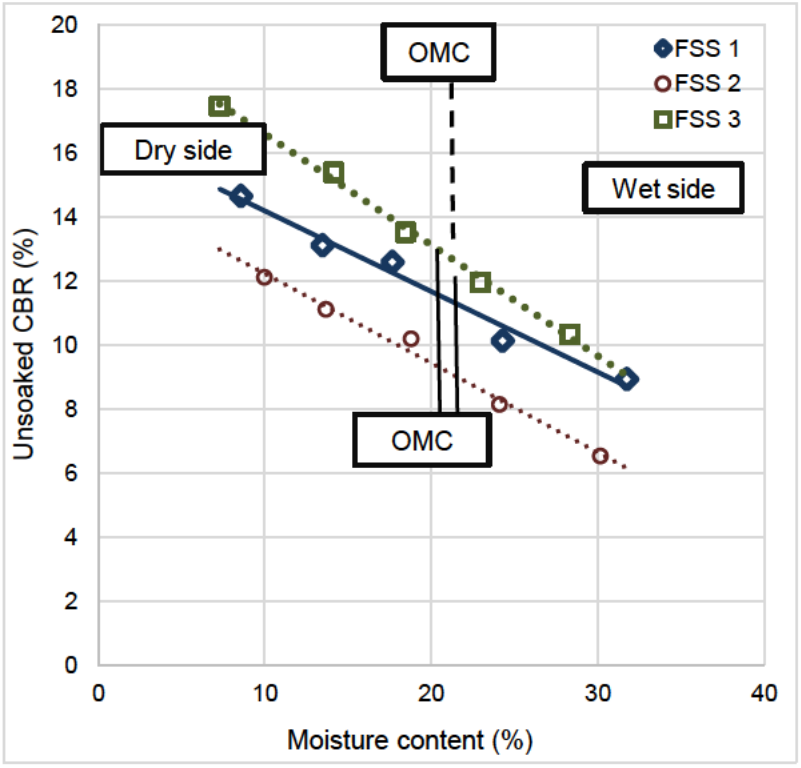

Figure 4.27: Unsoaked FSS CBR variation with water content

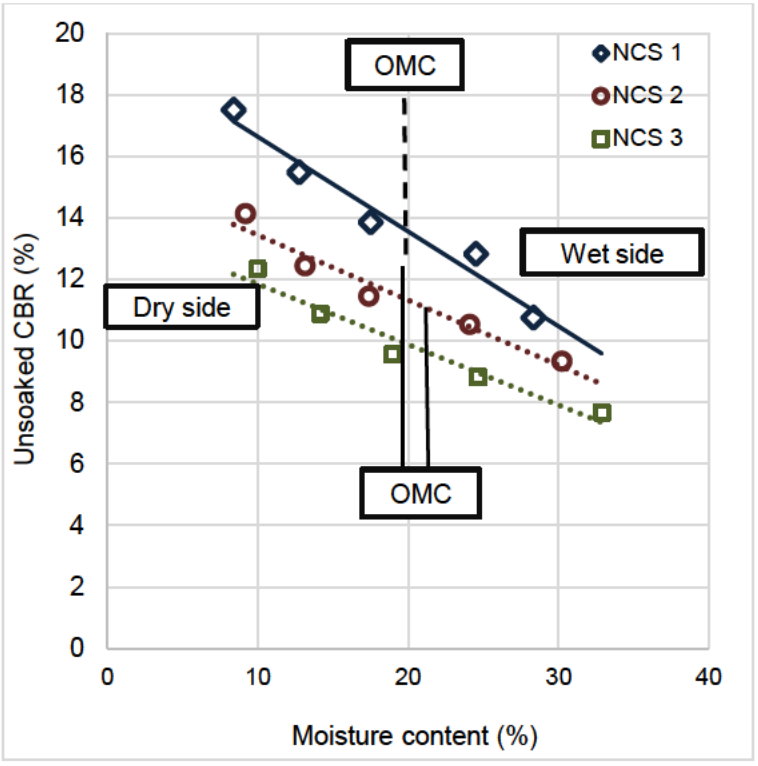

Figure 4. 28: Unsoaked NCS CBR variation with water content

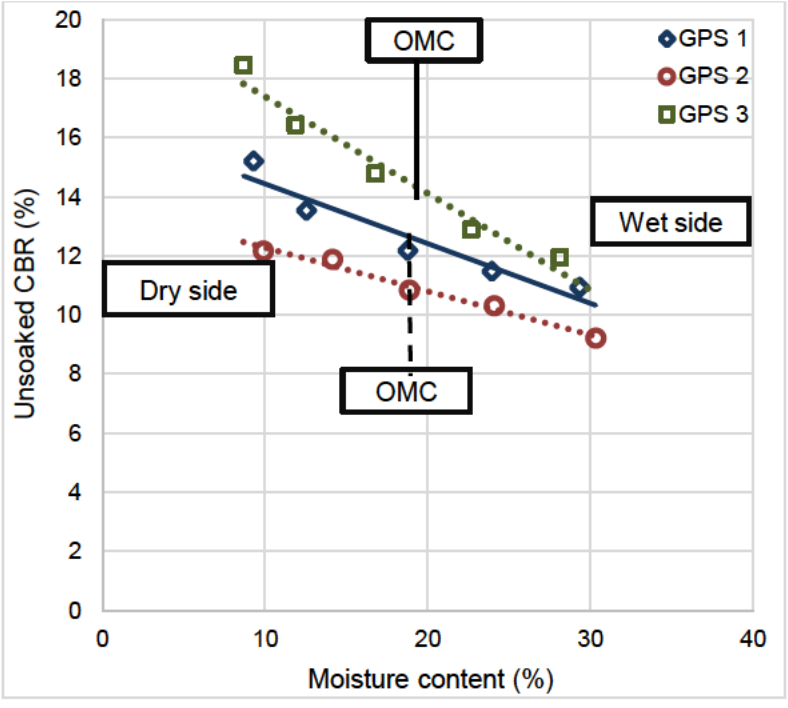

Figure 4. 29: Unsoaked GPS CBR variation with water content

Figures 4.27 through 4.29 illustrated the effect of Mc on CBR values of the tested soils and a general trend of decrease in CBR with increase in soil Mc across drying and wetting paths. The result is consistence with the results published by Sanchez-Leal

(2002), Ampadu (2007), Cekerevac et al. (2009), and Purwana et al. (2012) for the variation of CBR with Mc in incompressible geomaterials. In addition, Figures 4.30 and 4.32, also emphasised that soils with higher fine content absorbed more water during the soaking period. Therefore, it resulted in an increased moisture quantity within the soil's voids and as a result recorded low CBR values. Furthermore, the soil samples located on the drying curve possess lower water contents and as such trigged higher CBR values even after four days soaking period. As a result, the CBR versus water content curve followed a hysteresis effect from wetting to drying which is a non-linear relationship.

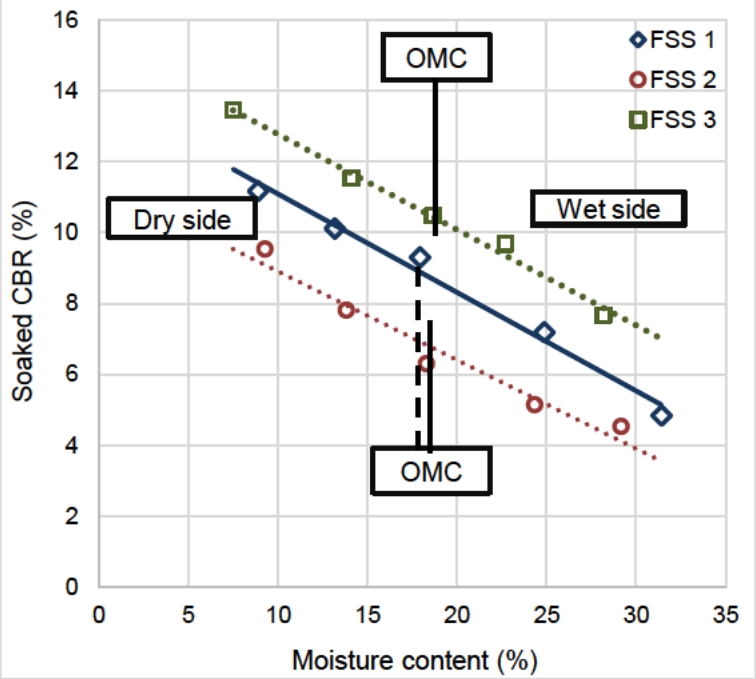

Figure 4.30: Soaked FSS CBR Variation with water content

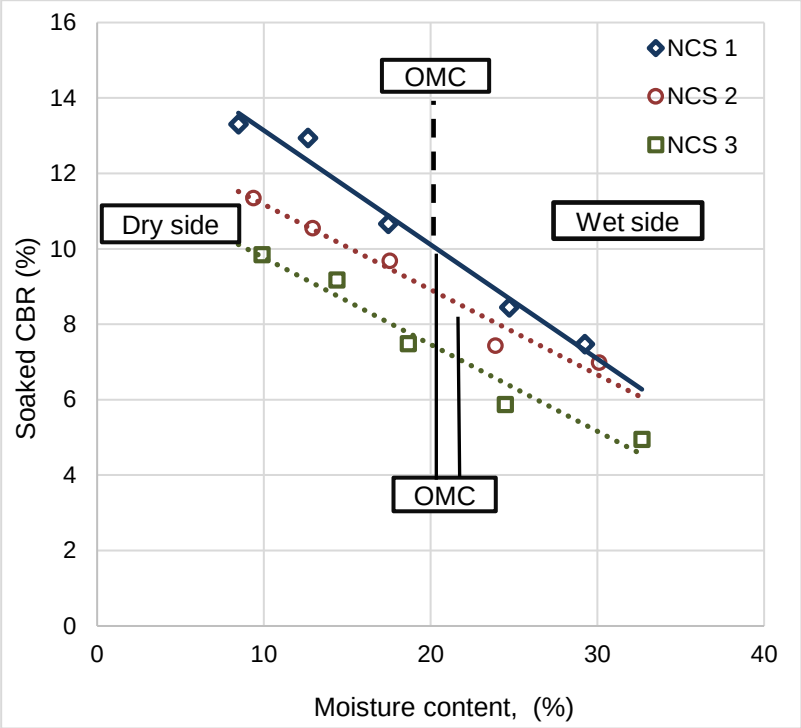

Figure 4.31: Soaked NCS CBR Variation with water content

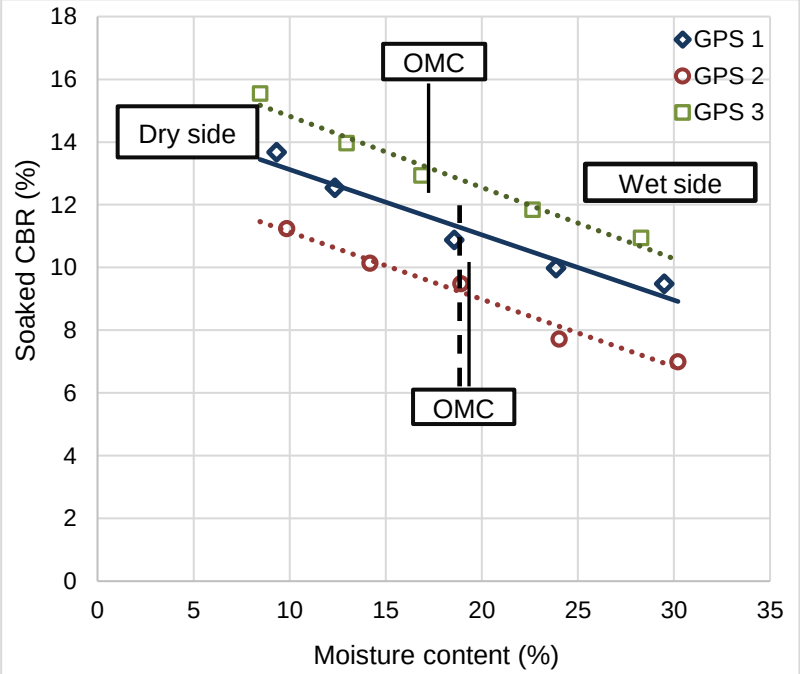

Figure 4.32: Soaked GPS CBR Variation with water content

Consequently, the influence of matric suction on CBR of compacted soils were investigated as part of the unsaturated CBR test. Sets of identical specimens were prepared for both soaked and unsoaked CBR test. One set of the prepared samples

were used for CBR testing, while the other set was used for suction measurement (filter paper method Whitman No. 42).

4.5.4 Unsaturated CBR effect on matric suction

The result portrayed that decrease in moisture content, led to the increase in matric suction and subsequently caused increase in CBR value. Figures 4.33 through 4.35 explained moisture content decrease due to drying, and this caused the rise in capillary pressure within the soil's particles thus led to increase in matric suction. Probably, a bi-linear relationship between CBR and matric suction was observed from the curve.

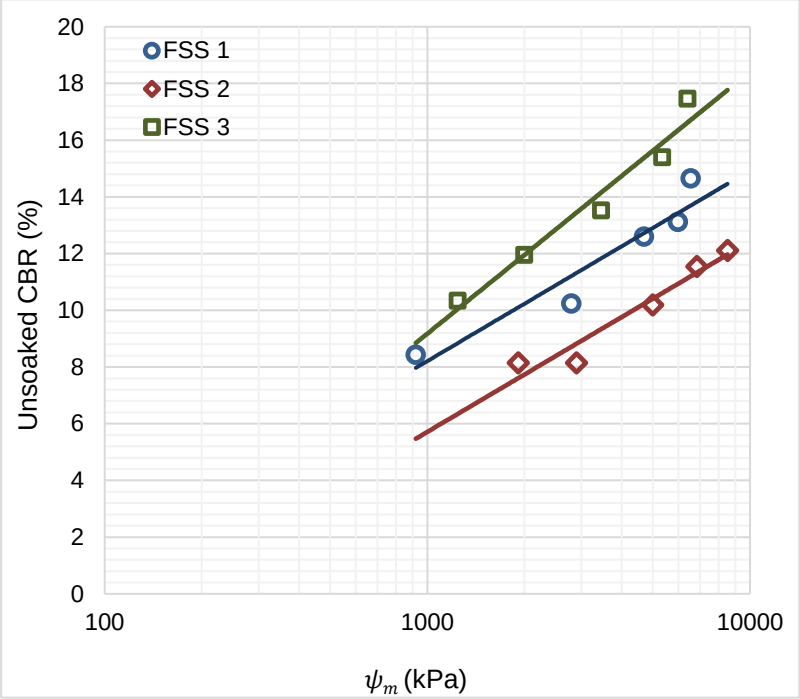

Figure 4.33: Variation of unsoaked FSS CBR versus matric suction

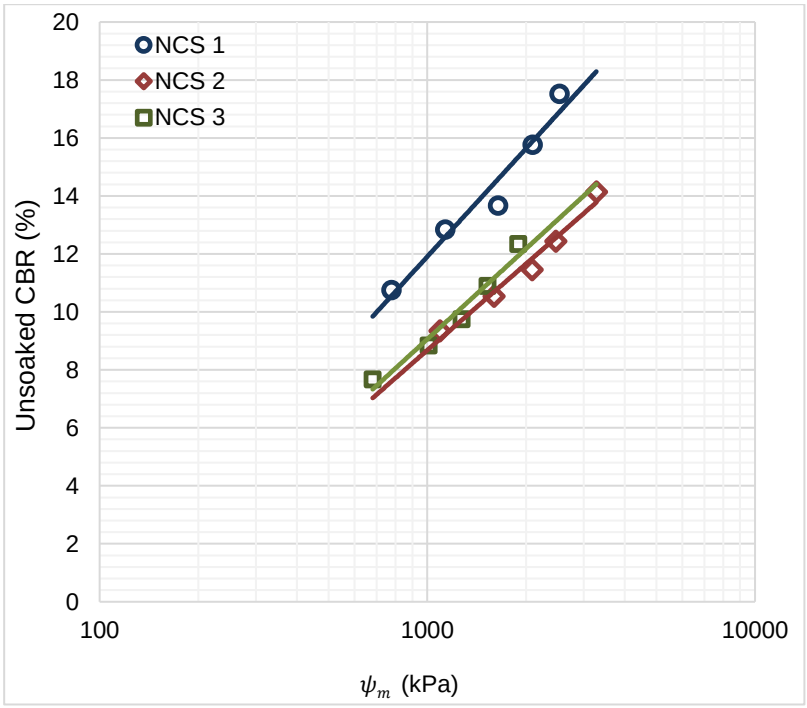

Figure 4. 34: Variation of unsoaked NCS CBR versus matric suction

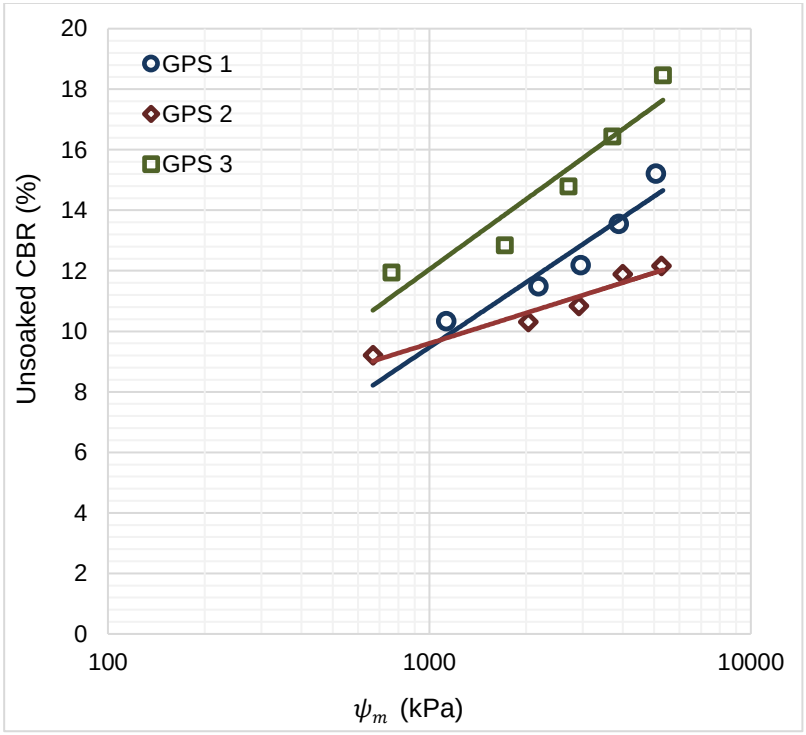

Figure 4. 35: Variation of unsoaked GPS CBR versus matricsuction

Furthermore, the experimental results in Figures 5.34 through 4.35 showed increment of matric suction due to the drying process that increased CBR values of unsoaked specimens. However, the CBR values increases as matric suction increased along the drying and wetting paths. This trend agrees with the observations of Paraire (1987) and Ampadu (2007) for the soil samples examined along the wetting paths. Based on this extrapolation of the dry densities used in this study and the corresponding matric suction values, $(u_a - u_w)$, all test points were estimated using Equation 4.1. The suction matric values are plotted against the unsaturated CBR, (CBR_u) in Figures 4.36 and 4.38. The results portrayed an equation that is expressed as:

$$CBR_u = CBR_s \times \left(\frac{u_a - u_w}{u_e}\right)^n \quad (4.1)$$

where CBR_s is the soaked CBR, u_e is the air-entry value and n is the regression parameters for the model presented in Equation 4.1. A regression model was developed for parameter n and as well used to optimise the parameter n in Equation 4.1. The values for parameter n, in this study ranges from 0.21 to 0.382. This values differs from Ampadu's values for parameter n, that ranges from the order of 1.4 and about 0.5, for lower and for higher dry densities respectively, and constant for suction values up to about 15,000 kPa. The parameter n obtained from the regression model differs from that proposed by Ampadu (2007). The differences in values could be attributed to soil type, variation in moisture content and dry densities. However, the results of CBR_u were discovered to be 1.5 to 2 times higher than that of the conventional CBR values. Whereas, the CBR_u values obtained using the developed models were found to be close to the predicted unsaturated CBR values obtained from Ampadu's models.

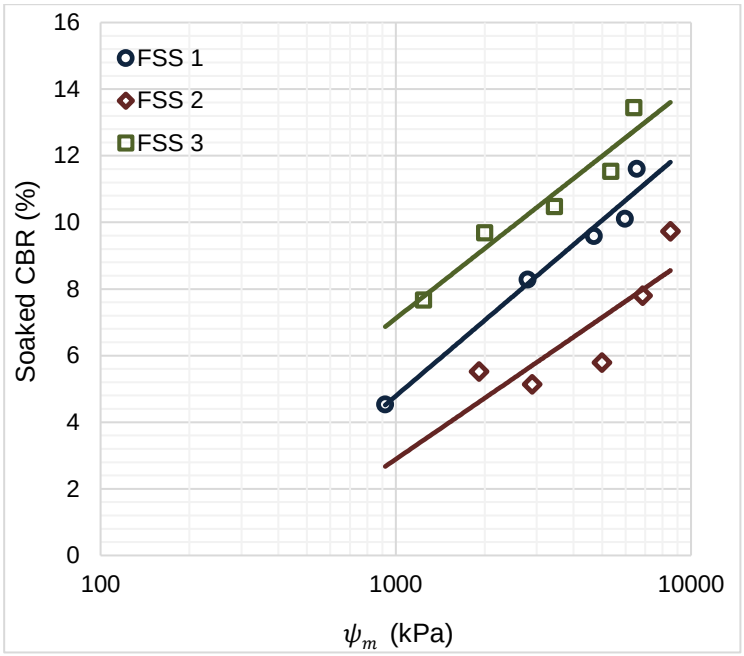

Figure 4. 36: Variation of soaked FSS CBR versus matric suction

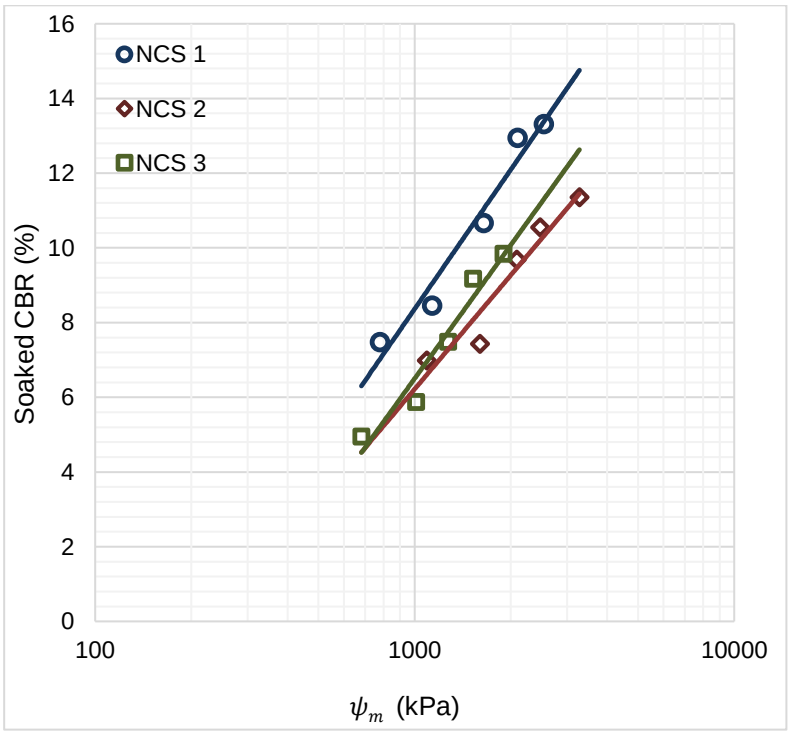

Figure 4. 37: Variation of soaked NCS CBR versus matric suction

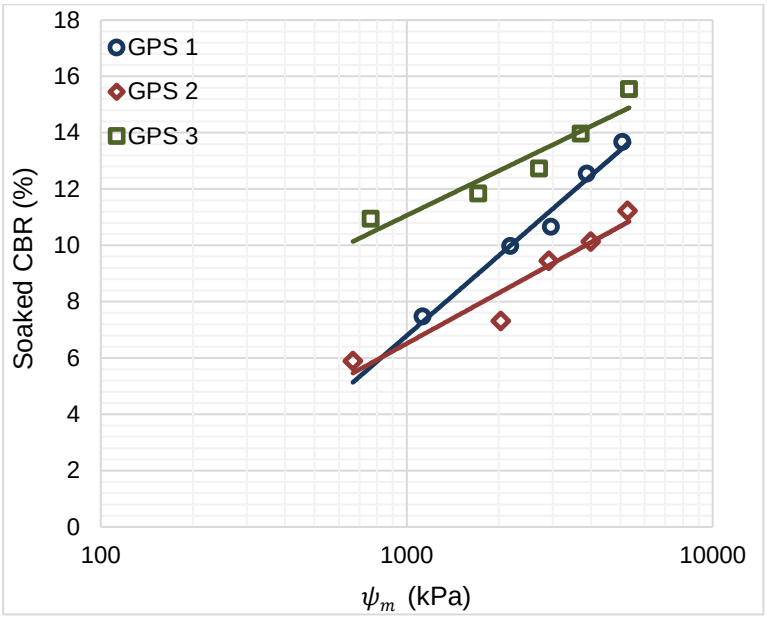

Figure 4.38: Variation of soaked GPS CBR versus matric suction

4.5.5 Developed predictive equation for unsaturated CBR

NCSS 11 mathematical software was used in this study and the software package has excellent predictability analytical capacity and graphical features. The interrelationship of variables is formulated by an equation that linked the dependent variable and one or multiples predictor variables. The response variable is designated as Z and the set of the predictor variables are denoted as $Y_1, Y_2, \ldots\ldots Y_n$, where n depicts the number of predictor variable. Accurate relationship between Z and $Y_1, Y_2, \ldots\ldots Y_n$ can be approximated by the regression model.

$$Z = f(Y_1, Y_2, \ldots\ldots Y_n) + \varepsilon, \tag{4.2}$$

Where ε is assumed to be the random error representing approximation divergence and it accounts for the failure of the model that failed to fittingly optimize the data. The function $f(Y_1, Y_2, \ldots\ldots Y_n)$ describes the relationship between Z and $Y_1, Y_2, \ldots\ldots Y_n$. An example is the linear regression model.

$$Z = \alpha_0 + \alpha_1 Y_1 + \alpha_2 Y_2 + \cdots\ldots\ldots + \alpha_n Y_n + \varepsilon, \tag{4.3}$$

Where $\alpha_0, \alpha_1, \ldots\ldots, \alpha_n,$ are known as the regression parameters and are usually determined from the data. The predictor variables are also known as independent variables, regressors, factors and carriers. Most commonly, the term independent variable is used during regression exercise.

The NCSS software was used to develop a mathematical predictive models for CBR_u, using suction matric, dry density, AEV and soaked CBR (CBR_s) as independent variables. While, CBR_u is used as dependent variable. The regression analysis results demonstrate that AEV has the highest effect on CBR_u, followed by matric suction, dry density and lastly CBR_s. The R^2 for each independent variable are presented in Table 4.10. The developed models are presented as follow:

$$\mathrm{CBR_u}(\%) = -\beta_0 + \beta_1(\mathrm{CBR_s}) - \beta_2(\gamma_\mathrm{d}) - \beta_3\log(\psi_\mathrm{m}) + \beta_4(\mathrm{S_e}) \ldots\ldots\ldots\ldots\ldots\ldots\ldots\ldots\ldots\ldots (4.4)$$

$$\mathrm{CBR_u}(\%) = -\xi_0 + \xi_1 \log(\psi_\mathrm{m}) - \xi_2(P_s) + \xi_3(CBR_s) + \xi_4(S_e) + \xi_5(\gamma_d) \ldots\ldots\ldots\ldots\ldots\ldots (4.5)$$

Where: CBRu is the unsaturated CBR and the values of each symbol are summarized in the table below:

Table 4.10: Parameters symbols and their corresponding values

Denotations	Meaning	Values	R^2
Equation 4.4			
$-\boldsymbol{\beta_0}$	Intercept	16.9485	-
$\boldsymbol{\beta_1}$	Coff. for CBRs	4.6696	-
$\mathbf{CBR_s}$	CBRs	-	0.8511
$\boldsymbol{\beta_2}$	Coff. for dry density	0.9766	-
$\boldsymbol{\gamma_d}$	Dry density		0.9182
$\boldsymbol{\beta_3}$	Coff. for suction matric	0.0001	-
$\boldsymbol{\psi_m}$	Suction matric	-	0.9234
$\boldsymbol{\beta_4}$	Coff. for Air-entry values (AEV)	0.1085	-
$\boldsymbol{S_e}$	Air-entry values	-	0.9332
Equation 4.5			
$-\boldsymbol{\xi_0}$	Intercept	-14.9392	-
$\boldsymbol{\xi_1}$	Coff. for matric suction	6.237E-05	-
$\boldsymbol{\psi_m}$	Matric suction	-	0.9415
$\boldsymbol{\xi_2}$	Coff. for swelling pressure	0.0016	-
$\boldsymbol{P_s}$	Swelling pressure	-	0.7865
$\boldsymbol{\xi_3}$	Coff. for CBRs	4.4837	-
$\mathbf{CBR_s}$	CBRs	-	0.9177
$\boldsymbol{\xi_4}$	Coff. for Air-entry values (AEV)	0.0983	-
$\boldsymbol{S_e}$	Air-entry values	-	0.9195
$\boldsymbol{\xi_5}$	Coff. for Dry density	0.9173	-
$\boldsymbol{\gamma_d}$	Dry density	-	0.9501

The curve of measured CBR_u against predicted CBR_u values showed that Models 1 and 2 closely predicted the measured values because of the convergence data with high R^2 values of 0.9496 (Figure 4.39).

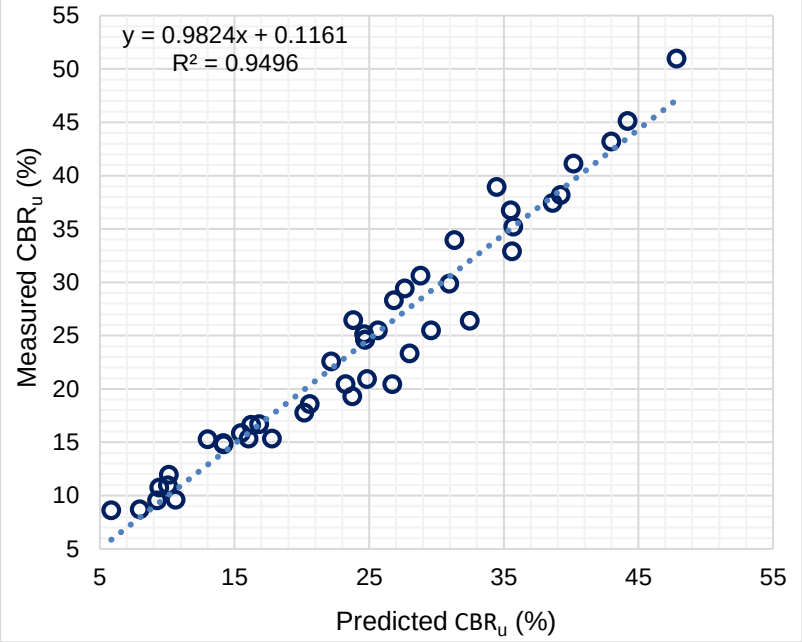

Figure 4.39: Measured versus predicted unsaturated CBRu model 1

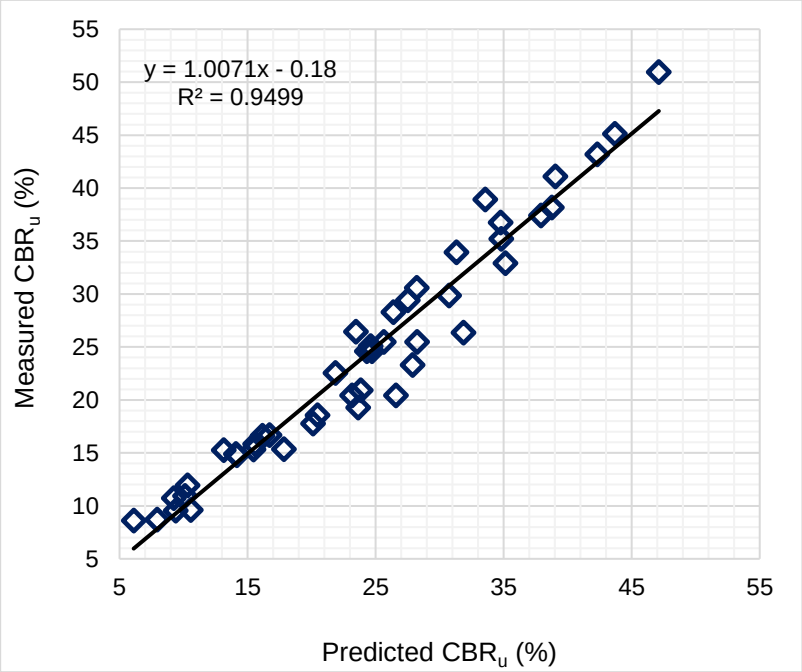

Figure 4.40: Measured versus predicted unsaturated CBRu model 2

Table 4.11: Values of unsaturated CBR

Soaked samples	Dry density (%)	$\mathbf{CBR_s}$ (%)	$\boldsymbol{\psi_m}$ (kPa)	$\mathbf{n}$	$\boldsymbol{S_e}$ (kPa)	Measured $\mathbf{CBR_u}$ (%)	Model 1 (%)	Model 2 (%)
							Authors Model	
FSS 1								
	1293	11.60	6541	0.30	132	37.41	38.63	37.91
	1680	10.11	5976	0.28	132	29.40	27.66	27.52
	1772	9.59	4689	0.26	132	24.26	24.61	24.71
	1636	8.28	2793	0.25	132	17.76	20.19	20.12
	1330	4.53	921	0.33	132	8.60	5.85	6.10
FSS 2								
	1274	9.73	8517	0.25	158	26.36	32.48	31.86
	1589	7.80	6843	0.23	158	18.56	20.58	20.45
	1729	5.79	4989	0.21	158	11.95	10.95	10.32
	1440	5.14	2895	0.26	158	10.95	10.05	10.11
	1233	4.52	1913	0.30	158	9.55	9.24	9.37
FSS 3	1388	13.44	6398	0.30	113	45.11	44.20	43.68
	1782	11.53	5345	0.28	113	33.95	31.34	31.32
	1891	10.47	3450	0.26	113	25.47	25.65	25.64
	1737	9.68	1998	0.24	113	19.29	23.75	23.63
	1392	7.66	1240	0.29	113	15.34	17.77	17.23
NCS 1								
	1641	13.31	2534	0.35	101	41.11	40.18	39.04
	1926	12.94	2098	0.33	101	35.21	35.72	34.82
	1975	10.66	1643	0.30	101	24.61	24.70	24.30
	1788	8.45	1134	0.28	101	16.63	16.24	16.16
	1585	7.47	778	0.35	101	15.26	13.00	13.13
NCS 2								
	1578	11.35	3278	0.38	128	38.92	34.48	33.55
	1790	10.55	2465	0.36	128	30.60	28.81	28.22
	1885	9.68	2087	0.34	128	26.44	23.82	23.46
	1725	7.43	1598	0.32	128	16.67	16.83	16.71
	1585	6.98	1091	0.35	128	14.78	14.20	14.15
NCS 3								
	1445	9.84	1895	0.36	135	25.47	29.60	28.23
	1617	9.17	1525	0.34	135	20.91	24.86	23.82
	1716	7.48	1272	0.32	135	15.33	16.05	15.46
	1626	5.87	1010	0.30	135	10.74	9.42	9.24
	1327	4.94	681	0.35	135	8.70	7.98	7.93
GPS 1								
	1750	13.67	5071	0.31	124	43.19	42.99	42.32
	1984	12.54	3884	0.28	124	32.90	35.61	35.12
	2225	10.66	2959	0.27	124	25.10	24.63	24.60
	2046	9.98	2183	0.25	124	20.44	23.26	23.16
	1647	7.47	1128	0.34	124	15.83	15.48	15.58
GPS 2								
	1571	11.23	5263	0.33	145	36.74	35.53	34.77

	1963	10.13	3989	0.31	145	28.30	26.85	26.37
	2132	9.45	2914	0.29	145	22.56	22.18	21.86
	1928	7.31	2029	0.27	145	14.91	14.17	14.10
	1623	5.89	667	0.32	145	9.60	10.63	10.56
GPS 3								
	1912	15.55	5331	0.30	102	50.96	47.85	47.12
	2049	13.96	3708	0.28	102	38.18	39.22	38.76
	2331	12.73	2707	0.26	102	29.86	30.95	30.74
	2209	11.84	1715	0.24	102	23.31	28.00	27.88
	1923	10.94	763	0.31	102	20.42	26.73	26.59

In summary, pavement design procedures which are commonly based on CBR test, can be extended to account for suction under unsaturated condition. Moreover, resilient modulus (Mr) test is widely accepted in the design of pavements in various transportation agencies around the world. However, determination of Mr value is costly, time-consuming, and somewhat complicated. Based on this reason, Unsaturated CBR test can be used as an alternative, as demonstrated in is study. Recommendation for the interpretation of CBR results considering the influence of suction, gave an insightful knowledge about suction correlation with CBR. These results are encouraging as they not only provide a valid frame work to understand the influence of soil suction on the engineering behaviour of highway pavements, but proved to be reliable for unsaturated soil mechanics.

4.6 Unconfined Compressive Strength (UCS) Results

Compressive strength of soil is a significant factor, used in evaluating subgrade strength of pavement. UCS test was prepared according to TMH1 METHOD 14. The studied subgrade soils were demoulded after compaction and kept in a curing chamber for 7days, as to evaluate the effects of moulding Mc on soil's strength. The result revealed that the compressive strength of the subgrades decreases as water contented increases. Furthermore, the strength gained by these soils were as result of compaction effort and the soils are categorized as stiff and very stiff subgrade according to (Das, 1994) classification.

The results demonstrated that the densest specimens absorbed less water and were found to have higher compressive strength. Similarly, the least dense material (soils with higher fine content) tends to have more water intake and this led to lower compressive strength values.

The curves in Figures 4.41 through 4.43 indicated that density and strength are highly sensitive to moulding water content. Furthermore, the curves demonstrated that the effect of moulding water content is prominent for specimens with higher percentage of fine. This showed that specimens compacted on the dry side portrayed higher strength than those specimens compacted on the wet-side.

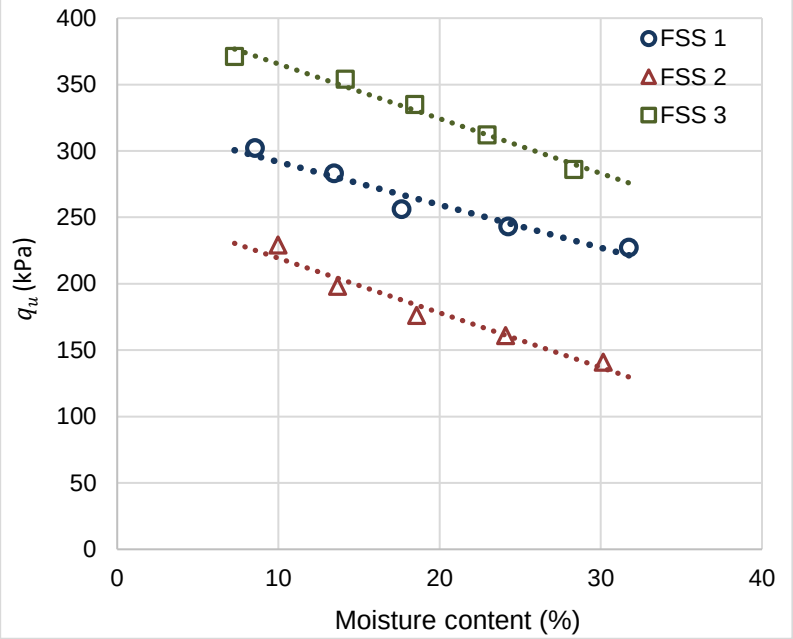

Figure 4.41: FSS seven days UCS values

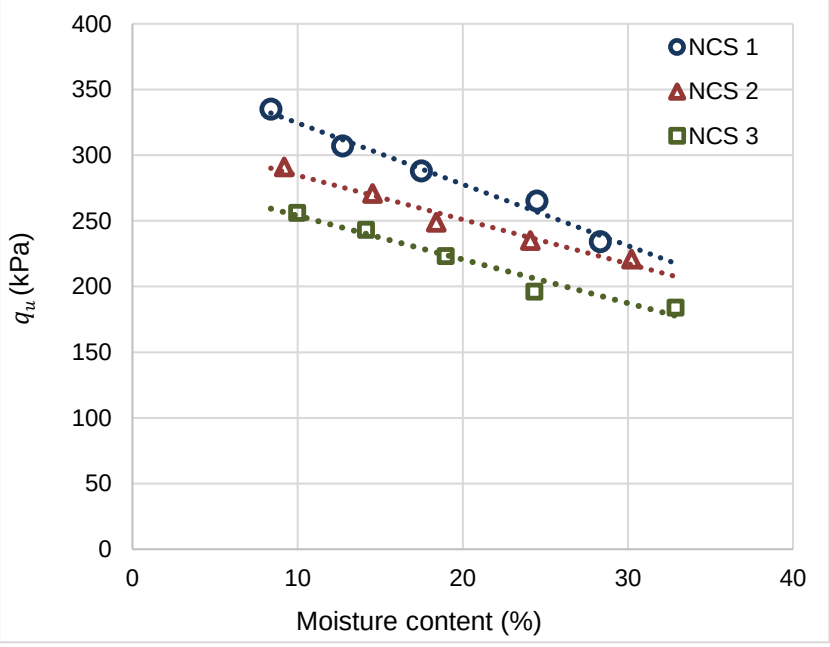

Figure 4.42: NCS seven days UCS values

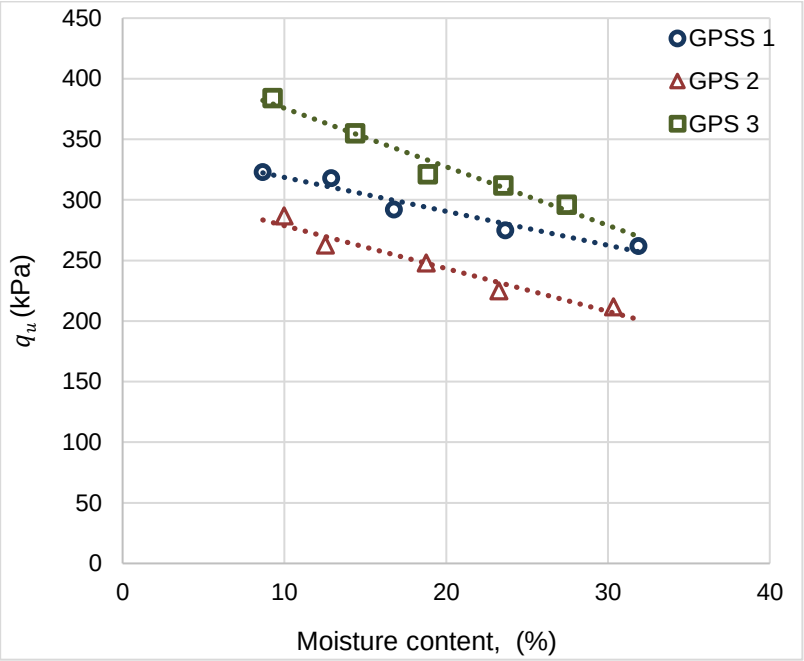

Figure 4.43: GPS seven days UCS values

The low strength values with the increased moulding water content (wet-side) can be attributed to relatively high-water content. Thus, on the wet-side soil particles of the specimen dispersed, thereby becomes too difficult to be compacted especially with the soils that contained higher amount of expansive clay minerals. Whilst on the dry side, the soil particles fussed together resulting in closed packed pore water within the soil, this caused the soil particles to be densest and thus led to more compacted specimens that yielded relatively high strength.

CHAPTER 5: CONSOLIDATED UNDRAINED TEST RESULT

5.1 Overview

This part of the experimental work, gives emphases on the changes in shear strength parameters with respect to moulding water content and matric suction. Further description of Mohr-Coulomb failure criteria with shear strength parameters i.e. friction angles, (ϕ^0) and cohesion, C' under unsaturated soil mechanics for studied soils were also illustrated.

5.2 Saturated Soil Shear Strength (τ) Result

Shear stresses are induced as the soil is loaded, thus when shear stresses reach a limiting value, shear deformation sets in, leading to soil failure. Therefore, shear strength is the resistance of soil to deform by continuous shear displacement of the soil particles upon the action of stress. The failure conditions for soil is expressed as ultimate shear stress, known as shear strength. Nonetheless, series of consolidated undrained shear test on the prepared specimens was performed to obtain effective τ parameters (c' and ϕ^0) for all the tested soils at different Mc. Three different confining stresses i.e. 20kPa, 50kPa, and 100kPa were considered, to significantly evaluate the behaviour of the studied soils at different confining stresses.

5.2.1 Stress- strain response of the studied soils

During consolidated undrained test, the stress-displacement responses of the nine tested subgrades were assessed. The soils were tested at different Mc, ranging from the dry to wet side of the optimum. The influence of Mc on stress-strain behaviour of the tested soils were evaluated. Figures 5.1 through 5.27 in Appendix C shows stress-strain as a function of vertical displacement for FSS, NCS and GPS at normal stresses (σ_n) of 20, 50 and 100kPa. The strain at failure was found to be within 0.030 to 0.035%, at σ_n of 20kPa for FSS1 on the dry side. Furthermore, the strain at failure was obtained with the range of 0.06% to 0.07% at σ_n of 50k and 0.12% to 0.14% at σ_n of 100 kPa for FSS 2 and 3 respectively. The shear stress increases with respect to strain up until the maximum value and at the point beyond failure strain. The stress start to decrease at faster rate (residual stress), hence increasing the elastic modulus of the soils. The behaviour was as a result of the flocculated structure formed on the dry side, as the soil

particles oriented randomly, with an increase in stress and suddenly failed at a higher stress value.

All tested soils followed similar trend, due to gradually increase of stress with respect to increase in strain to the ultimate stress capacity of each soil. Furthermore, the soil structures were dispersed, as the soil particles were more in a parallel arrangement perpendicular to the direction of applied stress for the specimens prepared with higher moisture content. The stress-strain curves of the soils portrayed brittle stress-strain behaviour on dry side of the optimum. Whereas, ductile responses were observed on the wet-side of the optimum, this result agrees with the report published by (Fang, 2006).

5.2.2 Effects of moulding water content on shear strength parameters

Changes in shear strength parameters with varying moisture content were assessed. The results demonstrated the behaviour of the studied soils at different Mc, ranging from dry side of the optimum (DOP) to the wet side (WOP) with respect to shear strength parameters i.e. c' and ϕ'. The parameter values at 8.55% water content for specimen FSS1, gave . c' and ϕ' 58.10 kPa and 49.29^0 values. At 13.46% Mc, significant change was observed, thereby causing the parameter values to decrease to the values of 53.52 kPa and 43.38^0 c' and ϕ^0. More changes were recorded in shear strength parameters at the optimum moisture content (OPT). When compared with strength parameters values at 8.55% Mc as the soil yielded 51.2 kPa and 41.4^0 for both c' and ϕ^0. Whereas, at 24.27% Mc, the soil shear strength parameter values were measured to be 46.59 kPa and 37.67^0. Furthermore, at 31.75% Mc, . c' and ϕ' values decrease of 8.1 kPa and 6.62^0 were recorded. Therefore causing the soil to yield shear strength parameter values of 43.11 kPa and 34.78^0 respectively for c' and ϕ^0. Furthermore, the FSS recorded lower shear strength parameters, compared to NCS and GPS, as FSS contained higher clay content than rest of the soils. Similar trends were observed on the rest of the tested soils, as the soils exhibits bilinear relationship between the shear stress and bulk stress for Mohr-Coulomb failure envelop as the Mc increases. The failure envelops of the studied soils are presented in Appendix C, ranging from Figures 5.28 through 5.50.

Generally, the shear strength response of the studied soils is attributed to the amount of clay fraction and clay minerals within the subgrades, as the soils with higher content of expandable clay i.e. montmorillonite reduces the shear strength. Thus, shear strength is basically low for fully expanded clays (Morrow et al., 1984).

The shear strength parameters of the studied soils were obtained automatically at each Mc from the intron's software and failure envelopes were produced by plotting shear stress and bulk stress with a tangent line drawn to the failure stress circles. The shear strength values for each tested soil were calculated using equation 2.19. The shear strength parameter of the saturated and unsaturated tested soils is summarised in Table 5.1 in Appendix C.

5.2.3 Shear strength and swelling pressure relationship

Shear strength is important engineering properties of soil and it is the property, that materially influences the bearing capacity of pavement. Figures 5.73 through 5.75 showed that an exponential relationship exists between shear strength and swelling pressure. The results proved that swelling pressure reduces shear strength of compacted soil. This implies that increased swelling pressure in subgrade, causes decrease in shear resistance of the subgrade and this will in turn trigger fatigues that eventually will lead to cracking. Considering the swelling potential of the compacted studied soils, the shape of the exponential shear strength versus swell pressure curve demonstrated a smooth decrease in shear strength values with increase in moisture content for all the studied soils. Alternatively, exponential relation between shear strength and swelling pressure for sample FSS, which recorded the highest swelling potential values among the other studied soils, showed a sudden decrease in shear strength of 16% and 28 % when compared to NCS and GPS respectively. This response is associated with the quantities of expansive clay mineral that are present in FSS. Thus, FSS has the highest content of expandable clay montmorillonite according to XRD results in Appendix A. This result is consistent with the report published by (Morrow et al., 1984) which stated that the expandable clay montmorillonite is by far the weakest of the clay minerals. Therefore, the soil-moisture reaction of the is clay minerals, will reduce shear strength of soils due to swelling potentials.

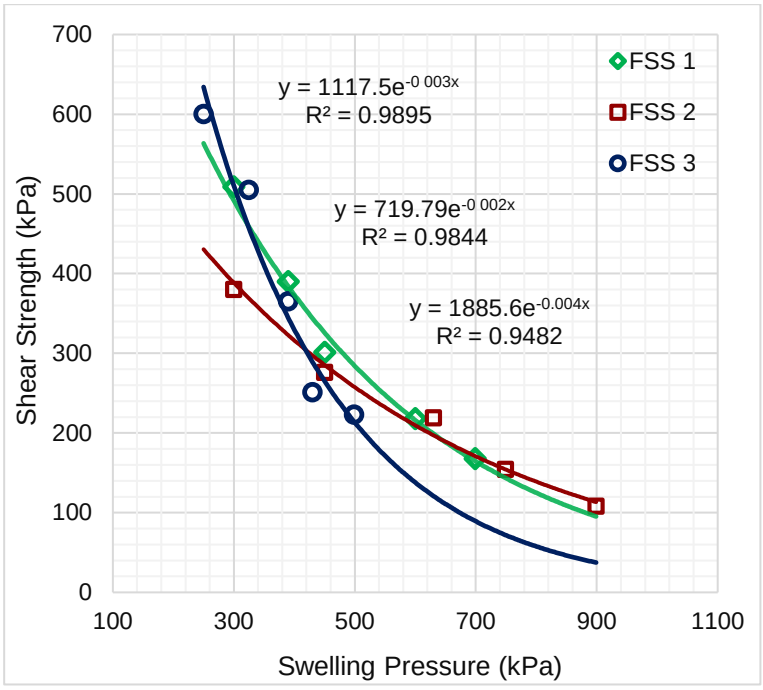

Figure 5. 51: FSS Shear strength – swelling pressure relationship

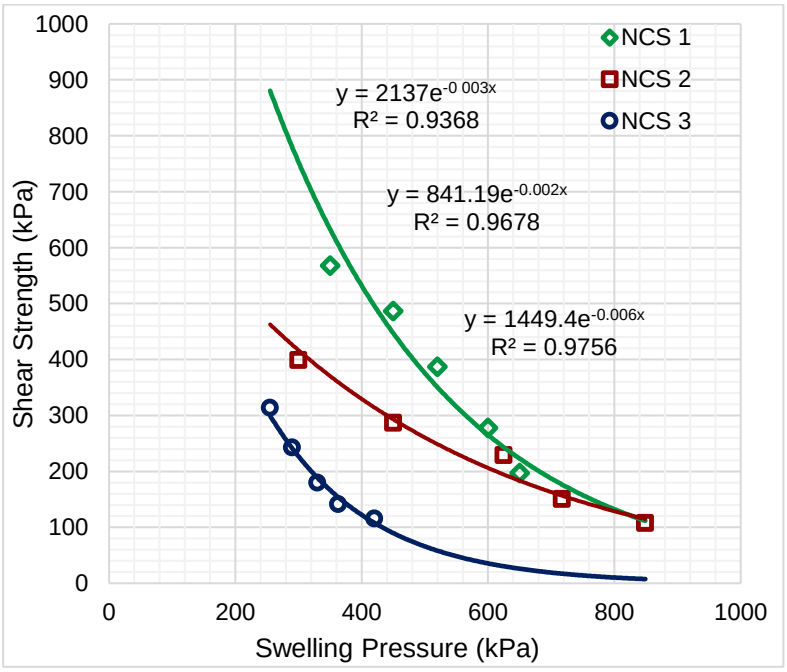

Figure 6. 52: NCS Shear strength – swelling pressure relationship

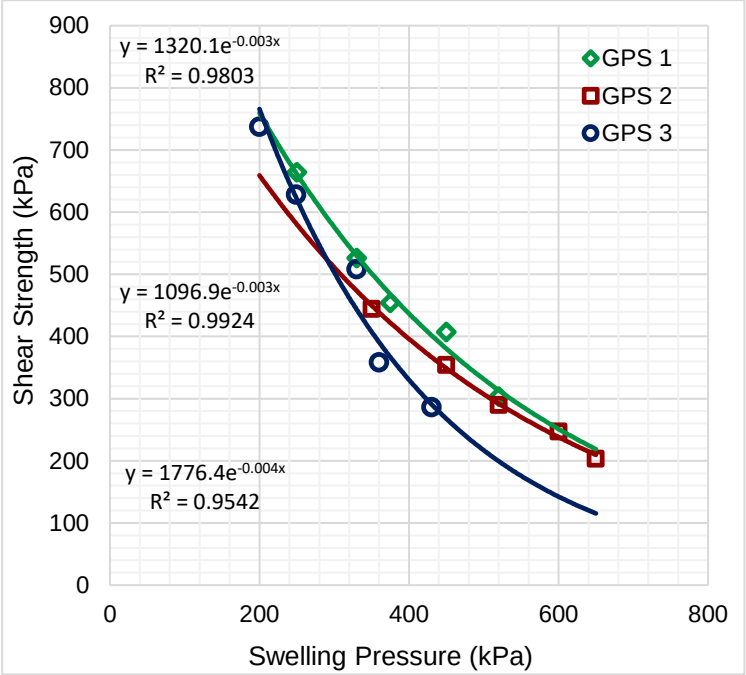

Figure 5.53: GPS Shear strength – swelling pressure relationship

The mathematical expression of shear strength relationship with swell pressure for the studied soils are given in Figures 5.51 through 5.53 by adding trendline in Excel software. These relationships were analysed with several functions such as linear, exponential and polynomial functions. Thus, exponential function was suitable for all the studied soils. The high values of coefficient of determination, R^2 was the decisive factor on the part of regression analysis fittingly for the tested soils.

5.2.4 Shear strength and suction relationship

The relation between the shear strength and suction, depicts the unsaturated failure criteria of the studied soils. The friction angle ($\emptyset^b$) due to shear is associated with matric suction. This gives resistance of the particles to being pulled apart due to surface tension of the thin layer of water surrounding each particle. Figures 6.76 through 6.84 illustrates the variation of shear strength and matric suction values of the studied soil. The curves proved that non-linear relationship between shear strength and matric suction exists. Thus, the soil shear strength values increase with respect to an increase in matric suction which is defined by the angle ($\emptyset^b$). This result agrees with research published by Escario and Juca (1989) which demonstrated an experimental study performed over a large range of suction values shown that the variation of shear strength with respect to suction is non-linear.

Furthermorehe, slope of the curve denoted by $\emptyset^b$, implied that the rate of shear strength increase due to the increase in matric suction. According to the results gotten from this study, the friction angles of the unsaturated soil was evaluated to be less compared to friction angles of the saturated soil. According to Fredlund and Rahardjo (1993), the magnitude of $\emptyset^b$, was normally equal or smaller than the effective friction angle ∅'. Owning to the fact that $\emptyset^b$ recorded in this study is low compared to the saturated ϕ^0. The laboratory result in this research for unsaturated angle of internal friction, is in consistence with the report published by (Donald, 1957, Likos, et al. 2010, Nam et al., 2011) were $\emptyset^b$ is less than ∅' ($\emptyset^b$ > ∅'). The curves showed that $\emptyset^b$ is the angle indicating the rate of variation in shearing strength due to the contribution of matric suction. The result portrayed that shear strength increased with increasing matric suction, this implied that increase in shear strength contribution for matric suction is characterised by $\emptyset^b$. This response of unsaturated shear strength of the tested soils, are simply governed by soil type, high suction values, dilation and different mechanisms of particle interaction due to initial void ratios as a result of the complex response of unsaturated clay, significantly contributed to the low $\emptyset^b$ values.

The stress at failure and the corresponding matric suction of each tested specimens from the consolidated undrained shear strength tests were plotted as a function of unsaturated soil version of failure envelopes. The saturated shear strength of the studied soils was calculated using equation 2.19, while the unsaturated shear strength of the studied soils was calculated using equation 2.27. Whereas, the unsaturated friction angle of soils was determined from the slope between the shear strength and matric suction curves. The shear strength and friction angle for saturated and unsaturated soil mechanics are summarized in Appendix C Table 5.1. Hence, it evidenced from the curves that the shear strength values of the unsaturated soil increase with increase in negative pore water pressure (matric suction), though the increase is non-linear.

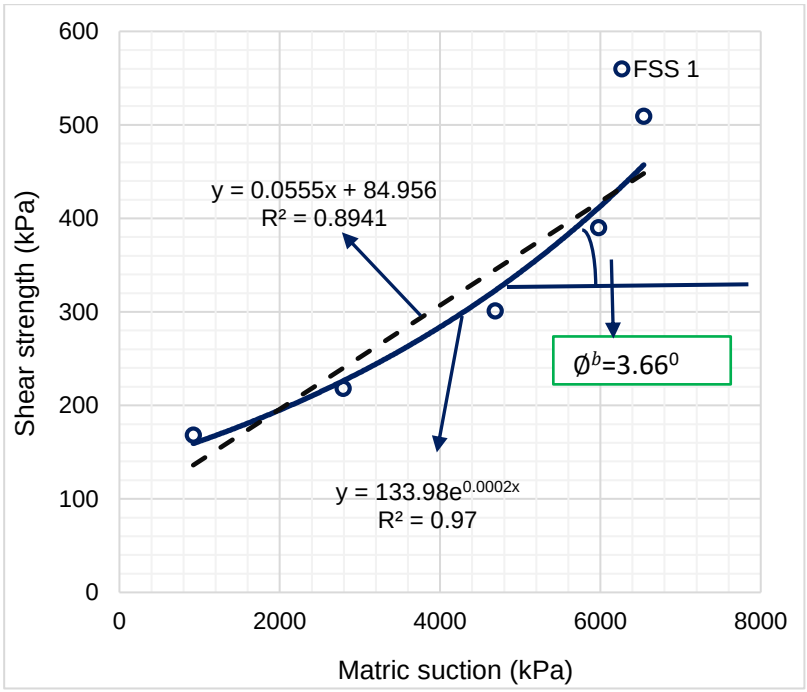

Figure 5.54: Unsaturated failure envelope for FSS1

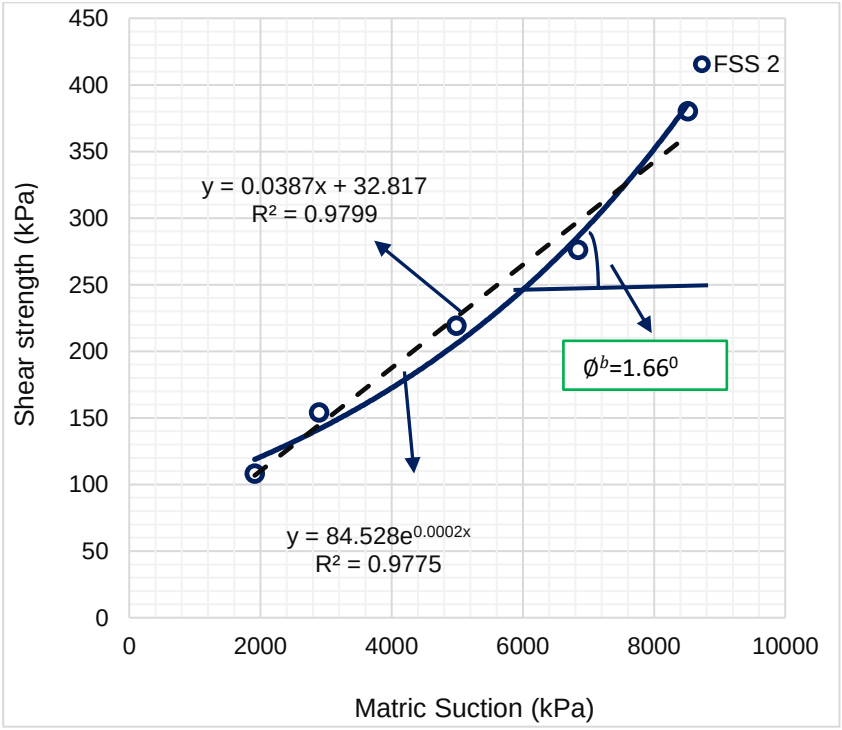

Figure 5.55: Unsaturated failure envelope for FSS2

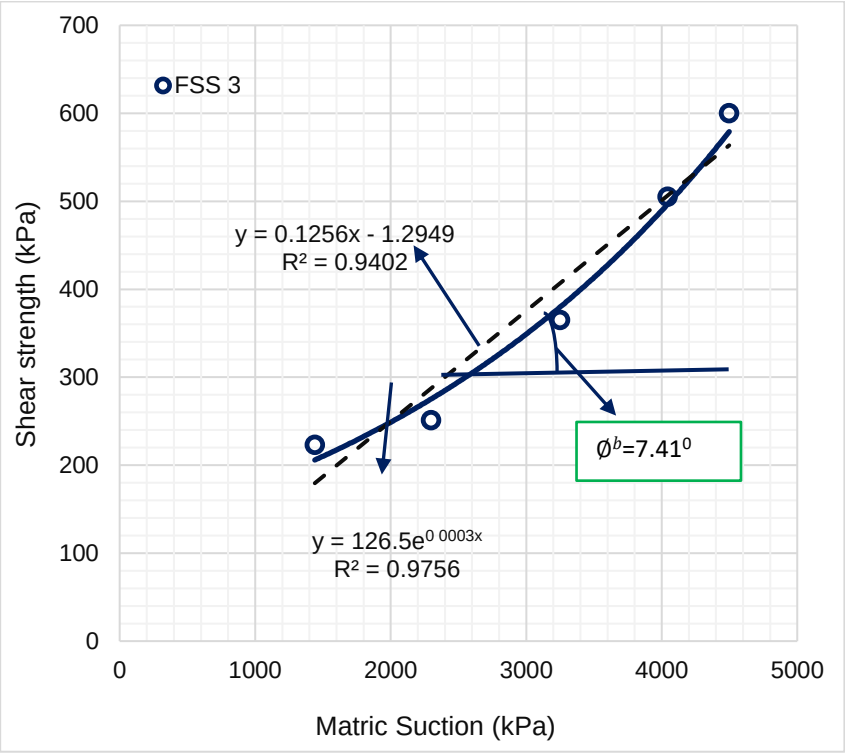

Figure 5.56: Unsaturated failure envelope for FSS3

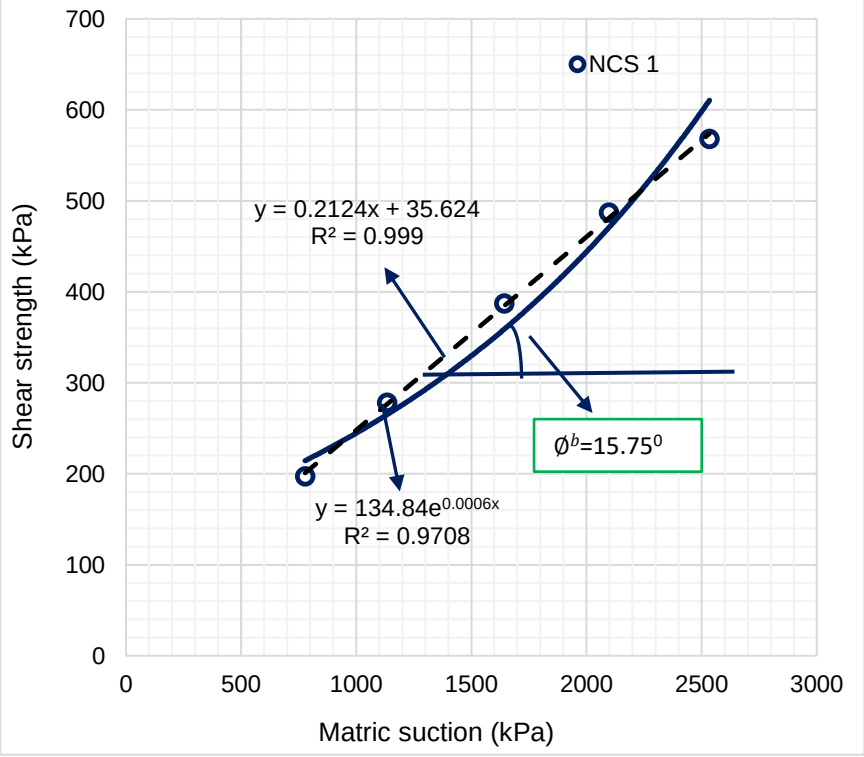

Figure 5.57: Unsaturated failure envelope for NCS 1

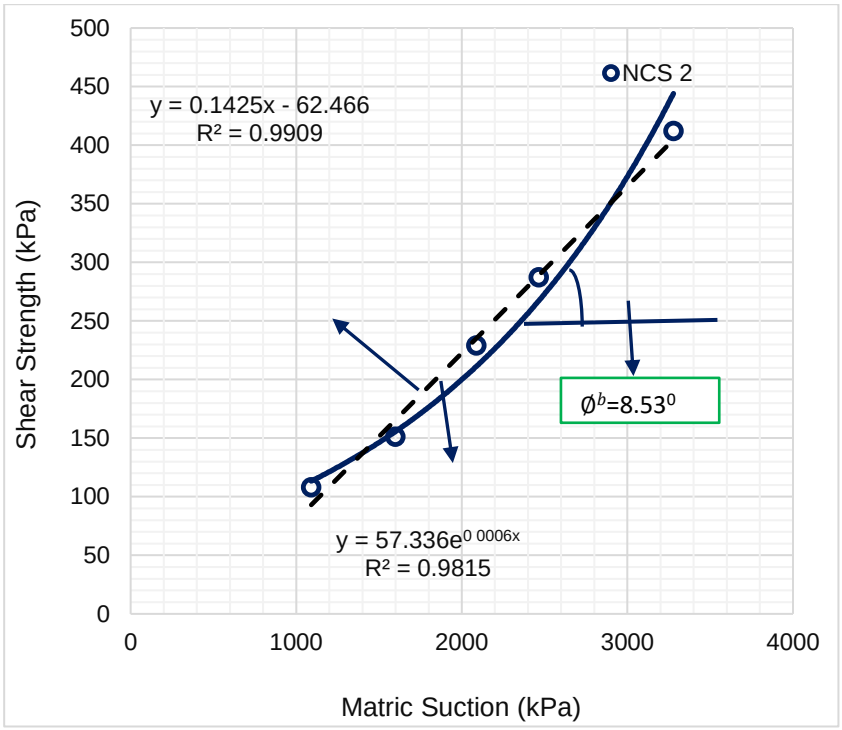

Figure 5. 58: Unsaturated failure envelope for NCS2

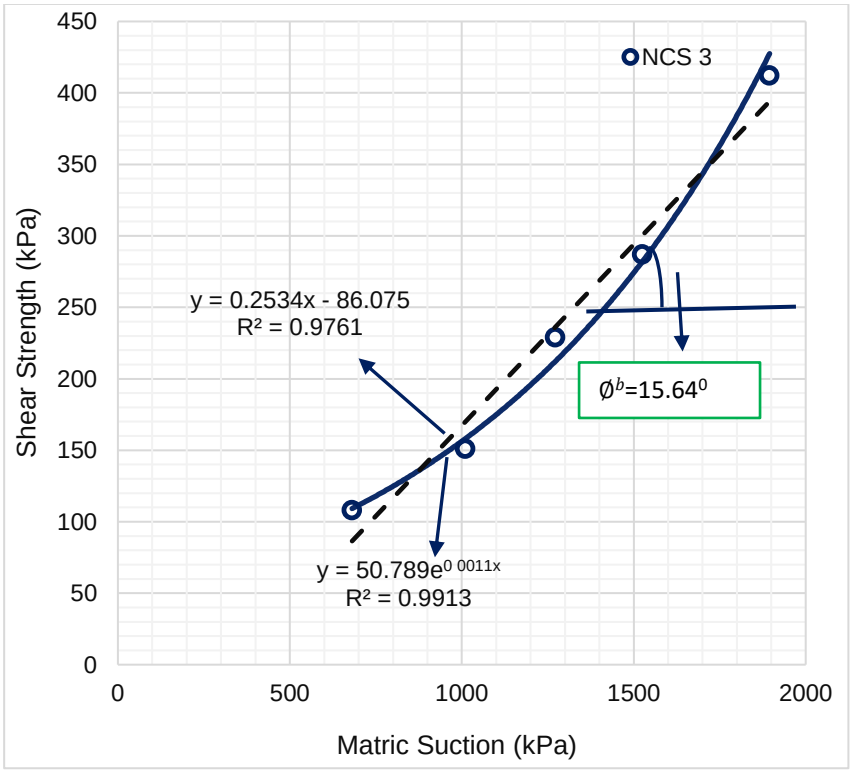

Figure 5. 59: Unsaturated failure envelope for NCS3

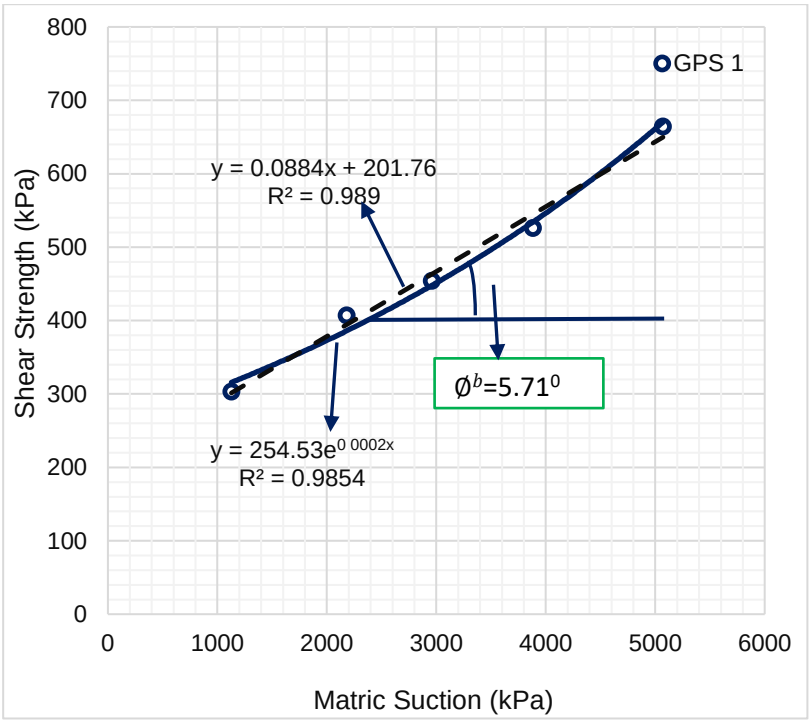

Figure 5.60: Unsaturated failure envelope for GPS 1

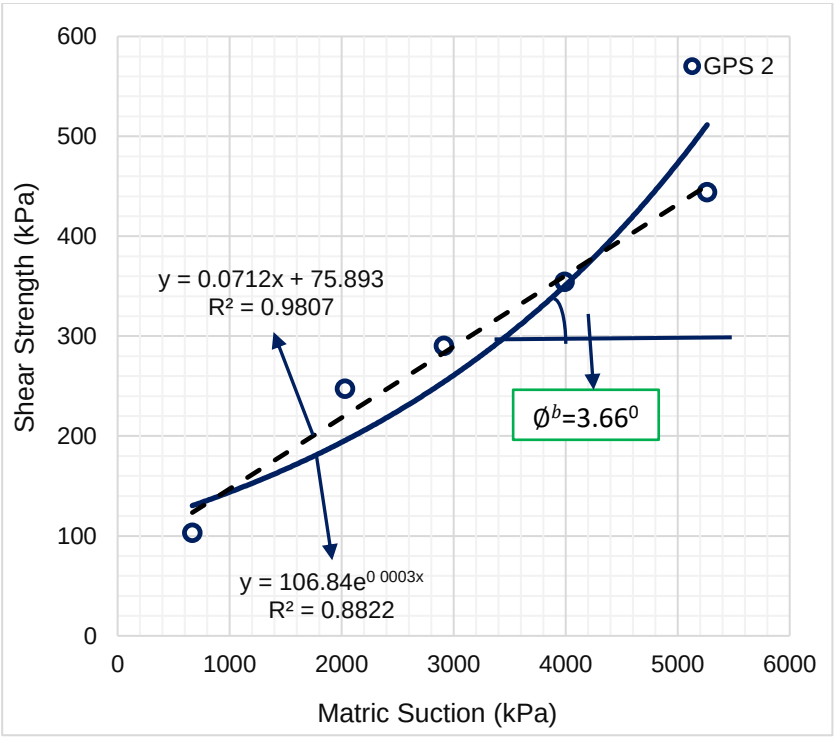

Figure 5.61: Unsaturated failure envelope for GPS 2

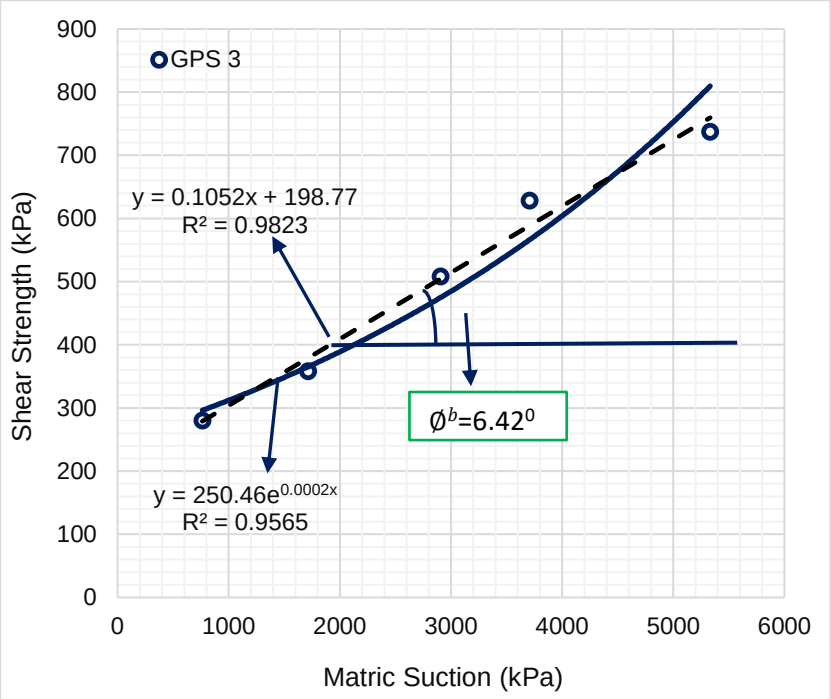

Figure 5.62: Unsaturated failure envelope for GPS 3

Conclusively, in the view of the experimental data, the connection between shear strength and matric suction under consistent net normal stresses is assessed to be non-straight as appeared in Figures 5.54 through 5.62. The collective comparison of the tested soils results and different conditions of saturated and unsaturated shear strength and shear strength parameters are presented in Appendix C Table 5.1. The shear strength of the studied soils i.e. FSS, NCS and GPS, under unsaturated condition increases with matric suction. Perhaps, the unsaturated shear strength values of the tested soils are 1.5 to 2.5 higher than the saturated shear strength values. The failure envelope moves up with the expanding net normal stress, subsequently causing the stress at failure to be high and thusly resulted in higher shear strength values under unsaturated condition.

CHAPTER 6: UNSATURATED RESPONSE OF PAVEMENT STRUCTURE UNDER CYCLIC LOADING

6.1 Overview

This chapter analyse the laboratory results of resilient modulus (M_r) test and as well demonstrated the effects of confining stress, deviatoric stress, moisture content, swelling stress and suction on M_r. The development of M_r predictive models using the test results obtained from various laboratory tests conducted in this research were also presented. A critical evaluation and validation of the developed M_r models and existing M_r models from literature review were assessed. In addition, comparison of pavement designs, using unsaturated soil M_r value and laboratory M_r value were also presented.

6.2 Laboratory Resilient Modulus Test Results

6.2.1 FSS resilient modulus result

The resilient modulus values for the subgrade soils were evaluated using Repeated Load Triaxial Test (RLTT). The axial load and displacement data recorded by M_r data collection was stored in 15 separate data files following the laboratory testing. Each of these data files consisted of the load stroke, and three LVDT displacement values recorded during the test. A software program installed into computer system that are connected to RLTT instron was use to convert these data files into resilient modulus values. The program searched for local maxima in the load and three displacement data sets; these peak values correspond to the peak load and displacement pulses observed during the haversine load pulse. Therefore, 100 load and displacement values were identified in each column. The average Mr values of last five sequences for the soils were recorded. Three identical specimens were tested at the same moisture content to illustrate the variation of Mr with deviatoric stress (σ_d) at different confining pressures (σ_c) of 19.96, 49.61, and 100.93 kPa as obtained from shear strength test. The results showed that the differences in resilient modulus values due to change in confining pressure are small. Figures 6.1 through 6.5 showed that the average difference in resilient modulus values relative to deviator stress is < 5% in FSS. Figure 6.1 is presented below while the rest of the Figures are presented in Appendix D.

Thus, this confirmed that confining pressure effected the resilient modulus values of the soils as the soils yielded high M_r values at higher confinement pressure. However, the trend in variation of M_r with deviator stress, represents strain softening response. This is common among expansive soils, as a result of molding moisture content, compaction effort and soils particle arrangement. Furthermore, the results showed that at low levels of repeated deviator stress, M_r decreases significantly as the deviator stress increases. Whilst, at greater value of deviator stress, M_r decreases slightly until constant value is reached. This result is in line with the report by (Wilson et al. 1990, Drumm et al. 1990).

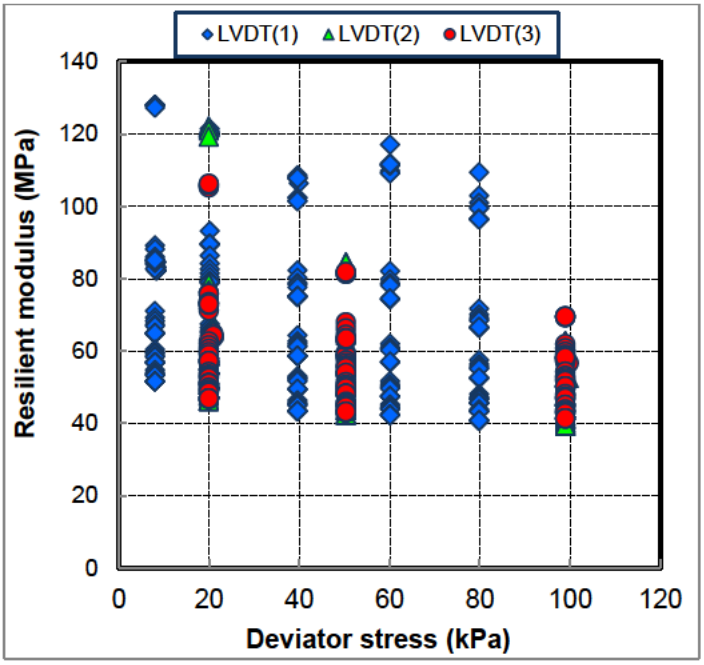

Figure: 6. 1: Variation of M_r of FSS1 at 8.55% moisture with deviatoric stress

6.2.2 NCS resilient modulus result

Typical results of the repeated load triaxial test conducted on the investigated Northern cape soils (NCS) are shown in Figures 6.6 below. Moreover, Figures 6.5 through 6.9 are presented in Appendix D. The test was conducted on NCS specimens 1, 2 and 3 compacted at different moisture content. The curves indicated that the M_r of NCS decreases with the increase in deviator stress under constant confining pressure. Under constant confining pressure of 100 kPa, the M_r decreased from 90.65 MPa to 59.87MPa at 20kPa for NCS 1 prepared with moisture content of 8.38%.

Furthermore, the resilient modulus increases with the increase of confining pressure at particular deviatoric stress, which reflects a typical softening response, that are affected significantly by the stress level. Similar trends were observed for NCS 2 and 3. Thus, NCS 3 recorded the lowest values of M_r. Where, NCS 1 yielded the highest M_r values followed by NCS 2. The low M_r values were due to higher percentage of fine content in NCS 3 according to particles size distribution carried out on the soils as reported in the previous chapter.

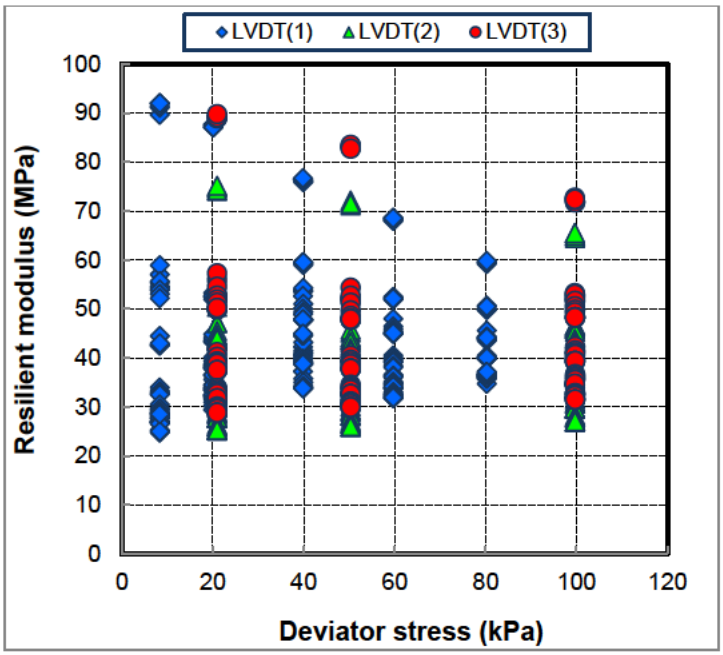

Figure 6. 6: Variation of M_r for NCS 1 at 8.38% moisture with deviatoric stress

6.2.3 GPS resilient modulus result

During the M_r test, average vertical deformation of the specimens were monitored and recorded by using three external variable displacement transducers (LVDTs) placed on the top of the triaxial cell. At each confining pressure, the resilient modulus values of the soils were determined by averaging the resilient deformation of the last five deviatoric cycles. The resilient modulus test results of the GPS specimens were determined based on the external displacement measurements and these results are presented in Figures 6.10, while the rest of the graphs are presented in Appendix D. The curves of the measured M_r were plotted as a function of different deviatoric and confining pressures. The M_r of soil samples showed high sensitivity to deviator stress and moisture variation.

This was as a result of the deviator stress increase, with increase in permanent deformation of the subgrade soils. As such, reduction in the M_r values occurred. The tested soils portrayed similar trend, as the report published by (Lekarp et al. 2000). The report evidenced that deviatoric stress has more effect on soil's stiffness than confinement pressure.

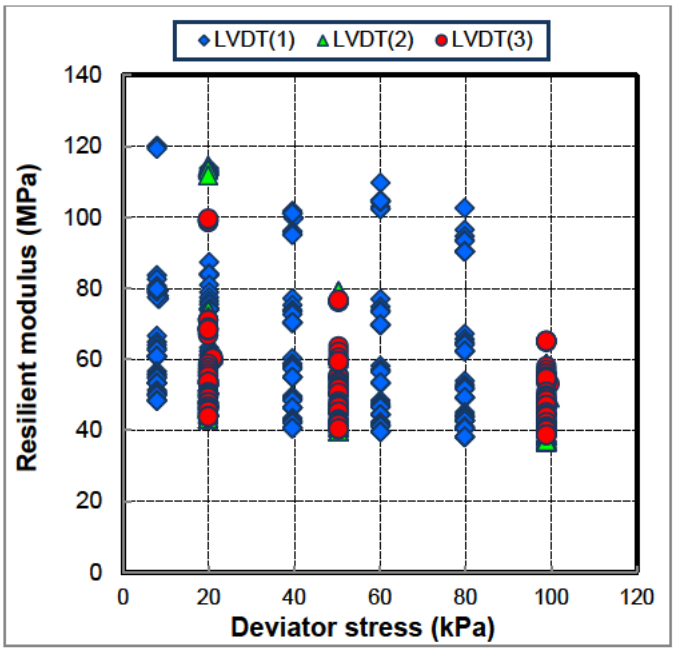

Figure 6. 10: Variation of M_r for GPS 1 at 9.28% moisture with deviatoric stress

Generally, the M_r of the studied soils decreases with an increase in deviatoric stress and M_r of subgrade soils is usually described as a function of deviatoric stress. Moreover, at a high level of deviatoric stress, the soils recorded average of 17.3% decrease in M_r of the studied soils at low deviatoric stress values. While, the effect of confining pressure on subgrades were slightly observed on the tested soils. Resilient modulus of the tested soils slightly increased at a higher confining pressure. This result is in agreement with the result published by Thompson and Robnett (1979). The result concluded that the resilient modulus of fine-grained soils does not depend on the confining pressure. The result stated as that confining pressures in the upper soil layers under pavements are normally less than 35 kPa. These tested subgrades portrayed the tendency to deform axially while bulging with increasing deviator stress. This had a softening effect on the specimens with increasing in deviator stress.

6.2.4 Effect of moisture on resilient modulus

The specimens were prepared at varying moisture content, as was obtained from moisture-density relationship in chapter 4 from section 4.2.1 through 4.2.3. The result demonstrated that moisture content has significant impact on the M_r of the studied subgrade soils. Subgrade M_r is critical in characterizing the support provided to the pavement structure by the underlying subgrade. Considering that the moisture content of a subgrade varies cyclically due to seasonal moisture changes. Therefore, it is imperative to evaluate the effects of moisture changes on M_r. Figure 6.16 illustrate decrease in M_r with increasing moisture content for FSS 1, 2 and 3. The soils prepared beyond the optimum moisture content failed at conditioning stage. Therefore, no M_r values were obtained at moisture content beyond the optimum. FSS 1 and 2 were more weakens by the increase in moisture content, the soils were more susceptible to failure at the optimum moisture content. Thus, failed completely at a point +2.5% moisture beyond the optimum moisture content. This behaviour could be attributed to an increased swelling pressure of the soils with higher PI and fine contents, because of expansive nature of the tested soils.

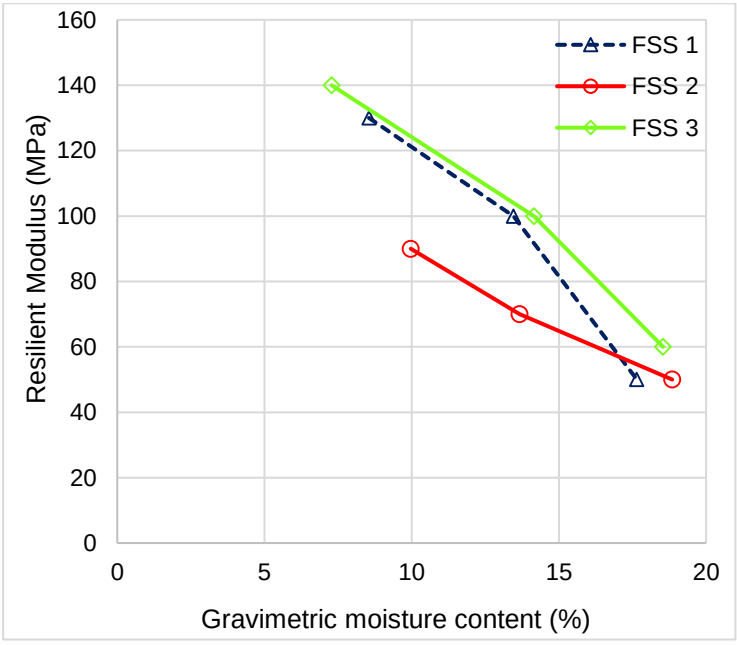

Figure 6.16: Mr – moisture content relationship for FSS

The pavement structures are usually compacted at a point below optimum water content. On the calculation that the subgrade moisture content will come to equilibrium with the surrounding subgrade soils due to seasonal moisture variation. However, the

degree of saturation of subgrade layer of pavement structures varies due to seasonal moisture changes. Therefore, it is important to examine the effects of moisture on the resilient deformation characteristics for the subgrade soils i.e. NCS 1, 2 and 3. To evaluate the resilient deformation characteristics of the subgrade soils, the resilient modulus tests for NCS 1, 2 and 3 under different moisture content were tested with the combinations of three confining 20, 50 and 100 kPa at five deviatoric stress. The effect of moisture content caused appreciable decrease in M_r values, but the decrease was more pronounced in NCS 3 as the soil recorded the lowest M_r values among the studied soils as shown in Figure 6.17. The results followed the same trends with the studied published by (Hossain, 2010), which shows decrease in M_r with increasing moisture content.

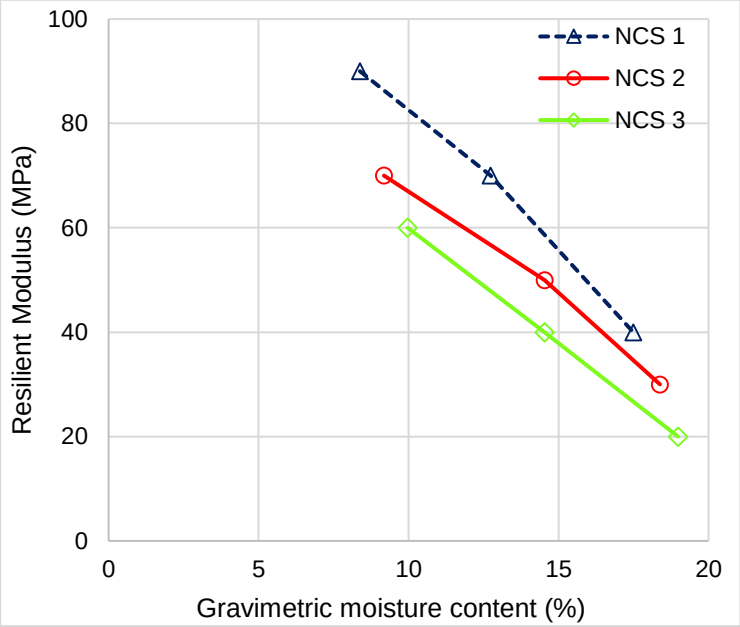

Figure 6.17: Mr – moisture content relationship for NCS

The variation in M_r values for specimens compacted at varying moisture content are represented in Figure 6.18. Comparatively, at a given moisture content, GPS 3 recorded the highest M_r value of 158 MPa at a moisture content of 8.28%. Whereas, at the same moisture content the corresponding M_r values of GPS 1 and 2, where obtained to be 120MPa and 90MPa respectively. This implied that moisture content strongly affected the M_r values of GPS 2, compared to GPS 1 and GPS 3. In addition, the M_r of the tested soils generally decreased with increase in moisture content, irrespective of soil type and deviatoric stress. Therefore, it was observed from the results that moisture content is among the factors that governs Mr of subgrade soils.

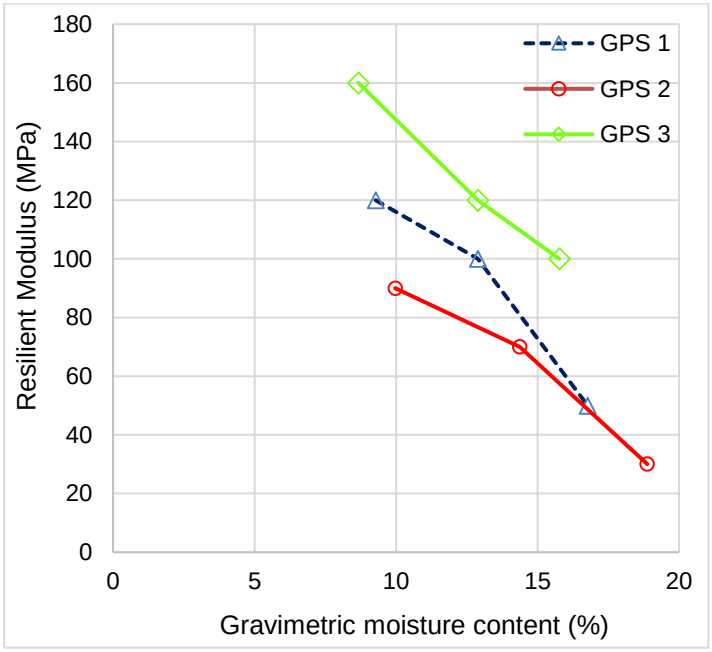

Figure 6.18: Mr – moisture content relationship for GPS

In addition, the highest M_r value was obtained on the dry of the OMC, even though the dry density of the sample at the dry side of OMC is not the maximum dry density. This can be explained due to the capillary suction and lack of lubrication at the dry side of the optimum. At the effect of capillary suction, soil particles moved close to each other, and this increases the shear stress with the soil's particles, therefore resulting to increase in M_r values. The specimens prepared on the wet side of the OMC failed during pre-conditioning stage. Thus, the smallest M_r values were recorded at the OMC as the specimens prepared beyond the OMC failed. Though, GPS 1, 2 and 3 survived the conditioning stage at a moisture content +2% beyond the OMC, but recorded M_r values of 20 MPa, 19MPa and 30MPa for GPS 1, 2 and 3 respectively.

6.2.5 Effect of swelling stress on M_r

Appropriate pavement design requires knowledge of stress-strain response of subgrade layer under cyclic loading. However, to accurately design a pavement, it is significant to consider swelling stress, hence the soil is expansive dealing with nature. Resilient modulus is an important property that characterizes subgrade behaviour through repeated load triaxial test (RLTT), with relatively high reliable testing procedures. Series of repeated load tests were conducted on FSS, NCS and GPS samples at different

moisture content, as to evaluate the stress relationship between of M_r and swelling stress. Figures 6.19 through 6.21 of the tested soils revealed and exponential decreasing in M_r values with increasing swelling pressure. This result, is similar to the result obtained from shear strength modulus variation with swelling stress presented in section 5.2.3, page 125.

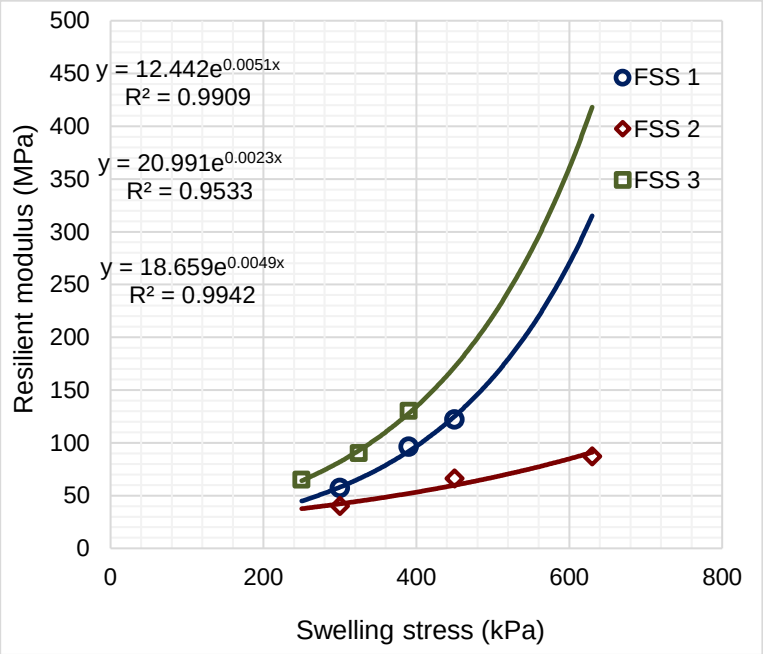

Figure 6.19: M_r – swelling pressure relationship for FSS

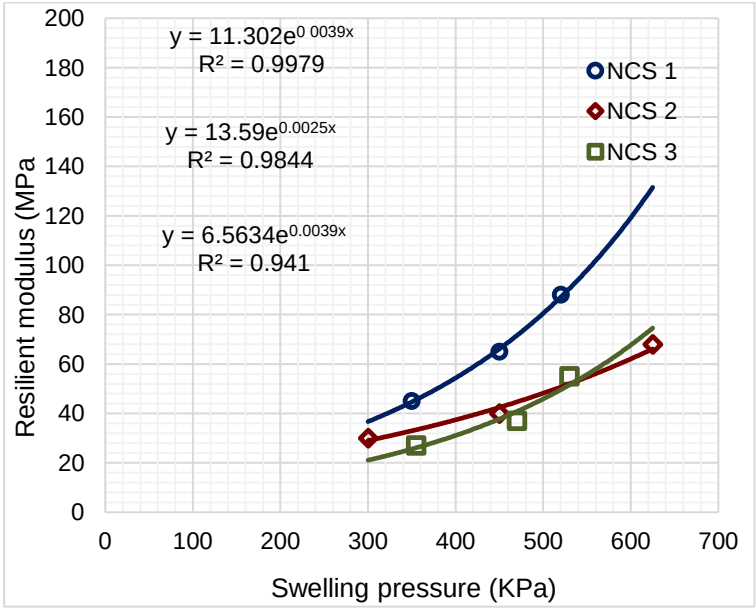

Figure 6.20: M_r – swelling pressure relationship NCS

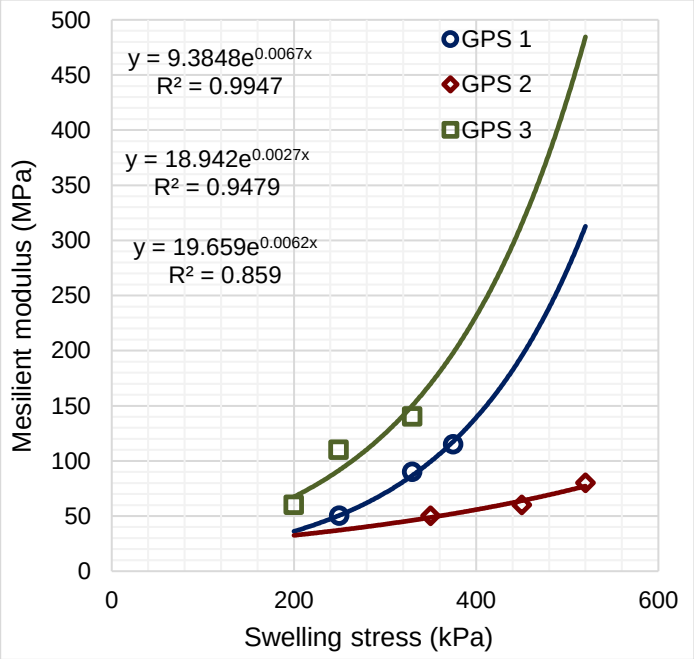

Figure 6.21: M_r – swelling pressure relationship for GPS

The tested soils were allowed to swell by absorbing water before M_r test was conducted on the specimens. The results showed reduction range of 2.18%-3.17% in resilient modulus values of the compacted soils, compared to the M_r values of the specimens that were not subjected swelling. This implies that increased swelling pressure in the studied subgrade, caused some decrease in shear resistance of the subgrades. As this is one the factors that triggers fatigues that leads to cracking on pavement structures constructed on expansive soil. Considering the swelling potential of the compacted studied soils, the shape of the exponential M_r versus swell pressure curve demonstrated a smooth decrease in M_r values with increase in swelling stress of all the studied soils.

6.3 Resilient modulus Estimation Based on Soil Geotechnical Properties

This section centres on build-up and development of mathematical predictive models, for estimating M_r using other geotechnical soil properties. Multiple regression analysis was used to develop mathematical model to predict M_r based on selected conducted geotechnical tests with respect to saturated soil mechanics. Forward and backward stepwise regressions were performed using NCSS11, with M_r as the dependent variable and independent variables are: γ_d, CBR, M_c, P_s, UCS, τ_S, P_{200} and LL. Forward stepwise regression starts without independent variables and sequentially adds variables to the

model in order of their significance in predicting the dependent variable. A backward stepwise regression begins with all independent variables and sequentially removes variables from a model that are least significant in predicting the dependent variable were both explored. Independent variables were added or removed until only those variables that are mathematically significant as measured by a T-test are included in the model. A significance level of 0.05 accuracy was obtained as a result of mathematical significance, of each independent variable and developed mathematical predictive. The accuracy level showed how reliable and accurate the developed models are and the models are presented as follows:

$$M_r(\mathrm{MPa}) = \zeta_0 + \zeta_1(\gamma_{dry}) - \zeta_2(P_{\#200}) - \zeta_3(M_c) - \zeta_4(\mathrm{LL}) - \zeta_5(P_s) \ldots\ldots\ldots\ldots\ldots (\mathrm{Model\ 1})$$

$$M_r(\mathrm{MPa}) = \lambda_0 + \lambda_1(\gamma_{dry}) - \lambda_2(CBR) - \lambda_3(M_c) - \lambda_4(P_s) + \lambda_5(q_u) + \lambda_6(\tau_s) \ldots\ldots (\mathrm{Mode\ 2})$$

$$\mathrm{M_r(MPa)} = \eta_0 + \eta_1(\gamma_{\mathrm{dry}}) - \eta_2(\mathrm{CBR}) - \eta_3(\mathrm{P_{\#200}}) - \eta_4(\mathrm{M_c}) + \eta_5(\mathrm{LL}) - \eta_6(\mathrm{P_s}) + \eta_7(\mathrm{q_u}) + \eta_8(\tau_s) \ldots\ldots\ldots\ldots\ldots\ldots\ldots\ldots\ldots\ldots\ldots\ldots\ldots\ldots\ldots\ldots\ldots\ldots\ldots\ldots\ldots\ldots\ldots\ldots\ldots. (\mathrm{Model\ 3})$$

The values of each symbol and the intercept are summarized in the Table 6.1 Appendix D. Three predictive models were developed using sets of laboratory data. The validation of the models was satisfactory. Comparing the M_r values obtained from the laboratory exercise and M_r values predicted by the developed models (Figures 6.22 through 6.24). The model has an adjusted coefficient of determinations (R^2) of 0.866, 0.936 and 0.939 for model 1, 2 and 3 respectively. The independent variables had p-values < 0.0001 (i.e., << 0.05). The negative coefficient of swelling pressure (P_s) on the three models infers that M_r decreases with increasing swelling pressure.

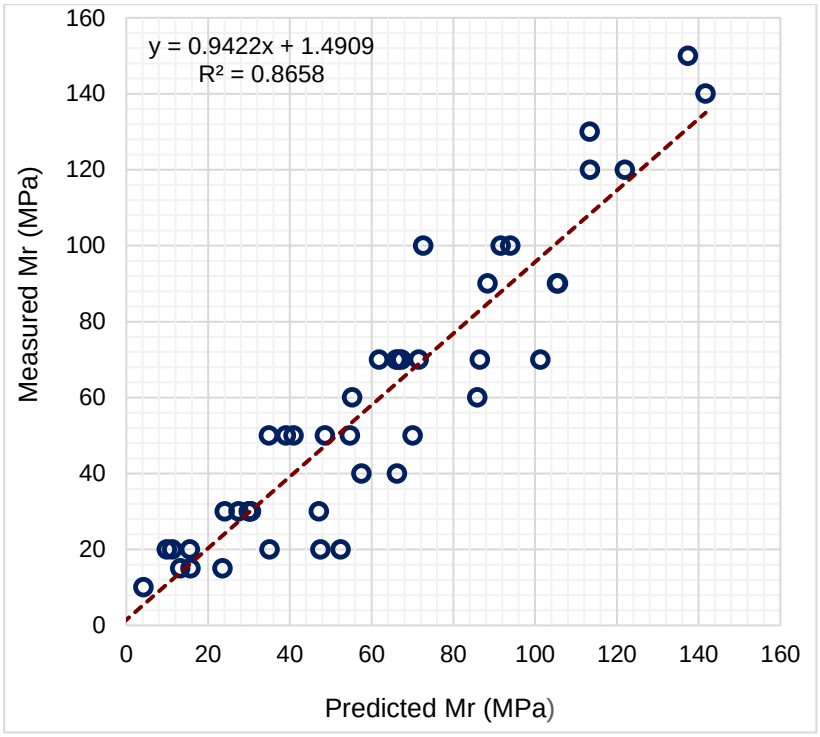

Figure 6. 22: Measured versus Predicted Mr for Model 1

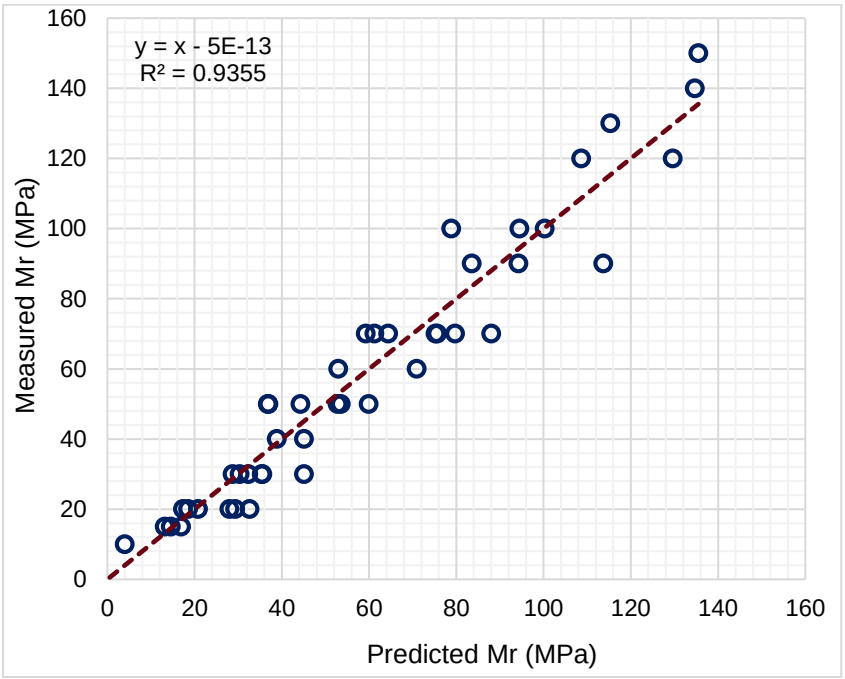

Figure 6. 23: Measured versus Predicted Mr for Model 2

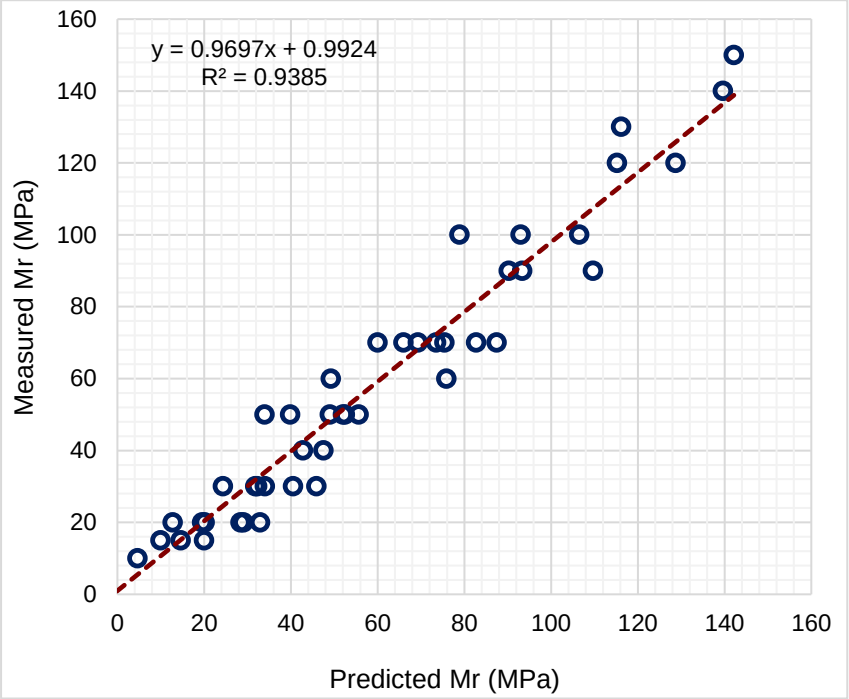

Figure 6.24: Measured versus Predicted Mr for Model 3

The M_r values obtained from the developed models were compared with the measured values. The data trend in Figure 6.22 through 6.24 indicates that there is a good agreement between the measured and predicted M_r values and this result proved the validity of the developed models.

6.4 Resilient Modulus- Matric Suction Relationship

Resilient modulus-matric suction relationship in Figures 6.25 through 6.27 shows variation of Mr with different suction values obtained at various moisture contents. This curves analysed the effects of suction on Mr. This was achieved by correlation of gravimetric moisture content of Mr specimens to the corresponding volumetric moisture content on the SMR, for the matric suction values for each Mr test soils. The results demonstrated that matric suction changes with respect to change in soil moisture conditions. The curves were plotted to understand the overall correlations between Mr and matric suction of the soils. The scattered plot in Figures 6.25 through 6.27 showed that compacting soils in unsaturated state induced suction increase as the Mr values increases. Therefore, a bi-linear relationship exists among Mr and matric suction.

Thus, increase in Mr values is pronounced due to the fact that dry state of soil initiated high suction. This is due to much lower capillary suction and these behaviours are typical

for fine grained soils as reported by Fredlund and Morgenstern, (1977), Drumm et.al. (1997), Huang, (2001). The correlation is considered reliable enough in this study, for estimating unsaturated soil Mr values for the tested subgrade soils. Though, coefficient of determination (R^2) for FSS and NCS were obtained to be 0.6349 and 0.6171 respectively, while that of GPS was obtained to be 0.8148 generally, there is a good correlation between Mr and matric suction since the suction is key independent variable that was used for the development of predictive models for Mr. The laboratory results indicated that matric suction could serve as a good predictor variable for observing the changes in Mr due to variation in moisture content for unsaturated soils.

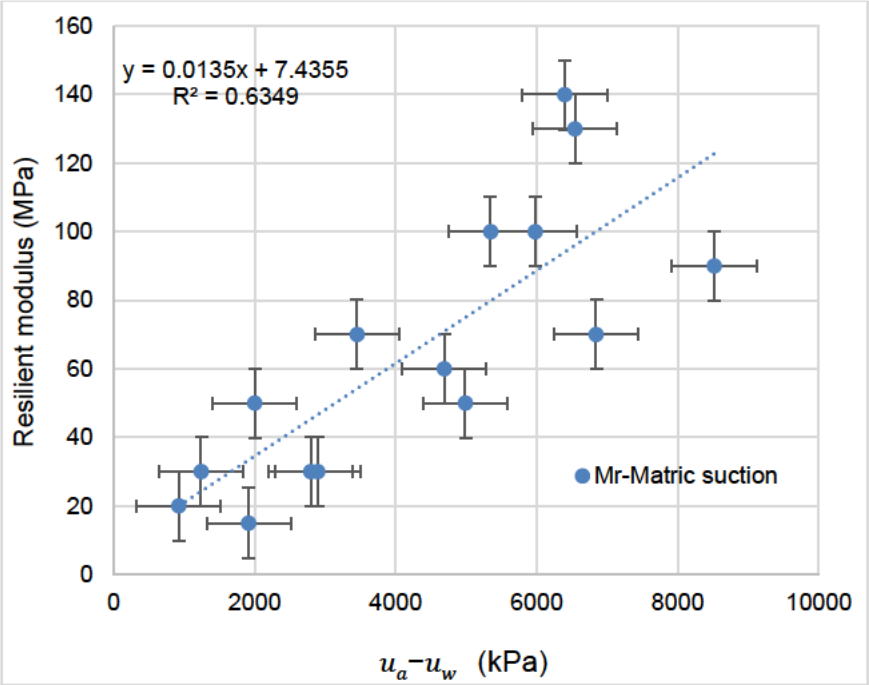

Figure 6.25: Mr – matric suction relationship for FSS

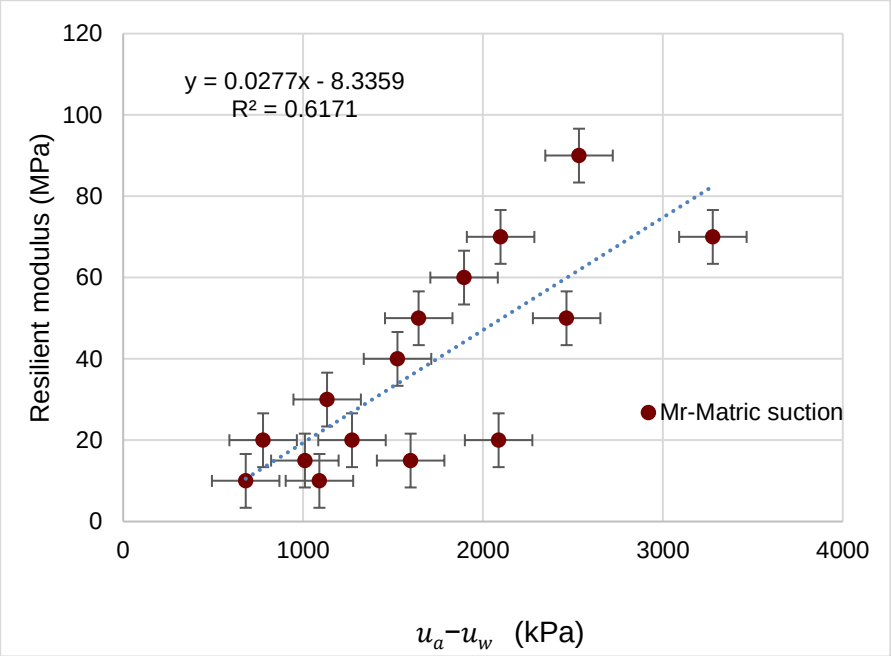

Figure 6.26: Mr – matric suction relationship for NCS

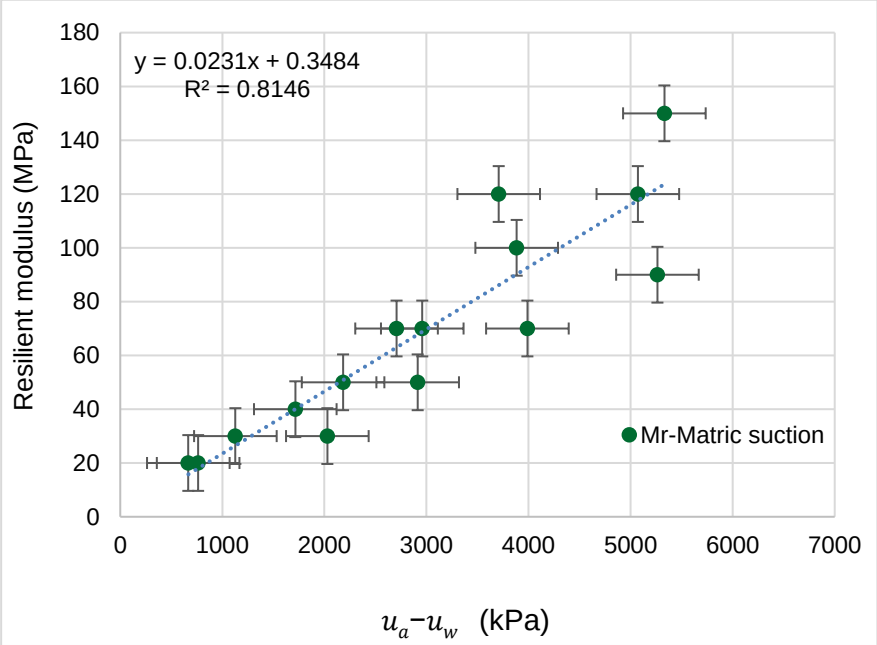

Figure 6.27: Mr – matric suction relationship for GPS

Generally, the scattered plots in Figures 6.25 and 6.27 provided a better theoretical framework for unsaturated soils with respect to suction. This relationship can adequately take into account the effect of moisture variation on changes in M_r.

6.5 Unsaturated Soil M_r

In the field, subgrade soils are normally subjected to continual seasonal moisture variations and this behaviour of unsaturated subgrade soils is governed by two stress state variables which are net normal stress and matric suction. Therefore, it is imperative to evaluate the unsaturated resilient modulus of a soil applying suction. The unsaturated Mr values of the specimens were determined by preparing two sets of identical specimens as mentioned earlier on section 3.5.4 page 68, at different moisture content as obtained from compaction exercise. One set of the identical specimens were used to measure the soils suction, while remaining set of the specimens were used to measure Mr. Furthermore, the unsaturated M_r of the studied soils were computed using Equation 2 2.61 and 2.65 by Yang et. al (2005) and Lian et.al (2008) in the literature review on pages 42 and 46 respectively.

This models considered the influence of deviator, matric suction and the lower impact of confining stress in terms of bulk stress. The test data were fitted into this model and the regression parameters K_1, K_2 and K_3 for each model at different moisture content and dry density, were obtained, using multiple linear regression statistical software package named NCSS11. Each model parameters K_1, K_2 and K_3 are presented in Tables 6.3 through 6.5. Furthermore, two more models were developed using matric suction, air-entry values, unsaturated CBR, dry density and swelling stress, to evaluate the unsaturated M_r of the studied soils. The model coefficients of each developed models are presented in Table 2 Appendix D. Amongst other developed model is the extension of Yang's model in which swelling stress is negatively integrated, as the swelling pressure negatively affects Mr by reducing the soils Mr values. The five models that are used to evaluate M_r values of the tested soils are listed as follows:

$$\mathrm{M_r(MPa)} = \mathrm{k_1}(\sigma_\mathrm{d} + x\psi_\mathrm{m})^{\mathrm{k_2}} \quad \text{Yang et. al 2005} \ldots\ldots \text{(Model 4)}$$

$$\mathrm{M_r(MPa)} = \mathrm{k_1}(\sigma_\mathrm{d} + x\psi_\mathrm{m})^{\mathrm{k_2}} - \mathrm{P_{S_n}} \quad \text{Extension of Yang et. al 2005 model} \ldots\ldots \text{(Model 5)}$$

$$\mathrm{M_r(MPa)} = (\mathrm{k_1 P_a}\left(\frac{\theta + x\psi_\mathrm{m}}{\mathrm{P_a}}\right)^{\mathrm{k_2}}\left(\frac{\tau_\mathrm{oct}}{\mathrm{P_a}} + 1\right)^{\mathrm{k_3}} \quad \text{Liang et. al 2008} \ldots\ldots \text{(Model 6)}$$

$$M_r\mathrm{(MPa)} = \xi_0 + \xi_1(\psi_\mathrm{m}) - \xi_2(S_e) + \xi_3(CBR_u) - \xi_4\left(P_{S_n}\right) \quad \text{Author's} \ldots\ldots \text{(Model 7)}$$

$$\mathrm{M_r(MPa)} = \alpha_0 + \alpha_1(\psi_\mathrm{m}) - \alpha_2(\mathrm{S_e}) - \alpha_3\left(\mathrm{P_{S_n}}\right) + \alpha_4(\mathrm{CBR_u}) - \alpha_5(\gamma_\mathrm{dry}) \quad \text{Author's} \ldots\ldots \text{(Model 8)}$$

The M_r values of the studied soils were calculated at a constant deviatoric of σ_1- σ_3 and confining stress of, 100 kPa were considered. Thus, the studied soils recorded the highest M_r values, at this stresses. The of value $x = 1$ is considered for the calculation of the M_r, as x is the parameter representing contribution of suction on soil resilient stress. The equation coefficients for models 7 and 8 are available in Appendix D.

Table 6.3: Unsaturated resilient modulus using model 4

Soils	ω%	γ_d (kN/m^3)	K_1	K_2	R^2	ψ_m (MPa)	Measured M_r (MPa)	Predicted M_r (MPa)
FSS 1								
	8.35	12.45	375	-0.363	0.459	6.541	130	190.6
	13.56	16.63	289	-0.395	0.472	5.676	100	145.4
	17.48	17.32	198	-0.438	0.493	4.989	60	97.83
	24.27	15.90	-	-	-	2.793	Failed	Failed
	31.75	12.88	-	-	-	0.921	Failed	Failed
FSS 2								
	10.13	12.47	415	-0.542	0.456	8.517	90	130
	13.61	15.62	376	-0.687	0.428	6.343	70	106
	18.54	16.93	312	-0.753	0.416	5.189	50	90
	24.09	14.15	-	-	-	2.895	Failed	Failed
	30.16	12.12	-	-	-	1.913	Failed	Failed
FSS 3								
	7.33	11.45	525	-0.546	0.432	6.398	140	190.4
	14.19	17.61	473	-0.687	0.387	5.345	100	149.3
	18.48	16.59	418	-0.999	0.342	3.450	70	121
	22.91	16.93	-	-	-	1.998	Failed	Failed
	28.30	13.47	-	-	-	1.240	Failed	Failed
NCS 1								
	8.40	16.07	410	-1.256	0.348	2.534	90	127
	12.70	18.92	270	-1.289	0.377	2.098	70	103
	17.51	19.35	150	-1.297	0.421	1.643	50	78
	24.52	17.52	-	-	-	1.134	Failed	Failed
	28.35	16.18	-	-	-	0.778	Failed	Failed
NCS 2								
	9.20	15.45	377	-0.980	0.543	3.878	70	99.57
	14.18	17.52	200	-0.985	0.457	2.465	50	80
	18.40	18.52	100	-0.997	0.632	2.087	20	48
	24.91	18.89	-	-	-	1.598	Failed	Failed
	30.23	15.58	-	-	-	1.091	Failed	Failed
NCS 3								
	9.94	14.17	150	-1.181	0.567	1.595	60	86
	14.55	15.86	100	-1.198	0.584	1.545	40	59
	18.87	16.83	60	-1.299	0.632	1.172	20	42.49
	25.26	15.95	-	-	-	0.990	Failed	Failed
	32.92	13.02	-	-	-	0.681	Failed	Failed
GPS 1								

	8.69	16.47	415	-0.588	0.437	5.071	120	160
	13.48	19.46	387	-0.793	0.421	3.884	100	132
	17.30	21.83	200	-0.757	0.875	2.959	70	88
	24.31	20.07	295	-0.976	0.654	2.183	30	70
	32.72	16.16	-	-	-	1.128	Failed	Failed
GPS 2								
	9.95	15.45	377	-0.689	0.432	5.263	90	120
	13.69	19.23	318	-0.792	0.451	3.989	70	106
	18.56	20.89	200	-0.884	0.865	2.914	50	77.41
	24.11	18.96	249	-0.979	0.435	2.029	20	60
	30.14	15.96	-	-	-	0.667	Failed	Failed
GPS 3								
	9.30	18.13	525	-0.589	0.412	5.331	150	196
	14.18	21.63	474	-0.876	0.418	3.708	120	150
	18.85	22.84	250	-0.949	0.389	2.707	90	96.74
	22.91	21.71	130	-0.984	0.421	1.715	40	76
	27.30	18.83	-	-	-	0.763	Failed	Failed

***γ_d = dry unit weight *ψ_m = matric suction * M_r = resilient modulus * ω = moisture content**

Table 6.4: Unsaturated resilient modulus using model 5

Soils	ω%	γ_d (kN/m^3)	K_1	K_2	R^2	ψ_m (kPa)	P_{s_n} (kPa)	Measured M_r (MPa)	Predicted M_r (MPa)
FSS 1									
	8.35	12.45	375	-0.363	0.459	6.541	0.699	130	189.90
	13.56	16.63	289	-0.395	0.472	5.676	0.600	100	144.8
	17.48	17.32	198	-0.438	0.493	4.989	0.450	60	97.38
	24.27	15.90	-	-	-	2.793	0.390	Failed	Failed
	31.75	12.88	-	-	-	0.921	0.330	Failed	Failed
FSS 2									
	10.13	12.47	415	-0.542	0.456	8517	0.899	90	129.101
	13.61	15.62	376	-0.687	0.428	6343	0.749	70	105.251
	18.54	16.93	312	-0.753	0.416	4989	0.630	50	89.37
	24.09	14.15	-	-	-	2895	0.450	Failed	Failed
	30.16	12.12	-	-	-	1913	0.300	Failed	Failed
FSS 3									
	7.33	11.45	525	-0.546	0.432	6398	0.499	140	189.901
	14.19	17.61	473	-0.687	0.387	5345	0.450	100	148.85
	18.48	16.59	418	-0.999	0.342	3450	0.390	70	120.67
	22.91	16.93	-	-	-	1998	0.330	Failed	Failed
	28.30	13.47	-	-	-	1240	0.250	Failed	Failed
NCS 1									
	8.40	16.07	410	-1.256	0.348	2.534	0.650	90	126.35
	12.70	18.92	270	-1.289	0.377	2.098	0.600	70	102.4
	17.51	19.35	150	-1.297	0.421	1.643	0.520	50	77.48
	24.52	17.52	-	-	-	1.134	0.450	Failed	Failed
	28.35	16.18	-	-	-	0.778	0.350	Failed	Failed

NCS 2									
	9.20	15.45	377	-0.980	0.543	3878	0.630	70	98.94
	14.18	17.52	200	-0.985	0.457	2465	0.500	50	79.5
	18.40	18.52	100	-0.997	0.632	2087	0.450	20	47.55
	24.91	18.89	-	-	-	1598	0.400	Failed	Failed
	30.23	15.58	-	-	-	1091	0.350	Failed	Failed
NCS 3									
	9.94	14.17	150	-1.181	0.567	1595	0.830	60	85.17
	14.55	15.86	100	-1.198	0.584	1545	0.725	40	58.28
	18.87	16.83	60	-1.299	0.632	1172	0.650	20	41.84
	25.26	15.95	-	-	-	990	0.520	Failed	Failed
	32.92	13.02	-	-	-	681	0.400	Failed	Failed
GPS 1									
	8.69	16.47	415	-0.588	0.437	5071	0.490	120	159.51
	13.48	19.46	387	-0.793	0.421	3884	0.450	100	131.55
	17.30	21.83	200	-0.757	0.875	2959	0.375	70	87.63
	24.31	20.07	295	-0.976	0.654	2183	0.350	50	69.65
	32.72	16.16	-	-	-	1128	0.250	Failed	Failed
GPS 2									
	9.95	15.45	377	-0.689	0.432	5263	0.650	90	119.35
	13.69	19.23	318	-0.792	0.451	3989	0.600	70	105.4
	18.56	20.89	200	-0.884	0.865	2914	0.520	50	76.89
	24.11	18.96	249	-0.979	0.435	2029	0.450	30	59.55
	30.14	15.96	-	-	-	667	0.350	Failed	Failed
GPS 3									
	9.30	18.13	525	-0.589	0.412	5331	0.520	150	195.48
	14.18	21.63	474	-0.876	0.418	3708	0.425	120	149.58
	18.85	22.84	250	-0.949	0.389	2707	0.400	70	96.34
	22.91	21.71	130	-0.984	0.421	1715	0.300	40	75.7
	27.30	18.83	-	-	-	763	0.200	Failed	Failed

***γ_d = dry unit weight *ψ_m = matric suction * M_r = resilient modulus * ω = moisture content * P_{s_n} = swelling pressure**

Table 6.5: Unsaturated resilient modulus using model 6

Soils	ω%	γ_d (kN/m^3)	K_1	K_2	K_3	R^2	ψ_m (kPa)	Measured M_r (MPa)	Predicted M_r (MPa)
FSS 1									
	8.35	12.45	750	0.119	0.339	0.824	6.541	130	138.17
	13.56	16.63	500	0.148	0.453	0.943	5.676	100	105.44
	17.48	17.32	200	0.258	0.673	0.952	4.989	60	68
	24.27	15.90	-	-	-	-	2.793	Failed	Failed
	31.75	12.88	-	-	-	-	0.921	Failed	Failed
FSS 2									
	10.13	12.47	650	0.054	0.332	0.975	8.517	90	92.17
	13.61	15.62	500	0.067	0.432	0.934	6.343	70	76
	18.54	16.93	350	0.075	0.464	0.927	4.989	50	54.44
	24.09	14.15	-	-	-	-	2.895	Failed	Failed

	30.16	12.12	-	-	-	-	1.913	Failed	Failed
FSS 3									
	7.33	11.45	900	0.088	0.348	0.953	6.398	140	146
	14.19	17.61	700	0.093	0.359	0.843	5.345	100	114
	18.48	16.59	500	0.098	0.427	0.884	3.450	70	81.47
	22.91	16.93	-	-	-	-	1.998	Failed	Failed
	28.30	13.47	-	-	-	-	1.240	Failed	Failed
NCS 1									
	8.40	16.07	650	0.075	0.364	0.829	2.534	90	98
	12.70	18.92	500	0.084	0.395	0.942	2.098	70	73.43
	17.51	19.35	400	0.097	0.439	0.854	1.643	50	61
	24.52	17.52	-	-	-	-	1.134	Failed	Failed
	28.35	16.18	-	-	-	-	0.778	Failed	Failed
NCS 2									
	9.20	15.45	500	0.079	0.456	0.873	3.878	70	77.47
	14.18	17.52	400	0.085	0.487	0.842	2.465	50	62
	18.40	18.52	200	0.095	0.493	0.838	2.087	20	31.45
	24.91	18.89	-	-	-	-	1.598	Failed	Failed
	30.23	15.58	-	-	-	-	1.091	Failed	Failed
NCS 3									
	9.94	14.17	530	0.066	0.532	0.852	1.595	60	76
	14.55	15.86	410	0.069	0.583	0.689	1.545	40	60
	18.87	16.83	280	0.072	0.632	0.732	1.172	20	38
	25.26	15.95	-	-	-	-	0.990	Failed	Failed
	32.92	13.02	-	-	-	-	0.681	Failed	Failed
GPS 1									
	8.69	16.47	800	0.068	0.579	0.965	5.071	120	126
	13.48	19.46	650	0.073	0.591	0.987	3.884	100	103
	17.30	21.83	510	0.079	0.637	0.852	2.959	70	81.18
	24.31	20.07	380	0.085	0.689	0.842	2.183	50	62
	32.72	16.16	-	-	-	-	1.128	Failed	Failed
GPS 2									
	9.95	15.45	650	0.076	0.648	0.821	5.263	90	108
	13.69	19.23	470	0.079	0.681	0.873	3.989	70	78.07
	18.56	20.89	370	0.087	0.686	0.834	2.914	50	61.79
	24.11	18.96	260	0.094	0.734	0.794	2.029	30	43.70
	30.14	15.96	-	-	-	-	0.667	Failed	Failed
GPS 3									
	9.30	18.13	1185	0.046	0.437	0.843	5.331	150	160
	14.18	21.63	900	0.055	0.495	0.892	3.708	120	129
	18.85	22.84	570	0.063	0.561	0.836	2.707	70	84.10
	22.91	21.71	340	0.071	0.583	0.821	1.715	40	50.33
	27.30	18.83	-	-	-	-	0.763	Failed	Failed

***γ_d = dry unit weight *ψ_m = matric suction * M_r = resilient modulus * ω = moisture content**

Conclusively, Tables 6.3 through 6.5 presents the results obtained from the regression analysis performed on the measured M_r values by utilizing models 4 through 6. The values of the regression constants, along with coefficient of determination (R^2), are shown for each soil and moisture content tested. Some general trends due to changes in moisture conditions was observed amongst the regression constants. Generally, it was observed that k_1 coefficient attained maximum value on the dry side and this values decreases with increasing moisture content. This regression trend of the studied soils is in agreement with result published by Nazzal and Mohammad (2010). The regression result of the soils showed that k_1 is proportional to the stiffness of the material which is dependent on the effective stress of the soil. Under unsaturated soils, effective stress is dependent on matric suction, and matric suction increases with decreasing water content, therefore the increase in k_1 can be attributed to an increase in matric suction. The coefficient for k_2 is related to deviator stress for model 4. Thus, has negative values as it tend to decrease with increasing moisture content. While coefficient for k_2 in model 5 is positive, as it is related to bulk stress.

Generally, the value of k_3 coefficient is positive, as the regression analysis identified the best subset of independent variables that results in accurate correlation between resilient modulus model parameters k_i and basic soil properties. However, the k_3 coefficient describes the softening of the soils with increasing octahedral shear stress and values reduces with increasing moisture content. This implied that the soils at a higher moisture content are more susceptible to softening due to increase in shear stress.

6.5.1 Validation of the developed and existing models

In order to validate the models used in this study, five models with varying degrees of predictability were plotted against the laboratory measure M_r data. The M_r calculated using model 4, 5 and 6 best fitted the laboratory data, because this models coefficient of determination (R^2) were obtained to 0.9438, 0.9607 and 0.9533 respectively. In addition, the M_r of unsaturated subgrade soil mainly depend on suction, deviatoric stress level and confining pressure, which are the parameter coefficient in this models.

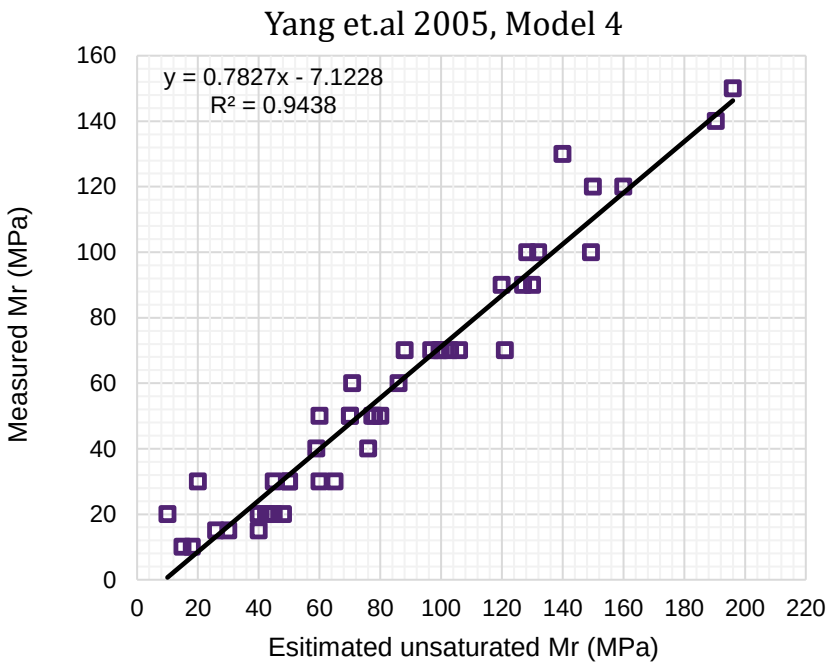

Figure 6. 28: Validation of model 4

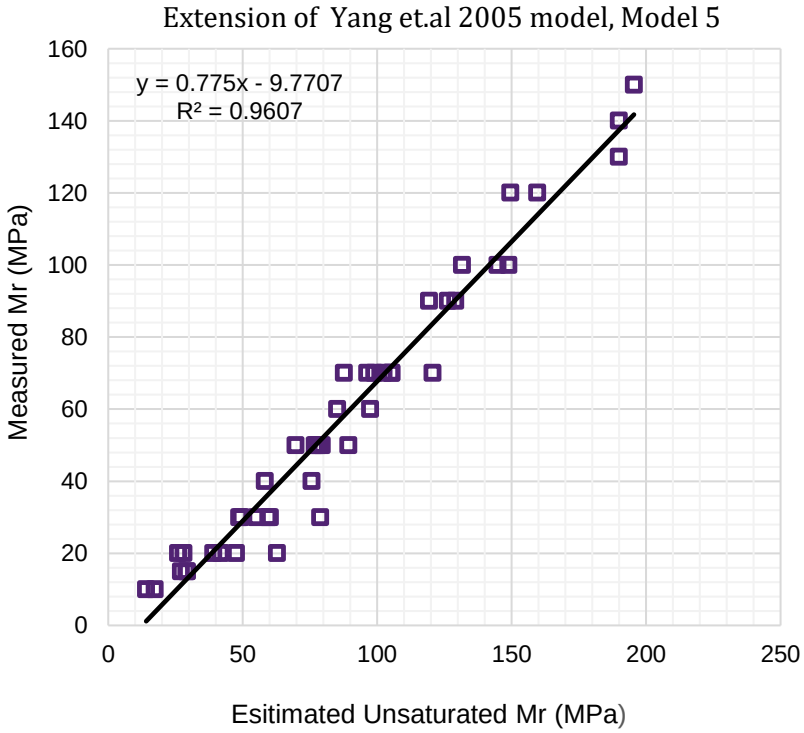

Figure 6. 29: Validation of model 5

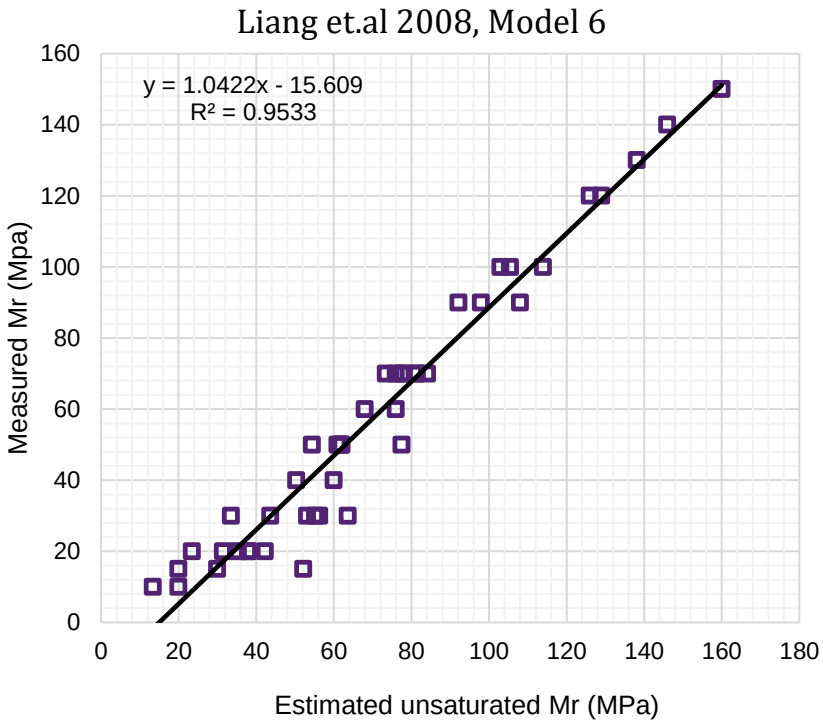

Figure 6.30: Validation of model 6

The results from the M_r tests were correlated with other unsaturated soil properties i.e. Air entry value, suction, unsaturated CBRu and dry densities. The developed models 7 and 8 for estimating M_r of studied soils showed strong correlation with R^2 of 0.9134 and 0.9139 for models 7 and 8 respectively. Though, models 4, 5 and 6 were found to have higher R^2 compared to models 7 and 8. The low value of R^2 for models 7 and 8 were expected as this models is given as function of suction, air-entry values unsaturated CBR and dry density.

Generally, this models were acceptable though deviatoric and confining stresses were not considered as independent variables during regression exercise. Moreover, there is a strong correlation between the predicted and measured M_r as shown in Figures 6.31 and 6.32. This implies that models 7 and 8 are suitable for predicting unsaturated M_r of expansive subgrade with high degree of accuracy.

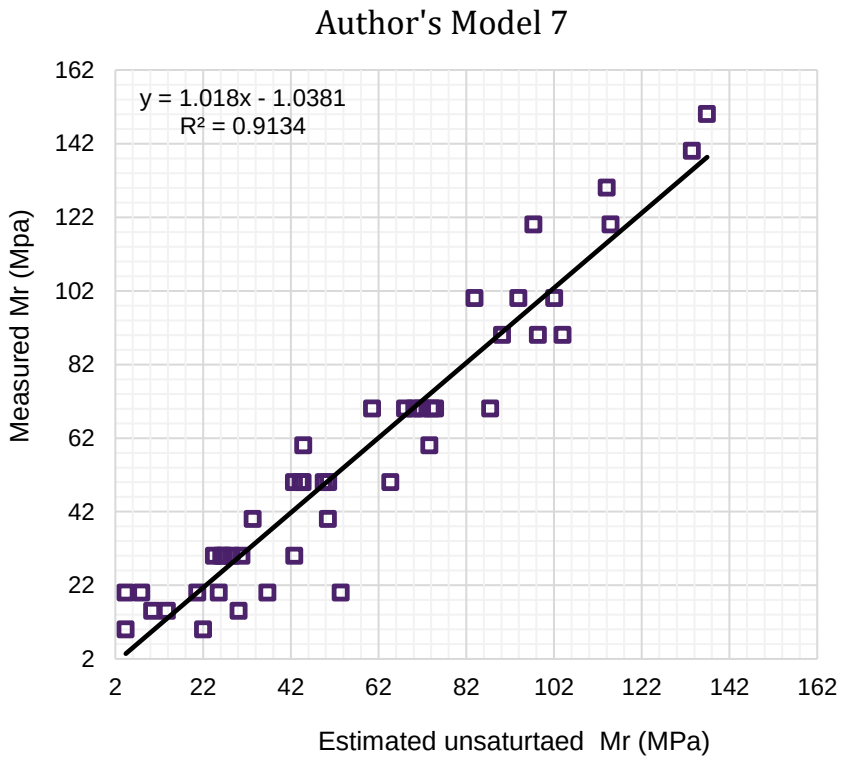

Figure 6.31: Validation of model 7

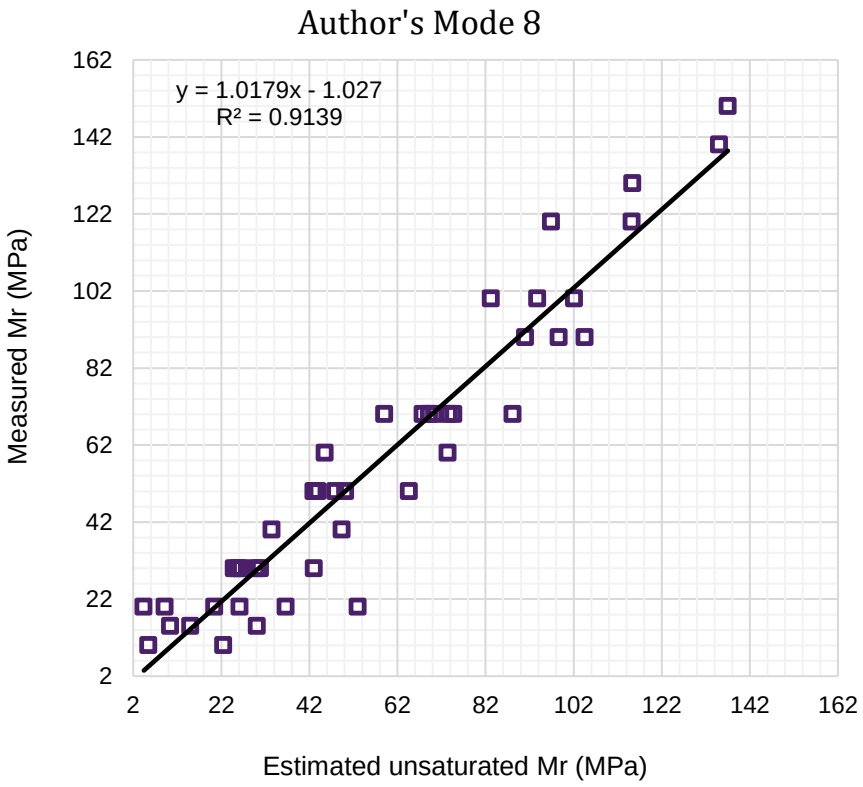

Figure 6.32: Validation of model 8

Figures 6.27 through 6.31 shows validation of different Mr models. The models were demonstrated as a function to simulate the behaviours of the M_r with respect to soil

suction using curve-fitting procedures and laboratory test data. It was observed that the predicted M_r default the measured M_r values by ± 0.048 on the average. However, the increase in M_r values were recognized at the dry side of the optimum. Whilst low M_r values were recorded as the moisture content of soil increases. Thus, the higher M_r values on the dry side is attributed to the integrity of soil structure and rigidity of soil skeleton, as higher suction stiffens the structure of the soil specimen, higher M_r is obtained.

6.6 Design Of Flexible Pavement Structure

Appropriate pavement design requires knowledge of stress-strain response of subgrade layer under cyclic loading. Pavement structure is generally under unsaturated conditions. Thus, to appropriately design a pavement, it is significant to consider unsaturated M_r values, as M_r is an important property that characterizes subgrade performance and pavement strength under unsaturated soil mechanics.

However, AASHTO Guideline for the Design of Pavements (1993) was followed in this research. This guideline gives a full description of the functional and structural performance of pavement. The method can be used for new and rehabilitation pavement design. The design equations for asphalt pavements structure include is stated below:

$$\log(W_{18}) = Z_R \times S_o + 9.36\log(SN+1) - 0.20 + \frac{\log\left(\frac{\Delta PSI}{4.2-1.5}\right)}{0.40 + \frac{1094}{(SN+1)^{5.19}}} + 2.32\log(M_R) - 8.07 \quad (6.1)$$

Where:

W_{18} = predicted number of 18 − kip (80kN) single axle load applications

Z_R = standard normal deviate

S_0 = combined standard error of the traffic and performance predictions

SN = structural number of the total pavement thickness

ΔPSI = difference between the PSI_o and terminal PSI_t serviceability indices

M_{ER} = effective resilient modulus adjusted for seasonal variation (MPa)

However, the structural number is given by the equation 6.2 below:

$$SN = a_1D_1 + a_2D_2m_2 + a_3D_3m_3 \quad (6.2)$$

Where:

$\mathrm{SN} = \text{structural number of the total pavement thicknes}$

$a_i = \text{layer coefficient}$

$D_i = \text{layer thickness}$

$m_i = \text{layer drainage coefficient}$

The design equations are provided to design pavement structure to the predetermined degree of assurance in order to guarantee performance of service life period which it was designed.

6.6.1 Design of flexible pavement structure using laboratory M_r value

This design approach followed layer thickness determination using layered analysis technique. Moreover, salient features were considered during pavement design in this research, such as:

- Traffic consideration in terms of equivalent standard axle load repetitions (18-kip).
- Equivalent axle load factors.
- Layer coefficients for different types of materials
- Single index structural number was used to represent the pavement structure at each layer.

$W_{18} = \mathrm{f}(\mathrm{M_r}, \mathrm{SN}, \mathrm{Z_R}, \mathrm{S_{o,}}\ \Delta\mathrm{PSI})$

Table 6.6: Parameters for design of a 3-layered pavement structure

Selected design input	Design values
Expected ESAL, $\mathbf{SC_{W18}}$	$10{,}000{,}000, 18 - \text{kip standard axles}$
$\mathbf{Realiability, R}$	95%
$\mathbf{Z_R}$	-1.645
$\boldsymbol{S_O}$	0.45
$\mathbf{M_r}$ surface asphalt (assumed)	2758 MPa
$\mathbf{M_r}$ base (assumed)	172.37MPa
$\mathbf{M_r}$ subbase (assumed)	89.632
FSS 1 $\mathbf{M_r}$ subgrade obtained from Lab	60MPa at Optimum moisture content
$\boldsymbol{P_i}$	4.5
$\boldsymbol{P_t}$	2.1
$\Delta \boldsymbol{PSI}$	2.4

The nomograph for flexible pavement, as presented in Figure 6.33 below, was used to trace the required structural number for each layer.

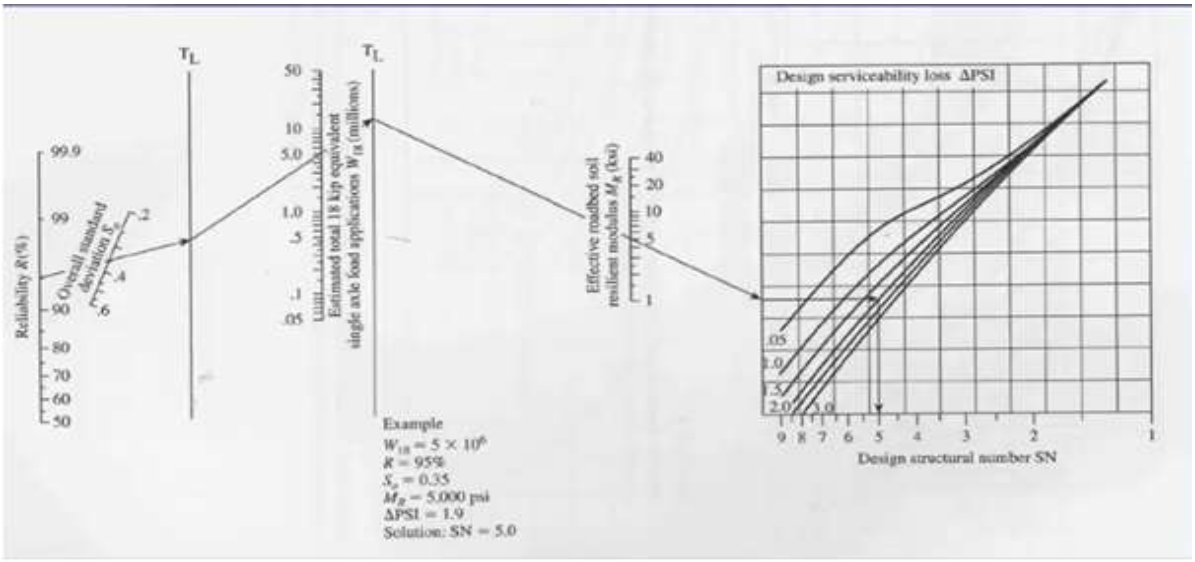

Figure 6.33: Nomograph for flexible pavement

Tests to determine parameters associated with pavement design need to be effective. Routine testing of soil subgrades to determine various parameters is an important feature in pavement design and construction. The resilient modulus is one important parameter in the determination of the structural capacity of pavements. However, the M_r and structural number of each layer are summerized in the Table 6.7 below:

Table 6.7: Resilient modulus layers thickness and structural number (SN) design one

	Structural number	Next lowest layer	Next lowest layers Mr	SN_i
Surface Asphalt	SN_1	Base	2758 MPa	3.20
Base	SN_2	Subbase	172.37MPa	4.00
Subbase	SN_3	Subgrade	60MPa	4.55

$$\textbf{Layer 1}, \mathbf{SN}_1 = a_1 d_1, \mathbf{SN}_1$$

From coefficient for asphalt chart, $a_1 = 0.44$, in Appendix D

$\mathrm{SN}_1 = 3.20 = 4.1(d_1)$

$d_1 = \dfrac{3.22}{0.44} = 7.3\ inches = 190mm, \qquad \therefore depth\ required, d_1^* = 7.5inches, 200mm$

$\mathrm{Min.thickness} = 3.5\ \mathrm{inches} = 90\mathrm{mm}\ \therefore\ d_1 > d_1^*,\ provide\ d_1 = 200mm\ depth\ okay$

$$\textbf{Layer 2}, \qquad \mathbf{SN}_2 = a_1 d_1^* + a_2 d_2 m_2,$$

Where:

$d_2 = is\ darinage\ coefficient = 1, fair$

$a_2 = 0.249(log\mathrm{M_r}) - 0.977 = 0.249(log13000\ psi) - 0.977, \qquad a_2 = 0.047$

$\therefore\ \mathrm{SN}_2 = 4.00, a_2 = 0.047$

$\mathrm{m}_2 = \text{is darinage coefficient} = 1, \text{fair}$

$\mathrm{SN}_2 = a_1 d_1^* + a_2 d_2 m_2 = 4.00 = 0.44(7.85) + 0.047 d_2(1)$

$$\therefore d_2 = \frac{0.546}{0.047} = 11.62\ inches = 295mm, \qquad \therefore depth\ required, d_2 = 300mm$$

$$d_2^* > \frac{\mathrm{SN}_2 - SN_1^*}{a_2 m_2} > \frac{4.00 - 3.3}{0.047 \times 1} > 14.89\ inches\ provide, d_2 = 380mm$$

Layer 3, $\mathbf{SN_3 = a_1 d_1^* + a_2 d_2^* m_2 + a_3 d_3 m_3}$

$\mathrm{m}_3 = \text{is darinage coefficient} = 1, \text{fair}$

$a_3 = 0.227(log\mathrm{M_r}) - 0.839 = 0.227(log8702.26\ psi) - 0.839, \qquad a_3 = 0.055$

$\therefore\ \mathrm{SN}_3 = 4.55, a_3 = 0.055$

$\mathrm{SN}_3 = a_1 d_1^* + a_2 d_2^* m_2 + a_3 d_3 m_3 = 4.55 = 0.44(7.3) + 0.047(14.89) + 0.055(1)\ d_3$

$$\therefore d_3 = \frac{4.55 - 3.990}{0.055} = 10.18\ inches = 254mm, \qquad \therefore depth\ required, d_2^* = 460mm$$

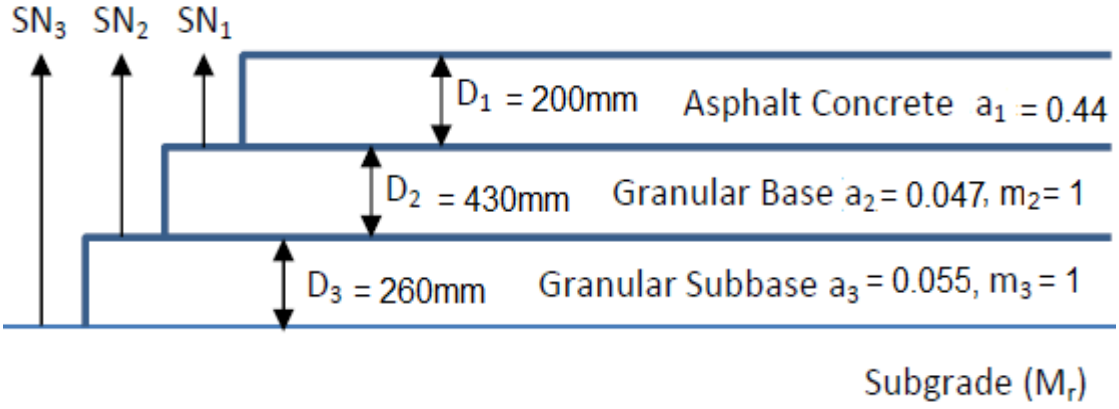

Figure 6.34: Pavement design thickness one

The designed depth for subgrade is not sufficient to provide support for the pavement structure, therefore the roadbed/subgrade required stabilization or reinforcement. The design showed that structural performance of the subgrade required higher $\mathrm{M_r}$ value in order to provide the required support for pavement structure.

6.6.2 Flexible pavement design using unsaturated M_r value from model 4

The second pavement design was done using unsaturated M_r value evaluated using model 4. The subgrade thickness of pavement layers are optimized to fulfil both structural and economical requirements based on the resilient strength of the roadbed. The selected design parameters structural numbers are summarized in Tables below:

Table 6.8: Parameters for 3-layered pavement structure for design two

Selected design input	Design values
Expected ESAL, $\mathbf{SC_{W18}}$	$10{,}000{,}000, 18 - \text{kip standard axles}$
$\mathbf{Realiability, R}$	95%
$\mathbf{Z_R}$	-1.645
$\boldsymbol{S_O}$	0.45
$\mathbf{M_r}$ surface asphalt (assumed)	2758 MPa
$\mathbf{M_r}$ base (assumed)	172.37MPa
$\mathbf{M_r}$ subbase (assumed)	89.63 MPa
FSS 1 $\mathbf{M_r}$ subgrade obtained from Lab	100MPa at Optimum moisture content
$\boldsymbol{P_i}$	4.5
$\boldsymbol{P_t}$	2.1
$\Delta \boldsymbol{PSI}$	2.4

According to the design presented below, the wearing course portrayed response of a dense graded hot mix asphalt (HMA) that has high resistance again deformation due to its value for M_r. Stone mastic asphalt (SMA) could be recommended for a high-volume roads as to increase the resistance against deformation.

Table 6.9: Resilient modulus layers thickness and structural number design two

	Structural number	Next lowest layer	Next lowest layers Mr	SN_i
Surface Asphalt	SN_1	Base	2758 MPa	3.22
Base	SN_2	Subbase	172.37MPa	4.00
Subbase	SN_3	Subgrade	100MPa	6.50

$$\mathbf{Layer\ 1, SN}_1 = \boldsymbol{a_1 d_1, SN}_1,$$

$\text{From coefficient for asphalt chart, a}_1 = 0.44, \text{in Appendix D}$

$\text{SN}_1 = 3.20 = 4.1(d_1)$

$d_1 = \dfrac{3.22}{0.44} = 7.3\ inches = 190mm, \qquad \therefore depth\ required, d_1^* = 7.5inches, 200mm$

$\text{Min. thickness} = 3.5 \text{ inches} = 90\text{mm} \ \therefore\ d_1 > d_1^*,\ provide\ d_1 = \ 200mm\ depth\ okay$

$$\textbf{Layer 2,} \qquad \textbf{SN}_2 = a_1 d_1^* + a_2 d_2 m_2,$$

Where:

$d_2 = is\ darinage\ coefficient = 1, fair$

$a_2 = 0.249(log\mathrm{M_r}) - 0.977 = 0.249(log13000\ psi) - 0.977, \qquad a_2 = 0.047$

$\therefore\ \mathrm{SN}_2 = 4.00, a_2 = 0.047$

$$\mathrm{SN}_2 = a_1 d_1^* + a_2 d_2 m_2 = 4.00 = 0.44(7.85) + 0.047 d_2(1)$$

$$\therefore d_2 = \frac{0.546}{0.047} = 11.62\ inches = 295mm, \qquad \therefore depth\ required, d_2 = 300mm$$

$$d_2^* > \frac{\mathrm{SN}_2 - SN_1^*}{a_2 m_2} > \frac{4.00 - 3.3}{0.047 \times 1} > 14.89\ inches\ provide, d_2 = 380mm$$

$$\textbf{Layer 3,} \qquad \textbf{SN}_3 = \mathbf{a_1 d_1^* + a_2 d_2^* m_2 + a_3 d_3 m_3}$$

$\mathrm{d}_3 = \text{is darinage coefficient} = 1, \text{fair}$

$a_3 = 0.227(log\mathrm{M_r}) - 0.839 = 0.227(log8702.26\ psi) - 0.839, \qquad a_3 = 0.055$

$\therefore\ \mathrm{SN}_3 = 4.55, a_3 = 0.055$

$\mathrm{m}_3 = \text{is darinage coefficient} = 1, \text{fair}$

$a_3 = 0.227(log\mathrm{M_r}) - 0.839 = 0.227(log14504\ psi) - 0.839, \qquad a_3 = 0.106$

$\therefore\ \mathrm{SN}_3 = 6.5, a_3 = 0.106$

$$\mathrm{SN}_3 = a_1 d_1^* + a_2 d_2^* m_2 + a_3 d_3 m_3 = 3.86 = 0.41(7.85) + 0.047(16.62) + 0.106(1)\ d_3$$

$$\therefore d_3 = \frac{6.50 - 3.997}{0.106} = 24\ inches = 609.6mm, \qquad \therefore depth\ required, d_3^* = 620mm$$

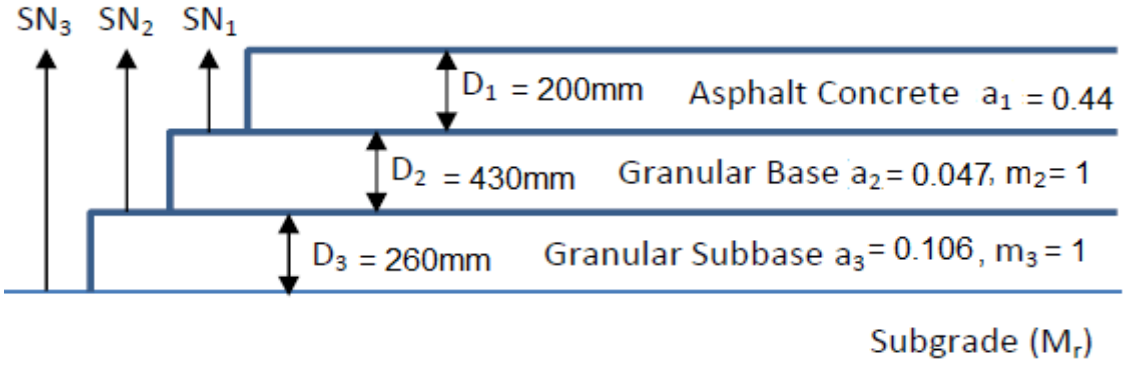

Figure 6.35: Pavement design thickness design two

The designed okay, design depth > d_1 and d_2.there for the subgrade is sufficient enough to provide support for the pavement structure. In addition, the empirical equation in the AASHTO method shows the different factors that are considered for design, for instance traffic, pavement performance (serviceability), road bed soil (subgrade), and drainage coefficients. The subgrade layer is characterized by its resilient modulus.

CHAPTER 7: SUMMARY, CONCLUSION AND RECOMMENDATIONS

7.1 SUMMARY

This research was carried out to study the effects of the geotechnical response of unsaturated subgrades for pavement structure under cyclic loading. Following the research objective, characterization of the identified subgrades soils using particles size distribution analysis (PSD) and consistency limit tests was accomplished. Base on the results, the subgrades were designated as high plastic clay (CH) for FSS and NCS respectively, and lean clay (CL) for GPS 1 and 2. Thus, GPS 3 was classified as elastic slit. Nonetheless, these soils were subjected to free swell index and swelling stress tests, to ascertain the their degree of expansiveness. In addition, XRD and XRF tests were also carried on the soil with the objective to quantify the clay minerals responsible for swelling behaviour of the soils and as a confirmation for the classification tests mentioned above.

However, an extensive laboratory testing exercise was carried out to assess the impact of suction, swelling stress and moisture content on Mr values of unsaturated subgrade soils of different plasticity indices. Repeated Load Triaxial (RLT) tests were conducted to evaluate the Mr response of nine identified subgrade soils, representing the range of problematic subgrade soils found across three provinces in South Africa. The influence of suction, swelling stress, deviator stress and confining stress variation on Mr were evaluated. As these stress state variable are mainly the parameters that governs the dynamics of unsaturated Mr. Additionally, Soil Water Retention Curves (SWRC) were established to evaluate the correlation between moisture content and matric suction for the tested subgrade soils.

After these laboratory tests were completed and results were obtained. Development of mathematical predictive models for both CBR and Mr under classical soil and unsaturated soil mechanics were achieved. The development of the mathematical models exercise, were followed by regression analysis as to develop and compute the regression constants (k_1, k_2, k_3,) for Yang et.al (2005) and Hang et. al constitutive model using NCSS 11 mathematical software Thus, the developed models were tested using laboratory data and results revealed that the values obtained under unsaturated soil

mechanics are 1.5 to 2 times higher compared to the results gotten under classical soil mechanics.

7.2 CONCLUSIONS

The aim of this research was directly pursued, as to characterize the geotechnical response of unsaturated soils for road pavement structure under cyclic loading. Based on the results of the laboratory testing program and the subsequent analyses, the following conclusions were reached:

- The particles size distribution analyse of the soils, showed that the soils fine content ranges from 75% to 95%. Whereas, the consistency limit test results revealed that the soils have liquid limit range of 40 to 70% and Plasticity index (PI) range of 17% to 45%. Furthermore, the soils free swelling index and swelling stress results were obtained to be within the bracket of 30% to 80% and 200 kPa to 900 kPa respectively. Based on these tests results, the soils were accurately classified as high plastic clay (CH) for FSS, low plastic clay (CL) for NCS, while, GPS 1 and 2 were classified as lean clay (CL) and GPS 3 as elastic slit (ML).

- The suction filter paper results for the soils, confirmed lower total and matric suction values on the wet side. Thus, this implies high capillary stresses in the soils and caused higher absorption of water within soils voids. Furthermore, the soils with higher PI on the dry side of the optimum recorded the highest matric suction values ranging from 5000 kPa to 10000kPa, due to higher percentage of fine content. However, matric suction of the soils were found to be 83.23% higher than that osmotic suction. This proved that matric suction is a dominant parameter of total suction. This is ascribed to the influence of soils capillarity, void size and the physiochemical interactions, that depends on the soil mineralogy and morphology. Thus, the result is in line with the investigation published by (Yang et al. 2005) which proved that hydromechanical response of soils are governed by matric suction.

- An increase in matric suction results stiffens the unsaturated soil specimens, as evidenced by the effective stress for unsaturated soils. Whereas, effective stress increases with increasing matric suction. The incorporation of matric suction in

predicting Mr values, provides the best theoretical approach since matric suction is a key parameter in describing the stress state variables of unsaturated soils.

- Based on the filter paper for soil-water retentivity, FSS, NCS and GPS displayed adsorptive unimodal shapes. Thus experimental test data were fitted with three different SWRC models developed by Van Genuchten 1980; Fredlund and Xing 1994; and Seki 2007 with a correction factor using a least squares regression. An Optimizer was used to optimize the parametric models to the measured data. This was followed by an iterative exercise, for the best sum of squared residuals (SSR) differences between the predicted and measured SWRC values. The sum of the SSR and Akaike information criterion (AIC) is an indication of how well the models fits with the measured data. Generally, it was observed that Seki's model best fitted the experimental data of the studied soils with R^2 ranging from 0.95458 - 0.99986, compared to the other models.

- SWRC curves establishes the relationship between the volumetric water content and matric suction. This demonstrated that matric suction increases with decreasing volumetric water content. However, the soils with higher PI values recorded higher air-entry values compared to the soils with lower PI values. This was expected due to unimodal shape of the SWRC. Hence higher PI soils have a higher water holding capacity due to surface charges and short-range adsorption.

- The resilient modulus values for subgrade soils were observed to be reliant on the stress state condition of the soil. The Mr results of the studied soils exhibited decrease in Mr with increasing deviatoric stress and as well an increase with confining pressure.

- The moisture content has a significant impact on the Mr of soils, such that Mr values decreased with increase in moisture content. CH and CL soils were the most susceptible to decreases in Mr when moisture content increased to the wet side of the optimum. The subgrades resilient response, displayed significant strain-softening behaviour on specimens prepared at the optimum moisture

contents. Whereas, the specimens prepared at the point beyond the optimum moisture content failed at the conditioning stage.

- The equations (models) developed in this research were based on statistical analysis of laboratory test results that were limited to the soil geotechnical properties specified. Estimation of resilient modulus of subgrade regression parameters (k_1, k_2, k_3) varies with soils moisture content, dry density and percentage fines.

- Existing constitutive models that incorporate matric suction for predicting Mr values for unsaturated soils i.e. Yang et al. (2005) and Liang et al. (2008) were validated. Through comparing the predicted Mr values with measured Mr values from this study. The results showed that Yang et al. (2005) and Liang et al. (2008) models had the ability to capture the effect of moisture variation on Mr through incorporating matric suction. The Yang et al. (2005) and Liang et al. (2008) models generally provided a good fit to the measured Mr data.

- Based on the experimental data of soils, three models were proposed in this study. These model includes the effect of dry densities, swelling pressure and air-entry values (AEV) on the contribution of Mr and the models also establishes an explicit correlation to matric suction by incorporating swelling stress and AEV into the model. Therefore, strong relationship between the matric suction and Mr is highlighted. Thus, the proposed models in this research can be a useful tool in the rational prediction of the Mr for routine engineering practice for unsaturated soil mechanics in pavement design practice.

- The swelling pressure decreased the resilient modulus and shear strength 1.45 to 3,2% of the initial Mr. Therefore, the effects of swelling should be considered in pavement design exercise and be neglected if the subgrade soil is not an expansive one.

- The unsaturated values of all the geotechnical tests results ranging from CBR shear strength and resilient modulus were 1.5 to 2 times higher than that of the classical laboratory soil mechanics values. This simply implied that designing

pavement structure using unsaturated soil mechanics value is very conservative, contrary to the design of pavement using classical soil mechanics values, that resulted in under-design of pavement structure, as demonstrated in this study.

7.3 RECOMMENDATIONS

In light of this research, the following recommendations are made to incorporate the effects of suction variation in assessing design value of Mr for unsaturated subgrades:

- A simpler procedures are needed to be established by adapting the conventional triaxial resilient modulus instrument in various research centres and universities in South Africa , in order to directly measure suction as at the same time of measuring resilient modulus and shear stress values. As this development will aid to lessen the time required to separately measure suction and resilient modulus. Therefore, reduce the time require to prepare many specimens and as well lessen the time specimens require to attain equilibration period.

- The proposed constitutive Mr-matric suction relationship was validated based on the results from the nine soil types utilised in this research. Wider range of soil types are required to validate the applicability of the developed model for a variety of soil types with different PI and moisture contents.

- The undergraduate geotechnical engineering courses has not been significantly modified in decades in South African universities. There, is no significant coverage of unsaturated soil mechanics. The student's depth of understanding of soil engineering would be greatly enhanced via introduction of geotechnical principles for unsaturated soil mechanics with the saturated soil case being presented as a subset of the broader theory. This will aid engineers in pavement, foundation, earth dam and rail track for better design.

REFERENCES:

AASHTO. 1994. Standard method of test for resilient modulus of unbound granular base/subbase materials and subgrade soils. AASHTO T294, Washington, DC.

AASHTO. 2002. Guide for the design of new and rehabilitated pavement structures. National Cooperative Highway Research Program, AASHTO NCHRP Project 1-37A. American Association of State Highway and Transportation Officials (AASHTO), Washington, D.C.

AASHTO. 2003. Standard method of test for determining the resilient modulus of soil and aggregate materials."

AASHTO T307. 2005. Standard methods of test for determining the resilient modulus of soils and aggregate materials.

AASHTO T 307-99. 2007. Standard method of test for determining the resilient modulus of soils and aggregate materials, American Association of State Highway and Transportation Officials, Washington, D.C.

AASHTO. 2008. Mechanistic-empirical pavement design guide, interim edition: A manual of practice. Washington, DC.

Abramento, M, and Carvalho, S. 1989. Goetechnical parameters for study of slope insatbilization at Serra do Mar-Brazilian Southeast. Proceedings of the 12th International Conference on Soil Mechanics and Foundation Engineering, Rio de Janeiro, 3: 1599-1602.

Agus, SS and Schanz, T, 2006a. Drying, wetting, and suction characteristic curve of bentonite-sand mixture. In: Proc 4th Int. Conf. on unsaturated soil, Arizona, USA, pp1405-1414.

Aitchison, GD. 1961. Relationship of moisture and effective stress functions in unsaturated soils Pore pressure and suction in soils, Butterworth, London.

Alam, TB Abdelrahman, M and Scharm, SA. 2009. Laboratory characteristics of Recycled Asphalt Pavement as a base layer. International Journal of Pavement Engineering, Vol. 11, No. 2, 123-131.

Allam, MM, and Sridharan, A. 1987. Stresses present in unsaturated soils. Journal of Geotechnical Engineering. ASCE. Vol. 113, 11, 1395-1399.

Alsherif, NA. and McCartney, JS. 2014. Effective stress in unsaturated silt at low degrees of saturation. Vadose Zone J. 13 doi:10.2136/ vzj2013.06.0109 (this issue).

Ampadu, S. (2007). A laboratory investigation into the effect of water content on the CBR of a subgrade soil. In T. Schanz (Ed.), Experimental Unsaturated Soil Mechanics (pp. 137–144). Berlin: Springer.

Arifin, YF and Schanz, T. 2009. Osmotic suction of highly plastic clays, Acta Geotechnical, 4 (3), pp. 177-191.

ASTM D4767 .1999. Standard test method for consolidated-undrained triaxial compression test on cohesive soils, 1999 Annual Book of ASTM, Vol..04 .08, Philadelphia P.A, pp.860-867.

ASTM D 5298-10. 2010. Standard test method for measurement of soil potential (suction) using filter paper.

ASTM D4546. 2013. Standard test method for expansion index of soils. Annual Book of ASTM Standards, PA 4546.

Austroads. 2012. A guide to the structural design of road pavements. *Austroads*.

Basma, AA., Al-Homoud, AS and Malkawi, AH. 1995. Laboratory assessment of swelling pressure of expansive soils. Applied Clay Science, 9, 355-368. 1995.

Baille, W, Tripathy, S and Schanz, T .2014. Effective stress in clays of various mineralogy. Vadose Zone J. 13 doi:10.2136/vzj2013.06.0112 (this issue).

Barksdale, RD and Itani, SY. 1989. Influence of aggregate shape on base behaviour. Transportation Research Record, No. 1227, Transportation Research Board, Washington, D. C., 173–182.

Bishop, AW. 1954. The use of pore pressure coefficients in practice. Geotechnique, 4, No 4,148-152.

Bishop, AW. 1959. The principle off effective stress. Norwegian Geotechnical Institute, vol. 32, pp 1–5.

Bishop, AW, Alan, I, Blight, GE and Donald, IB. 1960. Factors controlling the strength of partially saturated cohesive soils. Proc. Res. Conf. Shear Strength Cohes. Soils. ASCE, pp 503 532.

Bishop, AW, and Blight, GE. 1967. Some aspects of effective stress in saturated and unsaturated soils.” Géotechnique, 13(3), 177–197.

Blight, GE. 1967. Effective stress evaluation for unsaturated soils. ASCE journal of the soil mechanics and foundation division. 125-149.

Blight, GE. 2013. Unsaturated Soil Mechanics in Geotechnical Practice. Leiden The Netherlands, CRC Press/Balkema.

Bowles, J. 1992. Engineering properties of soil and their measurements. McGraw-Hill Boston, 4thEdition.

Bulut, R, Lytton, RL and Wray, WK. 2001. Soil suction measurements by filter paper. Geotechnical special publication number 115, Proceedings of Geo-Institute Shallow Foundation and Soil Properties Committee Sessions at the ASCE 2001 Civil Engineering Conference, pp. 243-261.

Butalia, TS, Huang, J, Kim, DG and Croft, F. 2003. Effect of moisture content and pore water pressure builds on resilient modulus of cohesive soils. *Resilient Modulus Testing for Pavement Components ASTM STP 1437*.

Burczyk, James, M, Ksaibati, Khaled., Anderson-Sprecher, Richard. 1994. Factors influencing determination of a subgrade resilient modulus value. in Transportation Research Record 1462, TRB, National Research Council, Washington, D.C. 1994, pp. 72-79.

Carmichael III RF. and Stuart, E.1978. Predicting Resilient Modulus: A study to determine the mechanical properties of subgrade soils. Transportation Research Record 1043, TRB, National Research Council, Washington, D.C., 1978, pp 20-28.

Cary, CE and Zapata, CE. 2010. Enhanced model for resilient response of soils resulting from seasonal changes as implemented in mechanistic-empirical pavement design guide.

Cary, CE, Zapata, CE, Witcizak, MW, Kaloush, K E. 2011. Pore- water pressure response of a soil subjected to traffic loading under saturated and unsaturated conditions. In *ASU Electronic Dissertations and Theses*. Arizona State University, 2011.

Cekerevac, C, Baltzer, S, Charlier, R, Chazallon, C, Erlingsson, S, Gajewska, B and Pavšic, P. 2009. ˇ Water influence on mechanical behaviour of pavements: Experimental investigation. In A. Dawson (Ed.), Water in road structures (pp. 217–242). Springer.

Chen, F.H. 1988. Foundations on expansive soils. Elsevier scientific publishing company, Amsterdam.

Cho, GC and Santamarina, JC. 2001. Unsaturated Particulate Materials - Particle Level Studies. ASCE Geotechnical Journal. Vol. 127. No. 1. pp. 84-96.

Coleman, JD. 1962. Stress strain relations for partly saturated soils. Geotechnique, 12**,** 348-350.

Cui, YJ and Delage, P. 1996. Yielding and plastic behaviour of an unsaturated silt, Géotechnique 46, No. 2, pp. 291-311.

Dai, S and Zollars, J. 2002. Resilient modulus of Minnesota road research project subgrade soil. Transportation Research Record No. 1786, *Transportation Research Board*, pp. 20–28.

Darter, MI, Elliot, RP and Hall, KT. 1991. Revision of AASHTO pavement overlay design procedures, Appendix: Documentation of Design Procedures. National Cooperative Highway Research Program Study 20-7, TRB, National Research Council, Washington, D.C., April 1991.

Das, BM. 1984. Principles of foundation engineering. USA: Brooks/Cole Eng. Division. Elias, V. (1994). Strategies for managing unknown bridge foundations. USA: federal highway administration.

Das, BM. 2006. Principles of geotechnical engineering. Stamford, CT: Learning College.

Donald, IB. 1957. Effective stresses in unsaturated non-cohesive soils with controlled negative pore pressure. M.Eng. Sc. Thesis, University of Melbourne, Melbourne, Australia.

Drumm EC, Boateng-Poku, Y and Johnson Pierce, T. 1990 Estimation of Subgrade Resilient Modulus from Standard Tests. Journal of Geotechnical Engineering, Vol. 116, No.5, May 1900. pp 774-789.

Drumm, EC, Reeves, JS, Madgett, MR, and Trolinger, WD.1997. Subgrade resilient modulus correction for saturation effects. Journal of Geotechnical and Geoenvironmental Engineering, 123(7): p. 663–670.

Ekblad, J. 2008. Water in coarse granular materials: Resilient and retentive properties. pp.117–123.

Erzin, Y and Erol, 0. 2004. Correlations for quick prediction of swell pressures. The Electronic Journal of Geotechnical Engineering [serial online], 9(F): Paper No. 0476.

Escario, V and Juca, JFT. 1989. Shear strength and deformation of partly saturated soils. Proceedings of the 12th International Conference on Soil Mechanics and Foundation Engineering, Rio de Janerio, 2: 43-46.

Fang, Z and Yin JH. 2006. Physical modelling of consolidation of Hong Kong marine clay with prefabricated vertical drains. Canadian Geotechnical Journal **43**(6): 638-652.

Farrar, MJ and Turner, JP. 1991. Resilient Modulus of Wyoming Subgrade Soils. Mountain Plains Consortium Report No 91-1, The University of Wyoming, Luramie, Wyoming.

Fattom, M and Barakat, S. 2000. Investigation of Three methods for Evaluating Swelling pressure of Soils. Environmental & Engineering Geoscience, Vol. VI, No. 3, pp. 293-299. 2000.

Feng, G, Meiri, A and Letey, J. 2003. Evaluation of a model for irrigation management under saline conditions. Effects on plant growth. Soil Science Society of America Journal, 67**,** 71-76.

Fleureau, JM, Kheirbek-Saoud, S, Soemitro, R and Taibi, S. 1993. Behaviour of clayey soils on drying-wetting paths. Can. Geotech. J. 30: 287-296.

Fredlund, DG, Bergan, AT and Wong, PK. 1977. Relation between resilient modulus and stress research conditions for cohesive subgrade soils. Transportation Research Record No. 642, *Transportation Research Board*, Washington, D.C., pp. 73–81.

Fredlund, DG and Morgenstern. NR. 1977. Stress state variables for unsaturated soils. Journal of Geotechnical and Geoenvironmental Engineering, 103, 447-466.

Fredlund, DG, Morgenstern, NR and Widger, RA. 1978. Shear strength of unsaturated soils. Canadian Geotechnical Journal, 15, 313-321.

Fredlund, DG and Rahardjo, H. 1993. Soil mechanics for unsaturated soils. New York. John Wiley and sons, Inc.

Fredlund, DG and Xing, A. 1994. Equations for the Soil-Water Characteristic Curve. Canadian Geotechnical Journal 31, no. 4 (August 1, 1994): 521–32.

Fredlund, DG. 1996. The scope of unsaturated soil mechanics. An overview. *In* Alonso and Delage (eds.). *Proceedings 1st International Conference on Unsaturated Soils,* Paris, France. Balkema Press.

Fredlund, DG. 1996. The emergence of unsaturated soil mechanics. The fourth Spencer J. Buchanan Lecture, College Station, Texas, A&M University Press, p. 39.

Fredlund, DG, Xing, A, Fredlund, MD and Barbour, S. L. 1996. The relationship of the unsaturated soil shear strength to the soil-water characteristic curve. Canadian Geotechnical Journal, Vol. 33, No. 3, pp. 440-448.

Fredlund, DG., Rahardjo, H, Leong, EC and Ng, CWW. 2001. Suggestions and recommendations for the interpretation of soil-water characteristic curves. In: Southeast Asian Geotechnical Conference, Hong Kong, (Vol. 1,), pp. 503–508.

Fredlund, DG. 2006. Unsaturated soil mechanics in engineering practice, Journal of Geotechnical and Geoenvironmental Engineering, Vol. 132, No. 3, pp. 286-321.

Fredlund, DG, Rahardjo, H and Fredlund, MD. 2012. Unsaturated soil mechanics in engineering practice., A Wiley-Interscience Publication, John Wiley & Sons, Inc, pp. 535.

Gallipoli, D, Gens, A., Sharma, R and Vaunat, J. 2003. An elasto-plastic model for unsaturated soil incorporating the effects of suction and degree of saturation on mechanical behaviour. Géotechnique,53**,** 123-136.

Geiser, F, Laloui, L and Vulliet, L. 2000. On the volume measurement in unsaturated triaxial test. Proc., The Asian Conference on Unsaturated Soil, pp. 669-679.

George, KP. 2004. Prediction of resilient modulus from soil index properties. Final report. University of Mississippi, Department of Civil Engineering, Oxford.

Goudie, A.S. 1973. Duricrusts in tropical and subtropical landscapes. Oxford.

Gupta, S, Ranaivoson, A, Edil, T, Benson, C and Sawangsuriya, A. 2007. Pavement design using unsaturated soil technology.

Hall, DK and Thompson, MR. 1994. Soil-property-based subgrade resilient modulus estimation for flexible pavement design. *Transportation Research Record, 1449*, TRB, National Research Council, Washington, D.C., pp. 30-38.

Heydinger, AG, Xie, QL, Randolph, BW and Gupta, JD. 1996. Analysis of resilient modulus of dense and open-graded aggregates. Transportation Research Record, No. 1547, Transportation Research Board, Washington, D.C., 1–6.

Heydinger, AG., 2003. Evaluation of seasonal effects on subgrade soils. Transportation Research Record No. 1821, *Transportation Research Board*, pp.47–55.

Hicks, RG. 1970. Factors influencing the resilient properties of granular materials. Ph.D. thesis, University of California, Berkeley, Berkeley, CA.

Hicks, RG and Monismith, CL. 1971. Factors influencing the resilient properties of granular materials. Highway Research Record. 345.

Hopkins, T, Beckham, TL., Sun, C and Ni, B. 2004. Resilient modulus of Kentucky Soils. Final research report for Kentucky transportation cabinet, Kentucky Transportation Centre, University of Kentucky.

Hossain, Z, Zaman, M, Doiron, C and Solanki, P. 2010. Characterization of Subgrade Resilient Modulus for Pavement Design. In Geo-Frontiers 2011. American Society of Civil Engineers, Reston, VA, 2011, pp. 4823-4832.

Huang, J., 2001. Degradation of resilient modulus of saturated clay due to pore water pressure build-up under cyclic loading. *Thesis (Master)*, Department of Civil Engineering and Environmental Engineering, Ohio State University.

India Standard (IS). 2020. Method of test for soils part xl determination of free swell index of soils, 24 *Bureau of Indian Standards,* 2720, Part XL.

Jaquin, PA, Augarde, CE, Gallipoli D. and Toll DG. 2009. The strength of rammed earth materials, Geotechnique. 59(5): 487–490.

Kamal, MA, Dawson, AR, Garouki, T, Hughes, DAB and Shaa'at, AA. 1993. Field and laboratory evaluation of the mechanical behaviour of unbound granular materials in pavements, Transportation Research Record No. 1406. 1993. pp 88-97.

Kancherla, A. 2004. Resilient modulus and permanent deformation testing of unbound granular materials., Master's Thesis, Texas A&M University.

Kang DH, Gupta, Ranaivoson, AZ, Roberson R and Siekmeier. 2011. Recycled materials a substitute for virgin aggregates in road construction II, Inorganic contaminant leaching." science society of America journal, Vol.75. No. 4 1276-1284.

Khoury, NN., and Zaman, MM. 2004. Correlation between resilient modulus, moisture variation, and soil suction for subgrade soils. *Transportation Research Record: Journal of the Transportation Research Board* 1874, no. 1 (2004): 99–107.

Khalili, N and Khabbaz, M. 1998. A unique relationship of chi for the determination of the shear strength of unsaturated soils. Géotechnique, 48.

Khalili, N, Geiser, F and Blight, GE. 2004. Effective stress in unsaturated soils: Review with new evidence. Int. J. Geomech., 4(2), 115–126.

Leong, EC., He, L and Rahardjo, H. 2002, Factors affecting the filter paper method for total and matric suction measurements. Geotech. Test. J., Vol. 25, No. 3, pp. 322–333.

Likos, WJ, Wayllace A, Godt, J, Lu, N. 2010. Modified direct shear apparatus for unsaturated sand at low suction and stress, Geotechnical Testing Journal, Vol.33, No. 4: p. 1-13.

.

Janoo, VC and Bayer II JJ. 2001. The effect of aggregate angularity on base course performance. U.S. Army Corps of Engineers, ERDC/CRREL TR-01-14.

Jennings, J. 1961. A revised effective stress law for use in the prediction of the behaviour of unsaturated soils. Pore Pressure and Suction in Soils**,** 26-30.

Jennings, JE and Burland, JB. 1962. Limitations to the use of effective stresses in partly saturated soils. Géotechnique, 12(2), 125–144.

Jones, MP and Witczak, M.W. 1977. Subgrade modulus on the San Diego Test Road. Transportation Research Record, TRR 641, Transportation Research Board, National Research Council, Washington, DC, pp. 1 6.

Lee, WJ., Bohra, NC., Altschaeffl, AG., and White, TD., 1995. Resilient modulus of cohesive soils and the effect of freeze-thaw. Canadian Geotechnical Journal, Vol. 32, 1995, pp. 559-568.

Lee, W, Bohra, NC, Altschaeffl, AG and White, TD. 1997. Resilient modulus of cohesive soils. Journal of Geotechnical and Geoenvironmental Engineering, Vol. 123, No. 2, 1997, pp. 131-135.

Leite, FC, Motta, RS, Vasconcelos, KL. 2011. Laboratory evaluation of recycled construction and demolition waste for pavements Construction and Building Materials, 25 (6) (2011), pp. 2972–2979.

Lekarp, F, Isacsson, U and Dawson, A. 2000. State of Art I: Resilient response of unbound aggregates. Journal of Transportation Engineering, ASCE, Vol (1) Jan/Feb. 2000.

Leong, EC, Tripathy, S and Rahardjo, R. 2003. Total suction measurement of unsaturated soils with a device using the chilled-mirror dew-point technique. Géotechnique, 53(2):173-182.

Liang, RY, Rabab'ah, S and Khasawneh, M. 2008. Predicting moisture-dependent resilient modulus of cohesive soils using soil suction concept. Journal of Transportation Engineering, 134(1): 34– 40.

Lu, N and Likos, WJ. 2004. Unsaturated soil mechanics. John Wiley & Sons, Inc., Hoboken, New Jersey.

Lu, N and Likos, WJ. 2006. Suction stress characteristic curve for unsaturated soil. Journal of Geotechnical and Geoenvironmental Engineering, 132**,** 131.

Lu, N, Godt, JW and Wu, DT. 2010. A closed-form equation for effective stress in unsaturated soil. Water Resources Research, 46**,** W05515.

Maatouk, A, Leroueil, S and La Rochelle, P. 1995. Yielding and critical state of a collapsible unsaturated silty soil. Geotechnique, 45(3):465-477.

Mallela, J, VonQuintus, H and Smith, KL. 2004. Consideration of lime-stabilized layers in mechanistic-empirical pavement design. Rep. prepared for The National Lime Association, National Lime Association, Arlington VA.

Mohammed, LN, Huang, B., Puppala, AJ., and Allen, A. 1999. Regression model for resilient modulus of subgrade soil. Transportation Research Record No. 1687, *Transportation Research Board*, Washington, D.C.

Morrow, C, Shi, LQ and Byerlee. J. 1984. Permeability of fault gouge under confining pressure and shear stress, J. Geophys. Res., 89, 3193–3200, doi:10.1029/JB089iB05p03193.

Muraleetharan, KK and Wei, C. 2000. A fully coupled analysis procedure for dynamic behaviour of unsaturated soils", in Advances in Unsaturated Soils, Geotechnical Special Publication No. 99 (ed. C. Shackleford, S.L. Houston and N-Y. Chang), Reston: American Society of Civil Engineers, pp. 165-179.

Nam, S, Gutierrez, M, Diplas, P, Petrie, J. 2011. Determination of the shear strength of unsaturated soils using the multistage direct shear test. Eng. Geol. 122 (3-4), 272–280.

National Cooperative Highway Research Program (NCHRP). 2002. Development of the 2002 guide for the design of new and rehabilitated pavement structures. *Project No. 1-37A*, NCHRP Transportation Research Board, Washington, D.C.

National Cooperative Highway Research program (NCHRP). 2004. Development of the 2002 Guide for Design of New and Rehabilitated Pavement structures". Phase2.

National Cooperative Highway Research program (NCHRP). 2003. Harmonized test method for laboratory determination of resilient modulus for flexible pavement design. Final Report 1-28A, National Cooperative Highway Research Program (NCHRPA), Transportation Research Board, National Research Council, Washington, D.C.

National Cooperative Highway Research program NCHRP. 2004. Guide for Mechanistic Empirical Design of New and Rehabilitated Pavement Structure: Part 2 Design Inputs: Chapter 3 Environmental Effects. Transportation Research Board, National Research Council.

Nazzal MD, Mohammad LN. 2010. Estimation of resilient modulus of subgrade soils for design of pavement structures. Journal of Materials in Civil Engineering 22(7): 726-734.

Ng, CWW and Pang, YW. 2000a. Experimental investigation of soil–water characteristics of a volcanic soil. Can. Geotech. J., 37(6), 1252–1264.

Ng, CWW and Pang, YW. 2000b. Influence of stress state on soil–water characteristics and slope stability. J. Geotech. and Geoenviron. Eng., ASCE. 26(2), ASCE, 157–166.

Ng, CWW and Chiu, CF. 2001. Behaviour of a loosely compacted unsaturated volcanic soil." J. of Geotech. and Geoenviron. Engrg., ASCE. 127(12), 1027–1036.

Ng, CWW and Chiu, CF. 2003a. Laboratory study of loose saturated and unsaturated decomposed granitic soil. J. of Geotech. and Geoenviron. Engrg., ASCE. 129(6), 550–559.

Ng, CWW. and Chiu, CF. 2003b. Invited keynote paper. Constitutive modelling of unsaturated loose soil slopes subjected to rainfall infiltration. Proc. 9th China National Conf. on Soil Mech. and Geotech. Engrg., Beijing. 1, pp. 187–200.

Ng, CWW. and Zhou, RZB. 2005. Effects of soil suction on dilatancy of an unsaturated soil. Proc. 16th Int. Conf. Soil Mech. & Geotech. Engrg. Osaka, Japan, 2, 559–562.

Ng, CWW, Zhou, C, Yuan, Q and Xu. 2013. Resilient modulus of unsaturated subgrade soil. Experimental and technical investigations Canadian Geotech. 50(2), 223-232.

Nicholson, P, Kashyap, V and Fuji, C. 1994. Lime and fly ash admixture improvement of tropical Hawaiian soils. Transportation Research Record 1440, National Research Council, Washington, D.C., 71–78.

Nishimura, T, Toyota, H, Vanapalli, SK and Oh, WT. 2007. Evaluation of critical state parameters for an unsaturated soil. Proc., 60th Canadian Geotechnical Conference, Ottawa (Canada), 1029-1036.

Noorany, I. 1984. Phase relations in marine soils. Journal of Geotechnical Engineering, ASCE, 110**,** 539-543.

Nokkaew, K, Tinjum, J. William L and Edil, T. 2014. Effect of matric suction on resilient modulus for compacted recycled asphalt base course in post compaction state. *transportation research record* (2014): i-iv.

Ooi, PSK, Archilla, AR., and Sandefur, KG. 2004. Resilient modulus for compacted cohesive soils. *Transportation Research Record*, No. 1874, pp. 115–124.

Oberg, A and Sallfors, G. 1997. Determination of Shear Strength Parameters of Unsaturated Silts and Sands Based on the Water Retention Curve. Geotechnical Testing Journal, Vol. 20, No. 1, pp. 40-48.

Paraire, J. 1987. Suction tests on CBR-diameter specimens. The bearing capacity suction relation. Crowthorne, GB: Transport and Road Research Lab (TRRL).

Pezo, R, Claros, G, Hudson, WR, and Stoke, KH. 1992. Development of a Reliable Resilient Modulus Test for Subgrade and Non-Granular Subbase Materials for Use in A Routine Pavement Design. Research Report 1177-4F., University of Texas-Austin.

Pham, HQ, Fredlund, DG and Lee Barbour, S. 2005. A study of hysteresis models for soil-water characteristic curves. Canadian Geotechnical Journal 42, no. 6 (December 2005): 1548–68.

Purwana, Y, Nikraz, H and Jitsangiam, P. 2012. Experimental study of suction-monitored CBR test on sand–kaolin clay mixture. International Journal of Geomaterials, 3(2), 419–422.

Pusch, R. and Yong, R. 2003. Water saturation and retention of hydrophilic clay buffer microstructural aspects, Applied Clay Science, Elsevier, 23, pp. 61-68.

Rahim, AM and George, KP. 2004. Subgrade soil index properties to estimate resilient modulus. *Transportation Research Board*, CD-ROM of Transportation Research Board Annual Meeting.

Rashed K. A. 1985. Swelling characteristics of compacted soil in Mosul Area. MSc. Thesis Mosul University.

Rassam, DW, and Cook, FJ. 2002. Predicting the shear strength envelope of unsaturated soils. Geotechnical Testing J. 28: 215-220.

Richter, C. 2006. Seasonal Variations in the Moduli of Unbound Pavement Layers. Publication No. FHWA-HRT-04-079, Turner–Fairbanks Highway Research Centre, McLean, Va.

Ridley, A. M. 1993. The measurement of soil moisture suction. PhD dissertation. Imperial College, University of London.

Saklecha, PP, Kedar, RS. and Saklecha, PK. 2013. Correlation of CBR with mechanical properties of foundation soil, Proc. of Indian Geotechnical Conference December 22-24, Roorkee, pp. 1-8, 2013.

Sánchez-Leal, F. 2002. Interpretation of CBR test results under the shear strength concept of unsaturated soil mechanics. 3rd international conference on unsaturated soils (pp. 663–668). Recife: CRC Press.

Santha, BL. 1994. Resilient modulus of subgrade soils: comparison of two constitutive equations. *Transportation Research Record No. 1462*, *Transportation Research Board*, Washington, D.C.

Sauer, EK. and Monismith, CL. 1968. Influence of Soil Suction on Behaviour of a Glacial till Subjected to Repeated Loading. Highway Research Record, No. 215, Washington, D.C., pp. 18-23.

Seki, K. 2007. SWRC fit – A nonlinear fitting program with a water retention curve for soils 10 having unimodal and bimodal pore structure. Hydrol. Earth System Sci. Discus, 4, 407- 11 437.

Sibley, JW and Williams, DJ. 1990. A new filter material for measuring soil suction. Geotech. Test. J., Vol. 13, No. 4, pp. 381–384.

Sivakumar, V and Wheeler, S. 2000. Influence of compaction procedure on the mechanical behaviour of an unsaturated compacted clay. Part 1: Wetting and isotropic compression. Geotechnique 2000; 50(4): 359-368.

South African national road agency limited (SANRAL). 2008. Framework for a highway system: integration of the pavement design method and a highway planning system." Report No. PB/2007/HPS.

Sreedeep, S. and Singh, D. 2006. Methodology for determination of osmotic suction of soils. Geotechnical and Geological Engineering, 24**,** 1469-1479.

Sridharan, A and Venkatappa Rao, G. 1973. Mechanisms controlling volume change of saturated clays and the role of the effective stress concept. Géotechnique 23(3), 359–382.

Tarantino, A. and De Col, E. 2008. Compaction Behavior of Clay. Geotechnique 58 (3): 199–213.

Terzaghi, K. 1936. The shearing resistance of saturated soils and the angle between the planes of shear. 1st International Conference on Soil Mechanics and Foundation Engineering.

Terzaghi, K. 1943. Theoretical Soil Mechanics." New York, USA, Wiley.

Theyse, HL. 2000. The development of mechanistic-empirical permanent deformation design models for unbound pavement materials from laboratory and accelerated pavement test data. Proc., Int. Symp. on Un-Bound Aggregates in Road Construction, A. A. Balkema, Rotterdam, The Netherlands, 285–293.

Tindall, JA. and Kundell, JR. 1999. Unsaturated zone hydrology for scientists and engineers. Prentice-Hall. 624 pages.

TMH1 (METHOD 7). 1986. Determination of the maximum dry density and optimum moisture content of gravel, soil and sand. Technical Methods for Highway.

TMH1 (METHOD 8). 1986. The determination of the determination of the California bearing ratio of untreated soils and gravels. Technical Methods for Highway.

TMH1 (METHOD 14). 1986. The determination of the dry bulk density, apparent relative density and water absorption of aggregate retained on a 4,75 Mm Sieve. Technical Methods for Highway.

Traylor. KL. 1971. Finite element analysis of layered road pavements. PhD Thesis, University of Nottingham.

Thompson, MR and Figueroa, JL. 1989. Mechanistic thickness design procedure for soil-lime layers.Transp. Res. Rec., 754, 32–36.

Thomson, MR and Robnett, QL. 1976. Resilient properties of subgrade soils. Final Report-Data Summary, Transportation Engineering Series 14, Illinois Cooperative Highway Research and Transportation Program Series, University of Illinois, Urbana.

Thomson MR, Robnett QL. 1979. Resilient properties of subgrade soils. Transportation Engineering J. ASCE 105.

Thom, NH and Brown, SF. 1987. The effect of moisture on the structural performance of a crushed limestone road base. Annual Transportation Research Board Meeting, Washington, D. C. 1987.

Thom, NH., and Brown, SF. 1989. The mechanical properties of unbound aggregates from various sources.'' Unbound aggregates in roads, edited by RH. Jones and AR. Dawson.

Vanapalli, SK, Fredlund, DG, Pufahl, DE and Clifton, AW. 1996. Model for the prediction of shear strength with respect to soil suction. Canadian Geotechnical Journal, Vol. 33, No. 3, pp. 379-392.

Van Genuchten, MT. 1980. A closed-form equation for predicting the hydraulic conductivity of unsaturated soils. Soil Science Society of America Journal, 44**,** 892-898.

Vinale, F, d'Onofrio, A., Mancuso, C, Santucci de Magistris, F and Tatsuoka, F. 2001. The pre-failure behaviour of soils as construction materials. Pre-Failure Deformation Characteristics of Geomaterials. Edited by M. Jamiolkowski, R. Lancellotta and D. LoPreti. Swets & Zeitlinger, Lisse. pp. 955-1007.

Von Quintus, H and Killingsworth, B. 1998. Analyses relating to pavement material characterizations and their effects on pavement performance. FHWA-RD-97-085. Federal Highway Administration, McLean, VA.

Wan, AWL, Gray, MN and Graham, J. 1995. On the relations of suction moisture content and soil structure in compacted clays. Proceedings of the 1st International Conference on Unsaturated Soils, Paris, France, pp. 215-222.

Wang, B, 2000. Stress effects of soil water characteristics curve on slope stability in expansive soils. MPhil Thesis, the Hong Kong University of Science and Technology, Hong Kong, China.

Wilson, BE, Sargand, SM, Hazen, GA and Green, R. (1990). “Multiaxial Testing of Subgrade”, Transportation Research Record, 1278, TRB, National Research Council, Washington, D.C., pp. 91-95.

Witczak, M and Uzan, J. 1998. The universal airport design system, Report I of IV. Granular material characterization. *Rep. to Department of Civil Engineering*, Univ. of Maryland, College Park, Md.

Wolfe, WE and Butalia, TS. 2004. Seasonal instrumentation of SHRP pavements. Final Report for Ohio Department of Transportation, Ohio State University, Columbus.

Yau, A and Von Quintus, H. 2002. Study of laboratory resilient modulus test data and response characteristics.” Report. No. FHWA-RD-02-051. FHWA, U.S. Department of Transportation, Washington, D.C.

Yang, SR, Huang, WH and Tai, YT. 2005. Variation of resilient modulus with soil suction for compacted subgrade soils. Transportation Research Record,1913: 99–106. doi:10.3141/1913-10.

Yang, SR, Lin, HD, Kung, JHS and Huang, WH. 2008. Suction controlled laboratory test on resilient modulus of unsaturated compacted subgrade soils. Journal of Geotechnical and Geo-Environmental Engineering, Vol. 134, No. 9, pp. 1375-1384.

Zaman, M and Khoury, N. 2007. Effect of soil suction and moisture on resilient modulus of subgrade soils in Oklahoma. Final Report for Oklahoma Department of Transportation. Norman. Oklahoma.

Zhan, LT. 2003. Field and laboratory study of an unsaturated expansive soil associated with rain-induced slope instability. PhD Thesis. Hong Kong University of Science and Technology.

Zienkiewic, ZOC, Chan, AHC, Pastor, M, Schrefler, BA and Shiomi, T. 1999. Computational geotechnics with special reference to earthquake engineering Wiley London.

APPENDIX A:

X-Ray Diffraction Analysis

General Information

Analysis date	2017/06/07 05:00:52 PM		
Sample name	FSS 1 sample one	Measurement date	2017/06/07 13:16:02
File name	FSS sample A: Raw	Operator: Aneke Frank	User: Aneke Frank
Comment	Full Chart		

Measurement profile (FSS1)

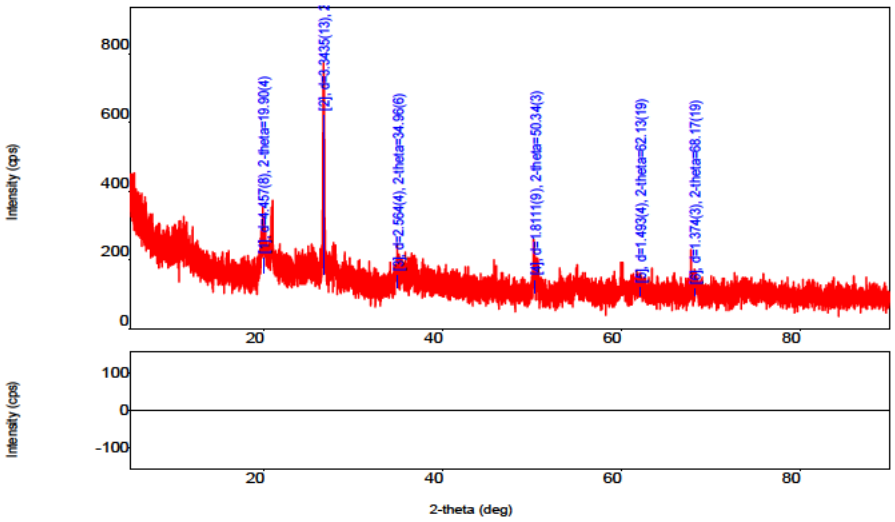

Qualitative analysis results

Phase name	Formula	Figure of merit	Phase reg. detail	DB card number
Quartz, syn	Si O2	0.513	ICDD (PDF2010)	00-046-1045
Orthoclase	K (Al Si3 O8)	0.263	ICDD (PDF2010)	01-086-0439
Kyanite	Al2 Si O5	0.140	ICDD (PDF2010)	01-074-1976
Bentonite	(Ca0.06 Na0.21 K0.27) (Al1.64 Fe0.06 Mg0.31) (Al0.29 Si3.71 O10 (O H)2)	2.113	ICDD (PDF2010)	01-076-7629
Kaolinite-2M	Al2 Si2 O5 (O H)4	2.801	ICDD (PDF2010)	01-075-0938
Illite-montmorillonite (NR)	K Al4 (Si, Al)8 O10 (O H)4 ·4 H2 O	2.929	ICDD (PDF2010)	00-035-0652
Muscovite-1M, magnesian, syn	K Al (Mg0.2 Al0.8) (Al0.42 Si3.58) O10 (O H)2	1.181	ICDD (PDF2010)	01-070-1868

Measurement profile (FSS 2)

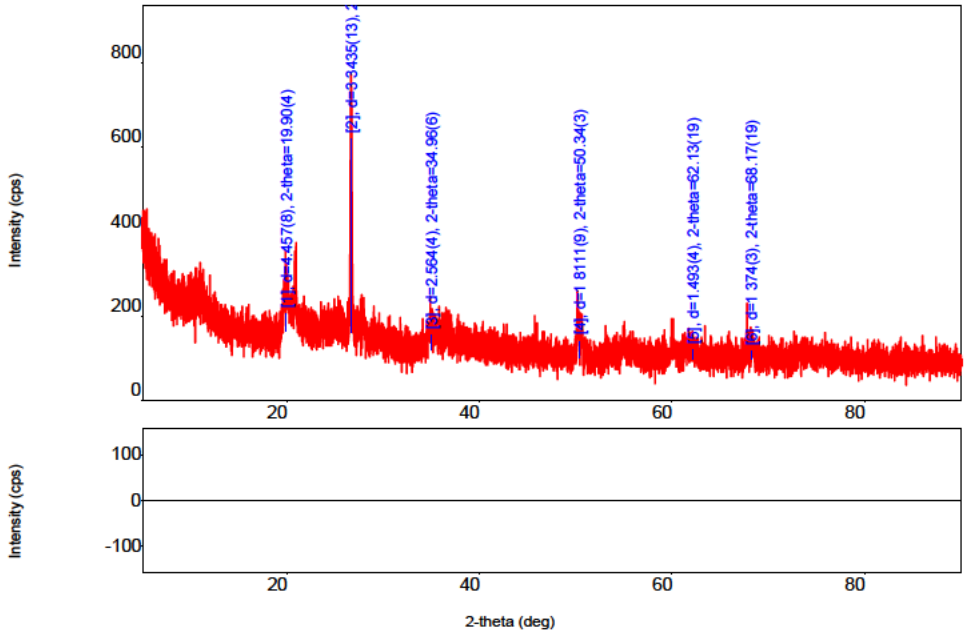

Qualitative analysis results

Phase name	Formula	Figure of merit	Phase reg. detail	DB card number
Quartz, syn	Si O2	0.213	ICDD (PDF2010)	00-046-1045
Orthoclase	K (Al Si3 O8)	0.342	ICDD (PDF2010)	01-086-0439
Kyanite	Al2 Si O5	0.983	ICDD (PDF2010)	01-074-1976
Bentonite	(Ca0.06 Na0.21 K0.27) (Al1.64 Fe0.06 Mg0.31) (Al0.29 Si3.71 O10 (O H)2)	5.151	ICDD (PDF2010)	01-076-7629
Kaolinite-2M	Al2 Si2 O5 (O H)4	0.212	ICDD (PDF2010)	01-075-0938
Illite-montmorillonite (NR)	K Al4 (Si, Al)8 O10 (O H)4 ·4 H2 O	2.929	ICDD (PDF2010)	00-035-0652
Muscovite-1M, magnesian, syn	K Al (Mg0.2 Al0.8) (Al0.42 Si3.58) O10 (O H)2	0.181	ICDD (PDF2010)	01-070-1868

Measurement profile (FSS 3)

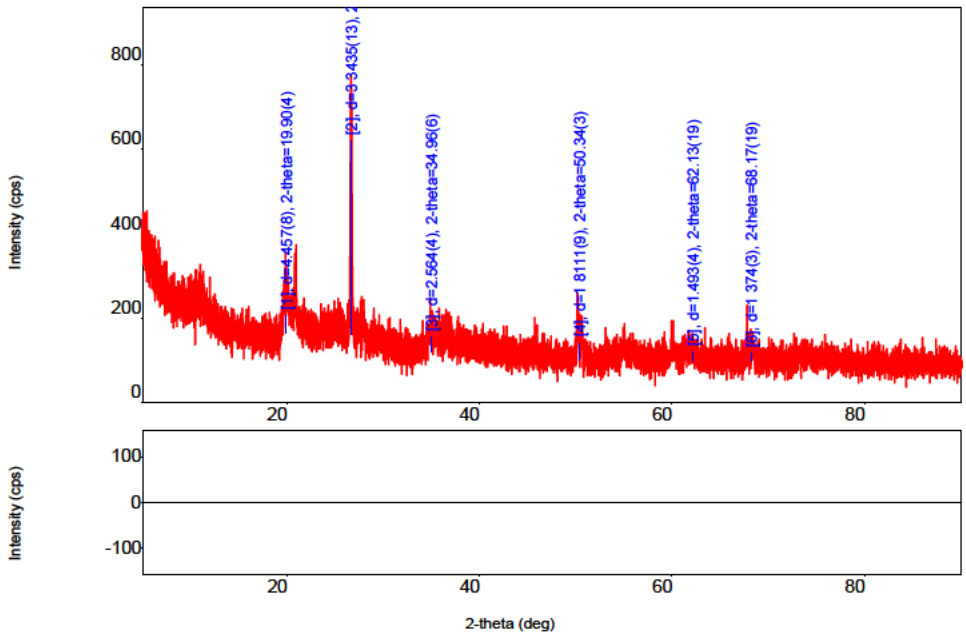

Qualitative analysis results

Phase name	Formula	Figure of merit	Phase reg. detail	DB card number
Quartz, syn	Si O2	2.151	ICDD (PDF2010)	00-046-1045
Orthoclase	K (Al Si3 O8)	1.092	ICDD (PDF2010)	01-086-0439
Kyanite	Al2 Si O5	0.983	ICDD (PDF2010)	01-074-1976
Bentonite	(Ca0.06 Na0.21 K0.27) (Al1.64 Fe0.06 Mg0.31) (Al0.29 Si3.71 O10 (O H)2)	2.221	ICDD (PDF2010)	01-076-7629
Kaolinite-2M	Al2 Si2 O5 (O H)4	0.457	ICDD (PDF2010)	01-075-0938
Illite-montmorillonite (NR)	K Al4 (Si, Al)8 O10 (O H)4 ·4 H2 O	1.759	ICDD (PDF2010)	00-035-0652
Muscovite-1M, magnesian, syn	K Al (Mg0.2 Al0.8) (Al0.42 Si3.58) O10 (O H)2	0.133	ICDD (PDF2010)	01-070-1868

APPENDIX A:

Measurement profile (NCS 1)

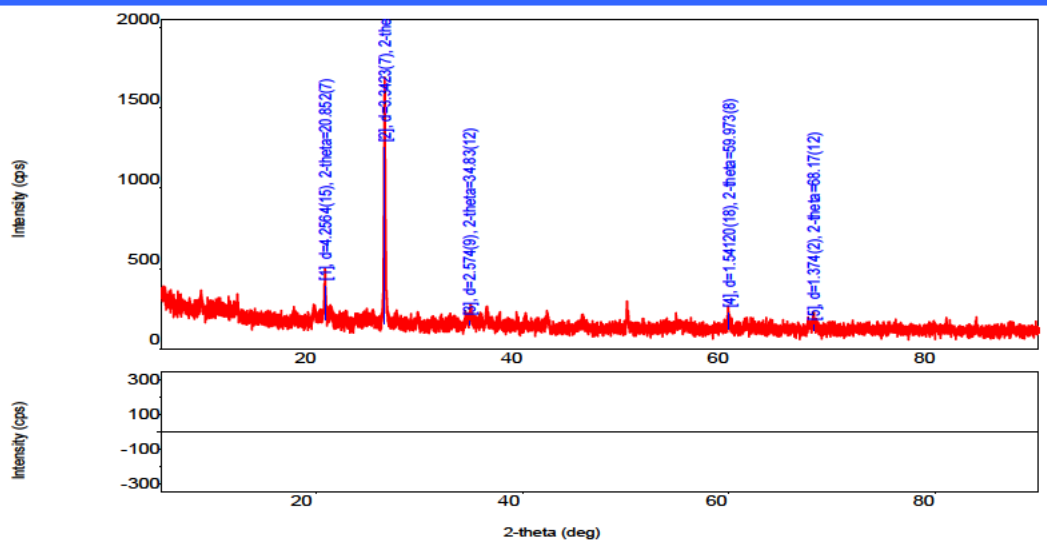

Qualitative analysis results

Phase name	Formula	Figure of merit	Phase reg. detail	DB card number
quartz low, alpha-Si O2	Si O2	0.927	ICDD (PDF2010)	01-086-1629
Iron Oxide	Fe2 O3	2.669	ICDD (PDF2010)	00-056-1302
Muscovite-1M, magnesian, syn	K Al (Mg0.2 Al0.8) (Al0.42 Si3.58) O10 (O H)2	1.467	ICDD (PDF2010)	01-070-1868
Kaolinite-1A	Al2 Si2 O5 (O H)4	1.575	ICDD (PDF2010)	01-072-2300
Bentonite	(Ca0.06 Na0.21 K0.27) (Al1.64 Fe0.06 Mg0.31) (Al0.29 Si3.71 O10 (O H)2)	3.069	ICDD (PDF2010)	01-076-7629
Goethite, cadmium, syn	(Fe0.99 Cd0.01) O (O H)	1.722	ICDD (PDF2010)	01-072-8205
Berthierine-1H	(Fe +2, Fe +3, Al)3 (Si, Al)2 O5 (O H)4	3.150	ICDD (PDF2010)	00-031-0618
Illite-montmorillonite (NR)	K Al4 (Si, Al)8 O10 (O H)4 ·4 H2 O	1.754	ICDD (PDF2010)	00-035-0652

Measurement profile (NCS 2)

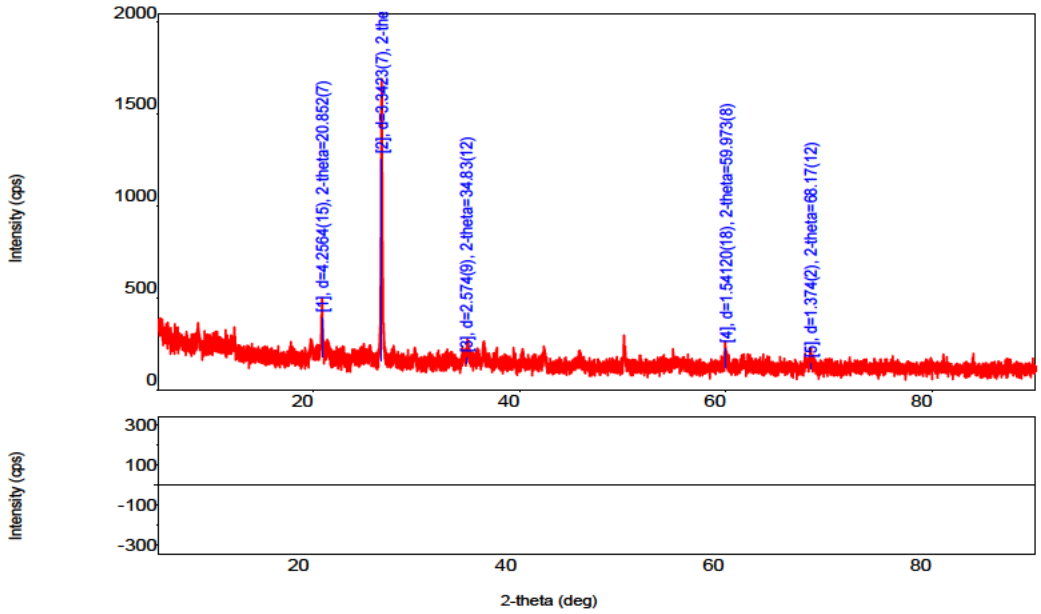

Qualitative analysis results

Phase name	Formula	Figure of merit	Phase reg. detail	DB card number
quartz low, alpha-Si O2	Si O2	0.887	ICDD (PDF2010)	01-086-1629
Iron Oxide	Fe2 O3	2.669	ICDD (PDF2010)	00-056-1302
Muscovite-1M, magnesian, syn	K Al (Mg0.2 Al0.8) (Al0.42 Si3.58) O10 (O H)2	1.33	ICDD (PDF2010)	01-070-1868
Kaolinite-1A	Al2 Si2 O5 (O H)4	1.435	ICDD (PDF2010)	01-072-2300
Bentonite	(Ca0.06 Na0.21 K0.27) (Al1.64 Fe0.06 Mg0.31) (Al0.29 Si3.71 O10 (O H)2)	6.014	ICDD (PDF2010)	01-076-7629
Goethite, cadmian, syn	(Fe0.99 Cd0.01) O (O H)	1.722	ICDD (PDF2010)	01-072-8205
Berthierine-1H	(Fe +2, Fe +3, Al)3 (Si, Al)2 O5 (O H)4	1.530	ICDD (PDF2010)	00-031-0618
Illite-montmorillonite (NR)	K Al4 (Si, Al)8 O10 (O H)4 ·4 H2 O	0.514	ICDD (PDF2010)	00-035-0652

Phase name	Formula	Space group	Phase reg. detail	DB card number
quartz low, alpha-Si	Si O2	152: P3121	ICDD (PDF2010)	01-086-1629
Iron Oxide	Fe2 O3	63: Cmcm	ICDD (PDF2010)	00-056-1302
Muscovite-1M, magnesian, syn	K Al (Mg0.2 Al0.8) (Al0.42 Si3.58) O10 (O H)2	5: C121, unique-b, cell-1	ICDD (PDF2010)	01-070-1868
Kaolinite-1A	Al2 Si2 O5 (O H)4	1: C1	ICDD (PDF2010)	01-072-2300
Bentonite	(Ca0.06 Na0.21 K0.27) (Al1.64 Fe0.06 Mg0.31) (Al0.29 Si3.71 O10 (O H)2)	12: C12/m1, unique-b, cell-1	ICDD (PDF2010)	01-076-7629
Goethite, cadmian, syn	(Fe0.99 Cd0.01) O (O H)	62: Pbnm	ICDD (PDF2010)	01-072-8205
Berthierine-1H	(Fe +2, Fe +3, Al)3 (Si, Al)2 O5 (O H)4	147: P-3	ICDD (PDF2010)	00-031-0618
Illite-montmorillonite (NR)	K Al4 (Si, Al)8 O10 (O H)4 ·4 H2 O	-	ICDD (PDF2010)	00-035-0652

Measurement profile (NCS 3)

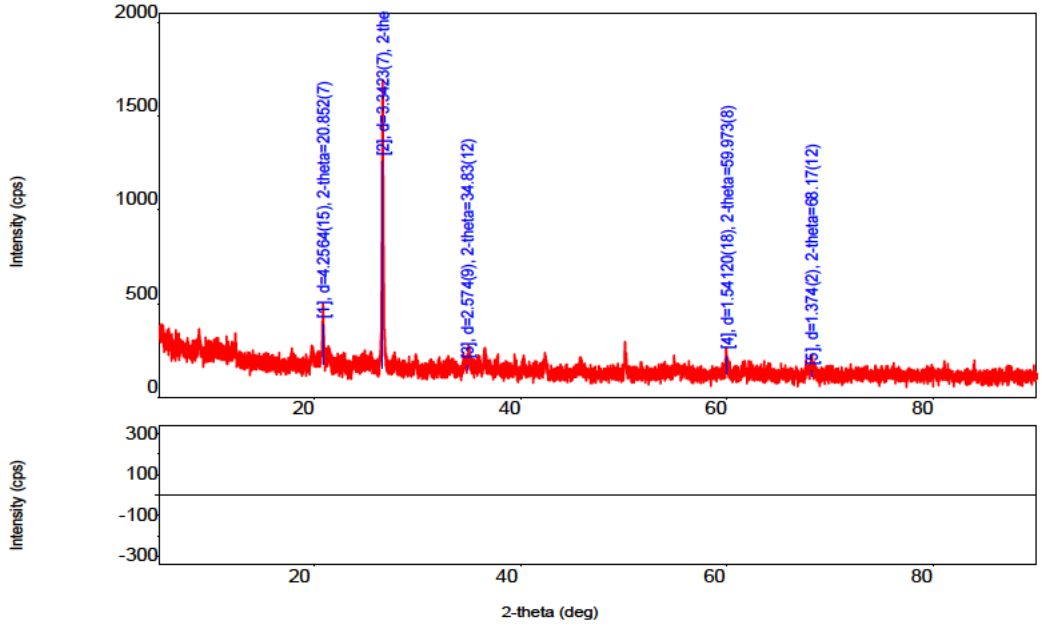

Qualitative analysis results

Phase name	Formula	Figure of merit	Phase reg. detail	DB card number
quartz low, alpha-Si O2	Si O2	0.887	ICDD (PDF2010)	01-086-1629
Iron Oxide	Fe2 O3	2.669	ICDD (PDF2010)	00-056-1302
Muscovite-1M, magnesian, syn	K Al (Mg0.2 Al0.8) (Al0.42 Si3.58) O10 (O H)2	1.33	ICDD (PDF2010)	01-070-1868
Kaolinite-1A	Al2 Si2 O5 (O H)4	1.435	ICDD (PDF2010)	01-072-2300
Bentonite	(Ca0.06 Na0.21 K0.27) (Al1.64 Fe0.06 Mg0.31) (Al0.29 Si3.71 O10 (O H)2)	6.014	ICDD (PDF2010)	01-076-7629
Goethite, cadmian, syn	(Fe0.99 Cd0.01) O (O H)	1.722	ICDD (PDF2010)	01-072-8205
Berthierine-1H	(Fe +2, Fe +3, Al)3 (Si, Al)2 O5 (OH)4	1.530	ICDD (PDF2010)	00-031-0618
Illite-montmorillonite (NR)	K Al4 (Si, Al)8 O10 (O H)4 ·4 H2 O	0.514	ICDD (PDF2010)	00-035-0652

Phase name	Formula	Space group	Phase reg. detail	DB card number
quartz low, alpha-Si	Si O2	152: P3121	ICDD (PDF2010)	01-086-1629
Iron Oxide	Fe2 O3	63: Cmcm	ICDD (PDF2010)	00-056-1302
Muscovite-1M, magnesian, syn	K Al (Mg0.2 Al0.8) (Al0.42 Si3.58) O10 (O H)2	5: C121, unique-b, cell-1	ICDD (PDF2010)	01-070-1868
Kaolinite-1A	Al2 Si2 O5 (O H)4	1: C1	ICDD (PDF2010)	01-072-2300
Bentonite	(Ca0.06 Na0.21 K0.27) (Al1.64 Fe0.06 Mg0.31) (Al0.29 Si3.71 O10 (O H)2)	12: C12/m1, unique-b, cell-1	ICDD (PDF2010)	01-076-7629
Goethite, cadmian, syn	(Fe0.99 Cd0.01) O (O H)	62: Pbnm	ICDD (PDF2010)	01-072-8205
Berthierine-1H	(Fe +2, Fe +3, Al)3 (Si, Al)2 O5 (O H)4	147: P-3	ICDD (PDF2010)	00-031-0618
Illite-montmorillonite (NR)	K Al4 (Si, Al)8 O10 (O H)4 ·4 H2 O	-	ICDD (PDF2010)	00-035-0652

APPENDIX A

GPS 1 X-Ray Diffraction analysis

General Information

Analysis date	2017/06/09 05:03:00 AM		
Sample name	GPS 1 sample one	Measurement date	2017/06/09 14:55:08
File name	GPS 1 sample: Raw	Operator: Aneke Frank	User: Aneke Frank
Comment	Full Chart		

Measurement profile (GPS 1)

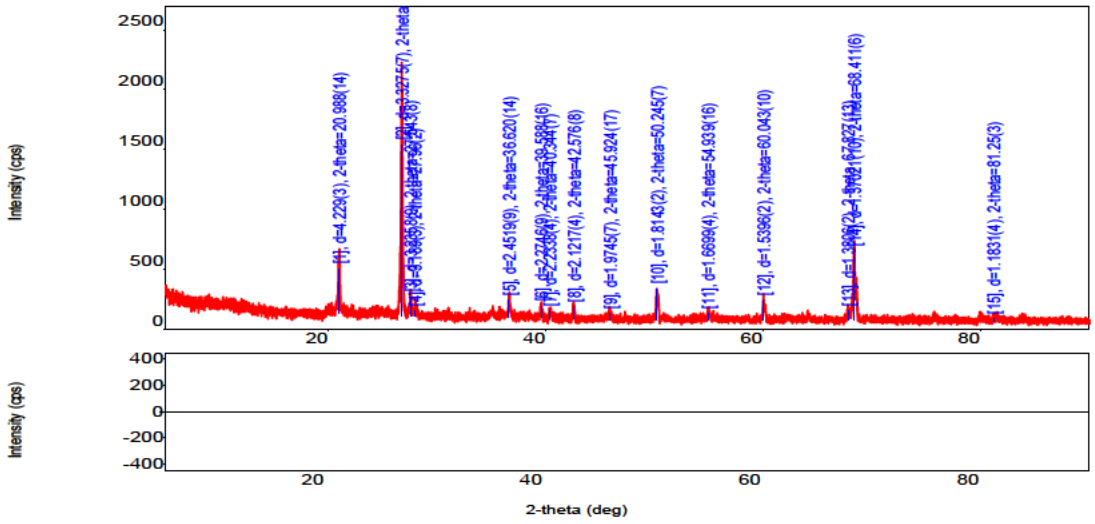

Measurement Qualitative analysis results

Phase name	Formula	Figure of merit	Phase reg. detail	DB card number
Quartz, syn	Si O2	0.625	ICDD (PDF2010)	00-033-1161
Anorthite, ordered	Ca Al2 Si2 O8	0.951	ICDD (PDF2010)	00-041-1486
Rutile, syn	Ti0.928 O2	0.862	ICDD (PDF2010)	01-089-0552
Goethite, cadmian, syn	(Fe0.99 Cd0.01) O (O H)	0.930	ICDD (PDF2010)	01-072-8205
Bentonite	(Ca0.06 Na0.21 K0.27) (Al1.64 Fe0.06 Mg0.31) (Al0.29 Si3.71 O10 (	0.895	ICDD (PDF2010)	01-076-7629
Kaolinite-1A	Al2 Si2 O5 (O H)4	1.366	ICDD (PDF2010)	01-072-2300
Berthierine-1H	(Fe +2, Fe +3, Al)3 (Si,Al)2 O5 (OH)4	1.540	ICDD (PDF2010)	00-031-0618
Muscovite-1M, magnesian, syn	K Al (Mg0.2 Al0.8) (Al0.42 Si3.58) O10 (O H)2	1.081	ICDD (PDF2010)	01-070-1868
Illite-montmorillonite (NR)	K Al4 (Si, Al)8 O10 (O H)4 ·4 H2 O	1.803	ICDD (PDF2010)	00-035-0652

Measurement profile (GPS 2)

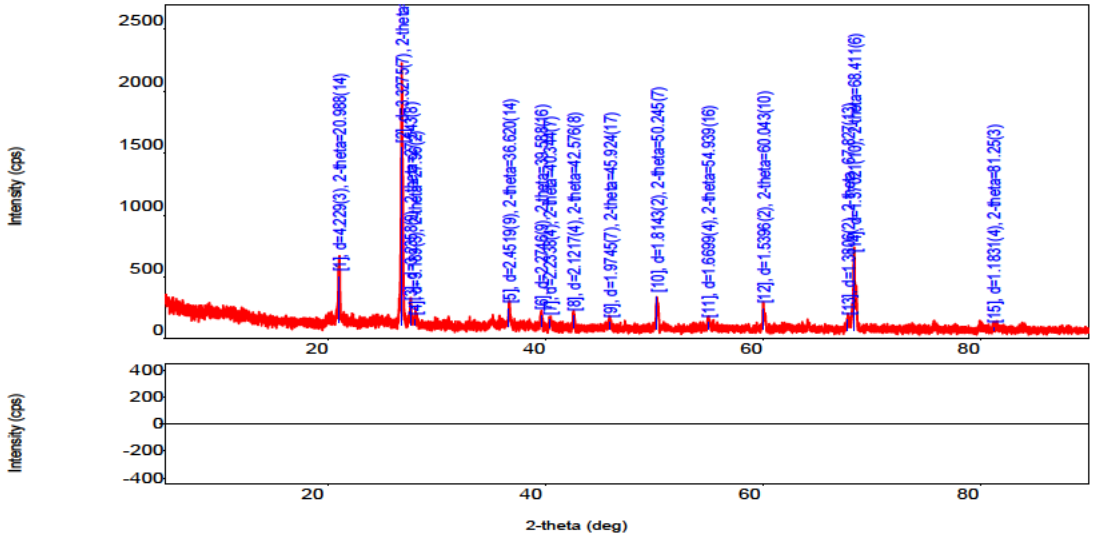

Measurement c Qualitative analysis results

Phase name	Formula	Figure of merit	Phase reg. detail	DB card number
Quartz, syn	Si O2	0.534	ICDD (PDF2010)	00-033-1161
Anorthite, ordered	Ca Al2 Si2 O8	0.951	ICDD (PDF2010)	00-041-1486
Rutile, syn	Ti0.928 O2	0.348	ICDD (PDF2010)	01-089-0552
Goethite, cadmian, syn	(Fe0.99 Cd0.01) O (O H)	0.930	ICDD (PDF2010)	01-072-8205
Bentonite	(Ca0.06 Na0.21 K0.27) (Al1.64 Fe0.06 Mg0.31) (Al0.29 Si3.71 O10 (O H)2)	3.243	ICDD (PDF2010)	01-076-7629
Kaolinite-1A	Al2 Si2 O5 (O H)4	0.213	ICDD (PDF2010)	01-072-2300
Berthierine-1H	(Fe +2, Fe +3, Al)3 (Si, Al)2 O5 (O H)4	0.931	ICDD (PDF2010)	00-031-0618
Muscovite-1M, magnesian, syn	K Al (Mg0.2 Al0.8) (Al0.42 Si3.58) O10 (O H)2	1.512	ICDD (PDF2010)	01-070-1868
Illite-montmorillonite (NR)	K Al4 (Si, Al)8 O10 (O H)4 ·4 H2 O	1.338	ICDD (PDF2010)	00-035-0652

Measurement profile (GPS 3)

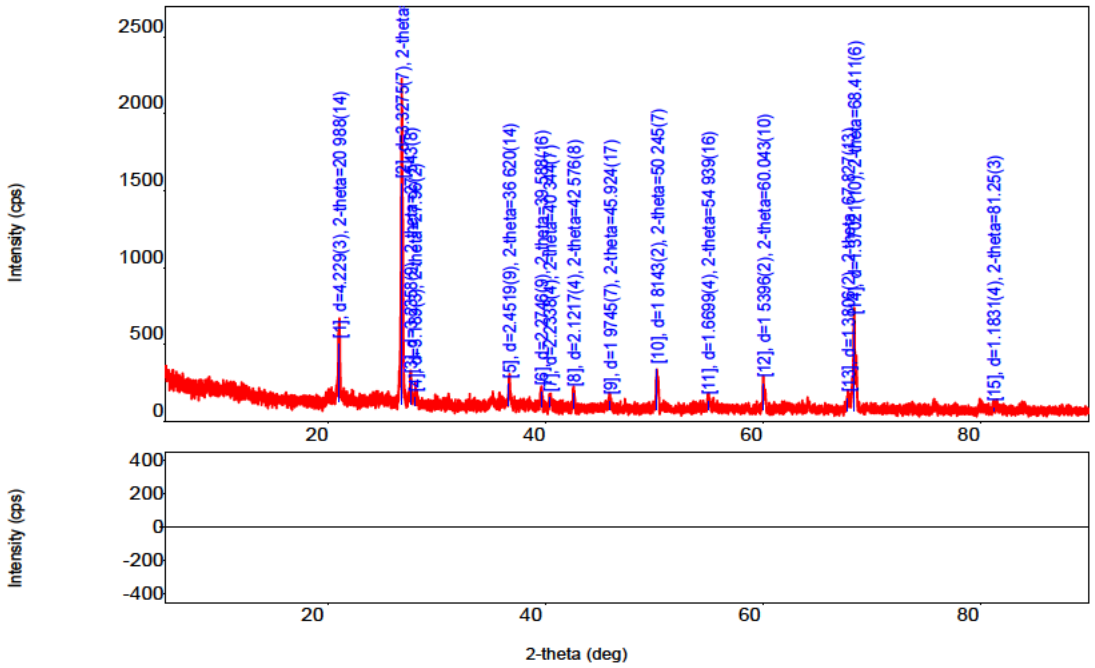

Measurement c Qualitative analysis results

Phase name	Formula	Figure of merit	Phase reg. detail	DB card number
Quartz, syn	Si O2	3.785	ICDD (PDF2010)	00-033-1161
Anorthite, ordered	Ca Al2 Si2 O8	0.235	ICDD (PDF2010)	00-041-1486
Rutile, syn	Ti0.928 O2	0.411	ICDD (PDF2010)	01-089-0552
Goethite, cadmian, syn	(Fe0.99 Cd0.01) O (O H)	0.884	ICDD (PDF2010)	01-072-8205
Bentonite	(Ca0.06 Na0.21 K0.27) (Al1.64 Fe0.06 Mg0.31) (Al0.29 Si3.71 O10 (O H)2)	1.212	ICDD (PDF2010)	01-076-7629
Kaolinite-1A	Al2 Si2 O5 (O H)4	0.632	ICDD (PDF2010)	01-072-2300
Berthierine-1H	(Fe +2, Fe +3, Al)3 (Si, Al)2 O5 (O H)4	0.854	ICDD (PDF2010)	00-031-0618
Muscovite-1M, magnesian, syn	K Al (Mg0.2 Al0.8) (Al0.42 Si3.58) O10 (O H)2	0.875	ICDD (PDF2010)	01-070-1868
Illite-montmorillonite (NR)	K Al4 (Si, Al)8 O10 (O H)4 ·4 H2 O	1.113	ICDD (PDF2010)	00-035-0652

APPENDIX A

FSS 1 X-Ray Fluorescence Analysis

Job name	EZ Scan
Application	EZS002XNV
Analysed date	2017- 6- 18 14:04
Sample	FSS 1 sample one
Operator	Frank

Component	Unit	Result	Det.limit	El. line	Intensity	w/o normal
Na2O	mass%	0.5260	0.0231	Na-KA	0.5447	0.3462
MgO	mass%	1.9588	0.02101	Mg-KA	5.4093	1.2892
Al2O3	mass%	21.4052	0.01852	Al-KA	169.0486	14.0879
SiO2	mass%	58.3918	0.02368	Si-KA	332.1282	38.4306
P2O5	mass%	0.0555	0.00466	P -KA	0.4837	0.0365
SO3	mass%	0.1603	0.00558	S -KA	1.1235	0.1055
Cl	mass%	0.0425	0.00837	Cl-KA	0.1679	0.0280
K2O	mass%	1.8978	0.00600	K-KA	37.0990	1.2490
CaO	mass%	1.7495	0.00577	Ca-KA	26.5813	1.1514
TiO2	mass%	1.1282	0.01516	Ti-KA	4.8382	0.7425
Cr2O3	mass%	0.0699	0.01037	Cr-KA	0.8585	0.0460
MnO	mass%	0.2025	0.06565	Mn-KB1	0.7682	0.1333
Fe2O3	mass%	12.0868	0.01024	Fe-KA	321.3238	7.9550
NiO	mass%	0.0268	0.00505	Ni-KA	1.0501	0.0177
CuO	mass%	0.0164	0.00437	Cu-KA	0.8364	0.0108
ZnO	mass%	0.0153	0.00393	Zn-KA	1.0466	0.0101
Br	mass%	0.0054	0.00239	Br-KA	1.0636	0.0035
Rb2O	mass%	0.0513	0.01294	Rb-KB1	2.6441	0.0337
SrO	mass%	0.0209	0.00248	Sr-KA	5.1276	0.0138
ZrO2	mass%	0.0559	0.01483	Zr-KB1	3.5744	0.0368
BaO	mass%	0.1333	0.03667	Ba-KA	3.5993	0.0877

APPENDIX A

FSS 2 X-Ray Fluorescence Analysis

Job name	EZ Scan
Application	EZS002XNV
Analysed date	2017- 6- 19 18:04
Sample	FSS 2 sample two
Operator	Frank

Component	Unit	Result	Det.limit	El. line	Intensity	w/o normal
Na2O	mass%	0.4233	0.02316	Na-KA	0.4336	0.2344
MgO	mass%	1.8534	0.02101	Mg-KA	6.3182	1.1823
Al2O3	mass%	19.3143	0.01852	Al-KA	158.139	12.0678
SiO2	mass%	33.2341	0.02368	Si-KA	241.237	33.4567
P2O5	mass%	0.0555	0.00466	P -KA	1.3746	0.0401
SO3	mass%	0.1603	0.00558	S -KA	0.2348	0.1102
Cl	mass%	0.0425	0.00837	Cl-KA	0.7845	0.0198
K2O	mass%	1.8978	0.00600	K-KA	30.8855	1.6335
CaO	mass%	4.6584	0.00577	Ca-KA	27.0781	1.2378
TiO2	mass%	0..2373	0.01516	Ti-KA	3.9065	0.3461
Cr2O3	mass%	0.0912	0.01037	Cr-KA	0.3451	0.0321
MnO	mass%	0.3114	0.06565	Mn-KB1	0.4562	0.2894
Fe2O3	mass%	13.1773	0.02524	Fe-KA	302.2121	5.4568
NiO	mass%	0.0379	0.00637	Ni-KA	1.0671	0.0234
CuO	mass%	0.0275	0.00348	Cu-KA	0.5691	0.0119
ZnO	mass%	0.0264	0.00482	Zn-KA	1.0674	0.0212
Br	mass%	0.0042	0.00348	Br-KA	1.0679	0.0049
Rb2O	mass%	0.0328	0.02387	Rb-KB1	1.4556	0.0337
SrO	mass%	0.0413	0.00389	Sr-KA	4.2347	0.0289
ZrO2	mass%	0.0331	0.02343	Zr-KB1	4.6342	0.0455
BaO	mass%	0.2441	0.04759	Ba-KA	5.0654	0.0743

APPENDIX A

FSS 3 X-Ray Fluorescence Analysis

Job name	EZ Scan
Application	EZS002XNV
Analysed date	2017- 6- 19 22:52
Sample	FSS 3 sample three
Operator	Frank

Component	Unit	Result	Det.limit	El. line	Intensity	w/o normal
Na2O	mass%	0.4353	0.04531	Na-KA	0.5354	0.4321
MgO	mass%	1.8581	0.03923	Mg-KA	6.6729	1.4567
Al2O3	mass%	19.8201	0.04252	Al-KA	158.3492	12.0459
SiO2	mass%	58.4352	0.02368	Si-KA	241.9024	38.4591
P2O5	mass%	0.6493	0.00563	P -KA	1.3953	0.0567
SO3	mass%	0.5639	0.00523	S -KA	0.6313	0.5643
Cl	mass%	0.0435	0.00321	Cl-KA	0.7452	0.0455
K2O	mass%	1.5202	0.00617	K-KA	37.1273	1.0987
CaO	mass%	1.5262	0.00891	Ca-KA	26.3987	1.1238
TiO2	mass%	1.9605	0.01781	Ti-KA	4.5610	0.8901
Cr2O3	mass%	0.0533	0.08915	Cr-KA	0.5623	0.0678
MnO	mass%	0.5362	0.04321	Mn-KB1	0.9013	0.4580
Fe2O3	mass%	12.4362	0.01654	Fe-KA	321.3901	7.8907
NiO	mass%	0.0456	0.00567	Ni-KA	1.0562	0.0568
CuO	mass%	0.0321	0.00891	Cu-KA	0.3893	0.0113
ZnO	mass%	0.0557	0.00531	Zn-KA	1.0569	0.0432
Br	mass%	0.0056	0.00910	Br-KA	1.0657	0.0089
Rb2O	mass%	0.0592	0.01264	Rb-KB1	2.5674	0.0321
SrO	mass%	0.0176	0.00290	Sr-KA	5.2891	0.0432
ZrO2	mass%	0.0492	0.01238	Zr-KB1	3.6373	0.0589
BaO	mass%	0.7472	0.08943	Ba-KA	3.6353	0.6738

APPENDIX A

NCS 1 X-Ray Fluorescence Analysis

Job name	EZ Scan
Application	EZS002XNV
Analysed date	2017- 6- 23 13:41
Sample	NCS 1 sample one
Operator	Frank

Component	Unit	Result	Det.limit	El. line	Intensity	w/o normal
Na2O	mass%	0.0515	0.02703	Na-KA	0.0505	0.0414
MgO	mass%	0.6437	0.01886	Mg-KA	2.0357	0.5174
Al2O3	mass%	19.8008	0.01668	Al-KA	183.2614	15.9174
SiO2	mass%	55.1435	0.02103	Si-KA	377.9683	44.3286
P2O5	mass%	0.0579	0.00347	P -KA	0.6245	0.0465
SO3	mass%	0.0412	0.00458	S -KA	0.3584	0.0331
Cl	mass%	0.0191	0.00621	Cl-KA	0.0934	0.0154
K2O	mass%	3.7728	0.00489	K-KA	91.1422	3.0329
CaO	mass%	0.2234	0.00432	Ca-KA	4.0481	0.1796
TiO2	mass%	0.7559	0.00982	Ti-KA	4.0266	0.6076
V2O5	mass%	0.0310	0.01216	V -KA	0.3043	0.0249
Cr2O3	mass%	0.0551	0.00750	Cr-KA	0.8993	0.0443
MnO	mass%	0.1388	0.00703	Mn-KA	3.3050	0.1116
Fe2O3	mass%	18.9925	0.03432	Fe-KB1	112.2866	15.2676
Co2O3	mass%	0.0200	0.00682	Co-KA	1.7914	0.0161
NiO	mass%	0.0176	0.00435	Ni-KA	0.7022	0.0142
CuO	mass%	0.0088	0.00386	Cu-KA	0.4575	0.0071
ZnO	mass%	0.0128	0.00341	Zn-KA	0.8832	0.0103
Rb2O	mass%	0.0289	0.00205	Rb-KA	6.7093	0.233
ZrO2	mass%	0.0515	0.00214	Zr-KA	14.2720	0.0414
BaO	mass%	0.1092	0.02955	Ba-KA	3.0095	0.0878
PbO	mass%	0.0240	0.00631	Pb-LA	1.2702	0.0193

APPENDIX A

NCS 2 X-Ray Fluorescence Analysis

Job name	EZ Scan
Application	EZS002XNV
Analysed date	2017- 6- 23 18:38
Sample	NCS 2 sample two
Operator	Frank

Component	Unit	Result	Det.limit	El. line	Intensity	w/o normal
Na2O	mass%	0.0563	0.02231	Na-KA	0.0423	0.0212
MgO	mass%	0.5369	0.01976	Mg-KA	2.0301	0.4512
Al2O3	mass%	15.5373	0.01890	Al-KA	183.2213	15.2313
SiO2	mass%	52.5235	0.02119	Si-KA	377.3421	44.2159
P2O5	mass%	0.0633	0.00390	P -KA	0.2341	0.0349
SO3	mass%	0.0567	0.00423	S -KA	0.2123	0.0890
Cl	mass%	0.0342	0.00602	Cl-KA	0.0345	0.0341
K2O	mass%	4.7432	0.00412	K-KA	91.1211	3.0112
CaO	mass%	0.5353	0.00490	Ca-KA	4.0411	0.1234
TiO2	mass%	0.5755	0.00993	Ti-KA	4.0123	0.3219
V2O5	mass%	0.0672	0.01456	V -KA	0.2121	0.0124
Cr2O3	mass%	0.0892	0.00789	Cr-KA	0.2122	0.0671
MnO	mass%	0.9012	0.00718	Mn-KA	3.1212	0.0345
Fe2O3	mass%	16.8422	0.04567	Fe-KB1	112.0132	15.2311
Co2O3	mass%	0.0267	0.0046	Co-KA	1.0324	0.0321
NiO	mass%	0.0291	0.00482	Ni-KA	0.2019	0.0231
CuO	mass%	0.0067	0.00197	Cu-KA	0.0245	0.0021
ZnO	mass%	0.0321	0.00789	Zn-KA	0.2342	0.0212
Rb2O	mass%	0.0347	0.00298	Rb-KA	6.6231	0.2331
ZrO2	mass%	0.0532	0.00459	Zr-KA	14.1100	0.0231
BaO	mass%	0.1018	0.07384	Ba-KA	3.0012	0.0890
PbO	mass%	0.0232	0.00892	Pb-LA	1.1011	0.0112

APPENDIX A

NCS 3 X-Ray Fluorescence Analysis

Job name	EZ Scan
Application	EZS002XNV
Analysed date	2017- 6- 23 23:54
Sample	NCS 3 sample
Operator	Frank

Component	Unit	Result	Det.limit	El. line	Intensity	w/o normal
Na2O	mass%	0.0536	0.01231	Na-KA	0.0122	0.0414
MgO	mass%	0.5363	0.01098	Mg-KA	2.0130	0.5174
Al2O3	mass%	17.636	0.02100	Al-KA	153.1216	15.9174
SiO2	mass%	51.526	0.01218	Si-KA	356.1197	44.3286
P2O5	mass%	0.6738	0.00254	P -KA	0.6345	0.0465
SO3	mass%	0.7387	0.00564	S -KA	0.4689	0.0331
Cl	mass%	0.5262	0.00789	Cl-KA	0.0234	0.0154
K2O	mass%	3.1123	0.00213	K-KA	91.0678	3.0329
CaO	mass%	0.1525	0.00231	Ca-KA	4.0231	0.1796
TiO2	mass%	1.0242	0.00311	Ti-KA	4.0390	0.6076
V2O5	mass%	0.1003	0.02101	V -KA	0.2134	0.0249
Cr2O3	mass%	0.0129	0.00211	Cr-KA	0.2120	0.0443
MnO	mass%	0.1239	0.00123	Mn-KA	3.2897	0.1116
Fe2O3	mass%	15.0963	0.07826	Fe-KB1	110.2116	15.2676
Co2O3	mass%	0.2135	0.00213	Co-KA	1.6212	0.0161
NiO	mass%	0.0213	0.00213	Ni-KA	0.4987	0.0142
CuO	mass%	0.0021	0.00672	Cu-KA	0.5212	0.0071
ZnO	mass%	0.0321	0.00219	Zn-KA	0.3011	0.0103
Rb2O	mass%	0.0151	0.00209	Rb-KA	2.4543	0.233
ZrO2	mass%	0.0231	0.00112	Zr-KA	14.2720	0.0414
BaO	mass%	0.1212	0.01097	Ba-KA	3.0095	0.0878
PbO	mass%	0.0234	0.00321	Pb-LA	1.2702	0.0193

APPENDIX A

GPS 1 X-Ray Fluorescence Analysis

Job name	EZ Scan
Application	EZS002XNV
Analysed date	2017- 6- 25 13:19
Sample	GPS 1 sample one
Operator	Frank

Component	Unit	Result	Det.limit	El. line	Intensity	w/o normal
Na2O	mass%	0.3732	0.02108	Na-KA	0.4118	0.2553
MgO	mass%	0.7154	0.01938	Mg-KA	2.1248	0.4894
Al2O3	mass%	17.4958	0.01635	Al-KA	150.7877	11.9686
SiO2	mass%	66.5877	0.02428	Si-KA	420.4225	45.5516
P2O5	mass%	0.0722	0.00467	P -KA	0.6485	0.0494
SO3	mass%	0.0571	0.00540	S-KA	0.4124	0.0391
Cl	mass%	0.0230	0.00795	Cl-KA	0.0935	0.0157
K2O	mass%	2.9766	0.00534	K-KA	59.3967	2.0362
CaO	mass%	1.2703	0.00564	Ca-KA	19.2608	0.8690
TiO2	mass%	0.7756	0.91690	Ti-KA	3.3597	0.5306
V2O5	mass%	0.0344	0.01519	V-KA	0.2781	0.0235
Cr2O3	mass%	0.0545	0.00992	Cr-KA	0.7053	0.0373
MnO	mass%	1.0676	0.05835	Mn-KB1	4.2085	0.7303
Fe2O3	mass%	8.2910	0.00931	Fe-KA	231.2775	5.6718
NiO	mass%	0.0174	0.00470	Ni-KA	0.7660	0.0119
CuO	mass%	0.0128	0.00399	Cu-KA	0.7400	0.0088
Rb2O	mass%	0.0193	0.00208	Rb-KA	5.1317	0.0132
SrO	mass%	0.0135	0.00209	Sr-KA	3.7917	0.0092
ZrO2	mass%	0.0298	0.01226	Zr-KB1	2.1962	0.0204
Nb2O5	mass%	0.0039	0.00225	Nb-KA	1.3042	0.0027
BaO	mass%	0.1090	0.03737	Ba-LA	0.2144	0.0745

APPENDIX A

GPS 2 X-Ray Fluorescence Analysis

Job name	EZ Scan
Application	EZS002XNV
Analysed date	2017- 6- 25 13:19
Sample	GPS 2 sample two
Operator	Frank

Component	Unit	Result	Det.limit	El. line	Intensity	w/o normal
Na2O	mass%	0.3578	0.03234	Na-KA	0.3227	0.3421
MgO	mass%	0.5321	0.01865	Mg-KA	2.2237	0.3456
Al2O3	mass%	14.2341	0.03215	Al-KA	132.6531	11.4531
SiO2	mass%	68.1120	0.03221	Si-KA	406.3211	42.345
P2O5	mass%	0.0892	0.00671	P -KA	0.6352	0.0321
SO3	mass%	0.0231	0.00664	S-KA	0.3512	0.0401
Cl	mass%	0.0431	0.00897	Cl-KA	0.0765	0.0234
K2O	mass%	2.0167	0.00453	K-KA	54.3135	1.9865
CaO	mass%	1.2255	0.00432	Ca-KA	13.3421	0.5432
TiO2	mass%	0.2315	0.87815	Ti-KA	3.2134	0.5123
V2O5	mass%	0.0267	0.02317	V-KA	0.3245	0.0342
Cr2O3	mass%	0.0432	0.00678	Cr-KA	0.5432	0.0453
MnO	mass%	1.0342	0.04456	Mn-KB1	3.3421	0.4534
Fe2O3	mass%	5.3421	0.00812	Fe-KA	287.1113	6.1103
NiO	mass%	0.0231	0.00321	Ni-KA	0.74321	0.0231
CuO	mass%	0.0234	0.00321	Cu-KA	0.2314	0.0034
Rb2O	mass%	0.0452	0.00251	Rb-KA	6.3421	0.0456
SrO	mass%	0.0342	0.00221	Sr-KA	2.8974	0.0094
ZrO2	mass%	0.0190	0.02134	Zr-KB1	1.8976	0.0287
Nb2O5	mass%	0.0093	0.00453	Nb-KA	1.8712	0.0034
BaO	mass%	0.1134	0.05643	Ba-LA	0.3122	0.0632

APPENDIX A

GPS 3 X-Ray Fluorescence Analysis

Job name	EZ Scan
Application	EZS002XNV
Analysed date	2017- 6- 25 13:19
Sample	GPS 3 sample three
Operator	Frank

Component	Unit	Result	Det.limit	El. line	Intensity	w/o normal
Na2O	mass%	0.3241	0.02317	Na-KA	0.4321	0.2348
MgO	mass%	0.4542	0.02135	Mg-KA	1.9645	0.2689
Al2O3	mass%	14.3245	0.02415	Al-KA	127.4321	12.3145
SiO2	mass%	66.9132	0.02152	Si-KA	394.8713	45.112
P2O5	mass%	0.0732	0.00623	P -KA	0.4353	0.0213
SO3	mass%	0.0342	0.00567	S-KA	0.4567	0.0345
Cl	mass%	0.0231	0.00321	Cl-KA	0.0213	0.0324
K2O	mass%	2.0189	0.00563	K-KA	59.1218	1.2341
CaO	mass%	1.0765	0.00367	Ca-KA	17.4231	0.3213
TiO2	mass%	0.2751	0.64328	Ti-KA	2.3132	0.4123
V2O5	mass%	0.0311	0.01567	V-KA	0.2258	0.0231
Cr2O3	mass%	0.0521	0.00512	Cr-KA	0.4281	0.0223
MnO	mass%	1.0214	0.03321	Mn-KB1	2.2321	0.2341
Fe2O3	mass%	4.9871	0.00865	Fe-KA	265.9732	2.4341
NiO	mass%	0.0451	0.00456	Ni-KA	0.5690	0.0765
CuO	mass%	0.0342	0.00379	Cu-KA	0.3219	0.0098
Rb2O	mass%	0.0563	0.00462	Rb-KA	5.2311	0.0448
SrO	mass%	0.0812	0.00346	Sr-KA	1.4321	0.0128
ZrO2	mass%	0.0219	0.04352	Zr-KB1	1.9432	0.0291
Nb2O5	mass%	0.0099	0.00552	Nb-KA	1.2344	0.0099
BaO	mass%	0.1238	0.04322	Ba-LA	0.0262	0.0389

APPENDIX B

Table 4.2: Soils Moisture Conditions and Swelling Stress Characteristics

Soils	ω%	γ_d (kN/m^3)	Surcharge force (kN)	P_{s_n} (kPa)	Ring area (m^2)
FSS 1					
	8.35	12.45	1.37	699	0.01963
	13.56	16.63	1.18	600	0.01963
	17.48	17.32	0.88	450	0.01963
	24.32	15.90	0.46	390	0.01963
	31.64	12.88	0.59	300	0.01963
FSS 2					
	10.13	12.47	1.77	899	0.01963
	13.61	15.62	1.47	749	0.01963
	18.54	16.93	1.23	630	0.01963
	24.12	14.15	0.88	450	0.01963
	30.19	12.12	0.59	300	0.01963
FSS 3					
	7.33	11.45	0.98	499	0.01963
	14.19	17.61	0.88	450	0.01963
	18.48	16.59	0.77	390	0.01963
	22.91	16.93	0.65	330	0.01963
	28.30	13.47	0.49	250	0.01963
NCS 1					
	8.40	16.07	1.28	650	0.01963
	12.70	18.92	1.18	600	0.01963
	17.51	19.35	1.02	520	0.01963
	24.52	17.52	0.88	450	0.01963
	28.35	16.18	0.69	350	0.01963
NCS 2					
	9.20	15.45	1.28	630	0.01963
	14.18	17.52	0.98	500	0.01963
	18.40	18.52	0.88	450	0.01963
	24.91	18.89	0.78	400	0.01963
	30.23	15.58	0.69	350	0.01963
NCS 3					
	9.94	14.17	1.67	830	0.01963
	14.55	15.86	1.42	725	0.01963
	18.87	16.83	1.28	650	0.01963
	25.26	15.95	1.02	520	0.01963
	32.92	13.02	0.88	400	0.01963
GPS 1					
	8.69	16.47	0.96	490	0.01963
	13.48	19.46	0.88	450	0.01963
	17.30	21.83	0.74	375	0.01963
	24.31	20.07	0.69	350	0.01963
	32.72	16.16	0.49	250	0.01963
GPS 2					
	9.95	15.45	1.28	650	0.01963
	13.69	19.23	1.18	600	0.01963

	18.56	20.89	1.02	520	0.01963
	24.11	18.96	0.88	450	0.01963
	30.14	15.96	0.69	350	0.01963
GPS 3					
	9.30	18.13	1.02	520	0.01963
	14.18	21.63	0.83	425	0.01963
	18.85	22.84	0.78	400	0.01963
	22.91	21.71	0.59	300	0.01963
	27.30	18.83	0.39	200	0.01963

*γ_d = dry unit weight

* $\boldsymbol{P_{s_n}}$ = swelling pressure

* ω = moisture water content

Table 4.3: Suction Values at Varying Moisture Content

Soils	GWC (%)	Total suction FPWC (%)	$\boldsymbol{\psi_T}$ (kPa)	$\boldsymbol{\psi_M}$ (kPa)	($\boldsymbol{\psi_O}$) (kPa)
FSS 1					
	8.55	14.63	8283	6541	1742
	13.46	18.78	7311	5676	1335
	17.65	24.15	5593	4989	904
	24.27	28.32	3993	2793	600
	31.75	33.50	1327	921	406
FSS 2					
	9.97	14.93	10158	8517	1641
	13.53	18.48	8164	6343	1321
	18.58	23.93	6052	4989	1063
	24.09	28.11	3797	2895	902
	30.16	32.78	2634	1913	721
FSS 3					
	7.28	14.22	8454	6398	2056
	14.15	19.43	6768	5345	1423
	18.45	24.21	4689	3450	1239
	22.94	27.43	2931	1998	933
	28.33	31.12	1818	1240	578
NCS 1					
	8.38	18.97	3598	2534	1064
	12.73	25.91	2781	2098	683
	17.49	29.11	2198	1643	555
	24.49	32.31	1495	1134	361
	28.33	35.78	1093	778	315
NCS 2					
	9.18	19.23	4532	3878	1254
	14.15	26.52	3495	2465	1030
	18.38	30.34	3035	2087	948
	24.89	32.82	2474	1598	876
	30.22	34.34	1581	1091	490

NCS 3					
	9.97	19.45	2166	1595	971
	14.53	25.76	1998	1545	453
	18.98	29.65	1592	1172	310
	25.24	31.54	1193	990	303
	32.88	34.35	889	681	208
GPS 1					
	8.67	15.78	6554	5071	1483
	13.46	22.91	5192	3884	1308
	17.33	26.62	4253	2959	1294
	24.27	30.14	2895	2183	712
	32.75	33.32	1472	1128	344
GPS 2					
	9.97	14.96	6771	5263	1808
	13.67	19.65	5699	3989	1210
	18.58	25.98	4081	2914	1067
	24.09	29.23	2758	2029	529
	30.16	31.33	956	667	289
GPS 3					
	9.28	13.35	7280	5331	1949
	14.15	19.46	4974	3708	1266
	18.88	21.84	3642	2707	935
	22.94	30.29	2297	1715	582
	27.33	34.39	998	763	235

*GWC = Gravimetric water content
*FPWC = Filter paper water content
*ψ_T, ψ_M and ψ_O = Total, Matric and Osmotic suction

Table 4.4: Fitting Parameters of Difference SWRC Models for FSS

FSS 1				
Model	Equation	Parameters	R^2	AIC
Van Genuchten	$S_e = \left[\frac{1}{1+(\alpha h)^n}\right]^m$ (m= 1-1/n)	θ_s=0.54642 θ_r=3.97841e-05 α = 0.0025426 n= 1.3251	0.93016	-75.337
Fredlund and Xing	$S_e = Q\left[\frac{1}{ln\left[e+\left(h/a\right)^n\right]}\right]^m$	θ_s=0.59715 θ_r= 4.4119e-06 a= 2255.8 m=2.5655 n = 0.59392	0.95550	-79.198

Seki	$S_e = \omega_1 Q\left[\frac{\ln(h/h_{m1})}{\sigma_1}\right] + (1-\omega_1)Q\left[\frac{\ln(h/h_{m2})}{\sigma_2}\right]$	θ_s=0.60402 θ_r= 5.9737e-08 ω_1=0.18115 h_{m_1}=16.297 σ_1= 1.7275 h_{m_2}= 3767.5 σ_2= 1.6344	0.97754	-84.087
FSS 2				
Van Genuchten	$S_e = \left[\frac{1}{1+(\alpha h)^n}\right]^m (m = 1-1/n)$	θ_s=0.53788 θ_r=2.7835e-05 α = 0.0017918 n= 1.3507	0.93317	-78.051
Fredlund and Xing	$S_e = \left[\frac{1}{ln\left[e+\left(e\frac{h}{a}\right)^n\right]}\right]^m$	θ_s= 0.55708 θ_r= 3.4180e-06 a=4384.7 m= 2.8559 n=0.73219	0.96142	-83.195
Seki	$S_e = \omega_1 Q\left[\frac{\ln(h/h_{m1})}{\sigma_1}\right] + (1-\omega_1)Q\left[\frac{\ln(h/h_{m2})}{\sigma_2}\right]$	θ_s=0.56810 θ_r= 2.2280e-06 ω_1=0.18665 h_{m_1}= 54.936 σ_1= 0.93116 h_{m_2}= 5053.5 σ_2= 1.0062	0.99813	-118.58
FSS 3				
Van Genuchten	$S_e = \left[\frac{1}{1+(\alpha h)^n}\right]^m (m = 1-1/n)$	θ_s=0.50863 θ_r=1.9479e-07 α = 0.0032176 n= 1.3068	0.91957	-76.980
Fredlund and Xing	$S_e = \left[\frac{1}{ln\left[e+(h/a)^n\right]}\right]^m$	θ_s= 0.52975 θ_r= 1.6845e-05 a=2672.7 m= 2.6044 n=0.64936	0.94750	-80.527
Seki	$S_e = \omega_1 Q\left[\frac{\ln(h/h_{m1})}{\sigma_1}\right] + (1-\omega_1)Q\left[\frac{\ln(h/h_{m2})}{\sigma_2}\right]$	θ_s=0.53867 θ_r= 1.4097e-06 ω_1=0.20857 h_{m_1}=40.659 σ_1= 1.1023 h_{m_2}= 3791.6 σ_2= 1.0595	0.9898513	-97.887

Table 4.5: Fitting Parameters of Difference SWRC Models for NCS

Model	Equation	Parameters	R^2	AIC
NCS 1				
Van Genuchten	$S_e = \left[\frac{1}{1+(\alpha h)^n}\right]^m (m = 1 - 1/n)$	θ_s=0.49334 θ_r=3.2549e-05 α = 0.0019231 n = 1.5498	0.91356	-76.028
Fredlund and Xing	$S_e = \left[\frac{1}{ln\left[e + (h/a)^n\right]}\right]^m$	θ_s= 0.51977 θ_r= 3.6868e-06 a=1568.6 m= 2.7477 n=0.84386	0.93197	-77.141
Seki	$S_e = \omega_1 Q\left[\frac{\ln(h/h_{m1})}{\sigma_1}\right] + (1-\omega_1)Q\left[\frac{\ln(h/h_{m}2)}{\sigma_2}\right]$	θ_s=0.53365 θ_r= 2.2035e-06 ω_1=0.20987 h_{m_1}=29.232 σ_1= 1.2094 h_{m_2}= 1754.1 σ_2= 0.66531	0.99876	-125.25
NCS 2				
Van Genuchten	$S_e = \left[\frac{1}{1+(\alpha h)^n}\right]^m (m = 1 - 1/n)$	θ_s=0.52915 θ_r=3.25871e-05 α = 0.0014801 n = 1.6255	0.93152	-77.458
Fredlund and Xing	$S_e = \left[\frac{1}{ln\left[e + (h/a)^n\right]}\right]^m$	θ_s= 0.57650 θ_r= 1.3018e-05 a=1151.1 m= 2.1934 n=0.60755	0.89959	-70.481
Seki	$S_e = \omega_1 Q\left[\frac{\ln(h/h_{m1})}{\sigma_1}\right] + (1-\omega_1)Q\left[\frac{\ln(h/h_{m}2)}{\sigma_2}\right]$	θ_s=0.57028 θ_r= 0.024685 ω_1=0.22872 h_{m_1}=43.896 σ_1= 1.1845 h_{m_2}= 2109.3 σ_2= 0.57823	0.99986	-152.10
NCS 3				
Van Genuchten	$S_e = \left[\frac{1}{1+(\alpha h)^n}\right]^m (m = 1 - 1/n)$	θ_s=0.58368 θ_r=4.4307e-06 α = 0.005422 n = 1.3433	0.87339	-66.375
Fredlund and Xing	$S_e = \left[\frac{1}{ln\left[e + (h/a)^n\right]}\right]^m$	θ_s= 0.60885 θ_r= 2.9804e-05 a=1064.0 m= 2.5958 n=0.79245	0.92085	-70.482
Seki		θ_s=0.62055 θ_r= 0.043033	0.99970	-138.97

	$S_e = \omega_1 Q\left[\frac{\ln(h/h_{m1})}{\sigma_1}\right] + (1-\omega_1)Q\left[\frac{\ln(h/h_{m2})}{\sigma_2}\right]$	ω_1=0.23381 h_{m_1}= 26.594 σ_1= 1.1599 h_{m_2}= 1196.9 σ_2= 0.52036		

Table 4.6: Fitting Parameters of Difference SWRC Models for GPS

Model	Equation	Parameters	R^2	AIC
GPS 1				
Van Genuchten	$S_e = \left[\frac{1}{1+(\alpha h)^n}\right]^m (m = 1 - 1/n)$	θ_s=0.59867 θ_r=2.6553e-05 α = 0.004833 n = 1.3266	0.91231	-70.455
Fredlund and Xing	$S_e = \left[\frac{1}{ln\left[e + (h/a)^n\right]}\right]^m$	θ_s= 0.61057 θ_r= 8.8741e-08 a= 2102.1 m= 2.6498 n=0.69976	0.94392	-74.265
Seki	$S_e = \omega_1 Q\left[\frac{\ln(h/h_{m1})}{\sigma_1}\right] + (1-\omega_1)Q\left[\frac{\ln(h/h_{m2})}{\sigma_2}\right]$	θ_s=0.61742 θ_r= 5.4004e-06 ω_1=0.20791 h_{m_1}= 41.449 σ_1= 1.0729 h_{m_2}= 2847.3 σ_2= 0.79985	0.99942	-129.62
GPS 2				
Van Genuchten	$S_e = \left[\frac{1}{1+(\alpha h)^n}\right]^m (m = 1 - 1/n)$	θ_s=0.51900 θ_r= 5.3120e -05 α = 0.0051261 n = 1.2128	0.85796	-68.486
Fredlund and Xing	$S_e = \left[\frac{1}{ln\left[e + (h/a)^n\right]}\right]^m$	θ_s= 0.56468 θ_r= 1.4060e-05 a= 1900.6 m= 2.6818 n=0.55083	0.91031	-81.309
Seki	$S_e = \omega_1 Q\left[\frac{\ln(h/h_{m1})}{\sigma_1}\right] + (1-\omega_1)Q\left[\frac{\ln(h/h_{m2})}{\sigma_2}\right]$	θ_s=0.55899 θ_r= 0.0040401 ω_1=0.99989 h_{m_1}= 2649.7 σ_1= 3.1068 h_{m_2}= 5.19783+06 σ_2= 0.21145	0.95458	-68.463
GPS 3				
Van Genuchten	$S_e = \left[\frac{1}{1+(\alpha h)^n}\right]^m (m = 1 - 1/n)$	θ_s=0.51361 θ_r=2.3320e-07		

		α = 0.0046693 n = 1.1396	0.87927	-74.565
Fredlund and Xing	$S_e = \left[\frac{1}{ln\left[e + \left(h/a\right)^n\right]}\right]^m$	θ_s= 0.53769 θ_r= 6.3827e-06 a= 811.36 m= 1.9089 n=0.46674	0.93348	-80.304
Seki	$S_e = \omega_1 Q\left[\frac{\ln\left(h/h_{m1}\right)}{\sigma_1}\right] + (1-\omega_1)Q\left[\frac{\ln\left(h/h_{m2}\right)}{\sigma_2}\right]$	θ_s=0.53473 θ_r= 0.012003 ω_1=0.47621 h_{m_1}= 134.36 σ_1= 2.9783 h_{m_2}= 3819.8 σ_2= 0.62959	0.99937	-136.95

APPENDIX C

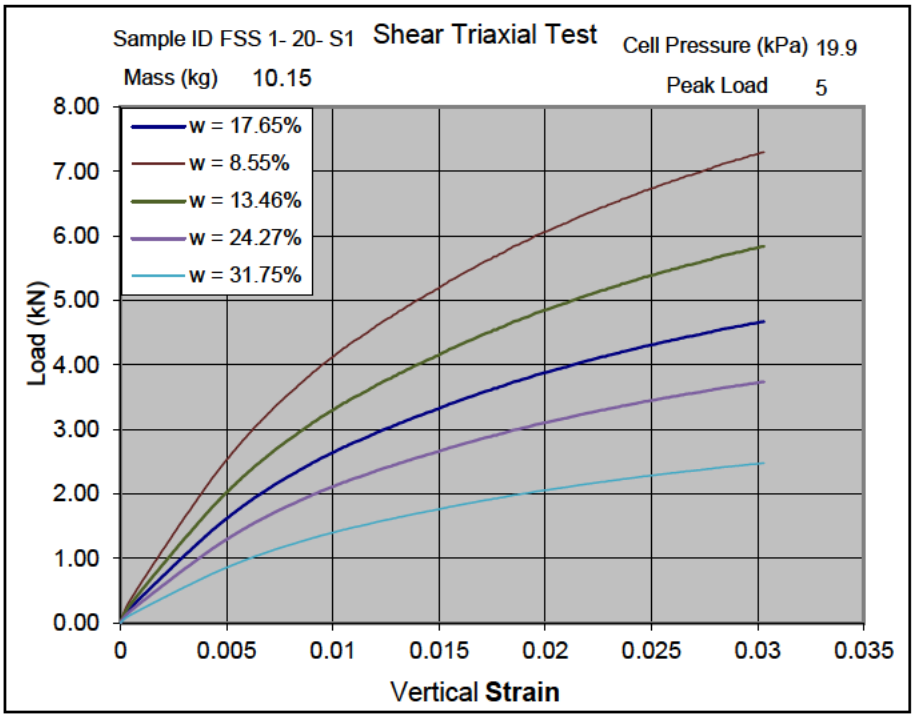

Figure 5.1: Stress − displacement curve of FSS 1 at $\sigma_c = 20kPa$

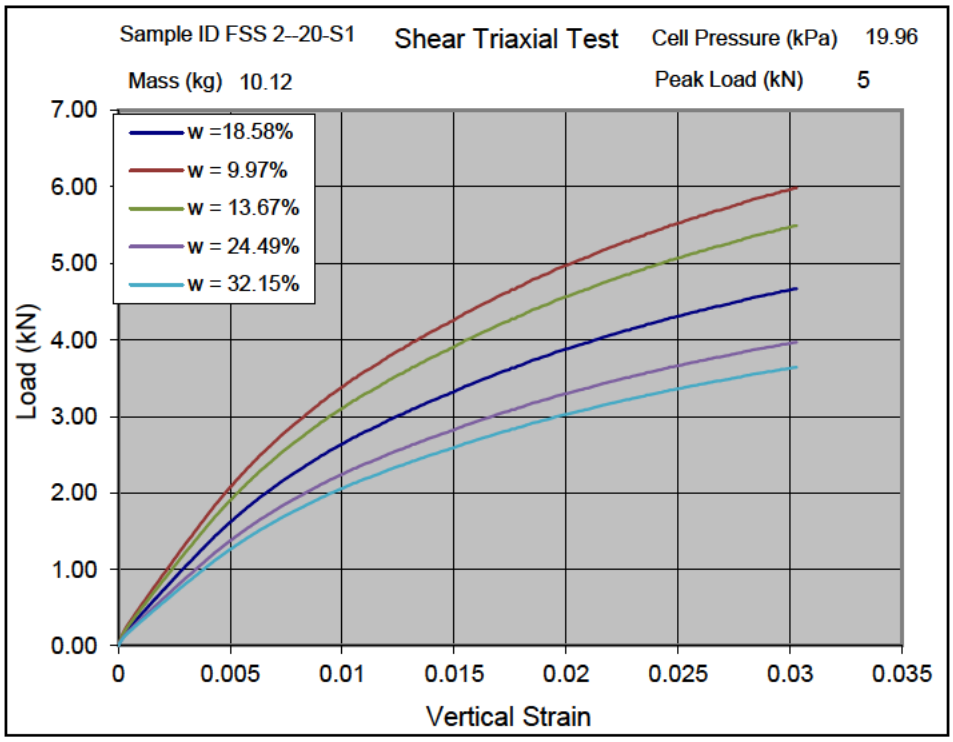

Figure 5.2: Stress − displacement curve of FSS 2 at $\sigma_c = 20kPa$

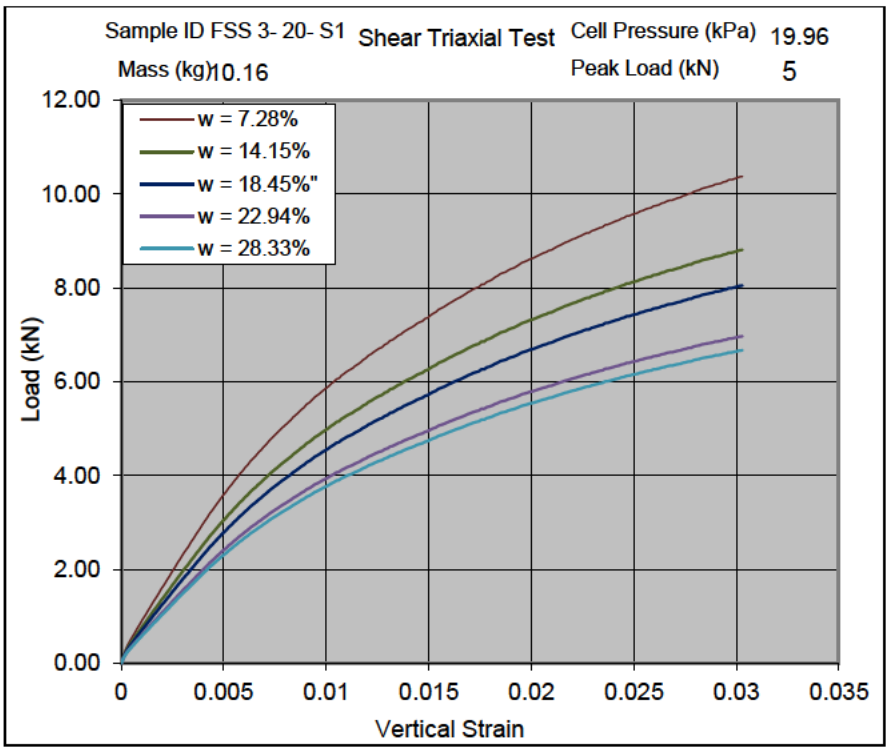

Figure 5.3: Stress – displacement curve of FSS 3 at $\sigma_c = 20$kPa

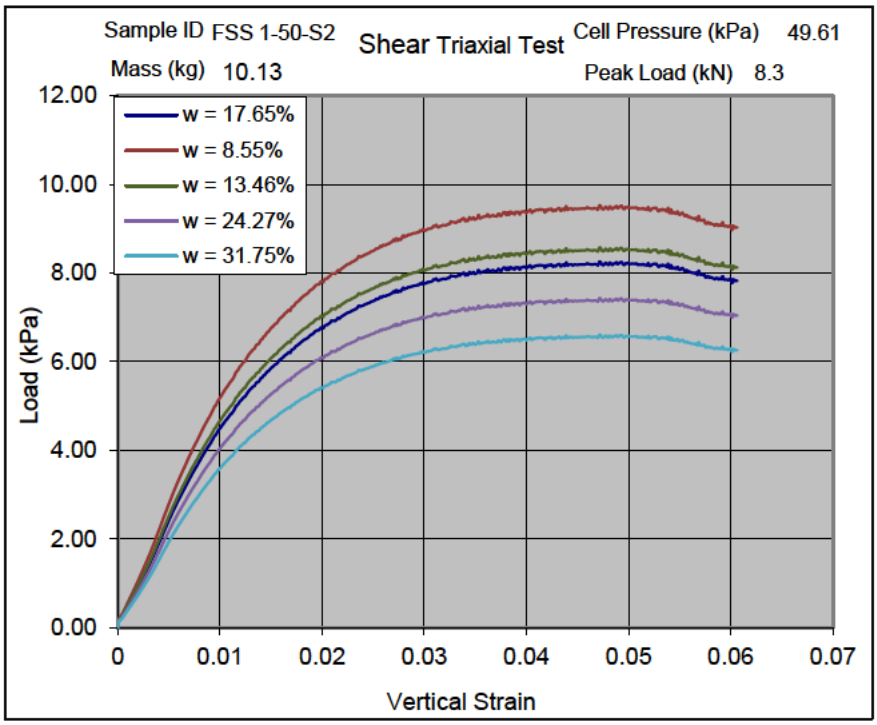

Figure 5.4: Stress – displacement curve of FSS 1 at $\sigma_c = 50$kPa

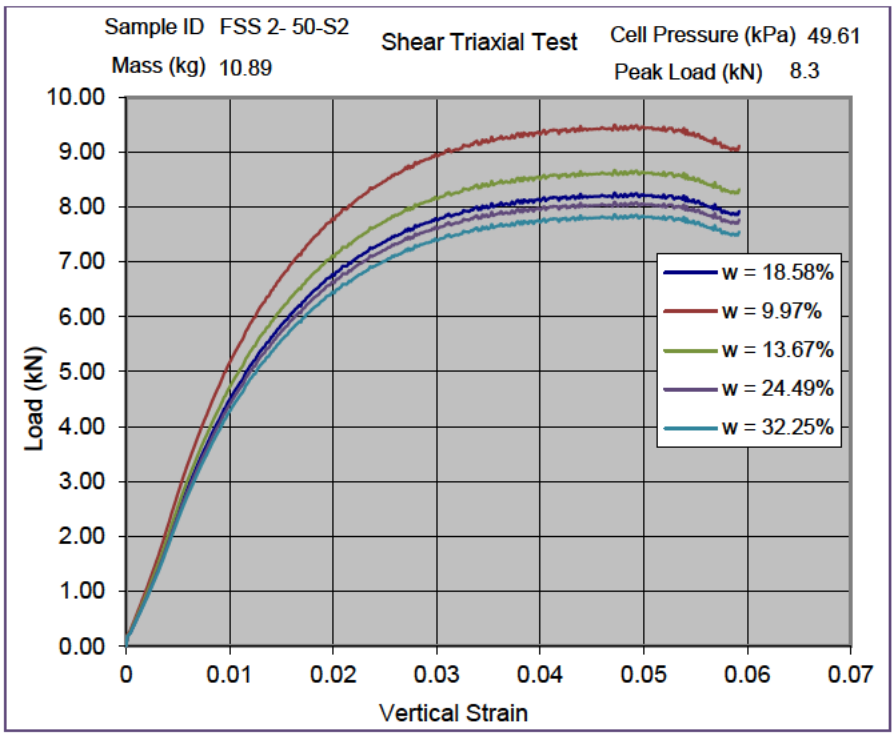

Figure 5.5: Stress – displacement curve of FSS 2 at $\sigma_c = 50$kPa

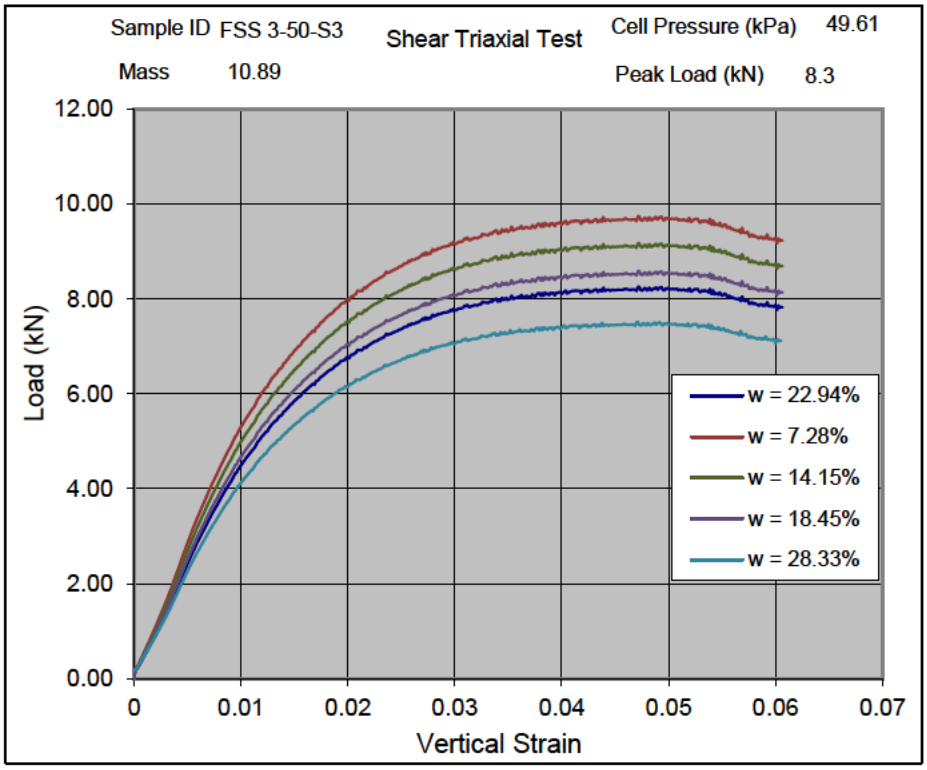

Figure 5.6: Stress – displacement curve of FSS 3 at $\sigma_c = 50$kPa

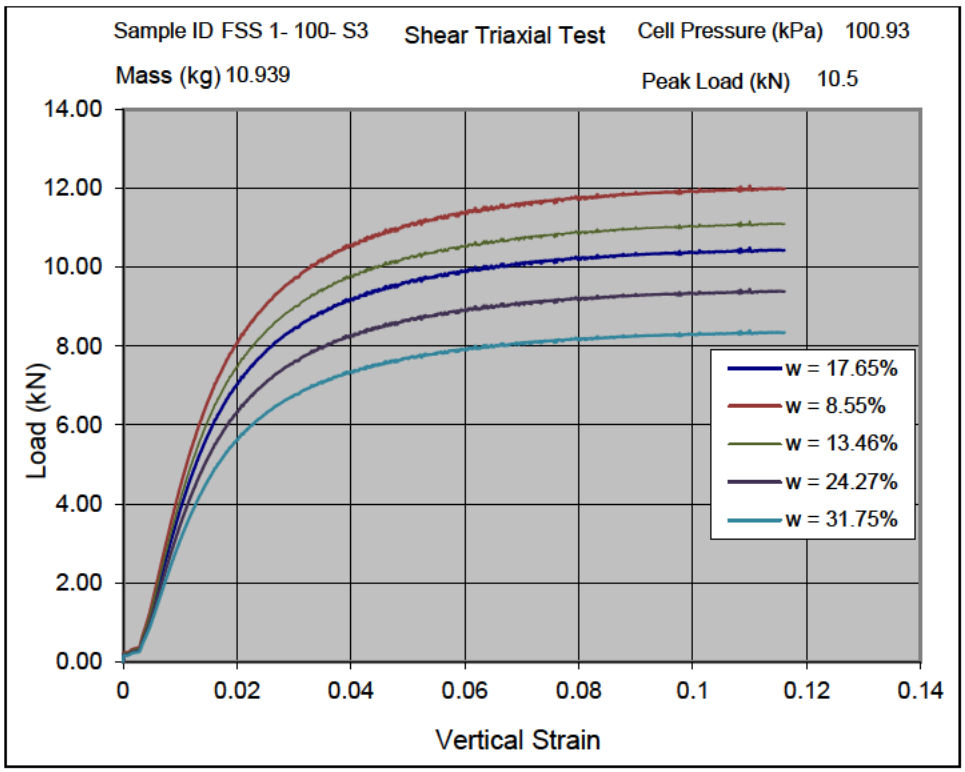

Figure 5.7: Stress – displacement curve of FSS 1 at $\sigma_c = 100$kPa

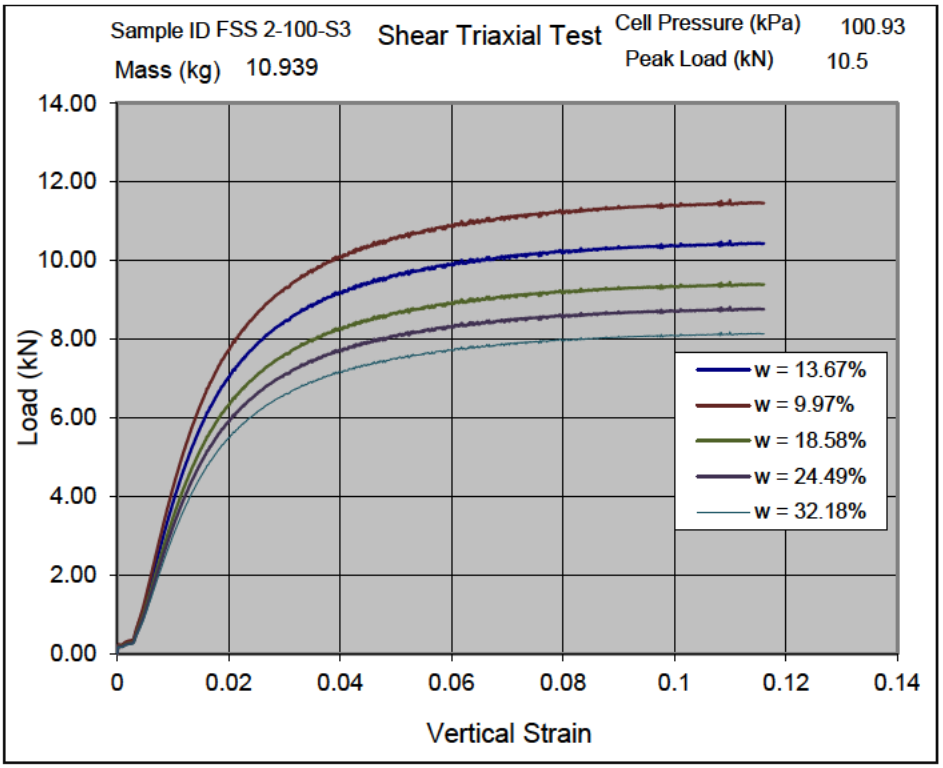

Figure 5.8: Stress – displacement curve of FSS 2 at $\sigma_c = 100$kPa

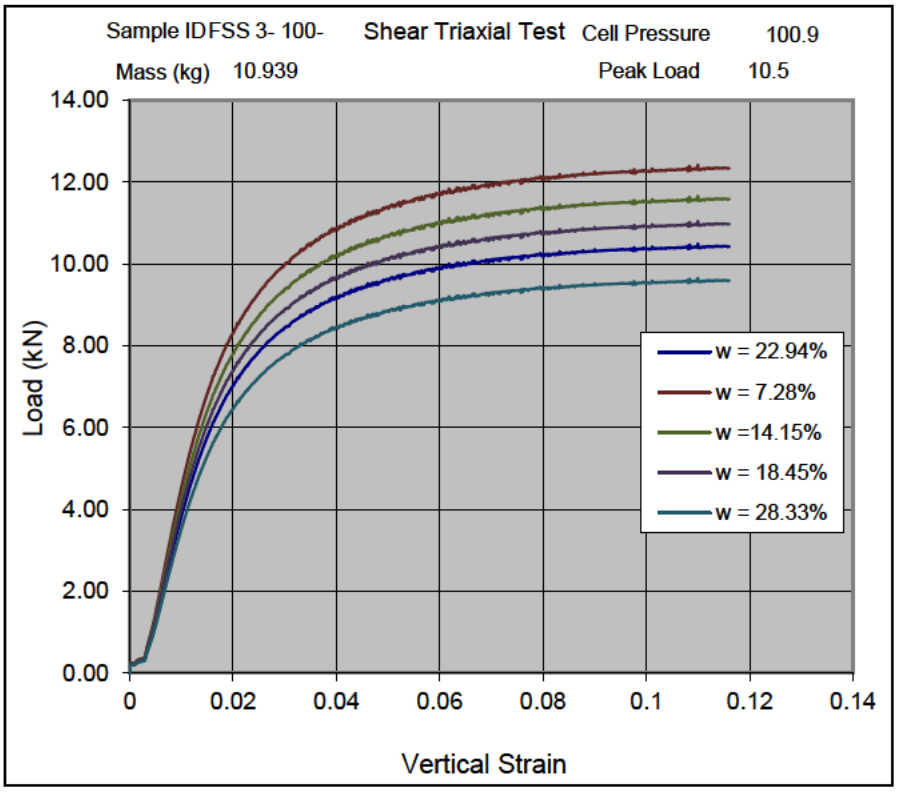

Figure 5.9: Stress − displacement curve of FSS 3 at $\sigma_c = 100$kPa

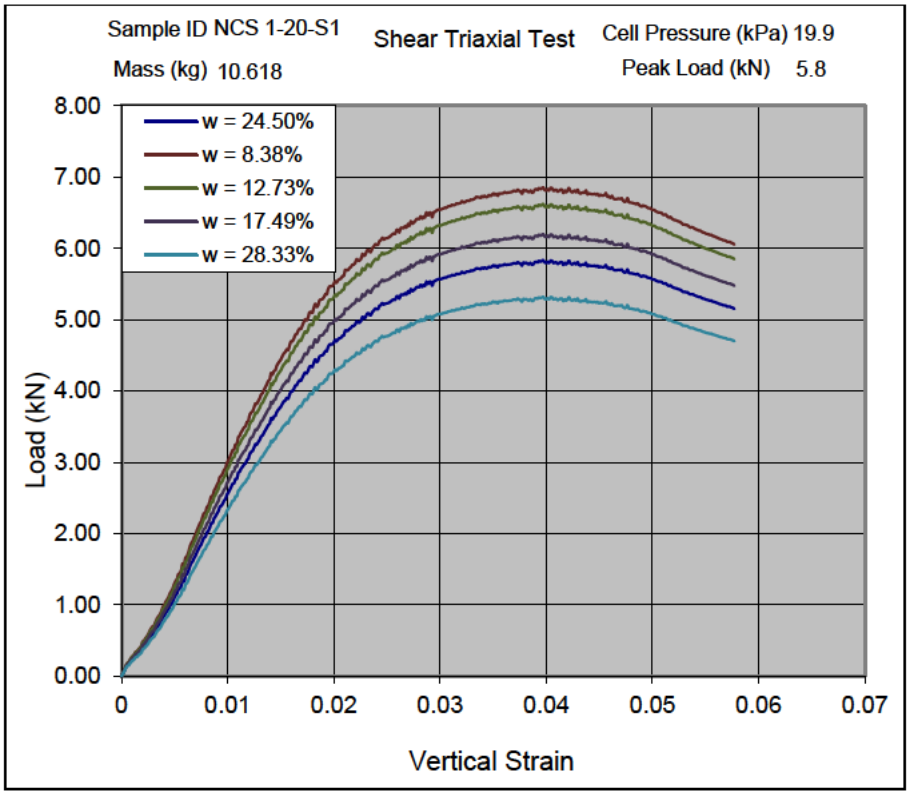

Figure 5.10: Stress − displacement curve of NCS 1 at $\sigma_c = 20$kPa

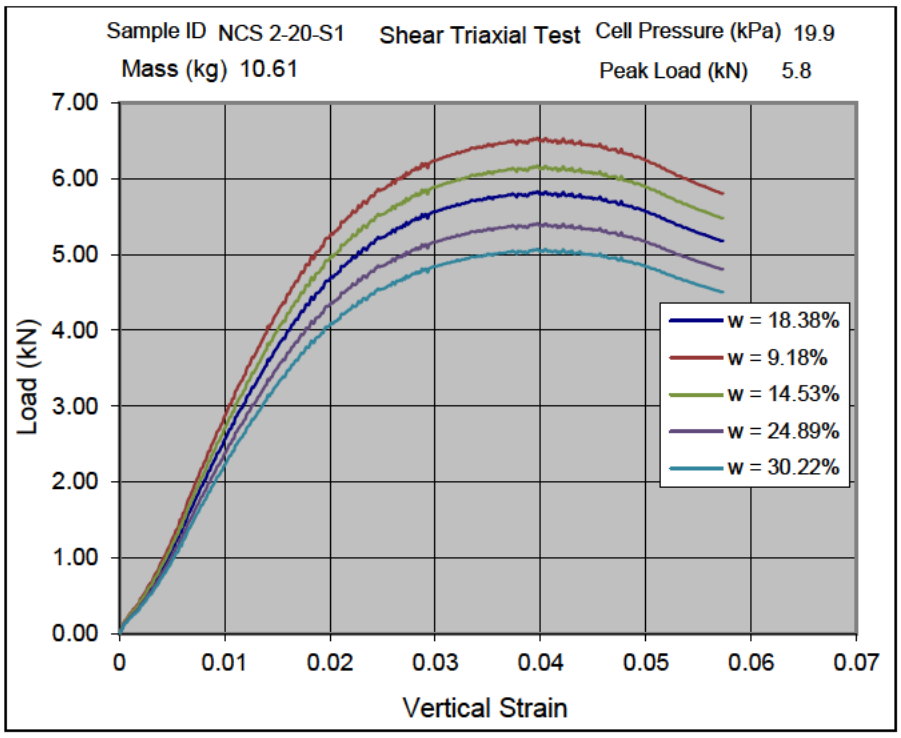

Figure 5.11: Stress – displacement curve of NCS 2 at $\sigma_c = 20$kPa

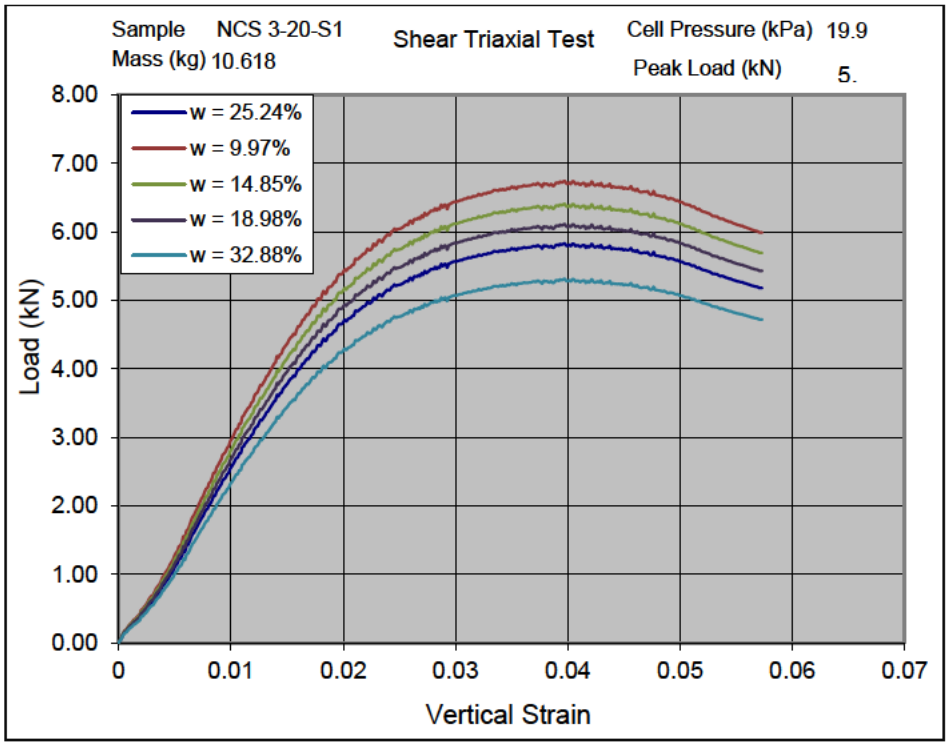

Figure 5.12: Stress – displacement curve of NCS 3 at $\sigma_c = 20$kPa

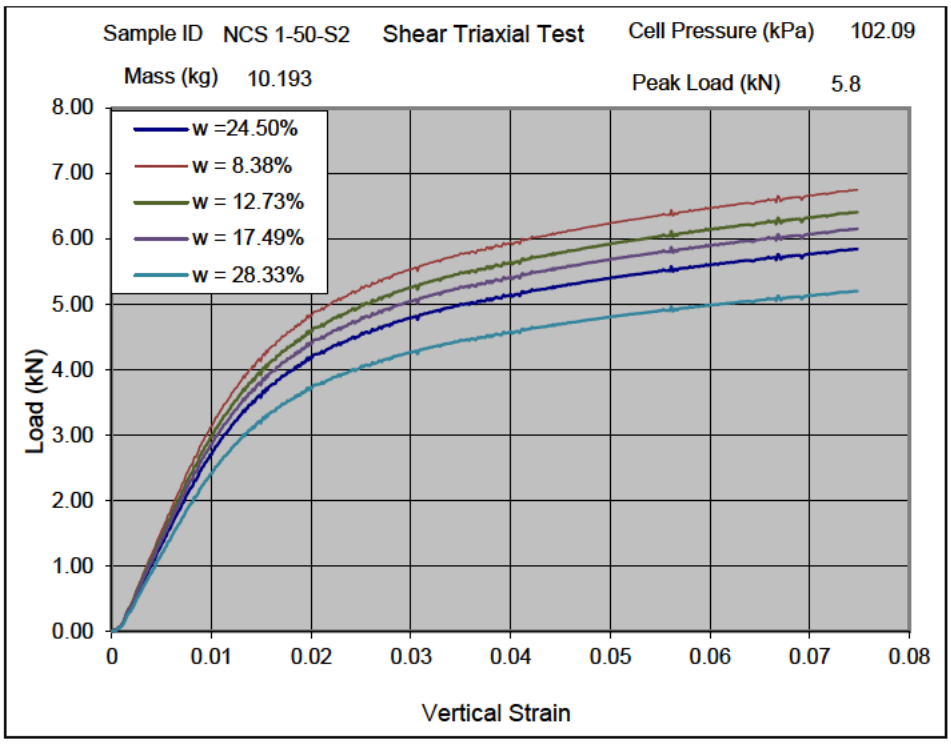

Figure 5.13: Stress − displacement curve of NCS 1 at $\sigma_c = 50$kPa

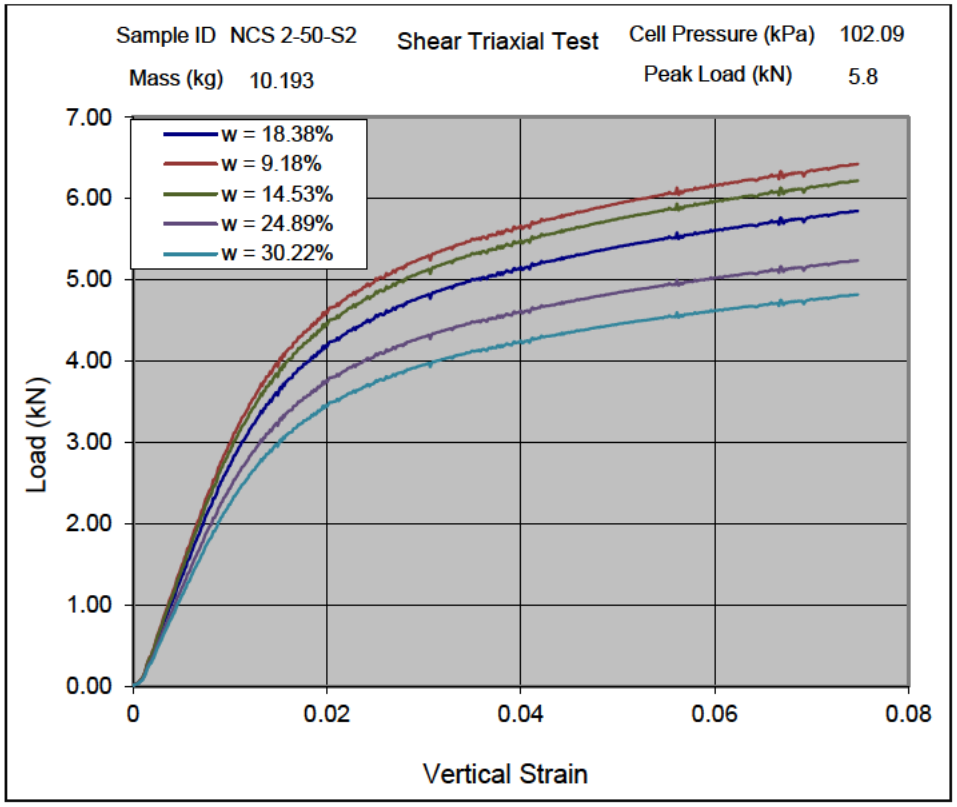

Figure 5.14: Stress − displacement curve of NCS 2 at $\sigma_c = 50$kPa

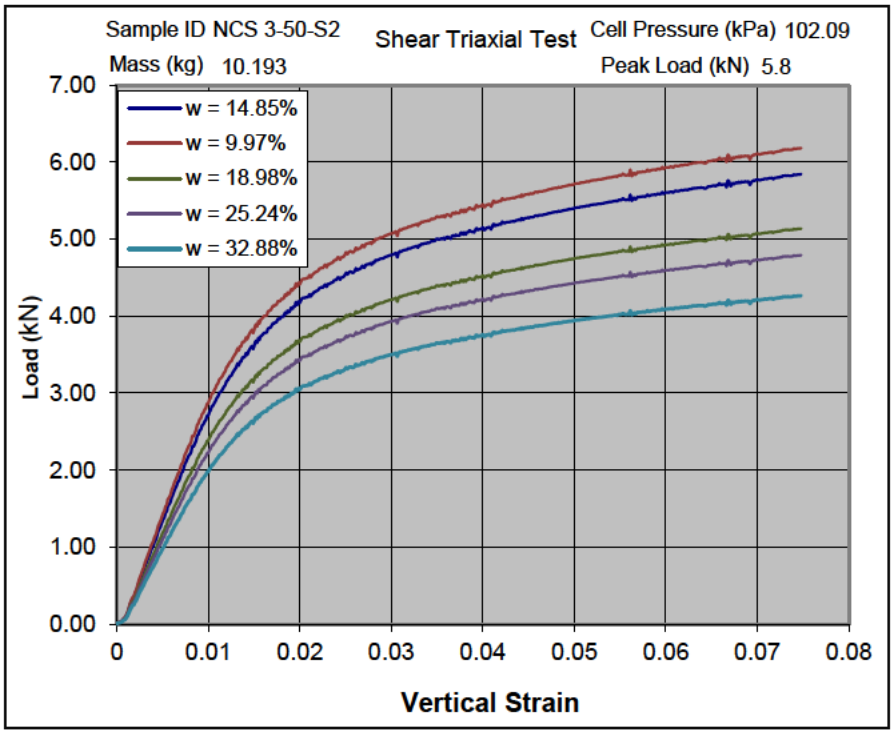

Figure 5.15: Stress – displacement curve of NCS 3 at $\sigma_c = 50$kPa

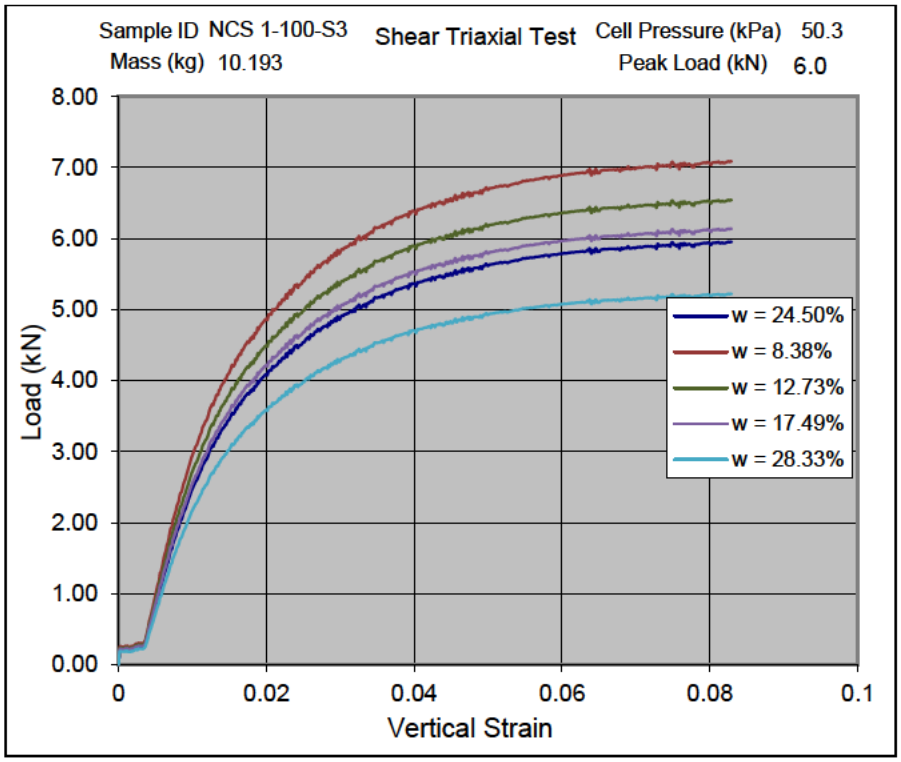

Figure 5.16: Stress – displacement curve of NCS 1 at $\sigma_c = 100$kPa

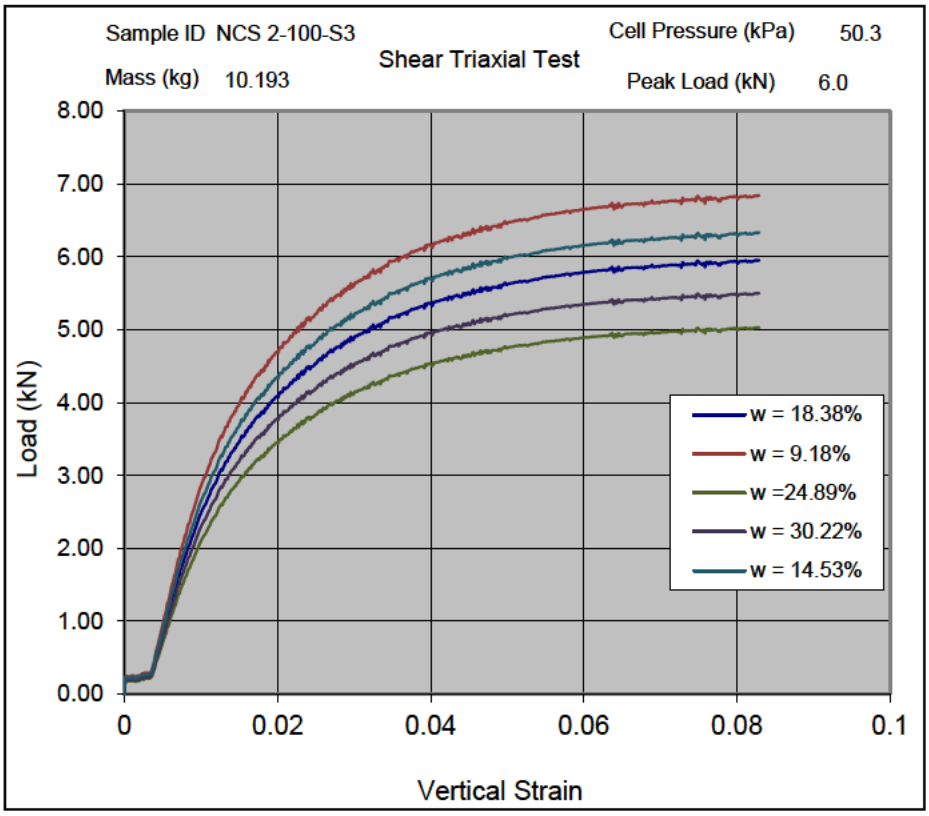

Figure 5.17: Stress – displacement curve of NCS 2 at $\sigma_c = 100$kPa

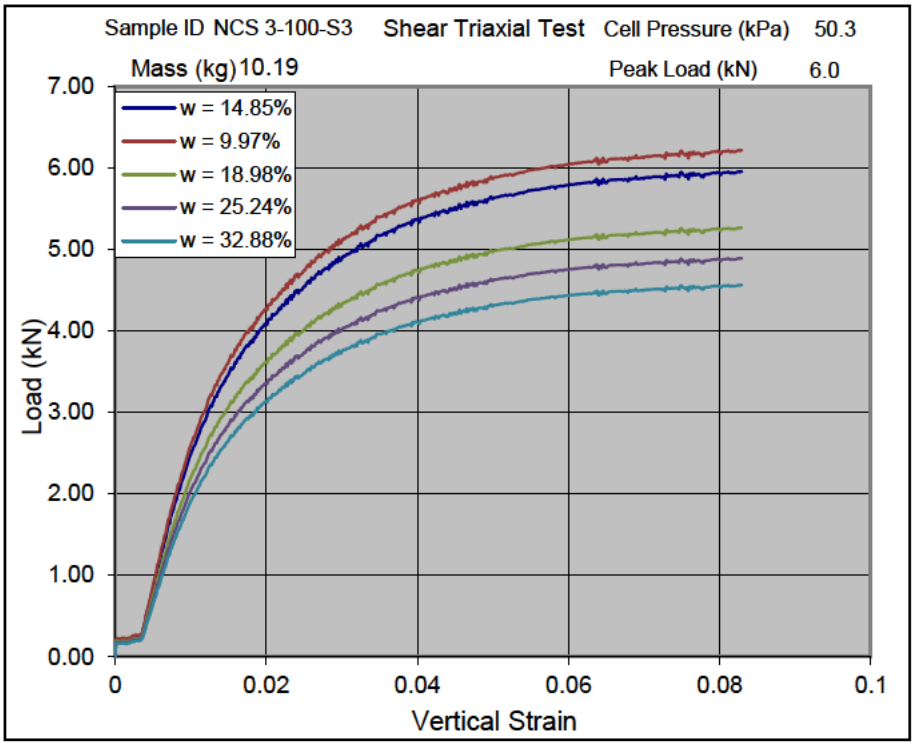

Figure 5.18: Stress – displacement curve of NCS 3 at $\sigma_c = 100$kPa

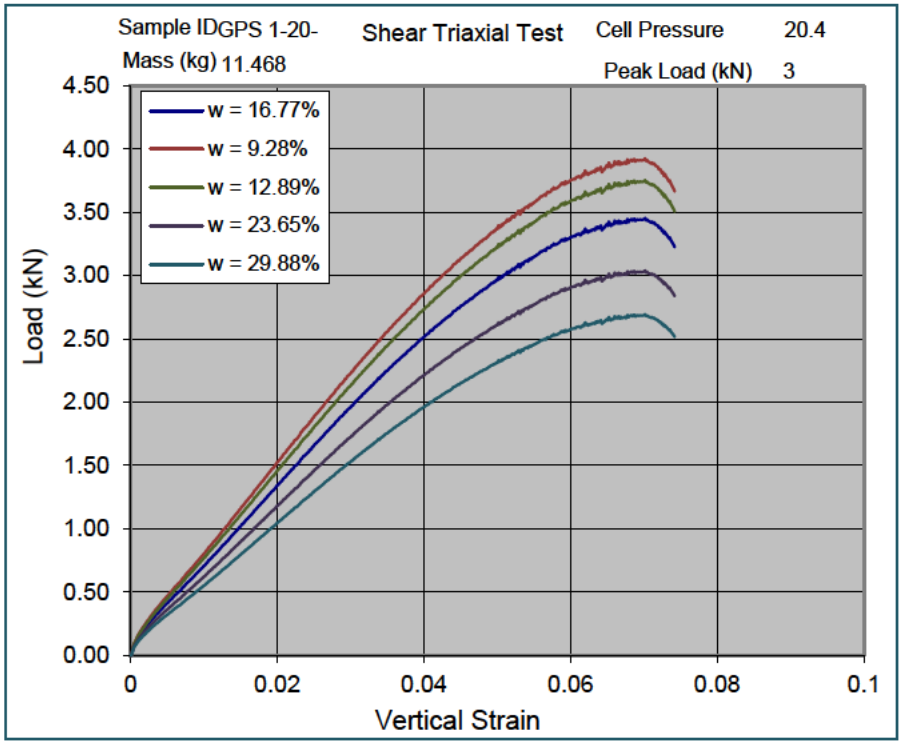

Figure 5.19: Stress – displacement curve of GPS 1 at $\sigma_c = 20$kPa

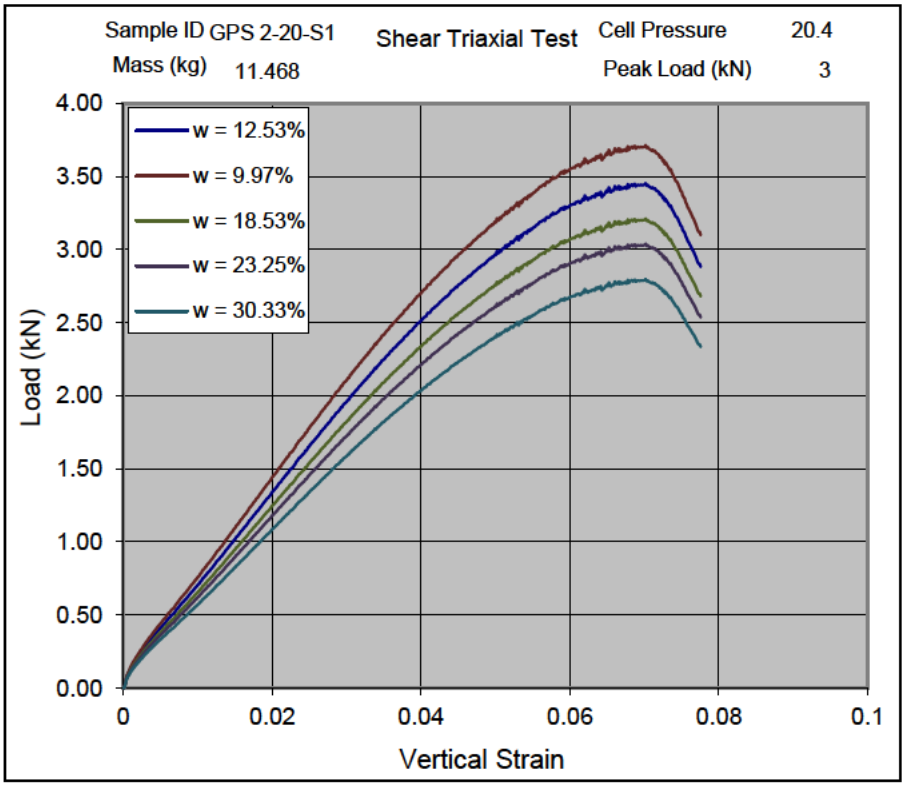

Figure 5.20: Stress – displacement curve of GPS 2 at $\sigma_c = 20$kPa

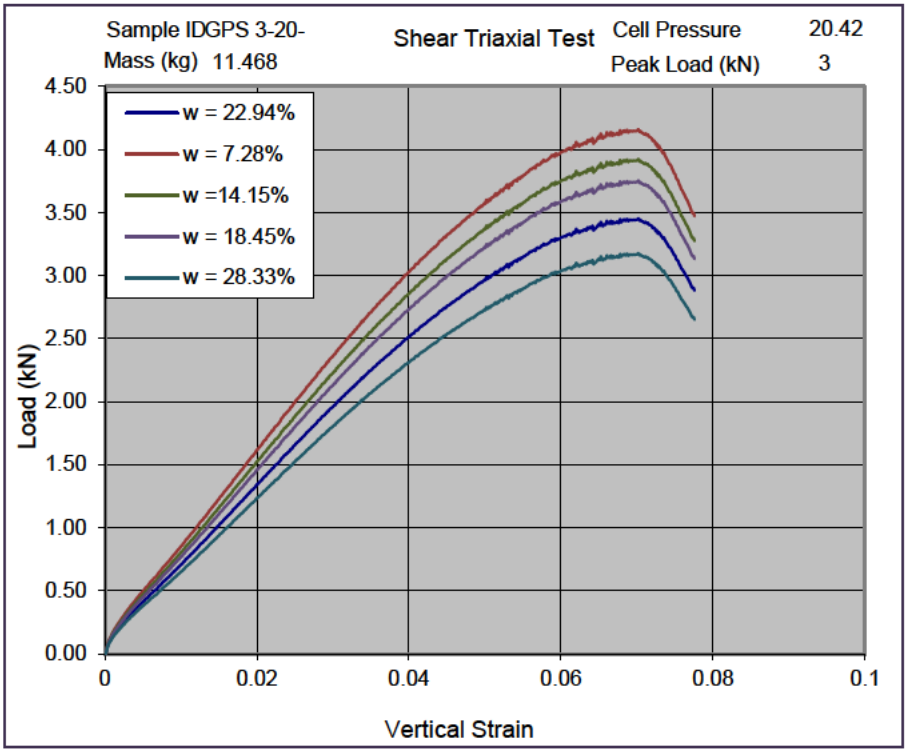

Figure 5.21: Stress − displacement curve of GPS 3 at $\sigma_c = 20$kPa

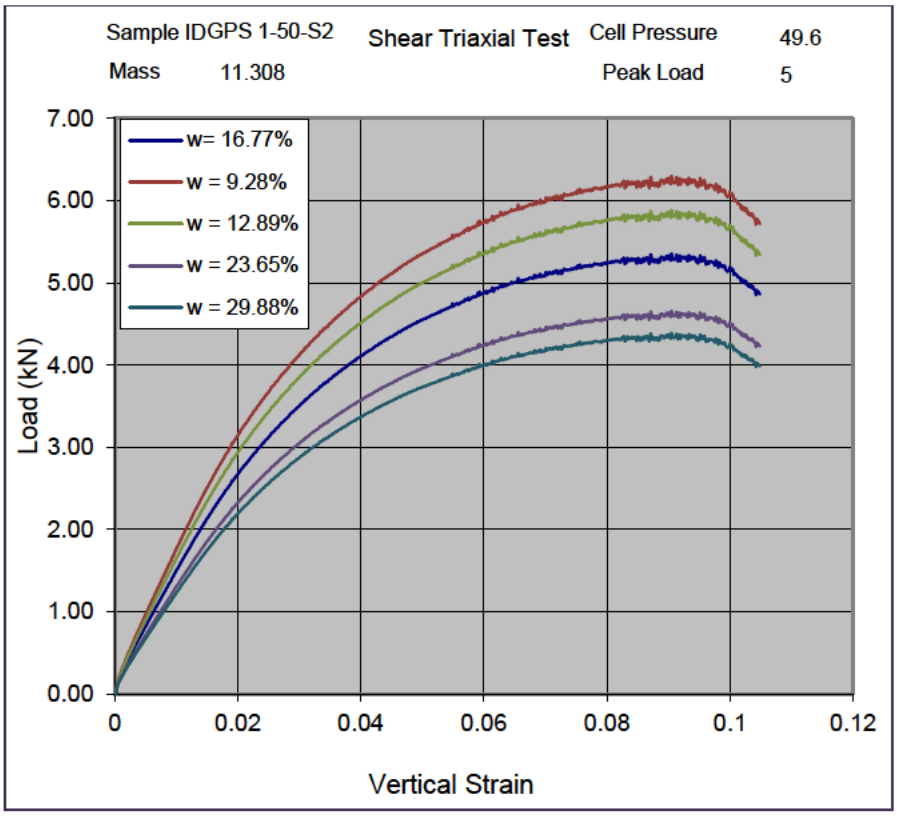

Figure 5.22: Stress − displacement curve of GPS 1 at $\sigma_c = 50$kP

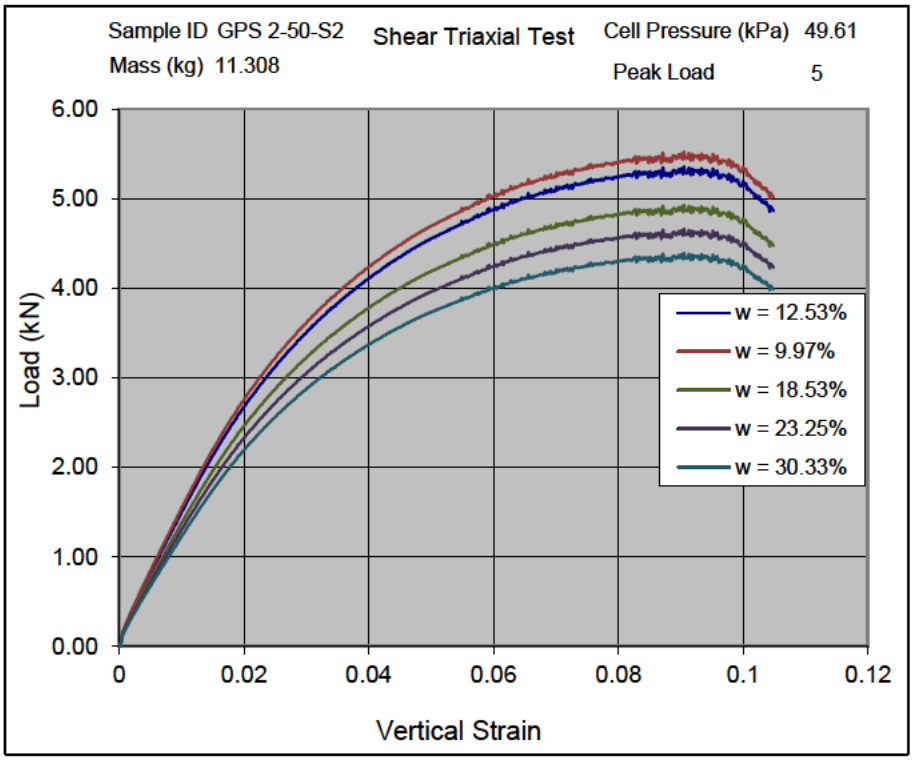

Figure 5.23: Stress − displacement curve of GPS 2 at $\sigma_c = 50$kPa

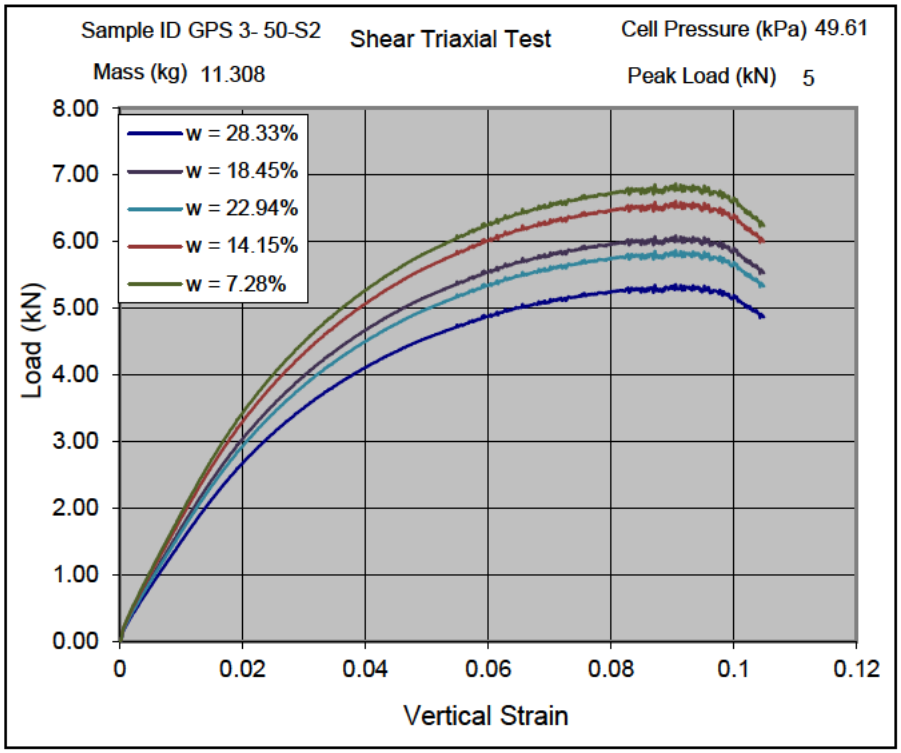

Figure 5.24: Stress − displacement curve of GPS 3 at $\sigma_c = 50$kPa

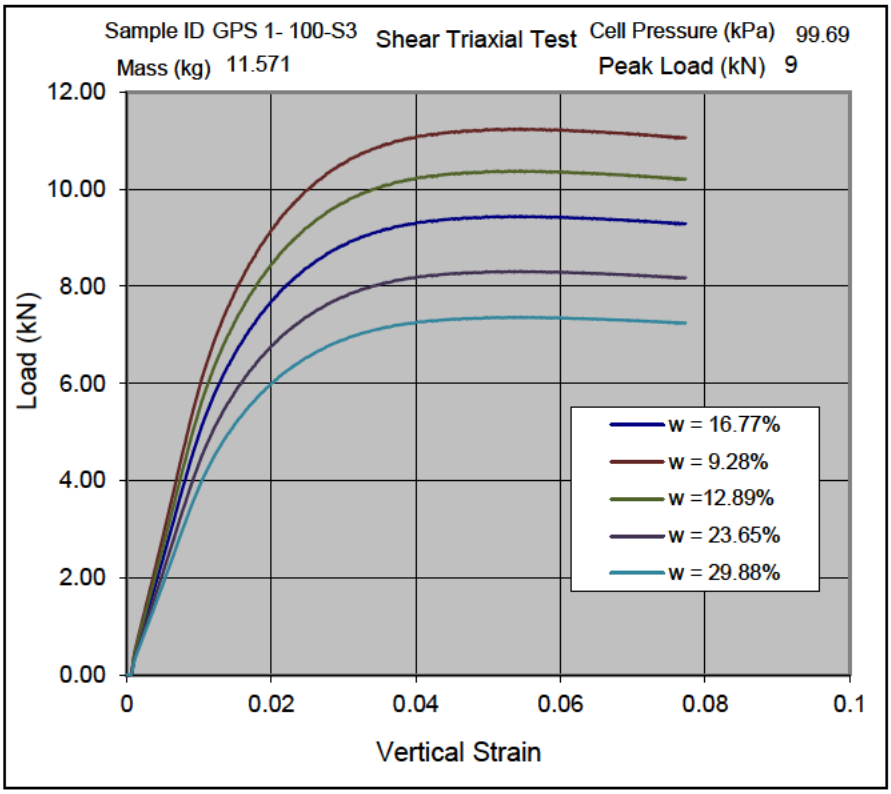

Figure 5.25: Stress − displacement curve of GPS 1 at $\sigma_c = 100$kPa

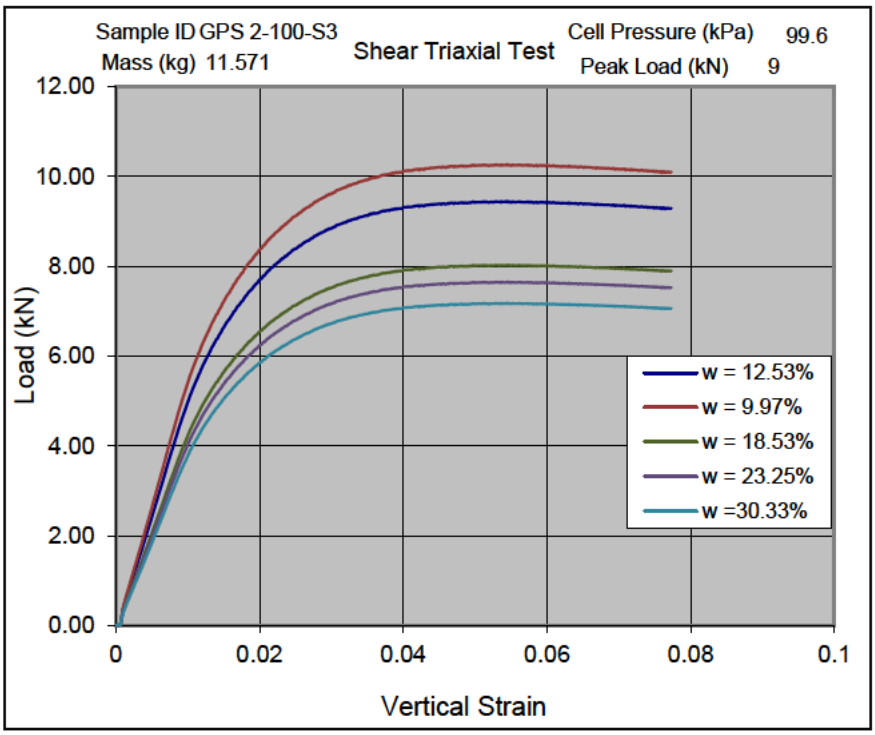

Figure 5.26: Stress − displacement curve of GPS 2 at $\sigma_c = 100$kPa

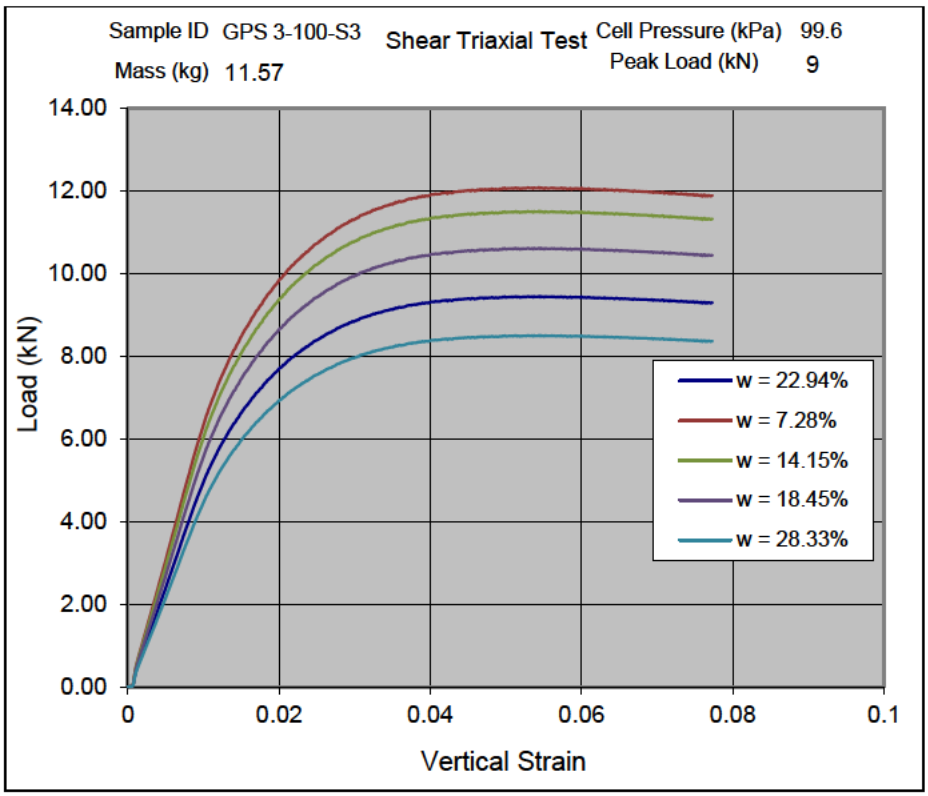

Figure 5.27: Stress − displacement curve of GPS 3 at σ_c = 100kPa

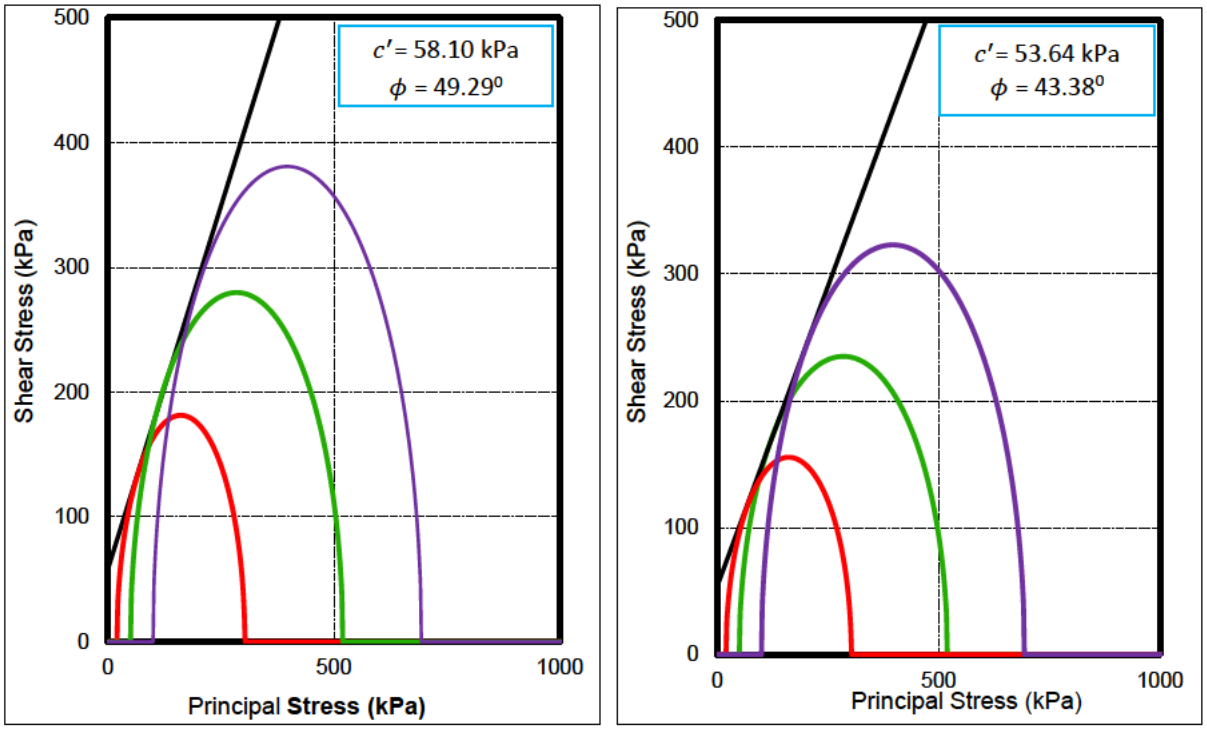

Figure 5.28: FSS 1 failure envelope at 8.55% and 13.46% moisture content

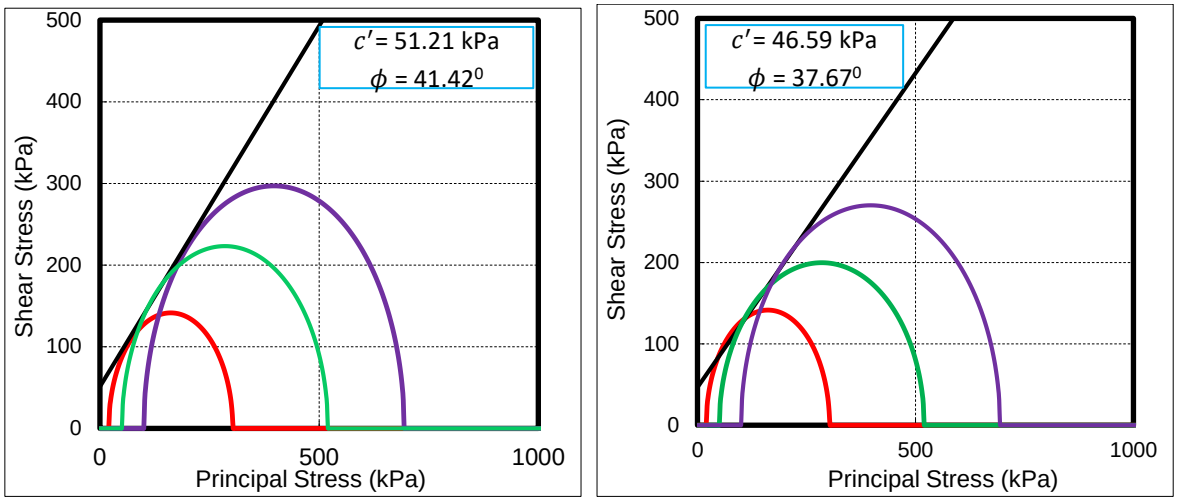

Figure 5.29: FSS 1 failure envelope at 17.65% and 24.27% moisture content

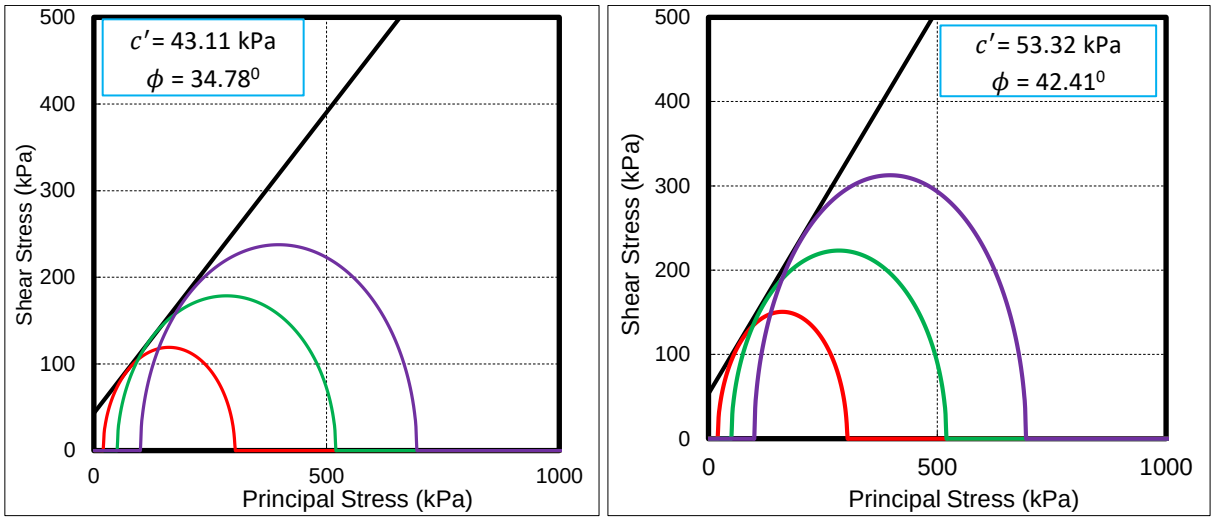

Figure 5.30: FSS 1, FSS 2 failure envelope at 31.75% and 9.97% moisture content

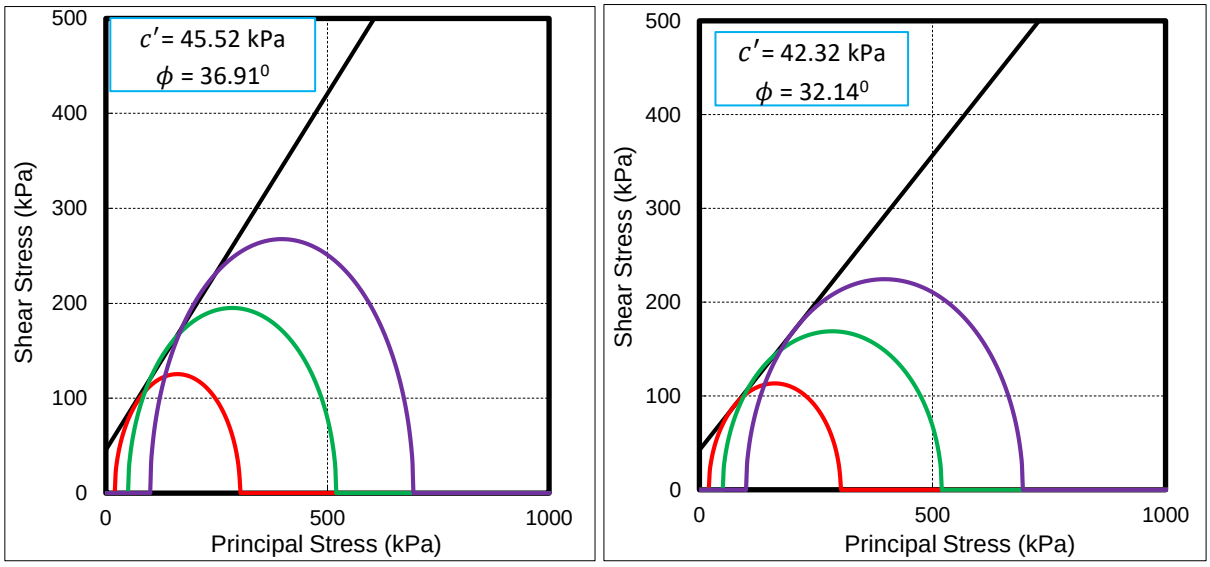

Figure 5.31: FSS 2 failure envelope at 13.67% and 18.58% moisture content

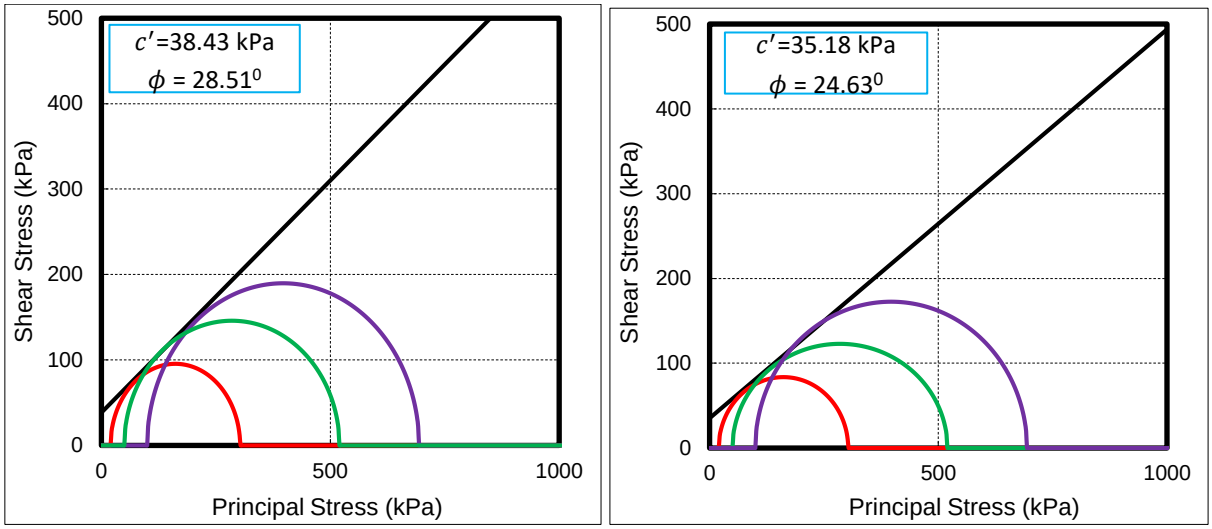

Figure 5.32: FSS 2 failure envelope criterion at 24.49% and 32.15% moisture content

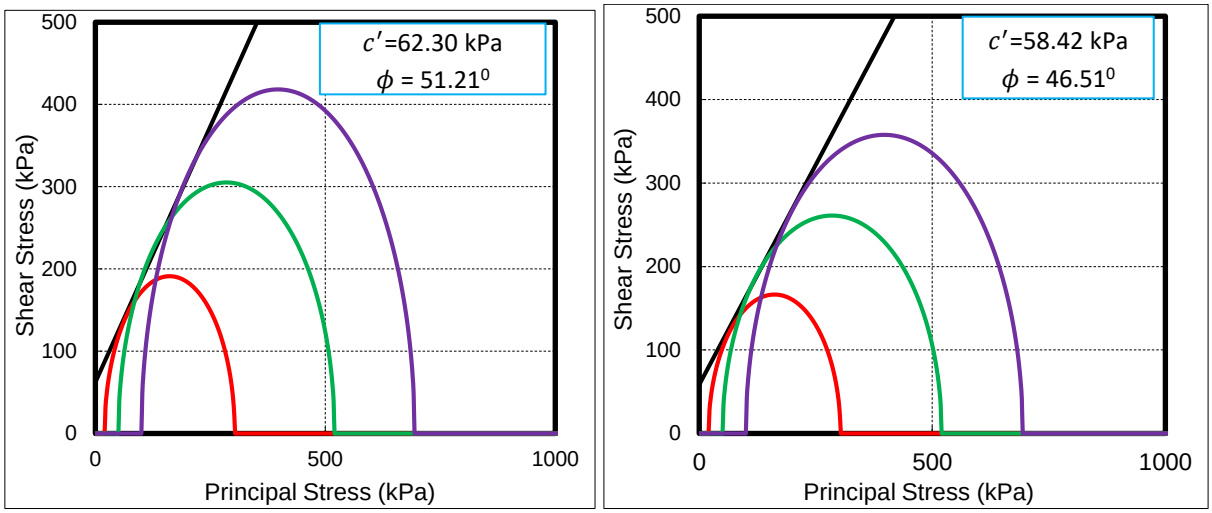

Figure 5.33: FSS 3 failure envelope at 7.28% and 14.15% moisture content

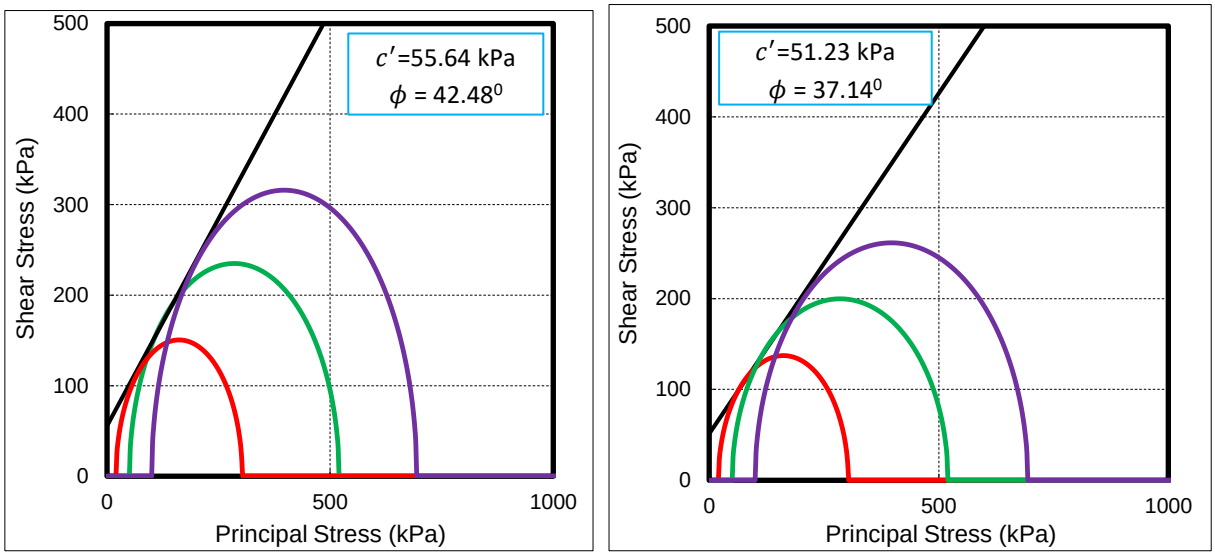

Figure 5.34: FSS 3 failure envelope at 18.54% and 22.94% moisture content

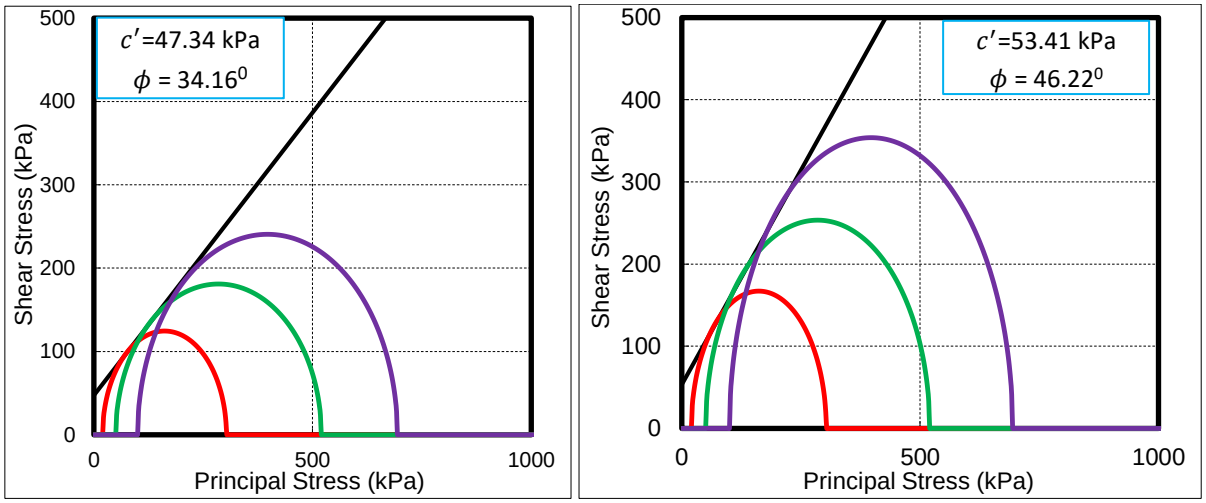

Figure 5.35: FSS 3, NCS 1 failure envelope at 28.33% and 8.38% moisture content

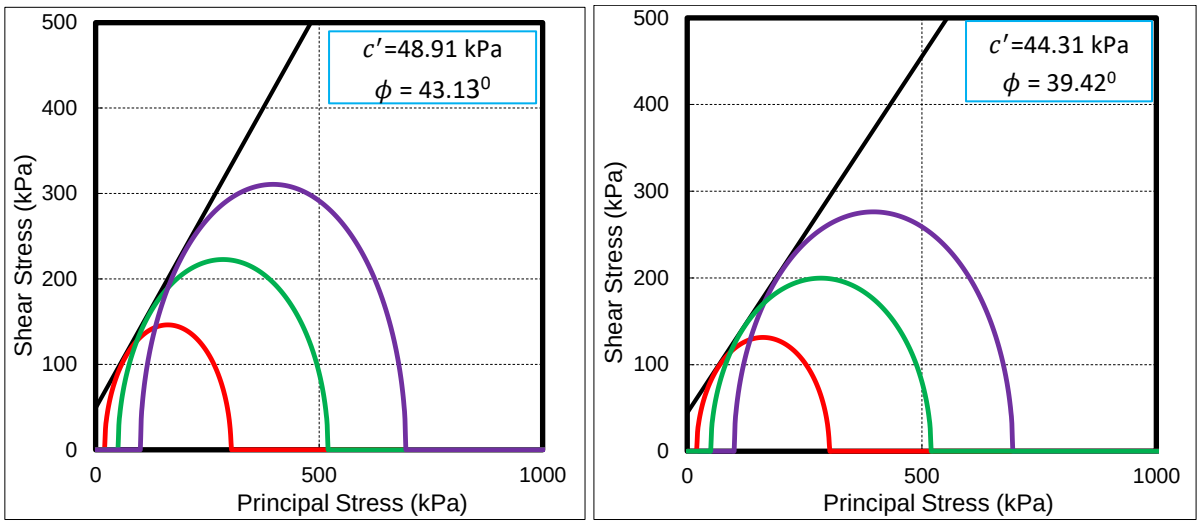

Figure 5.36: NCS 1 failure envelope at 12.73% and 17.49% moisture content

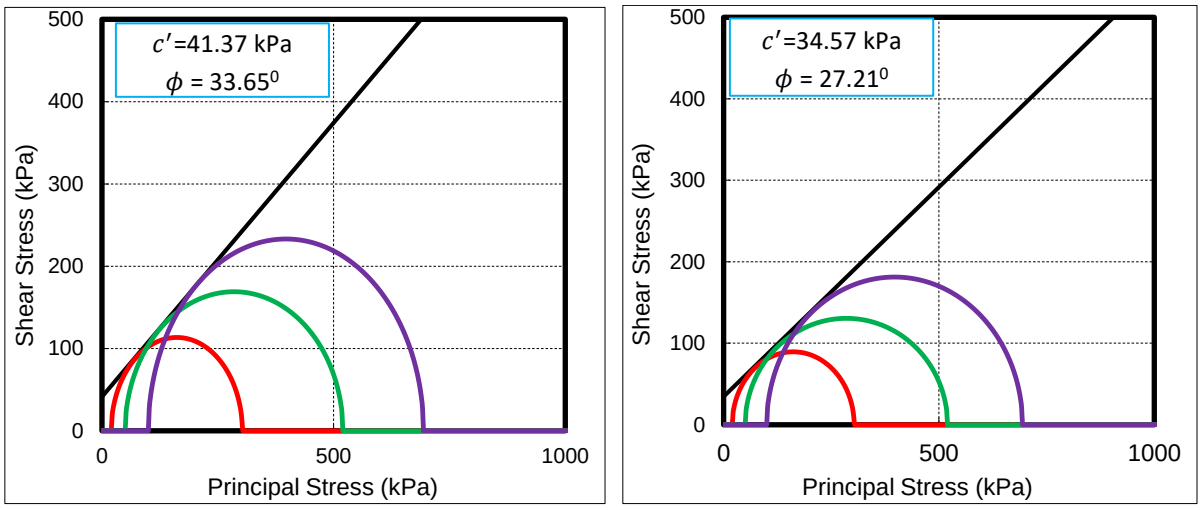

Figure 5.37: NCS 1 failure envelope at 24.40% and 28.33% moisture content

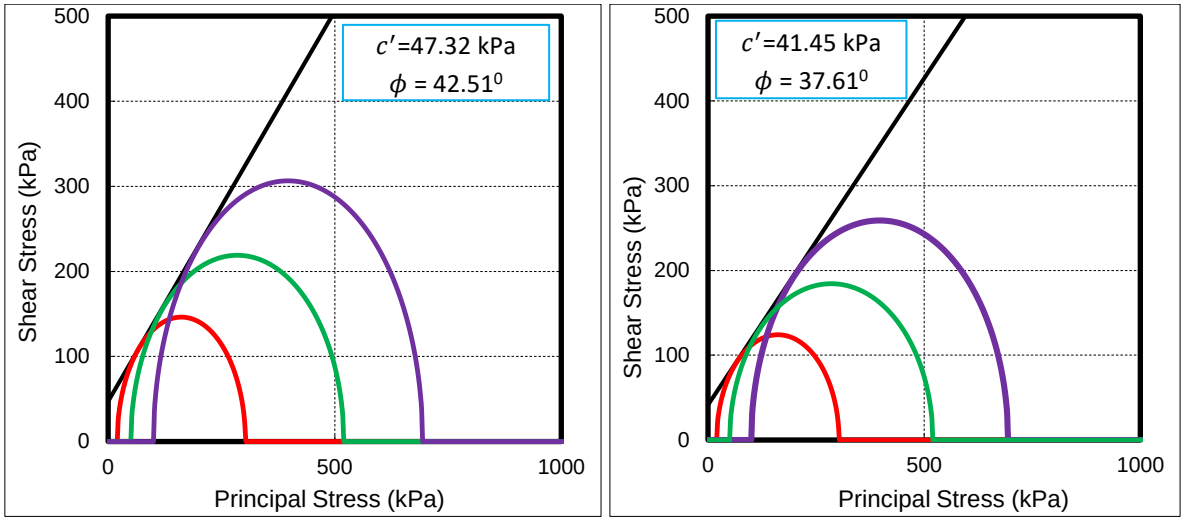

Figure 5.38: NCS 2 failure envelope at 9.18% and 14.53% moisture content

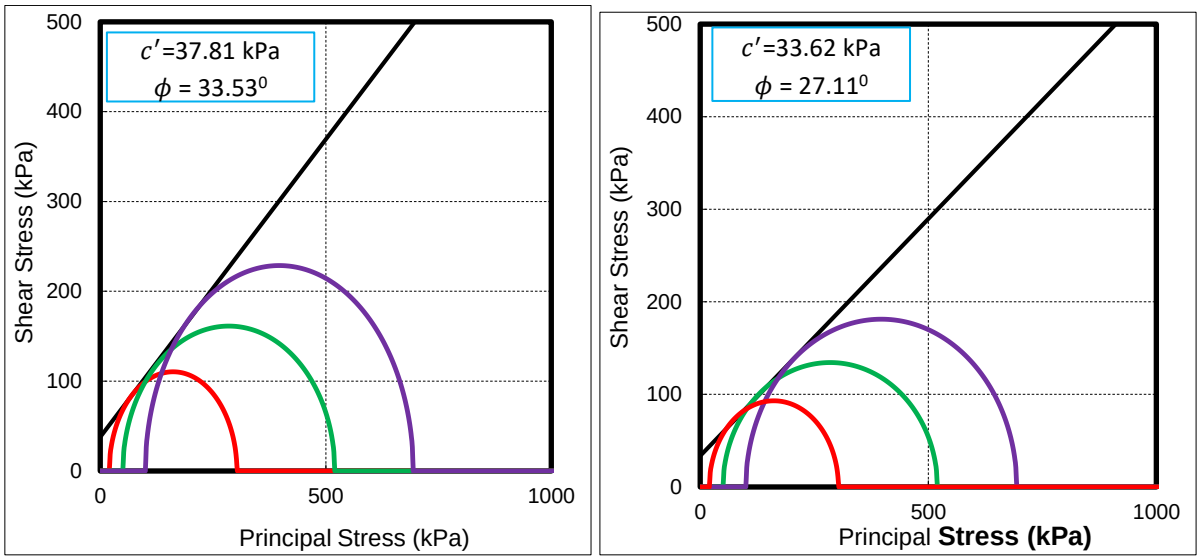

Figure 5.39: NCS 2 failure envelope at 18.38% and 24.89% moisture content

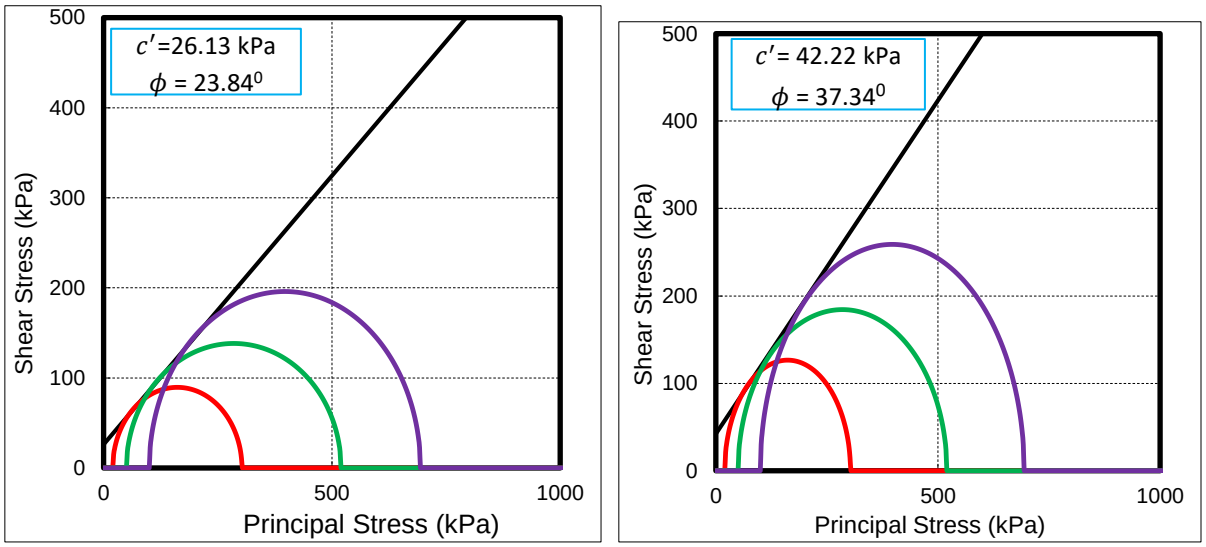

Figure 5.40: NCS 2, NCS 3 failure envelope at 30.22% and 9.97% moisture content

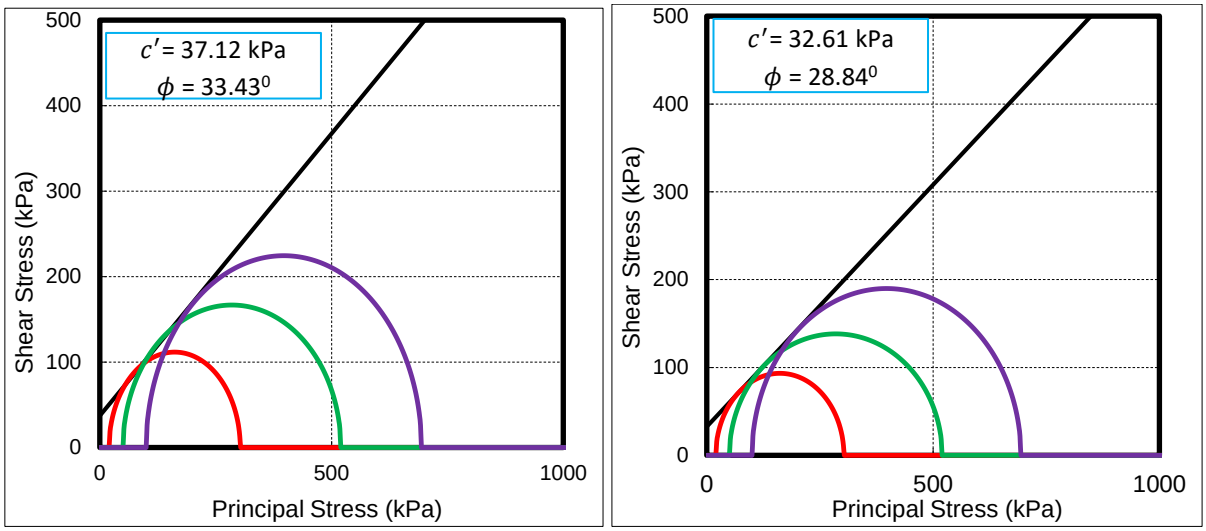

Figure 5.41: NCS 3 failure envelope at 14.53% and 18.9% moisture content

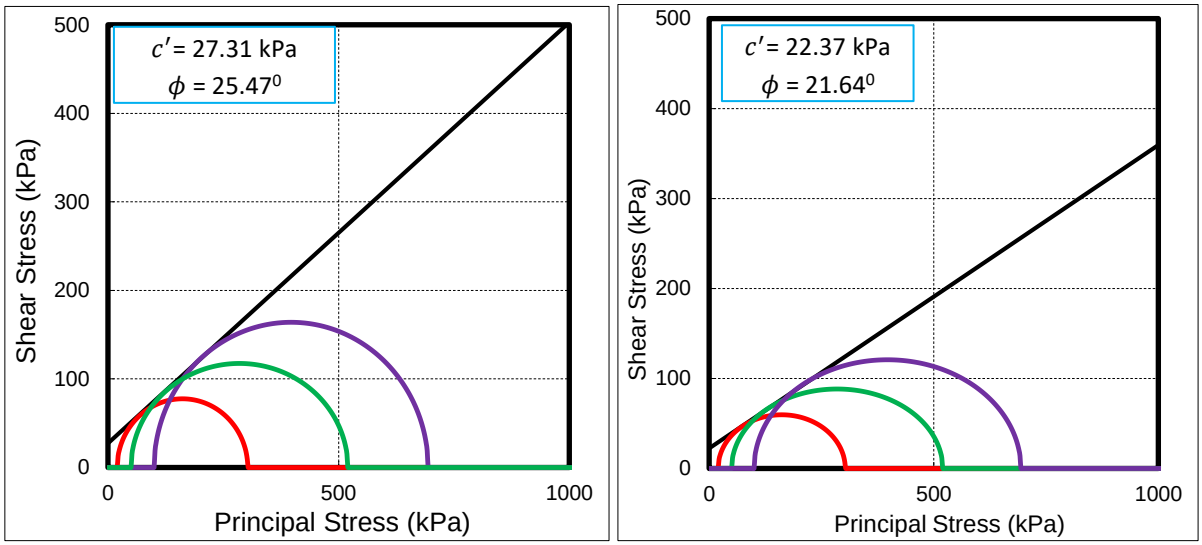

Figure 5.42: NCS 3 failure envelope at 25.24% and 32.88% moisture content

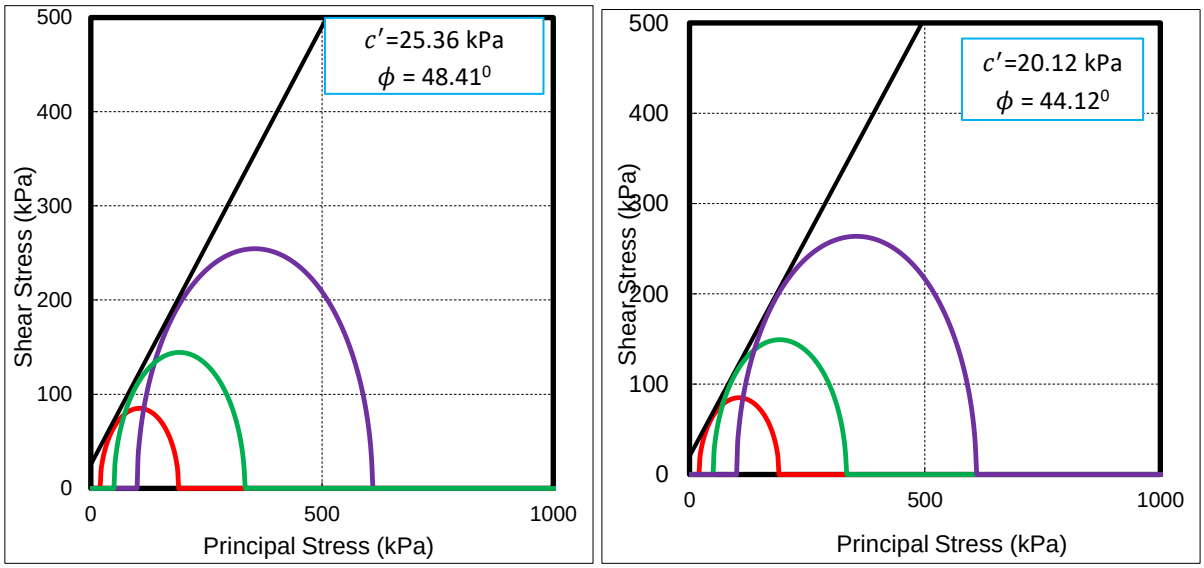

Figure 5.43: GPS 1 failure envelope at 9.28% and 12.89%moisture content

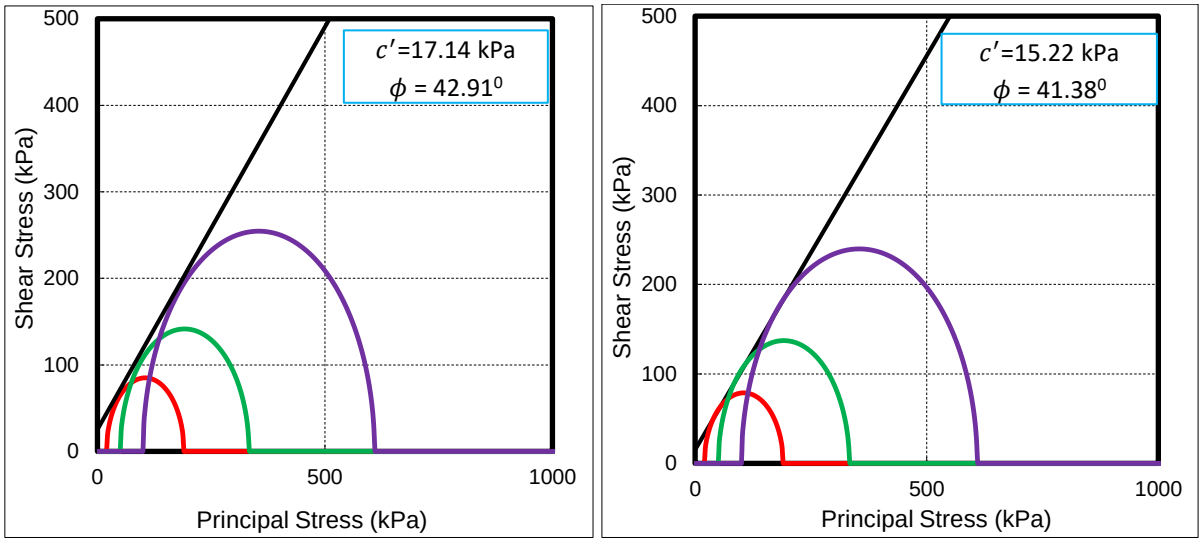

Figure 5.44: GPS 1 failure envelope at 16.77% and 23.65%moisture content

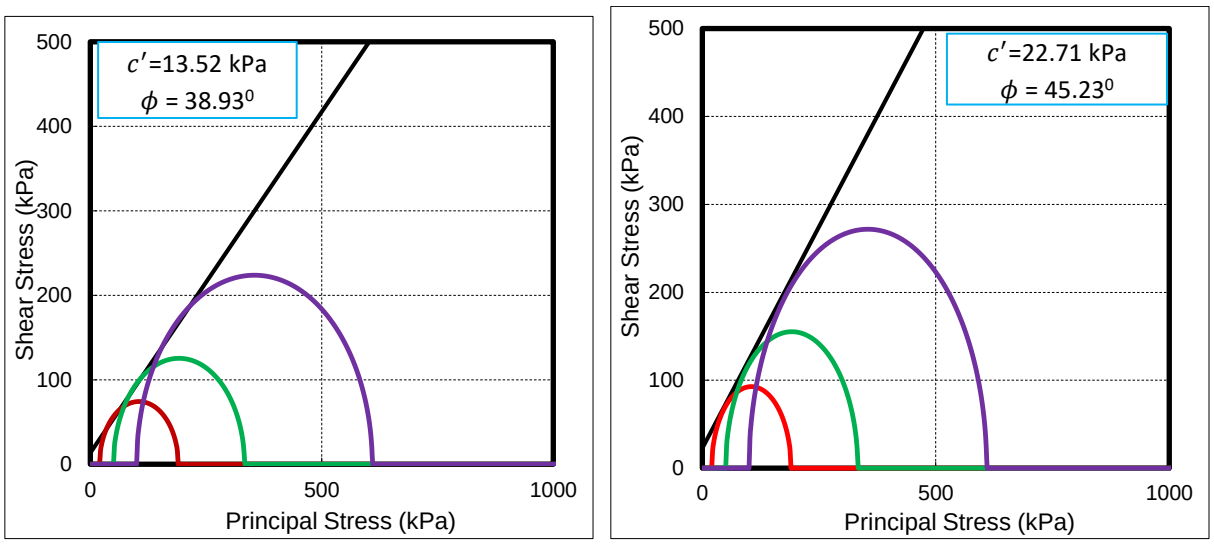

Figure 5.45: GPS 1, GPS 2 failure envelope at 29.88% and 9.97%% moisture content

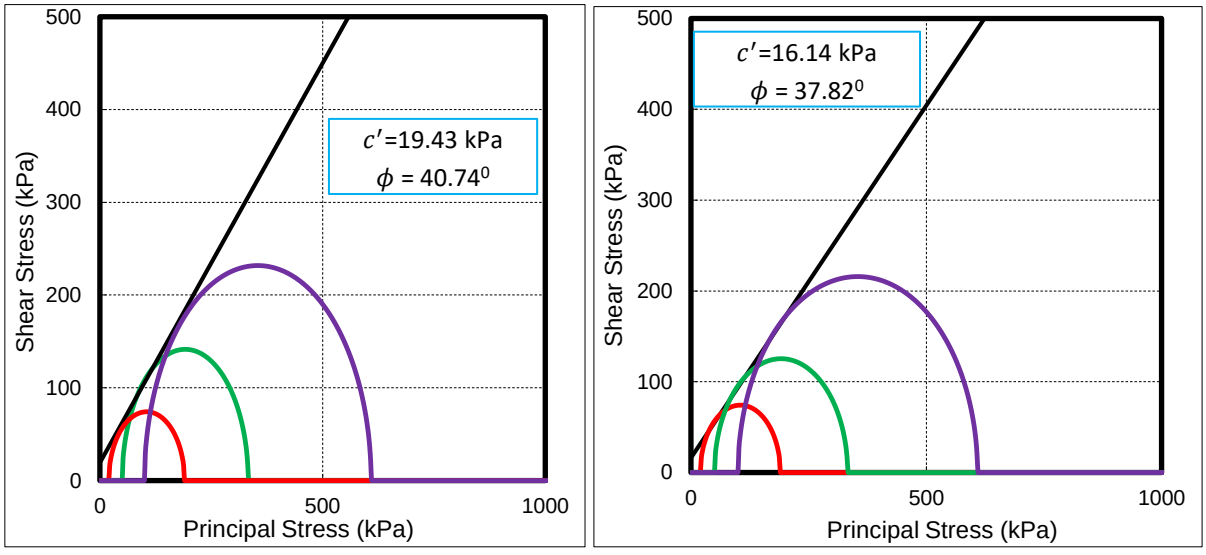

Figure 5.46: GPS 2 failure envelope at 12.53% and 18.53% moisture content

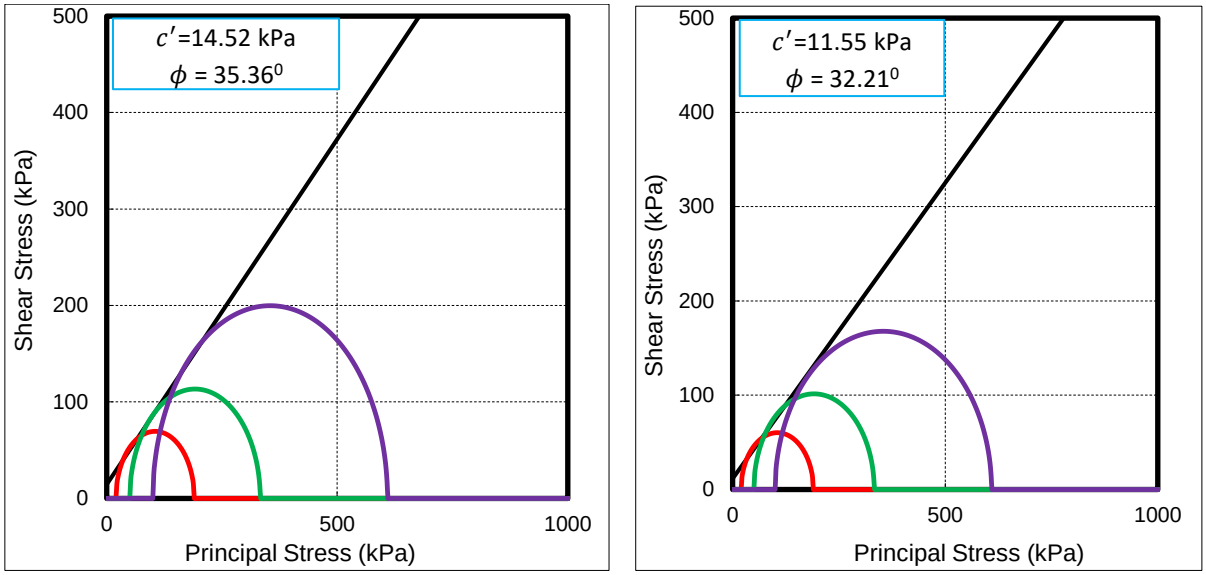

Figure 5.47: GPS 2 failure envelope at 23.25% and 30.33% moisture content

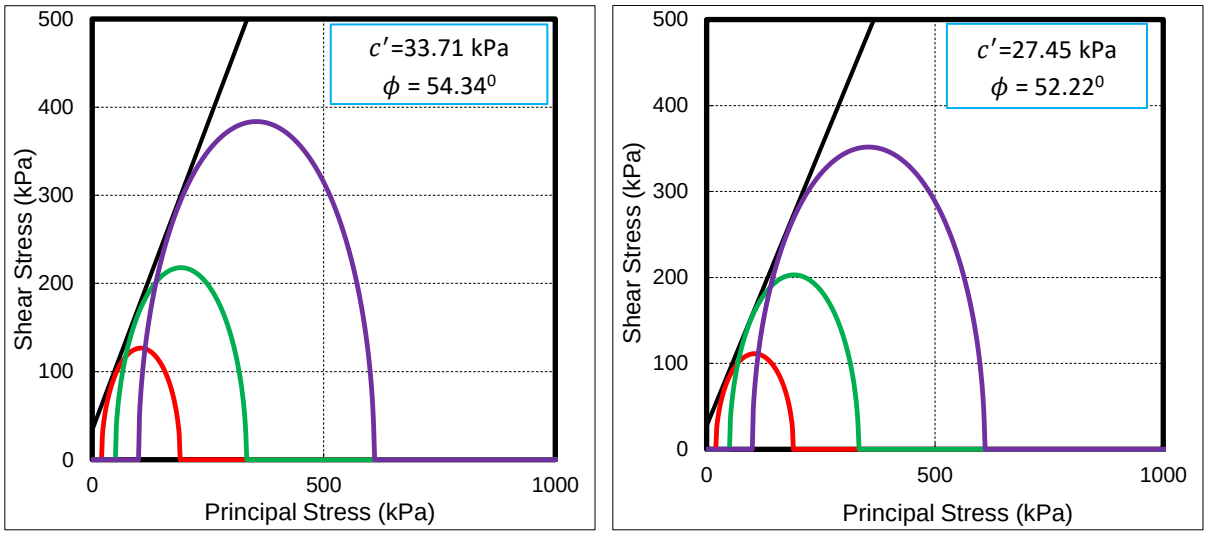

Figure 5.48: GPS 3 failure envelope at 9.28% and 14.37% moisture content

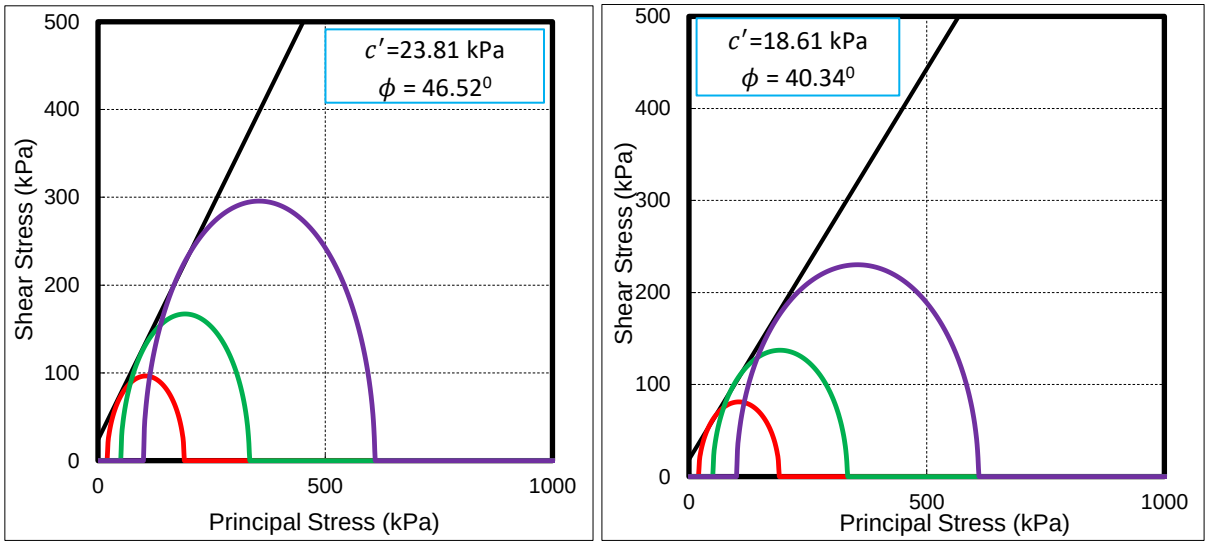

Figure 5.49: GPS 3 failure envelope at 18.88% and 23.53% moisture content

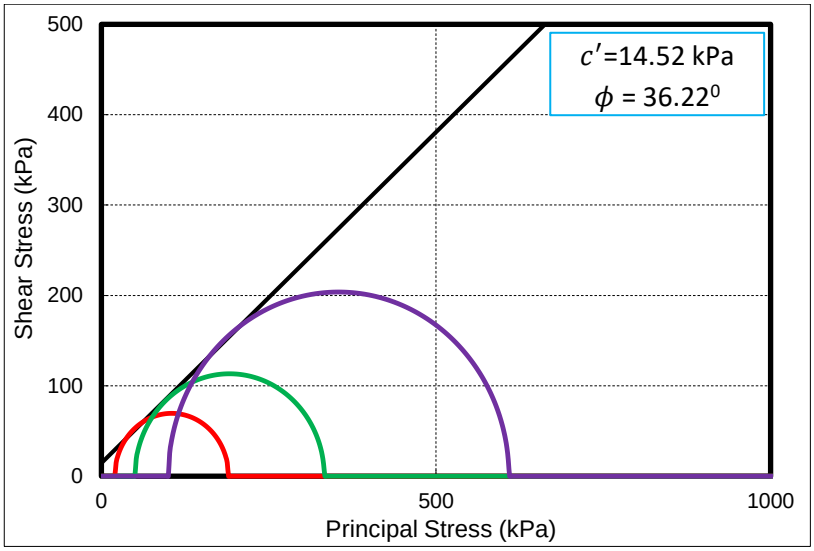

Figure 5. 50: GPS 3 failure criterion at 27.45% moisture content

Table 5.1: Saturated and unsaturated shear strength parameters

Soil moisture content (%)	C' (kPa)	σ_{nf} (kPa)	$tan\phi'$ (degree)	ψ_m (kPa)	$tan\phi^b$ (degree)	τ_s (kPa)	τ_u (kPa)	$(\tau_u - \tau_s)$ (kPa)
FSS 1								
8.55	58.10	388	49.29	6541		509	927	418
13.46	53.64	356	43.38	5976	3.66	390	772	382
17.65	51.21	283	41.42	4689		301	601	300
24.27	46.59	222	37.67	2793		218	397	179
31.75	43.11	178	34.78	921		168	226	58
FSS 2								
9.97	53.32	358	42.41	8517		380	627	247
13.67	45.52	306	36.91	6843		276	473	197
18.58	42.32	281	32.14	4989	1.66	219	364	145
24.49	38.43	212	28.51	2895		154	237	83
32.15	35.18	158	24.63	1913		108	163	55
FSS 3								
7.28	62.30	432	51.21	4498		600	1185	585
14.15	58.42	424	46.51	4045		505	1031	526
18.54	55.64	338	42.48	3250	7.41	365	788	423
22.94	51.23	264	37.14	2298		251	550	299
28.33	47.34	259	34.10	1440		223	410	187
NCS 1								
8.38	53.41	493	46.22	2534		568	982	414
12.73	48.91	468	43.13	2098		487	959	472
17.49	44.31	416	39.42	1643	12.68	387	726	339
24.40	41.37	355	33.65	1134		278	533	255
28.33	34.57	315	27.21	778		197	372	175
NCS 2								
9.18	47.32	398	42.51	3278		399	904	505

14.53	41.45	318	37.61	2465	8.53	287	657	370
18.38	37.81	288	33.53	2087		229	542	313
24.89	33.62	229	27.11	1598		151	397	246
30.22	26.13	189	23.34	1091		108	272	164
NCS 3								
9.97	42.22	356	37.34	1895	15.64	314	803	489
14.53	37.12	312	33.43	1525		243	670	427
18.98	32.61	267	28.84	1272		180	503	323
25.24	27.31	241	25.47	1010		142	398	256
32.88	25.37	227	21.64	681		116	307	191
GPS 1								
9.28	25.36	567	48.41	5021	5.71	664	1166	502
12.89	20.12	522	44.12	3884		526	914	388
16.77	17.14	470	42.91	2959		454	733	279
23.65	15.22	445	41.38	2183		407	610	203
29.88	13.52	392	38.93	1128		330	443	113
GPS 2								
9.97	22.71	418	45.23	5263	3.66	444	781	337
12.53	19.43	388	40.74	3989		354	589	235
18.53	16.14	358	37.82	2914		290	464	174
23.25	14.52	328	35.36	2029		247	377	130
30.33	11.55	303	32.21	667		203	245	42.4
GPS 3								
9.28	33.71	529	54.34	5331	6.42	737	1371	634
14.37	27.45	487	52.22	3708		628	1045	417
18.88	23.81	458	46.52	2907		508	834	326
23.53	18.61	422	40.34	1715		358	570	212
27.45	14.52	382	36.22	763		280	380	100

APPENDIX D

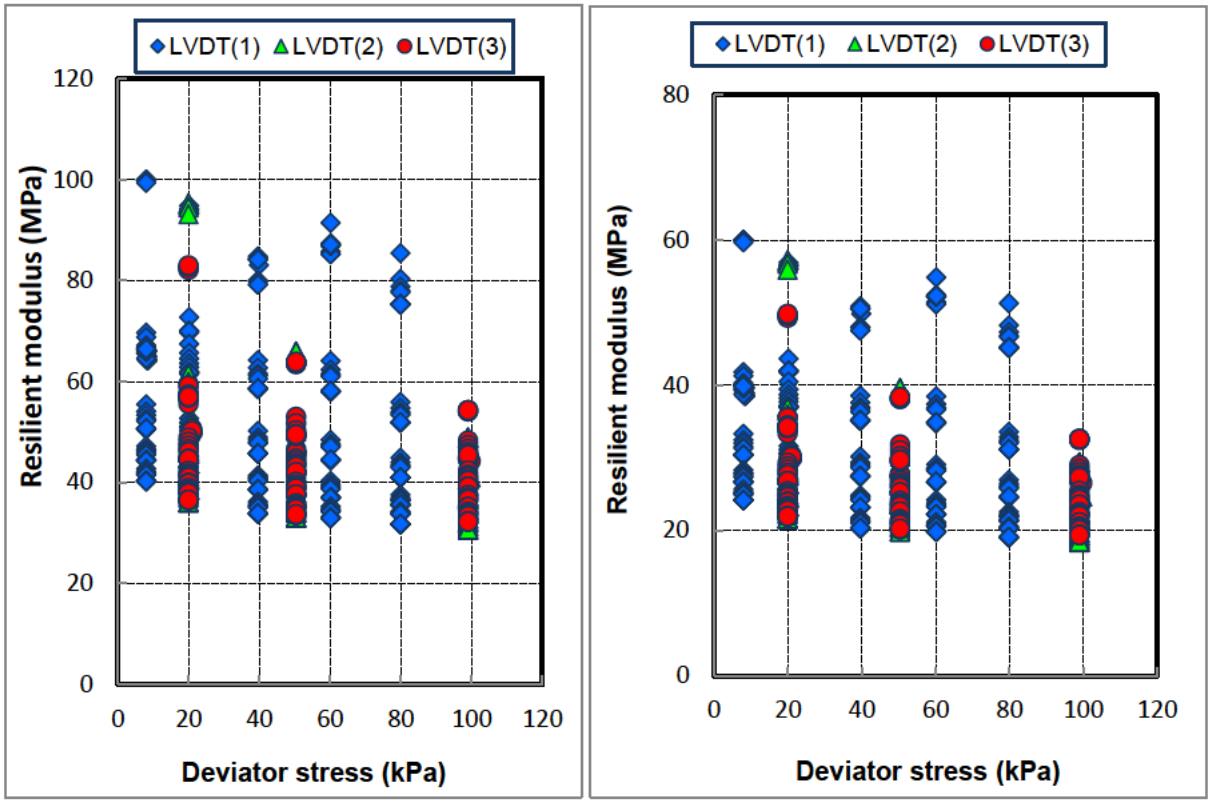

Figure 6.2: Variation of M_r for FSS1 at 13.67% and 17.65% moisture with deviatoric stress

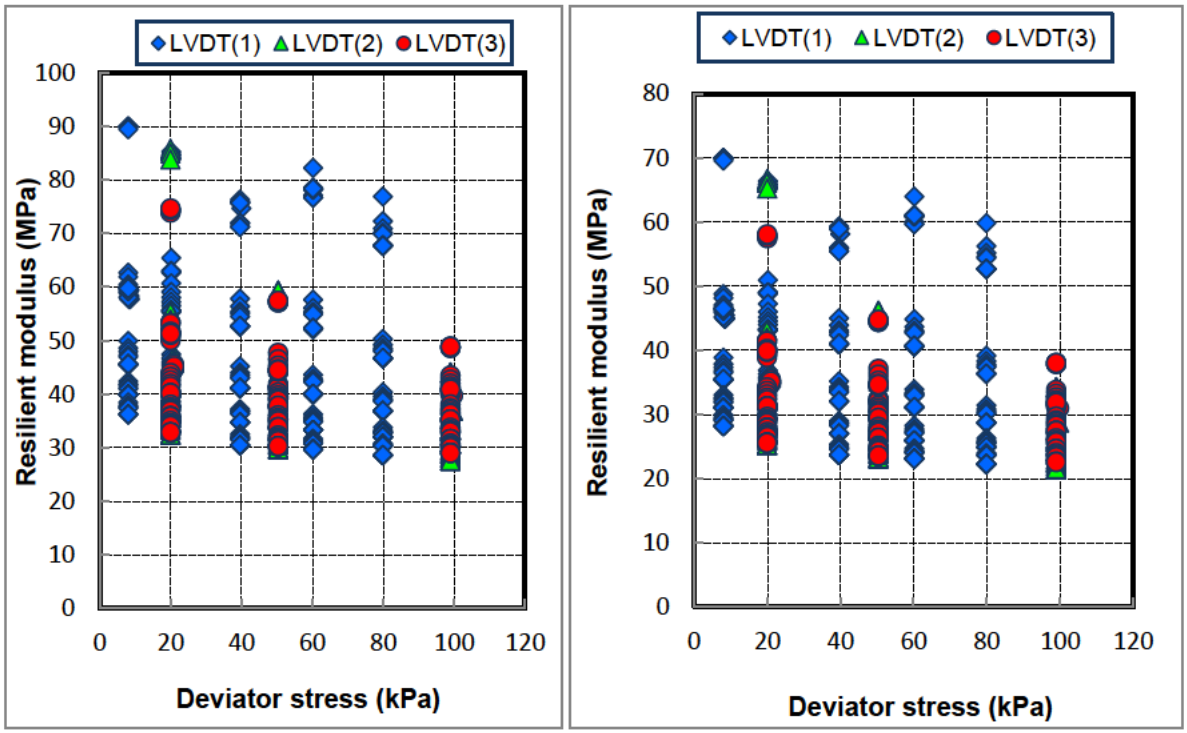

Figure 6.3: Variation of M_r for FSS 2 at 9.97% and 13.67% moisture with deviatoric stress

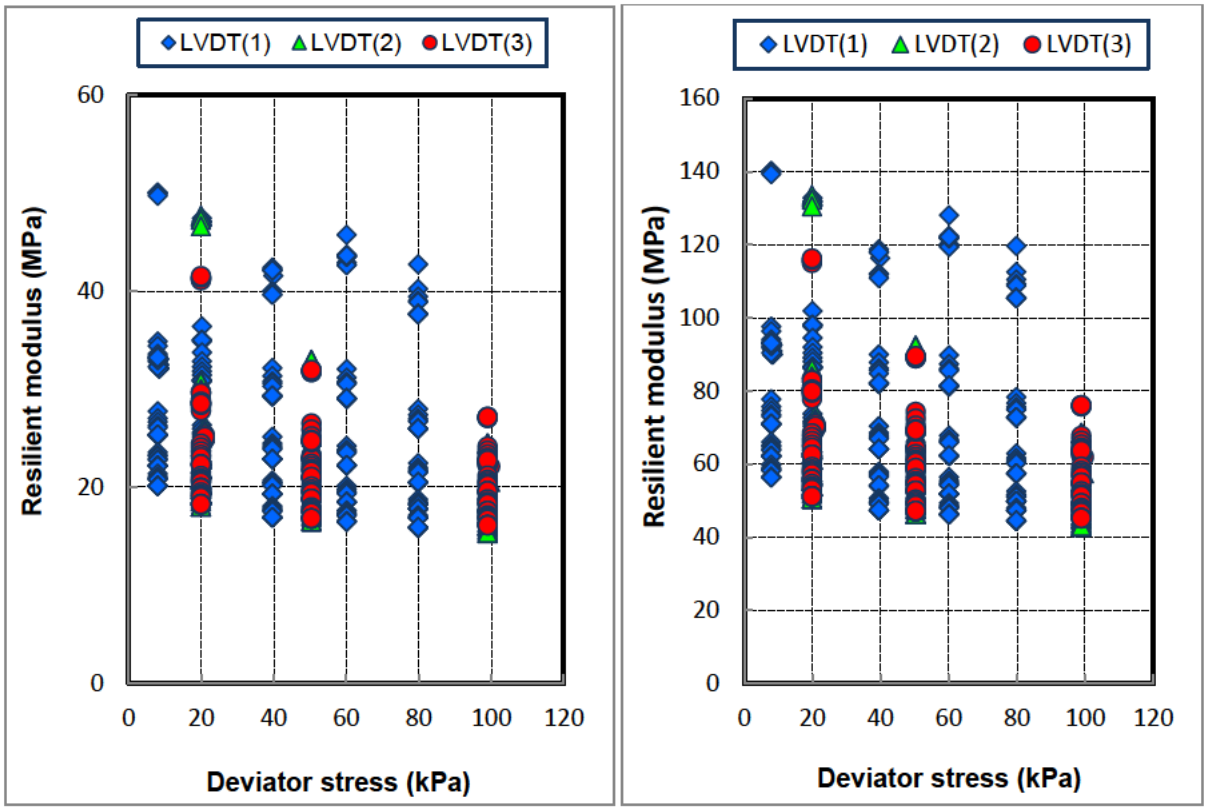

Figure 6.4: Variation of M_r for FSS 2, FSS 3 at 18.58% and 7.28% moisture with deviatoric stress

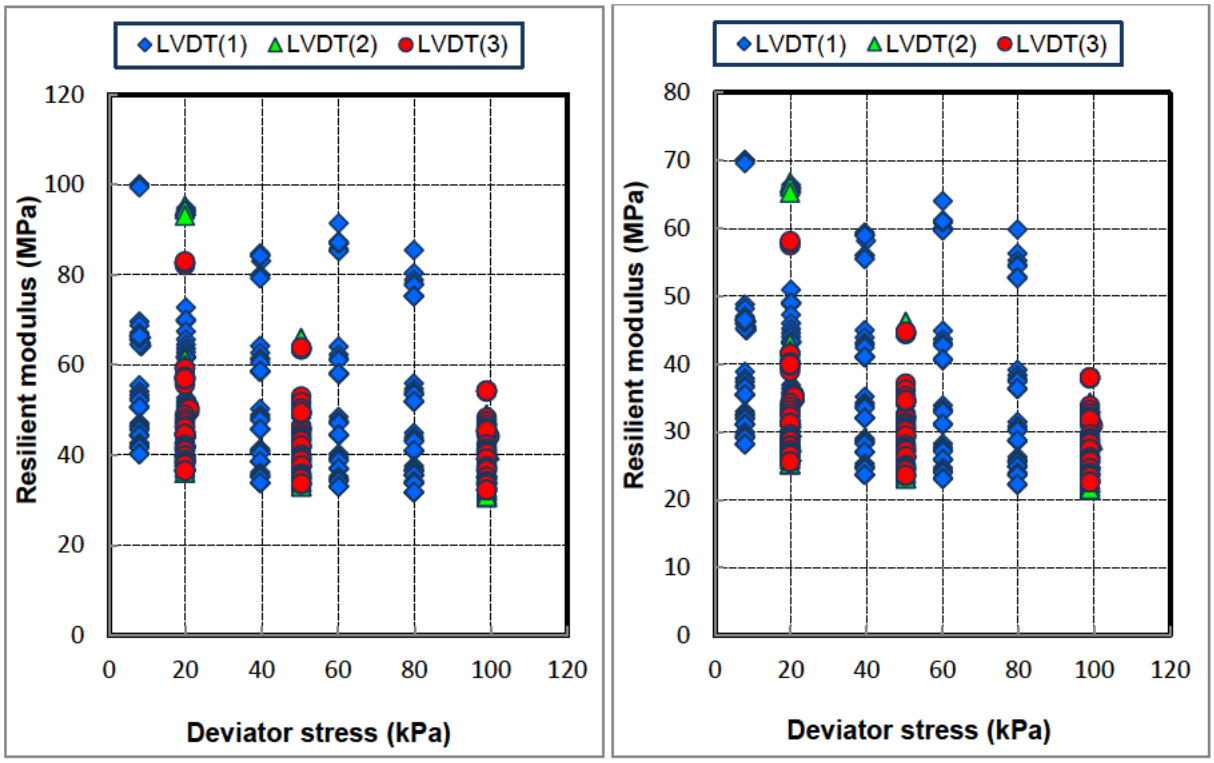

Figure 6.5: Variation of M_r for FSS 3 at 14.15% and 18.45% moisture with deviatoric stress

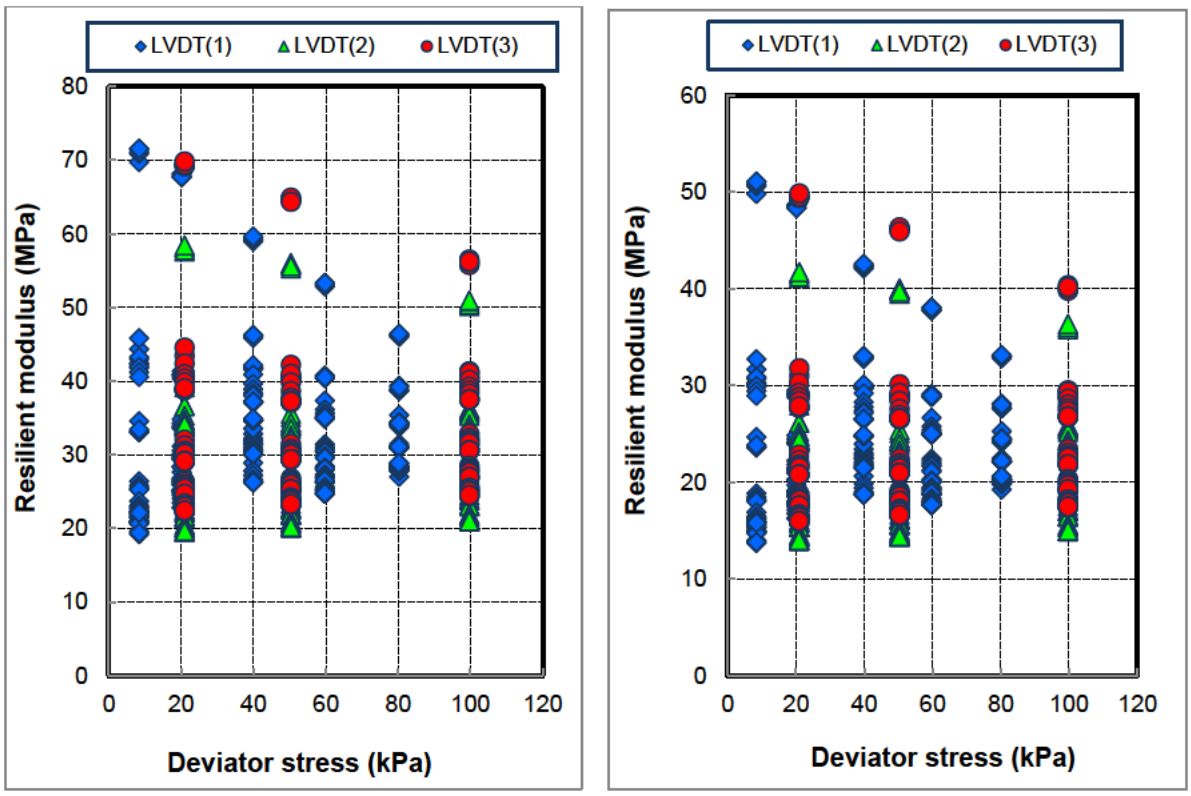

Figure 6.7: Variation of M_r for NCS 1 at 12.73% and 17.49% moisture with deviatoric stress

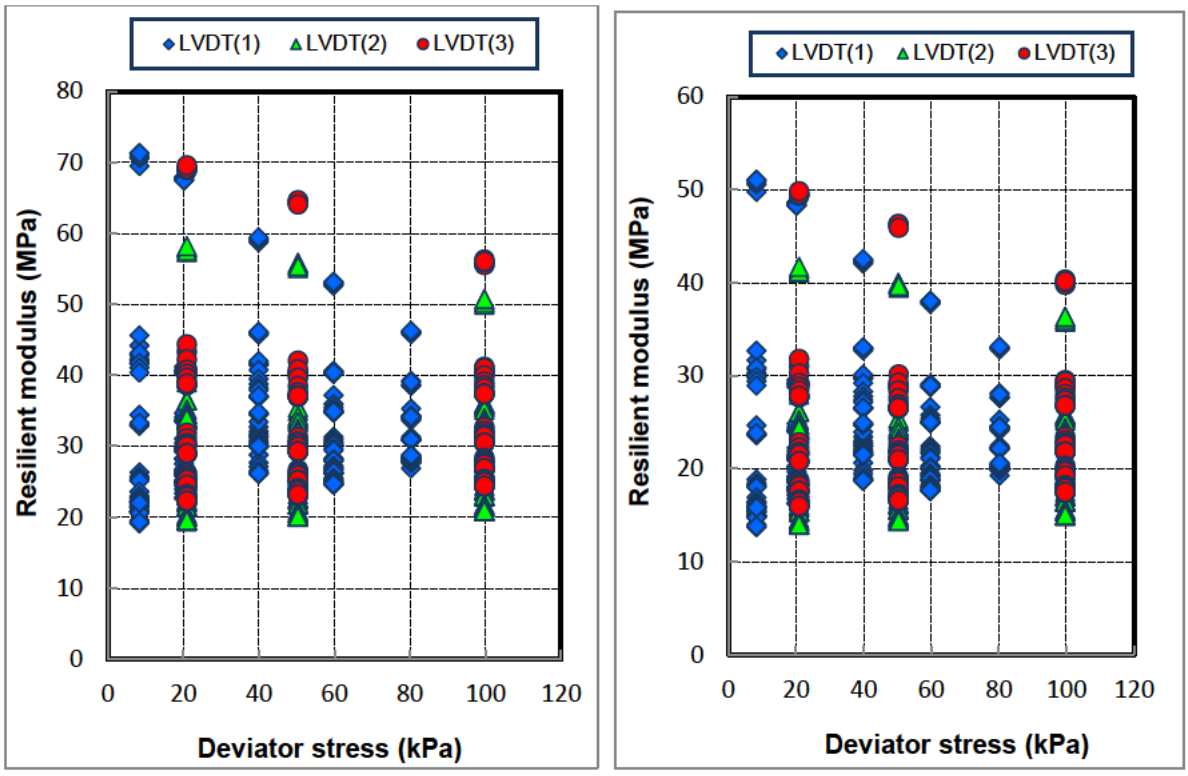

Figure 6.8: Variation of M_r for NCS 2 at 9.18% and 14.53% moisture with deviatoric stress

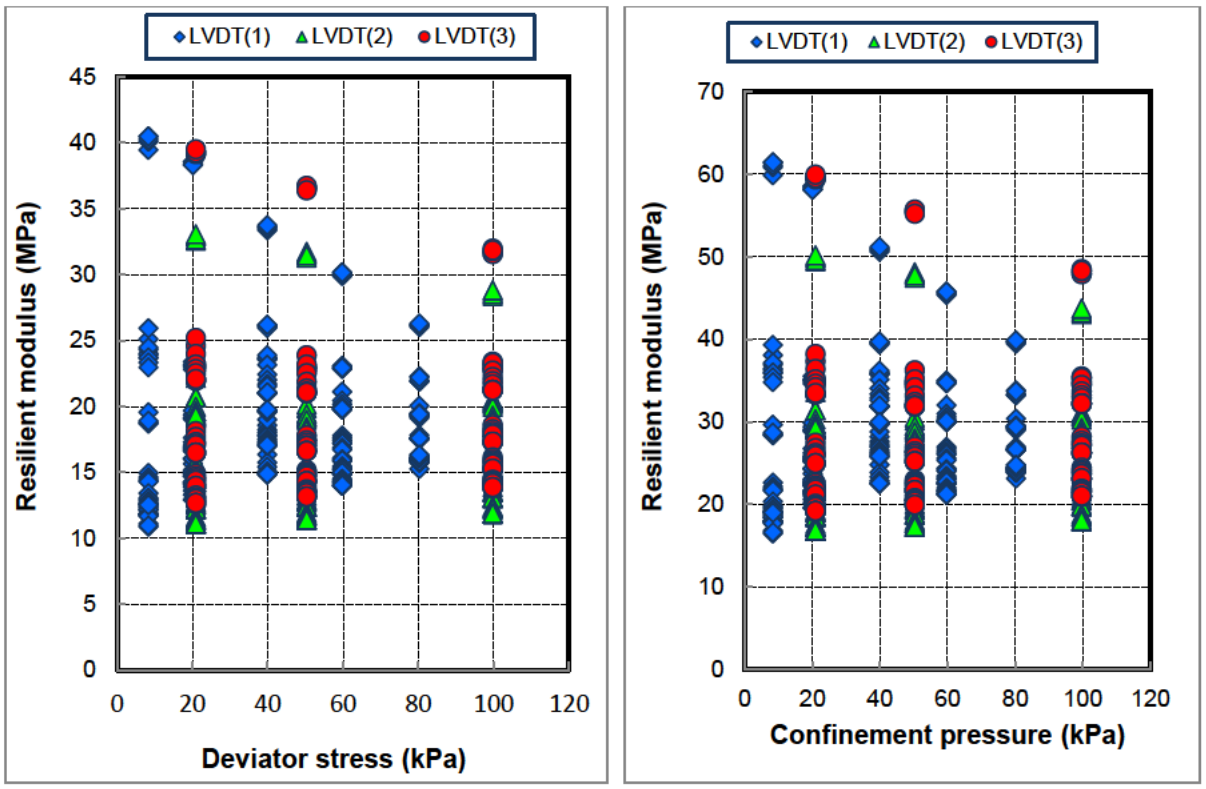

Figure 6: 9: Variation of M_r for NCS 2, NCS 3 at 18.38% and 9.97% moisture with deviatoric stress

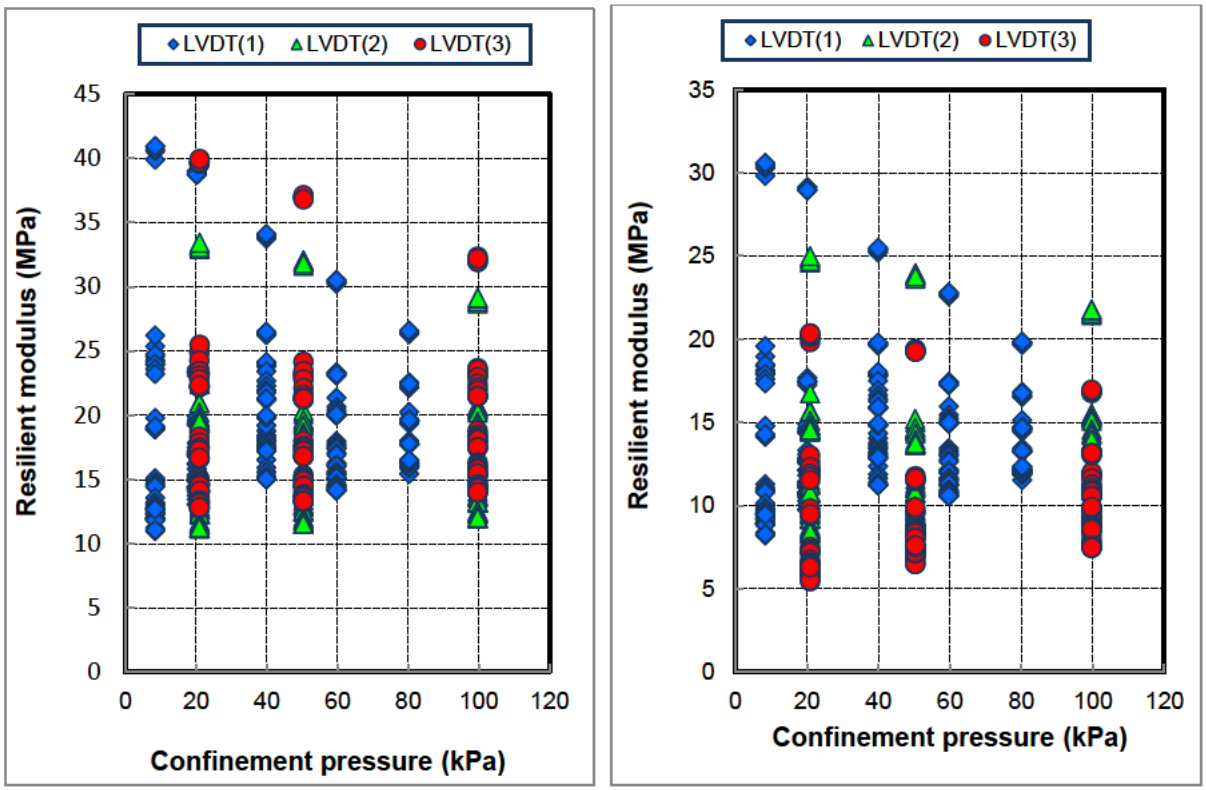

Figure 6. 10: Variation of M_r for NCS 3 at 14.85% and 18.89% moisture with deviatoric stress

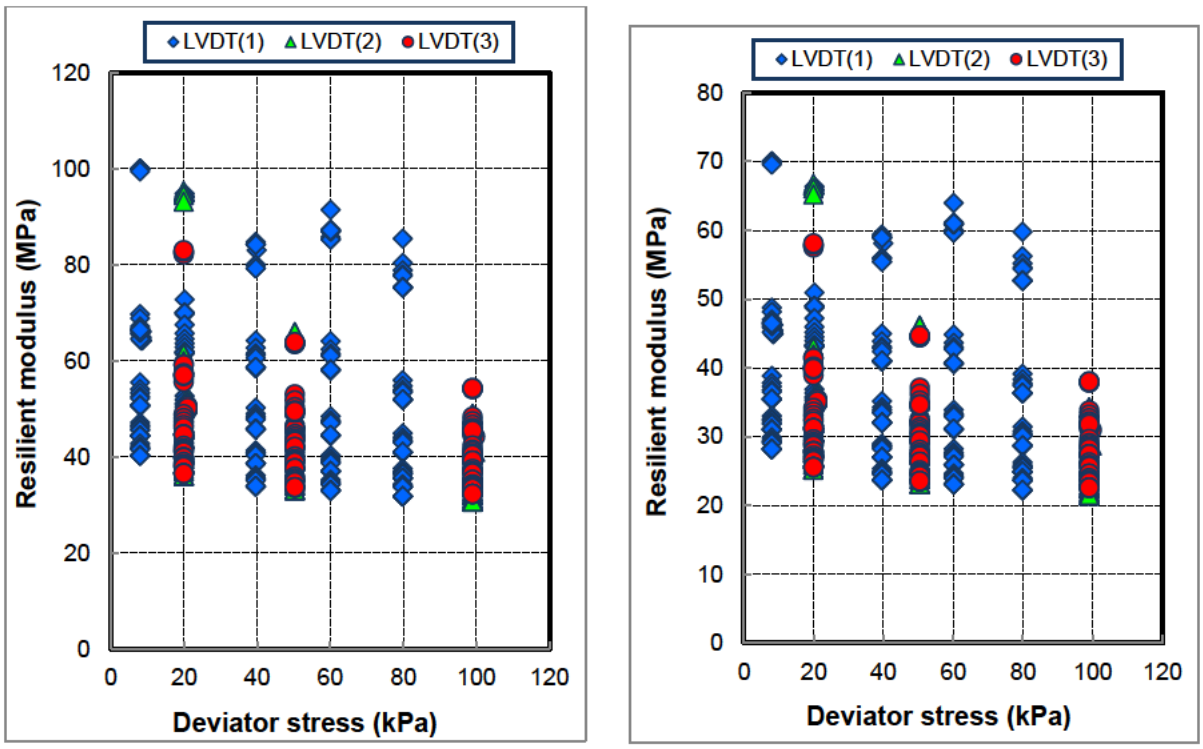

Figure 6.12: Variation of M_r for GPS 1 at 12.89% and 16.77% moisture with deviatoric stress

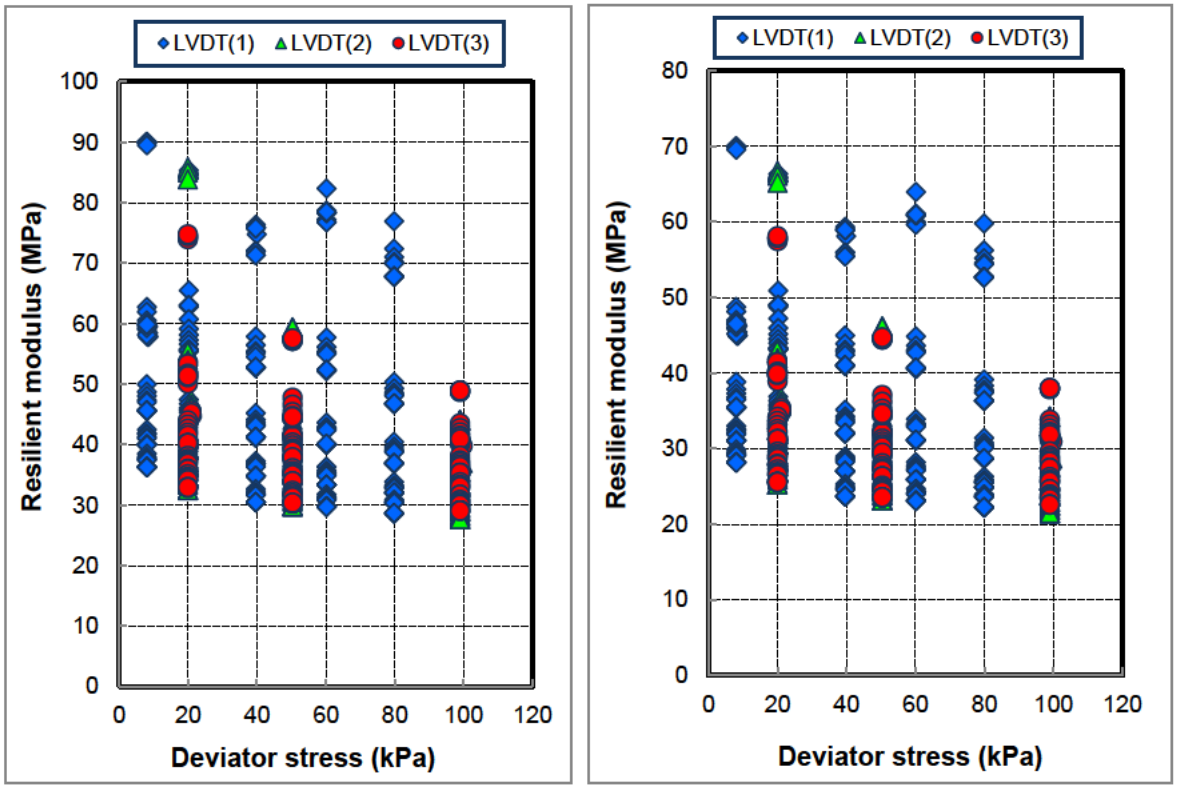

Figure 6.13: Variation of M_r for GPS 2 at 9.97% and 12.53% moisture with deviatoric stress

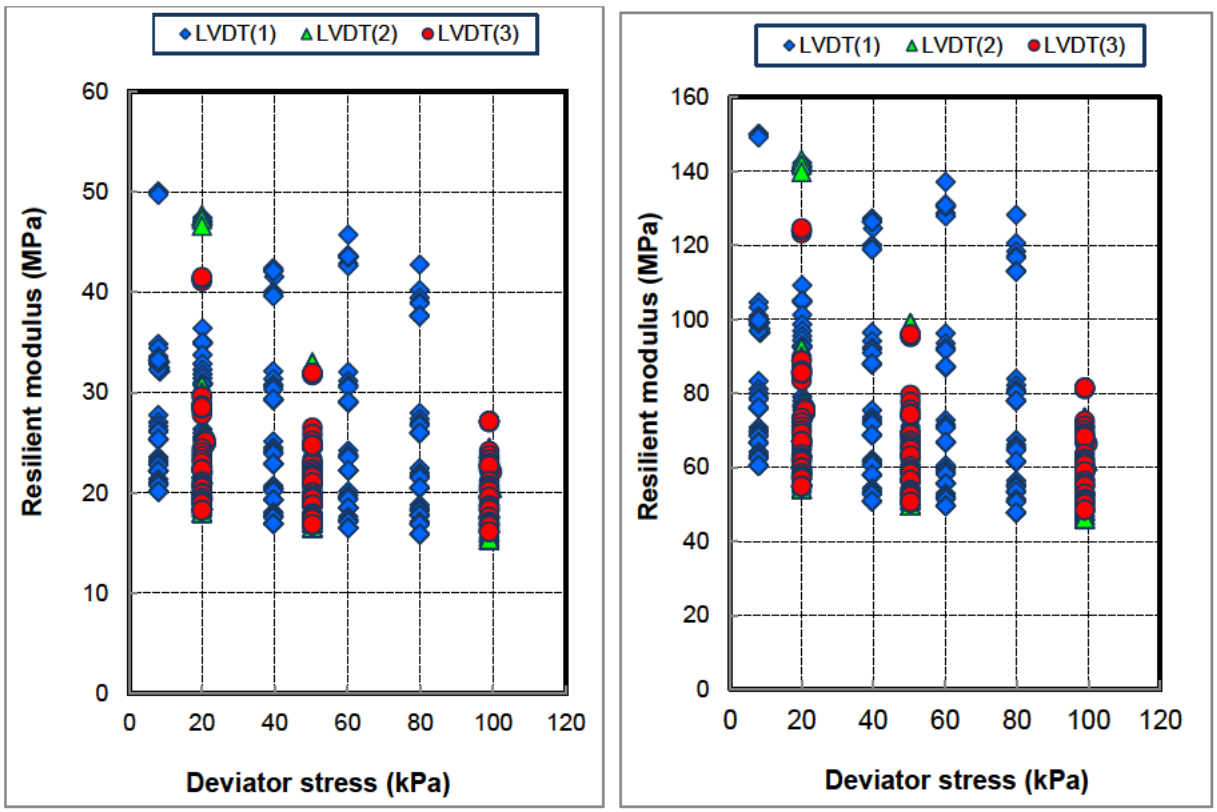

Figure 6.14: Variation of M_r for GPS 2, GP3 at 18.53% and 9.28% moisture with deviatoric stress

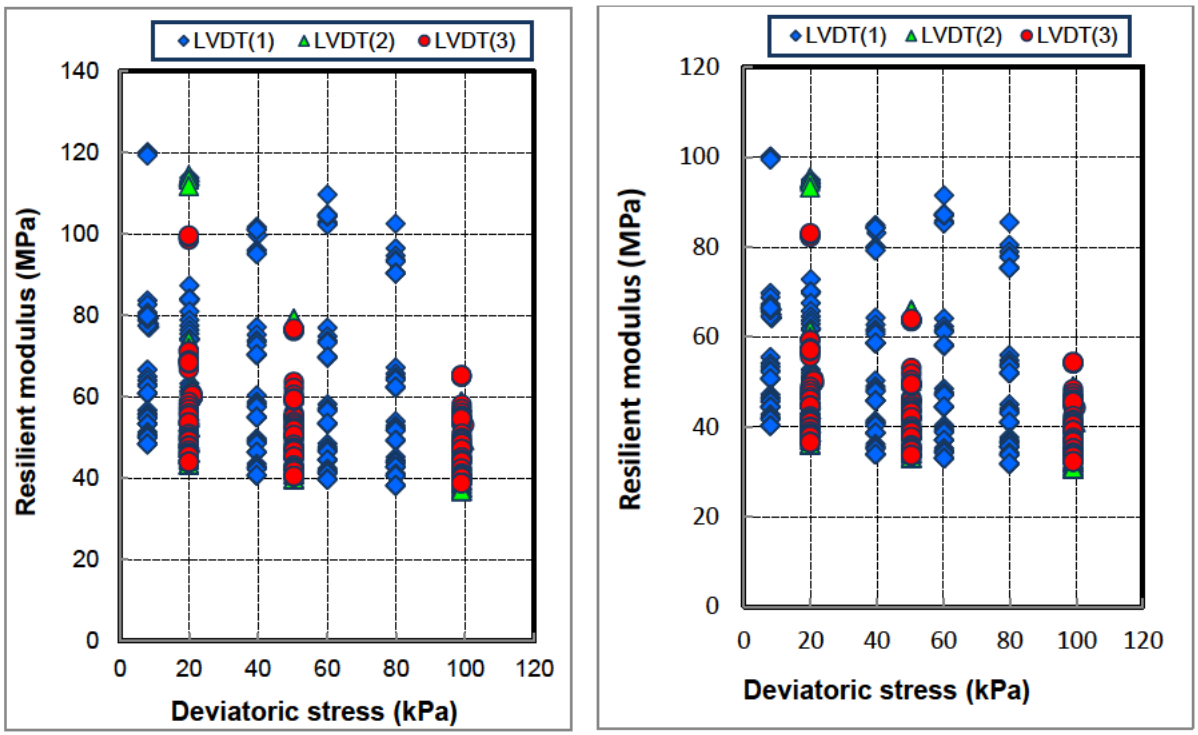

Figure 6.15: Variation of M_r for GPS 3 at 14.37% and 18.88% moisture with deviatoric stress

Table 6.1: Parameters symbols and their corresponding values

Denotations	Meaning	Values	R^2
Model 1			
ζ_0	Intercept	369.6004	-
ζ_1	Coff. for γ_{dry}	4.8039	-
γ_{dry}	Dry density	-	0.7271
ζ_2	Coff. for Percentage passing #200	1.1861	-
$P_{\#200}$	Percentage passing #200	-	0.7555
ζ_3	Coff. for Moisture content	5.3152	-
M_c	Moisture content	-	0.8640
ζ_4	Coff. for Liquid limit	0.0659	-
$\mathbf{LL}$	Liquid limit	-	0.8640
ζ_5	Coff. for Swelling pressure	0.0551	-
P_s	Swelling pressure	-	0.8740
Model 2			
λ_0	Intercept	135.6336	-
λ_1	Coff. for γ_{dry}	2.1865	-
$\gamma_{\mathbf{dry}}$	Dry density	-	0.7264
λ_2	Coff. for CBR	6.2707	-
$\mathbf{CBR}$	CBR		0.7464
λ_3	Coff. for Moisture content	3.0062	-
M_c	Moisture content	-	0.8068
λ_4	Coff. for Swelling pressure	0.0341	-
P_s	Swelling pressure	-	0.8358
λ_5	Coff. for Compression strength	0.0941	-
q_u	Compression strength	-	0.8445
λ_6	Coff. for Shear stress	0.1981	-
τ_s	Shear stress	-	0.9355
Model 3			
η_0	Intercept	188.2355	-
η_1	Coff. for γ_{dry}	2.1662	-
γ_{dry}	Dry density	-	0.7436
η_2	Coff. for CBR	8.9390	-
CBR	CBR	-	0.7825
η_3	Coff. for Percentage passing #200	0.7787	-
$P_{\#200}$	Percentage passing #200	-	0.7855
η_4	Coff. for Moisture content	3.3032	-
M_c	Moisture content	-	0.8643
η_5	Coff. for Liquid limit	0.5347	-
$\mathbf{LL}$	Liquid limit	-	0.8643
η_6	Coff. for Swelling pressure	0.0155	-
P_s	Swelling pressure	-	0.8751
η_7	Coff. for Compression strength	0.0940	-
q_u	Compression strength	-	0.8804
η_7	Coff. for Shear stress	0.2106	-
τ_s	Shear stress	-	0.9340

Table 6.2: Parameters symbols and their corresponding values

Denotations	Meaning	Values	R^2
Model 7			
ξ_0	Intercept	12.396	-
ξ_1	Coff. for Matric suction	0.0095	-
ψ_m	Matric suction	-	0.6117
ξ_2	Coff. for Air entry value (AEV)	1.1861	-
S_e	Air entry value	-	0.8106
ξ_3	Coff. for Unsaturated CBR_u	1.9574	-
CBR_u	Unsaturated CBR_u	-	0.9097
ξ_4	Coff. for Swelling pressure	0.0089	-
P_{S_n}	Swelling pressure	-	0.9104
Model 8			
α_0	Intercept	19.493	-
α_1	Coff. for Matric suction	0.0094	-
ψ_m	Matric suction	-	0.6117
α_2	Coff. for Air entry value (AEV)	0.2183	-
S_e	Air entry value (AEV)	-	0.8106
α_3	Coff. for Swelling pressure	3.0062	-
P_{S_n}	Swelling pressure	-	0.8169
α_4	Coff. for Unsaturated CBR_u	1.9782	-
CBR_u	Unsaturated CBR_u	-	0.9104
α_5	Coff. for Dry density	0.3311	-
γ_{dry}	Dry density	-	0.9109

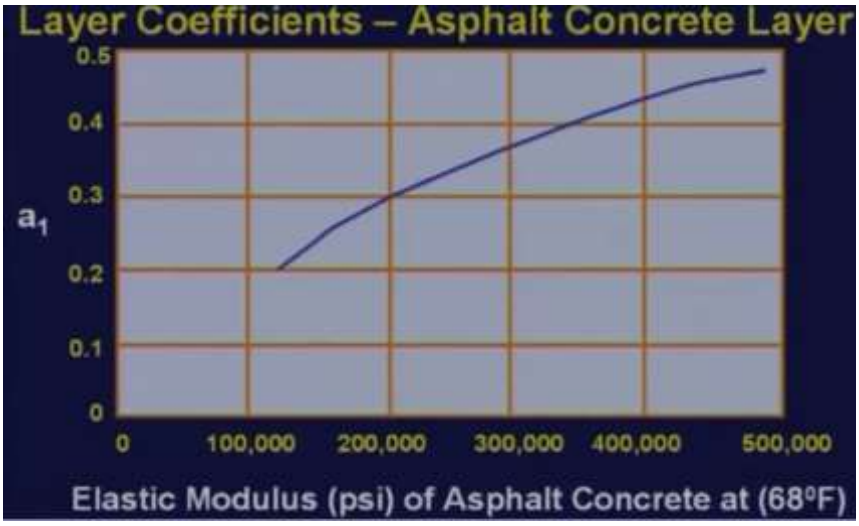

Figure 6.29: Layer coefficient for asphalt concrete

APPENDIX J

Table 6.23: Measurement of soil suction using filter paper- Data sheet

ASTM D 5298 (1994)

Geotechnical Laboratory, Department of Civil Engineering , CUT

Soil designation ……

Date tested: ……

Tested by: ……..

Sample		1-1		1-2		1-3		1-4		1-5	
Gravimetric water content of soil sample,W, (%)											
Tin No											
Top filter paper / Bottom filter paper		Top	Bot	Top	Bot	Top	Bot	Top	Bot	Top	Bot
Cold Tare Mass, g	Tc										
Mass of wet Filter paper + Cold Tare Mass, g	m1										
Mass of Dry Filter paper + Hot Tare Mass, g	m2										
Hot Tare Mass, g	Th										
Mass of water in Filter Paper, g M2-Th	Mf										
Mass of water in Filter Paper, g M1-M2-Tc+Th	Mw										
Water content of filter Paper,g (Mw/Mf) %	Wf										
Suction , kPa	Ψ										
Suction , logkPa	Ψ										
Suction, PF = logkPa+1	Ψ										